AD_____

Award Number DAMD17-94-J-4368

TITLE: pH Regulation by Breast Cancer Cells In Vitro and In Vivo

PRINCIPAL INVESTIGATOR: Robert J. Gillies, Ph.D.

CONTRACTING ORGANIZATION: University of Arizona
Tucson, Arizona 86719

REPORT DATE: September 1999

TYPE OF REPORT: Final

PREPARED FOR: U.S. Army Medical Research and Materiel Command
Fort Detrick, Maryland 21702-5012

REPORT DOCUMENTATION PAGE

Form Approved
OMB No. 074-0188

1. AGENCY USE ONLY (Leave blank)	2. REPORT DATE	3. REPORT TYPE AND DATES COVERED
	September 1999	Final (15 Aug 94 - 14 Aug 99)

4. TITLE AND SUBTITLE
pH Regulation by Breast Cancer Cells In Vitro and In Vivo

5. FUNDING NUMBERS
DAMD17-94-J-4368

6. AUTHOR(S)
Robert J. Gillies, Ph.D.

7. PERFORMING ORGANIZATION NAME(S) AND ADDRESS(ES)
University of Arizona
Tucson, Arizona 86719
E-MAIL:

8. PERFORMING ORGANIZATION REPORT NUMBER

9. SPONSORING / MONITORING AGENCY NAME(S) AND ADDRESS(ES)
U.S. Army Medical Research and Materiel Command
Fort Detrick, Maryland 21702-5012

10. SPONSORING / MONITORING AGENCY REPORT NUMBER

11. SUPPLEMENTARY NOTES
This report contains colored photos

12a. DISTRIBUTION / AVAILABILITY STATEMENT
Approved for public release; distribution unlimited

12b. DISTRIBUTION CODE

13. ABSTRACT *(Maximum 200 Words)*

Subject Terms: Metastasis, Spectroscopy, Intracellular pH, Blood Flow, In Vivo Tumor Models, Multidrug Resistance, H+ ATPase, Tumors

15. NUMBER OF PAGES
100

16. PRICE CODE

17. SECURITY CLASSIFICATION OF REPORT	18. SECURITY CLASSIFICATION OF THIS PAGE	19. SECURITY CLASSIFICATION OF ABSTRACT	20. LIMITATION OF ABSTRACT
Unclassified	Unclassified	Unclassified	Unlimited

FOREWORD

Opinions, interpretations, conclusions and recommendations are those of the author and are not necessarily endorsed by the U.S. Army.

___ Where copyrighted material is quoted, permission has been obtained to use such material.

___ Where material from documents designated for limited distribution is quoted, permission has been obtained to use the material.

___ Citations of commercial organizations and trade names in this report do not constitute an official Department of Army endorsement or approval of the products or services of these organizations.

X In conducting research using animals, the investigator(s) adhered to the "Guide for the Care and Use of Laboratory Animals," prepared by the Committee on Care and use of Laboratory Animals of the Institute of Laboratory Resources, national Research Council (NIH Publication No. 86-23, Revised 1985).

_ For the protection of human subjects, the investigator(s) adhered to policies of applicable Federal Law 45 CFR 46.

N/A In conducting research utilizing recombinant DNA technology, the investigator(s) adhered to current guidelines promulgated by the National Institutes of Health.

N/A In the conduct of research utilizing recombinant DNA, the investigator(s) adhered to the NIH Guidelines for Research Involving Recombinant DNA Molecules.

N/A In the conduct of research involving hazardous organisms, the investigator(s) adhered to the CDC-NIH Guide for Biosafety in Microbiological and Biomedical Laboratories.

Robert Gillies

PI - Signature Date

TABLE OF CONTENTS

PROJECT 1. MEASUREMENT OF TUMOR pH

INTRODUCTION

Prior to 1994, measurement of tumor pH was limited to microelectrodes, which measure the interstitial/extracellular pH (pHe), and ^{31}P MRS of inorganic phosphate, which measured the intracellular pH (pHi). In 1994, we developed a method to simultaneously measure the intra and extracellular pH of tumors, using exogenous 3-amino propyl phosphonate (3-APP) and inorganic phosphate (Pi) (Gillies et al., 1994, Am J Physiol 267, C195-C203). However, this method is limited to measuring average tumor pHe, and was not capable of reporting the pH range or localized values. MR-based pH measurement techniques have been improved in two ways. First, the data obtained from ^{31}P MRS of 3-APP have been more thoroughly analyzed to yield trans-tumoral pH ranges. Second, an alternative pH-sensitive marker has been developed to allow pH in mapping using multivoxel ^{1}H-MRS.

BODY/KEY RESEARCH ACCOMPLISHMENTS

- Deconvolution of ^{31}P spectra of 3-APP to yield pHe ranges was discussed in our annual report of 1996. The manuscript describing these results is still in preparation, since the method has been more or less superceded by the ^{1}H based MRSI technique. Nonetheless, the deconvolution method will hold some interest for a limited readership and thus, a publication will be forthcoming.
- Measurement of pHe maps using ^{1}H-MRSI of imidazoles was carefully characterized. This has been published [1]. Briefly, data are presented characterizing the behavior of ethoxycarbonyl propionic acid (IEPA) as a marker of extracellular pH. A significant effort was expended to characterize the source of errors in these measurements, which were estimated to be $\pm$0.1 pH unit in the worst case.

PROJECT 2. pH AND METASTASIS

INTRODUCTION

Prior work had shown that culturing cells at low pH induced them to become more metastatic in vivo (Schlappack et al., 1991, Intl. J. Cancer 64, 663-670). Our work had showed an acid pH in tumors (see above). One of our collaborators (MJC Hendrix) had developed a highly reproducible cell culture invasion assay, called MICS (Hendrix et all., 1987, Cancer Lett. 38, 137-147). Another collaborator (JA Backer) has produced a non-metastatic variant of a highly invasive breast cancer cell line. In this project we proposed to investigate the relationship between pH and metastasis in vitro and in vivo.
In the first study, we investigated simply if acute or chronic acid pH would affect the in vitro invasiveness of cancer cells. The ability of metastatic cells to regulate their pHi was also determined. Along with Joe Backer, we investigated whether prevention of metastasis affected pH regulation in vivo.

BODY

- Acid pH, whether acute or chronic, affected the migration and invasiveness of both melanoma and breast cancer cells. The results from melanoma cells were very conclusive and were published [2]. In brief, chronic exposure to low pH significantly increased the migration and invasion of both highly (C8161) and lowly (C375P) metastatic melanoma cells. Acute exposure to low pH (i.e. during the migration test), inhibited migration of cells grown at normal (7.2) pH values. This increased invasiveness was not related to pHi values since both chronic and acutely acidic cells had acidic pHi values.
- There was increased processing of gelatinase at low pHe, suggesting that this may be a relevant mechanism. The absolute pHi values did not correlate with metastasis. This was borne out in later studies, published in [3].

- To test the relationship between pH and metastasis further, highly metastatic MDA-mb-435 cells were rendered non-metastatic by transfection with nm-23, a gene product that inhibits metastasis through an unknown function [4]. When inoculated as tumors, the nm-23 transfectants were much less metastatic (0-2 metastatic nodules per animal average) compared to the non-transfectants (20 nodules). The major consistent difference between the nm-23 transfectants and the parental or vector control cells, was a lower pHi and a higher pHe. These data are consistent with a lower pHe being correlated to increased metastasis.

PROJECT 3. pH AND THERAPY.

INTRODUCTION

There are numerous studies that demonstrate, in vitro, that the extracellular pH can have a dramatic effect on the efficacy of chemotherapy. For example, it is well known that weakly basic chemotherapeutic agents distribute into acidic compartments based on the pH gradients. In cells these acidic environments are found in vesicles. In tumors, the pHe is acidic and hence, weakly basic drugs should sequester in the extracellular environment. This had yet to be tested in vivo. These studies investigated the relationship between pH and therapy in vitro by examining the role of vesicles in drug-resistance. In vivo the relationship was examined using tumor xenografts.

BODY

- We examined the role of acidic intracellular vesicle trafficking on drug resistance in breast cancer cells. Previous work in our lab had shown the presence of vacuolar-type H^+ ATPase activity at the plasma membrane so tumor cells. (Martinez-Zaguilan et al., 1993, Am. J. Physiol. 265, C1015-C1029). Efforts to visualize these pumps at the cell surface by immunocytochemistry were not successful, prompting us to hypothesize that the observed activity was an epiphenomenon of rapid endosomal recycling.
- This was investigated in drug-sensitive and drug –resistant MCF-7 cells [5]. The steady-state pHi of these different cells lines was not different, nor was there a difference in their endosomal/lysosomal pH values. However, both of the drug-resistant cell lines expressed a plasmalemmal V-ATPase activity, whereas the sensitive cells did not. Endosomal turnover was measured by monitoring the release of fluorescently tagged dextran, and the rates were much higher in the drug-resistant cells compared to the drug-sensitive cells. These data therefore suggest that drug-resistance is accompanied by a concomitant increase in endosomal turnover.
- In a companion manuscript [6], we examined the role of endosomal turnover on drug resistance theoretically and showed that it could be a potent force, if the endosomes expressed a drug/H^+ antiporter. PCR screening for known organic cation transporters has so far failed to identify such a protein in drug-resistant cells.
- The relationship between drug resistance and pH has been examined in vivo first by characterizing the pHe and pHi of drug resistant and sensitive tumors as the tumors grew [7]. Interestingly, the behavior of the two drug-resistant lines (PgP and MRP positive) were similar to each other, yet strikingly different from the pH-behavior of the drug sensitive cells. The observed large pH-gradient in the large drug-resistant tumors could contribute to increased drug resistance, and the smaller pH gradient in the small drug-resistance tumors would make them more sensitive. This is consistent with the observation that the drug-resistance increases with tumor size in their system, and suggests that pH gradients may play a role in "physiological" resistance to weakly basic chemotherapeutic agents.
- This was tested directly by alkalization of tumor pHe using bicarbonate [8]. Tumors with higher pHe were more sensitive to doxorubicin than were untreated tumors. Hence, alkalinization of tumor pH can be a potent sensitizer to doxorubicin therapy.

Project 4. THERAPY AND CELL VOLUME.

INTRODUCTION

There is evidence to suggest that cell volume is affected by successful chemotherapy. Since cell volume fraction is important to pH regulation and can be measured by many of the same techniques, we initiated a new project to investigate this phenomenon. Intra and extracellular volumes were measured directly, and indirectly, in tumor xenografts in response to therapy.

BODY

- Volume fractions can be measured in vivo using a variation of the pH-measurement technique. Since 3-APP is confined to the extracellular space, it can be used also as an extracellular volume marker. Dimethyl methyl phosphonate (DMMP) is a nontoxic marker of total cell volume and hence, in the same animal, the 3APP/DMMP ratio directly yields the extracellular volume fraction. This was tested in RIF-1 tumors treated with 5FU [9], and these data showed a high degree of concordance with "gold standard" destructive volume measurements using radiolabels. In this study, 5FU had no effect on tumor cell volumes. Volumes can also be measured indirectly by quantifying the apparent diffusion coefficient of water (ADC_w) using diffusion MRI. In these measurements, an increased ADC_w corresponds to an increased extracellular volume fraction. This was examined by determining the ADC_w in response to taxol chemotherapy in drug-sensitive and drug-resistance (D40) MCF7 cells [10].
- These data clearly showed that there was an early increase in the ADC_w that preceded any change in tumor volume, only in those tumors that eventually responded.

REPORTABLE OUTCOMES

1. **van Sluis R, Bhujwalla Z, Raghunand N, Ballesteros P, Alvarez J. Cerdan S Gillies RJ (1999) Imaging of extracellular pH of tumors using 1H MRSI.** ***Magnetic Resonance in Medicine*** **41: 743-750.** This paper describes a novel pH measurement technique that allows us to image the extracellular pH of tumors non-invasively in vivo. The technique is based on magnetic Resonance Spectral Imaging and employs a novel imidazole derivative developed by Drs. Cerdan and Ballesteros.

2. **Martinez-Zaguilan R, Seftor EA, Seftor RE, Chu YW, Gillies RJ, and Hendrix MJ (1996) Acidic pH enhances the invasive behavior of human melanoma cells.** ***Clinical & Experimental Metastasis, 14*****:176-86.** This manuscript describes the effect of acidic conditions on the migration and invasion of highly- and lowly-metastatic melanoma and breast cancer cells in vitro. It reports that growth at acidic conditions consistently renders all cells more invasive. In the case of melanoma cells, the lowly metastatic A375p cells grown at acidic pH (6.7) exhibited migration and invasion comparable to the highly metastatic C8161 cells grown at alkaline pH (7.4). These data support the hypothesis that metastasis might be augmented by hostile tumor environments (e.g. low pH).

3. **Martinez-Zaguilan R, Martinez GM, Gomez A and Gillies RJ (1998) Distinct regulation of pH and Ca by cells of differing metastatic potential.** ***J. Cell. Physiol*** **176:196-205.** This paper describes the occurrence of Vacuolar-type H^+ ATPases as a significant contributor to pH regulation in metastatic, compared to non-metastatic breast cancer and melanoma cells. We hypothesize at this juncture that the enhanced V-ATPase activity might result from rapid turnover of acidic vesicles, and not V-ATPase statically resident in the plasma membrane (see manuscripts 4 and 5 below).

4. **Bhujwalla ZM, Aboagye EO, Gillies RJ, Mendola CE and Backer JM (1998) Nm23-transfected MDA-MB-435 human breast carcinoma cells form tumors with altered phospholipid metabolism and pH. A ^{31}P NMR study In vivo and In vitro. *Magn. Reson. Med.* 41: 897-903.** NM-23 is a controversial family of proteins whose expression is correlated with reduced metastatic potential. In this study, we transfected highly metastatic MDA-mb-435 cells to express these proteins (2 isoforms, along with inactive mutant controls). When grown as tumor xenografts in SCID mice, the non-metastatic transfectants had significant alterations in their 31-P MR profiles, viz. significant alterations in both extracellular pH and phosphodiester levels. This is the first indication that the extracellular pH of tumors from metastatic cells may have a fundamental different pH environment than non-metastatic cells.

5. **Martinez-Zaguilan R, Raghunand N, Lynch, R, Bellamy, W, Martinez GM, Rojas B, Smith DJ, Dalton WS, and Gillies RJ, (1998) pH and drug resistance I. Drug-resistant breast cancer cells express plasma membrane V-ATPase. *Biochemical Pharmacology* 57: 1037-1046.** This paper is similar to MS #1, above, in that the mechanisms of pH regulation are compared between cells of different phenotypes. In this case, we compared drug-resistant and drug-sensitive MCF7 human breast cancer cells and observed that there were no significant differences between bicarbonate transport, Na/H exchange or resting pH in the cytosol or in the endosomes between these cell lines. however, the drug-resistant lines (both P-gp positive and –negative) had significant V-ATPase activity. We further postulated that this resulted from turnover of acidic vesicles and to support that hypothesis, showed that endosomal turnover rates were much more rapid in the drug-resistant lines, compared to the drug-sensitive lines. Furthermore, the drug-resistant lines trapped weakly basic chemotherapeutic agents (i.e. doxorubicin) into acidic vesicles, whereas the drug-sensitive cells did not.

6. **Martinez-Zaguilan, R, Raghunand N, Lynch RM, Bellamy W, Martinez GM, Rojas B, Smith DJ, Dalton WS, and Gillies RJ (1998) pH and drug resistance II. Turnover of acidic vesicles and resistance to weakly basic chemotherapeutics. *Biochemical Pharmacology* 57: 1047-1058.** This paper is a companion to the previous and explores, mathematically, the potential involvement of acidic vesicles in resistance to weakly basic chemotherapeutic drugs. It diverged from previous models in that it incorporated the turnover of vesicles and the facilitated transport of charged drug (e.g. organic cation transport, OCT). This model shows, for the first time, that acidic vesicles are equally effective as MDR-1 in conferring drug resistance, if the vesicles turn over and if there is significant OCT. We are currently following this up using RT-PCR of drug resistant cells for the presence of an OCT isoform.

7. **Raghunand N, Altbach MI, van Sluis R, Baggett B, Taylor CW, Bhujwalla ZM and Gillies RJ (1998) Plasmalemmal pH-gradients in Drug-Sensitive and Drug-Resistant MCF-7 Human Breast Carcinoma Xenografts Measured by ^{31}P MR Spectroscopy. *Biochemical Pharmacology* 57: 1037-1046.** This paper uses NMR to monitor the intra and extracellular pH of tumor xenografts of human breast cancer cells in SCID mice. It describes the observation that the extracellular pH in tumors from the drug-resistant lines is significantly lower than that from the drug-sensitive lines.

8. **Raghunand N, He X, van Sluis R, Mahoney B, Baggett B, Taylor C, Roe D, Bhujwalla Z and Gillies RJ (1998) Enhancement of Chemotherapy by Manipulation of tumor pH. *Br. J. Cancer* 80: 1005-1011.** In this paper, we examine the hypothesis that the acidic extracellular environment in tumors can contribute to resistance to weakly basic chemotherapeutic drugs. This hypothesis is supported by a preponderance of in vitro data. Using in vivo NMR, we show, for the first time, that

supplementation of drinking water with bicarbonate causes significant and substantial increases in the extracellular pH of tumors in vivo and that tumors thus treated are more sensitive to killing by doxorubicin. We plan to follow this up using a syngeneic system, which can tolerate higher doses of doxorubicin without compromising the animals' health.

9. **Bhujwalla ZM, McCoy CL, Glickson JD, Gillies RJ and Stubbs M (1998) Non-invasive estimations of intra- and extracellular volume and pH by 31-P MRS: applications to untreated and 5-FU treated RIF-1 tumors.** ***Br. J. Cancer*** **78: 606-611.** This paper describes the in vivo MR measurements of tumor cell volume using a combination of 3-APP, which is impermeant) and dimethylmethylphosphonate (DMMP), which is freely permeant. Such an approach was used previously by us in vitro, but this is the in vivo first report. Tumors that respond to 5-FU have significant and consistent reductions in their intracellular volumes.

10. **Galons J-P, Altbach MI, Taylor CW, Payne-Murrietta G and Gillies RJ (1999) Early Increases in Breast Tumor Xenograft Water Mobility in Response to Paclitaxel Therapy Detected by Non-Invasive Diffusion Magnetic Resonance Imaging.** ***Neoplasia*** **1(2), 113-117.** This manuscript describes the effect of Taxol chemotherapy on drug-sensitive and drug-resistant breast cancer tumors in vivo. We have used diffusion-weighted MRI to monitor the effect of taxol on individual tumors. This is an important study because the DWI effects can be observed within hours of taxol administration, whereas frank changes in tumor volume may not be apparent for days. Furthermore, conventional caliper measurements of tumor volume are compromised by a complex tumor morphology, much of which may be a cellular (i.e. edema or lipid deposits). Thus, MRI provides not only an early indicator of response, but also much more accurate morphometry. This approach will be followed up clinically.

11. **Raghunand N, van Sluis R, Altbach MI, Aiken NR, Bhujwalla ZM, Stubbs M and Gillies RJ (1997) Measurement of extracellular pH excursions in breast cancer xenografts: deconvolution of T2* effects.** ***Magnetic Resonance in Medicine.*** **(MS in preparation).** In earlier work, we developed a method to monitor the extracellular pH of tumors using an exogenous compound, 3-aminopropylphosphonate (3-APP). This work investigates the shape and width of the 3-APP resonance to render an estimate of the pH heterogeneity in tumors. This is a significant problem because many researcher feel that acid pH promotes carcinogenesis. This method will yield an estimate of the fraction of the tumor cells, which are in the lowest pH environments.

12. **van Sluis R, Bhujwalla Z, Raghunand N, Ballesteros P, Alvarez J. Cerdan S Gillies RJ (1998) Manipulation of tumor pH observed with novel pH imaging methodology.** ***Nature*** **(MS in preparation).** This paper applies the technique described in MS #3 to time-resolved images of tumor pH during imposed acidic (via carbogen) and basic (via bicarbonate) loads.

13. **Xie X, Gillies RJ and Gerner EW (1997) Characterization of a diamine exporter in Chinese hamster ovary cells and identification of specific polyamine substrates.** ***J. Biol. Chem. 272*****:20484-20489.** This paper describes the initial characterization of a novel polyamine exporter, which exchanges polyamine (organic cations) for protons. Such an activity may play a role in drug resistance, by transporting organic cations (e.g. anthracyclines) out of the cytosol and into recycling vesicles (see MS # 5).

GRANT PROPOSALS:

Mainly as a result of the success of this grant, we obtained NIH R01 funding to continue our studies on the "Causes and Consequences of Acid pH of Tumors" (CA77575). With this grant, we are continuing to improve our pH-measurement techniques and are investigating the relationship between tumor angiogenesis and pH.

The work with tumor pH and chemotherapy in continuing apace and will be the subject of an NIH proposal to be submitted in June, 2000.

The investigation of diffusion coefficient changes has also continued and is the subject of two NIH proposals (R01 and R21) to investigate the cellular aspect of $ADC_{w,,}$ and to move these studies to a clinical trial, respectively.

REFERENCES/APPENDICES

[1] van Sluis R, Bhujwalla Z, Raghunand N, Ballesteros P, Alvarez J, Cerdan S, and Gillies RJ (1999) Imaging of extracellular pH of tumors using 1H MRSI. *Magnetic Resonance in Medicine* 41:743-750.

[2] Martinez-Zaguilan R, Seftor EA, Seftor RE, Chu YW, Gillies RJ, and Hendrix MJ (1996) Acidic pH enhances the invasive behavior of human melanoma cells. *Clinical & Experimental Metastasis, 14*:176-86.

[3] Martinez-Zaguilan R, Martinez GM, Gomez A and Gillies RJ (1998) Distinct regulation of pH and Ca by cells of differing metastatic potential. *J. Cell. Physiol* 176:196-205.

[4] Bhujwalla ZM, Aboagye EO, Gillies RJ, Chacko VP, Mendola CE and Backer JM (1999) Nm23-transfected MDA-mb-435 human breast carcinoma cells form tumors with altered phospholipid metabolism and pH: A 31-P NMR study in vivo and in vitro. Magn. Reson. Med. 41, 897-903.

[5] Martinez-Zaguilan R. Raghunand N, Lynch RM, Bellamy W, Martinez GM, Rojas B, Smith DJ, Dalton WS and Gillies RJ (1999) pH and Drug Resistance I. Plasmalemmal V-type H+-ATPase is expressed in drug resistant human breast carcinoma cell lines. *Biochem. Pharmacol.* 57, 1037-1046.

[6] Martinez-Zaguilan R. Raghunand N, Lynch RM, Bellamy W, Martinez GM, Rojas B, Smith DJ, Dalton WS and Gillies RJ (1999) pH and Drug Resistance II. Turnover of acidic vesicles and resistance to weakly basic chemotherapeutic drugs. *Biochem. Pharmacol.* 57, 1047-1058.

[7] Raghunand N, Altbach MI, van Sluis R, Baggett B, Taylor CW, Bhujwalla ZM and Gillies RJ (1998) Plasmalemmal pH-gradients in Drug-Sensitive and Drug-Resistant MCF-7 Human Breast Carcinoma Xenografts Measured by ^{31}P MR Spectroscopy. *Biochem. Pharmacol.* 57, 309-312.

[8] Raghunand N, He X, van Sluis R, Mahoney B, Baggett B, Taylor CW, Paine-Murrietta G, Roe D, Bhujwalla ZM and Gillies RJ (1999) Enhancement Of Chemotherapy By Manipulation Of Tumor pH. *Br. J. Cancer* 80, 1005-1011.

[9] Bhujwalla ZM, McCoy CL, Glickson JD, Gillies RJ and Stubbs M (1998) Non-invasive estimations of intra- and extracellular volume and pH by 31-P MRS: applications to untreated and 5-FU treated RIF-1 tumors. *Br. J. Cancer.* 78, 606-611.

[10] Galons J-P, Altbach MI, Taylor CW, Payne-Murrietta G and Gillies RJ (1999) Early Increases in Breast Tumor Xenograft Water Mobility in Response to Paclitaxel Therapy Detected by Non-Invasive Diffusion Magnetic Resonance Imaging. *Neoplasia* 1(2), 113-117.

Magnetic Resonance in Medicine 41:743–750 (1999)

In Vivo Imaging of Extracellular pH Using ^{1}H MRSI

Robert van Sluis,[1] Zaver M. Bhujwalla,[2] Natarajan Raghunand,[1] Paloma Ballesteros,[3] José Alvarez,[4] Sebastián Cerdán,[4] Jean-Philippe Galons,[1] and Robert J. Gillies[1]*

Tumor pH is physiologically important since it influences a number of processes relevant to tumorigenesis and therapy. Hence, knowledge of localized pH within tumors would contribute to understanding these processes. The destructiveness, poor spatial resolution, and poor signal-to-noise ratio (SNR) of current technologies (e.g., microelectrodes, ^{31}P magnetic resonance spectroscopy) have limited such studies. An extrinsic chemical extracellular pH (pH_e) probe is described that is used in combination with ^{1}H magnetic resonance spectroscopic imaging to yield pH_e maps with a spatial resolution of $1 \times 1 \times 4$ mm^3. The principle of the technique is demonstrated on a phantom. Further data are shown to demonstrate its application in vivo, and results agree with previously reported pH values. The accuracy of the reported pH measurements is <0.1 pH units, as derived from a detailed analysis of the errors associated with the technique, the description of which is included. Magn Reson Med 41:743–750, 1999. © 1999 Wiley-Liss, Inc.

Key words: cancer; imidazole; MRSI; pH; tumor

Since the discovery of lactic acid production in tumors more than 50 years ago (1), it has generally been assumed that the pH of tumors is acidic. Indeed, numerous microelectrode measurements have shown that extracellular tumor pH (pH_e) is acidic (2). This acidic pH_e of tumors has been confirmed with less invasive ^{31}P magnetic resonance spectroscopy (MRS) measurements (3). Although the intracellular pH (pH_i) of tumors remains neutral to alkaline (4,5), it is somewhat influenced by the pH_e (6).

An acidic pH_e of tumors is physiologically important since it influences a number of processes relevant to carcinogenesis and therapy. Knowledge of localized pH within tumors, both intra- and extracellular, would allow more detailed study of these processes and relate them to intratumoral pH heterogeneity. For example, it has been found that low pH_e in vitro causes tumorigenic transformation of primary Syrian hamster embryo cells (7) and can lead to chromosomal rearrangements in Chinese hamster embryo cells (8,9). Furthermore, culturing cells at low pH causes them to be more invasive in vitro (10) and metastatic in vivo (11). Finally, the orientation of the pH gradient across the cell membrane may influence cell drug resistance (6,12)

Previously reported measurements of extracellular pH using either microelectrodes or ^{31}P MRS of 3-aminopropylphosphonate (3-APP) (3) have drawbacks. Microelectrodes are invasive and can destroy the membrane integrity, thereby disrupting the mechanism for maintaining the pH_e. ^{31}P MRS does not suffer this drawback and has the additional advantage of permitting simultaneous measurements of intracellular pH. However, the limited sensitivity of ^{31}P MRS allows measurements of pH_e only from relatively large tissue volumes. Hence, ^{31}P MRS provides measurements of pH ranges rather than different pH values for discrete spatial locations (13).

The use of ^{1}H MRS, inherently more sensitive than ^{31}P MRS, would allow measurements of pH over smaller tissue volumes. For example, the imidazole protons of histidine have long been useful as intracellular pH indicators in NMR (14,15).

Rabenstein and Isab (16) first proposed using imidazoles as extrinsic pH_e indicators. Gil et al (17) suggested several modifications of the basic structure of the imidazole molecule to improve its performance as an extrinsic pH probe. To date, the most promising candidate for a ^{1}H nuclear magnetic resonance (NMR)-sensitive pH_e indicator is the H2 resonance of (±) 2-imidazole-1-yl-3-ethoxycarbonyl propionic acid (IEPA), which has been shown to remain in the extracellular environment (17) Results from toxicity studies and preliminary in vivo data using IEPA have been reported previously (18,19).

Here, we present both phantom and in vivo data that demonstrate the feasibility of localized, multi-voxel pH_e measurements using ^{1}H magnetic resonance spectroscopic imaging (MRSI). Furthermore, a detailed discussion of the sources and (where possible) the quantification of errors associated with the proposed measurement technique is included.

MATERIALS AND METHODS

Titration of IEPA

Titration data for IEPA were obtained from bovine serum containing 20 mM IEPA, to which 20 mM EDTA and 10% v/v deuterium oxide (D_2O) were added for preservation and shimlock purposes, respectively. As a chemical shift reference, 10 mM 3-(trimethylsilyl) tetradeutero sodium propionate (TSP) was also added. The pH of the solution was adjusted at 37°C using 5 N solutions of NaOH and HCl to 19 pH values between 4.7 and 8.0 and the chemical shift of the H2 IEPA resonance was measured at 37°C in the spectrum for each pH value. Figure 1 shows the chemical structure and a high-resolution (9.4 T) ^{1}H spectrum of IEPA at pH 7.0.

[1]Departments of Biochemistry and Radiology, The University of Arizona, Tucson, Arizona.

[2]Department of Radiology, Johns Hopkins University School of Medicine, Baltimore, Maryland.

[3]Department of Chemistry, UNED, Madrid, Spain.

[4]Magnetic Resonance Laboratory, IIB CSIC, Madrid, Spain.

Grant sponsor: US Army Breast Cancer Initiative; Grant numbers: DAMD17–94-J-4368, DAMD17–96–1-6131, PB93–0037, and PB94–011.

Presented in part at the 1998 meeting of the ISMRM, Sydney, Australia, poster #1642.

*Correspondence to: Robert J. Gillies, The University of Arizona Health Sciences Center, PO Box 245042, Tucson, AZ 85724–5042.
E-mail: gillies@u.arizona.edu

Received 19 June 1998; revised 5 October 1998; accepted 5 October 1998.

The Henderson-Hasselbalch equation for IEPA is given by

$$pH = pK_a - \log_{10}\left(\frac{\delta_{obs} - \delta_{acid}}{\delta_{base} - \delta_{obs}}\right), \qquad [Eq.1]$$

where pH is the observed pH, pK_a is the negative $\log_{10}$ of the acid dissociation constant, and δ_{obs}, δ_{acid}, and δ_{base} are the chemical shifts of the observed, the fully protonated, and the fully deprotonated IEPA peaks, respectively. The experimental data were fitted to Eq.[1] through nonlinear regression (Sigmaplot 3.0, Jandel), and the results are shown in Fig. 2. The fit is characterized by the following set of parameters and their respective standard errors:

$$pK_a = 6.49 \pm 0.02;$$

$$\delta_{acid} = 8.92 \pm 0.01;$$

$$\delta_{base} = 7.77 \pm 0.01.$$

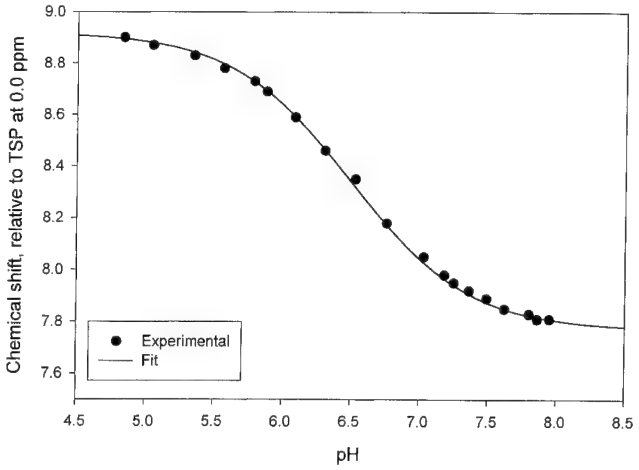

FIG. 2. Chemical shift of the H2-IEPA resonance relative to TSP, as a function of pH in bovine serum at 37°C. Measured data are shown as points, and the curve results from a nonlinear regression of the experimental data to Eq. [2].

MRSI Experiments

All MRSI experiments were performed on a 4.7 T GE Omega scanner, using the BASSALE sequence (20) and a two-turn ^{1}H surface coil. Two-dimensional (2D) water-suppressed MRSI data were obtained from a 4 mm coronal slice, phase-encoding dimensions of 2 × 2 mm^2 and 16 × 16 steps. The fields of view (FOVs) in all imaging and MRSI studies were 32 × 32 mm^2.

A three-compartment phantom was constructed, consisting of two 5 mm NMR tubes inside a larger, 12 mm glass cylinder. The two inner tubes were filled with 20 mM IEPA at pH values of 6.5 and 7.5, respectively. The third, outer compartment was filled with saline. ^{1}H MRSI data were acquired with a TE of 100 msec, TR of 2 sec, 512 points, spectral width (SW) of 6000 Hz, 4 averages. A separate data set was obtained without water suppression to correct for susceptibility effects.

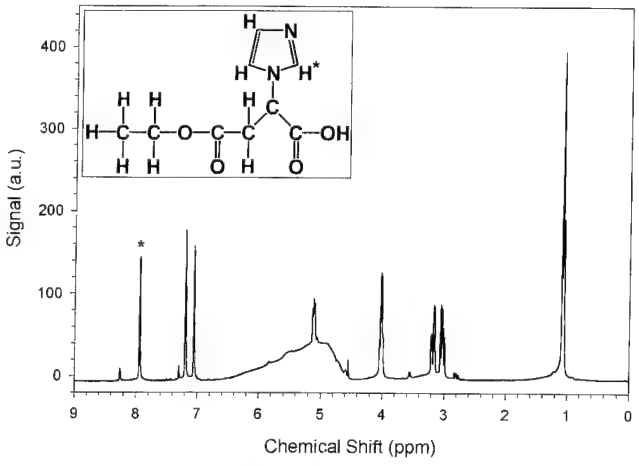

FIG. 1. Structure and 9.4 T ^{1}H NMR spectrum of IEPA in solution (pH 7.0). The pH-sensitive resonance and the C2 proton from which it originates are indicated by asterisks. The broad resonance in the center of the spectrum is due to residual water.

In vivo studies were performed on human breast cancer cells (MCF-7 and MDA^{mb}-435), grown in the mammary fat pad of severe combined immunodeficient (SCID) mice. Tumor volumes studied were 300–600 mm^3. The mice were anesthetized with ketamine (50 mg/kg) and acepromazine (5 mg/kg), and 0.15 ml of a 310 mM IEPA solution was injected intra-peritoneally. The animals were immobilized on a home-built MR cradle, and body temperature was maintained using a warm water blanket. ^{1}H MRSI data were acquired with a TE of 32 msec, TR of 2 sec, 128 points, SW of 6000 Hz, and 8 averages. The total measurement time was 34 min. A separate data set was obtained without water suppression to correct for susceptibility effects.

All data were processed using an MRSI processing program, developed in-house and written in Interactive Data Language (IDL, Research Systems, Boulder, CO). The raw ^{1}H MRSI data were Hanning filtered in *k*-space, and zero filled once in both *k*-space and in the time domain prior to 3D Fourier transformation.

RESULTS AND DISCUSSION

Phantom Data

The chemical shift of the H2 resonance of IEPA was determined for the maximum peak occurring between 7.77 and 8.92 ppm (the H2 proton titratable range) in each of the MRSI spectra. Chemical shifts in each voxel were referenced to unsuppressed water at 4.7 ppm to correct for susceptibility effects, and converted to pH values using Eq. [1]. The pH values from each voxel were color-encoded. Peaks lower than 10% of the maximum IEPA intensity were discarded, and results are shown in Fig. 3.

It is clear from Fig. 3b that the pH imaging technique allows the two compartments of the phantom to be distinguished. Furthermore, the reported pH values are in good agreement with the calibration values of 6.5 and 7.5 pH units. Note that the pH 6.5 compartment is spread over more voxels than the pH 7.5 compartment. Over the pH range 5–8, the T_2 of the C2 proton of IEPA decreases from 101 ± 12 msec to 61 ± 4 msec. In spin-echo sequences like

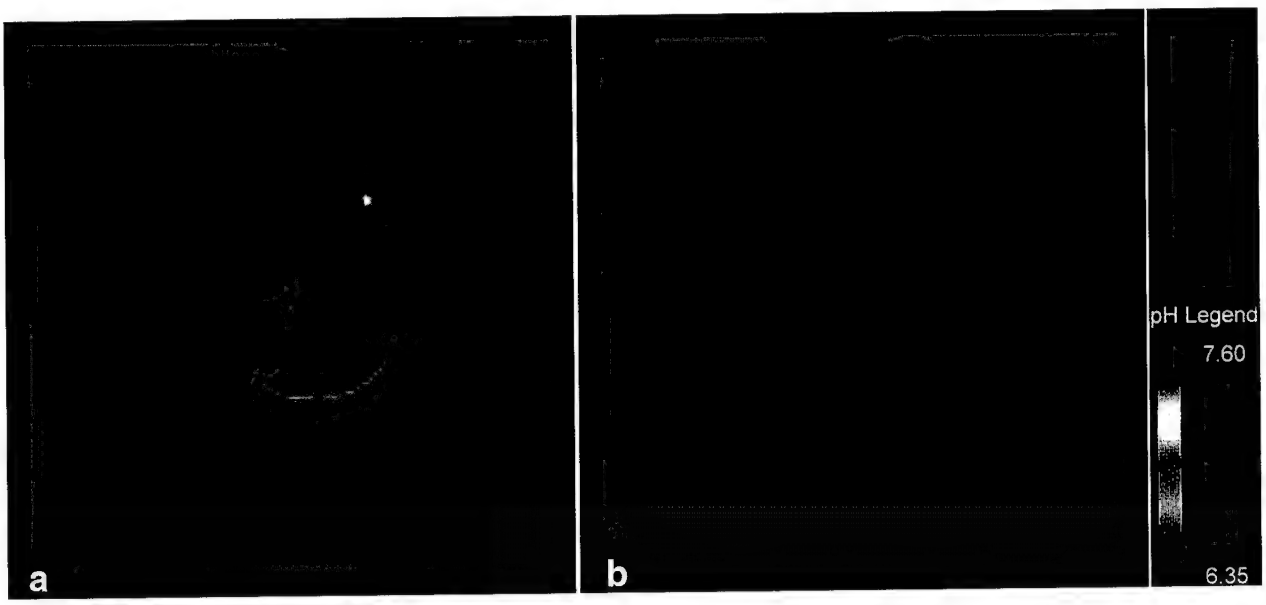

FIG. 3. **a:** Coronal image through the three compartment phantom, showing the two tubes with pH 6.5 (bottom left) and pH 7.5 (top right). The bright spot is a capillary filled with Gd-DTPA, used for orientation purposes. **b:** pH map and legend for the phantom. The pixel size in the pH map is 1 mm^2.

BASSALE, resonances with a longer T_2 will have a higher signal intensity than resonances with a shorter T_2. Since the T_2 of the C2 proton of IEPA decreases with increased pH, the H2-IEPA resonance from the lower pH compartment will have a higher intensity than the H2-IEPA resonance from the higher pH compartment. The degree of contamination due to the point spread function (PSF) is proportional to the intensity of the signal from which the contamination arises (21). As a result the contamination for the pH 6.5 compartment extends over more neighboring voxels compared with the pH 7.5 compartment. Furthermore, this T_2 weighting could lead to an underestimate of the reported pH value. The decrease of T_2 with increasing pH is consistent with the known increase in the exchange rate with solvent of protons from primary and secondary amines and amides (22). Increasing solvent exchange rate would tend to decrease T_2 values of the imidazolic protons because of an increased magnetization transfer to the surrounding solvent. Regardless of the exact underlying mechanisms of the T_2 dependence on pH, it is clear that ^1H MRSI of the H2 proton of IEPA allows us to produce a pH map of the phantom and distinguish between the two compartments, as shown in Fig. 3.

In Vivo Data

An illustration of the quality of our in vivo MRSI data, an array of 7 × 7 spectra, is shown in Fig. 4. These data demonstrate that the H2 resonance of IEPA is observable with good SNR in 15–20 voxels in the tumor. Pre-injection spectra contain a small resonance in the 7–9 ppm region corresponding to endogenous imidazole (data not shown). This resonance was smaller than that in, for example, voxel (9,12), and did not affect subsequent measurements.

Some voxels, in particular [10,8], [10,9], and [10,10], bracketed in Fig. 4, show the presence of a complex H2-IEPA resonance, which may result from the presence of two or more pools of distinct pH_e values. In all spectra, the H2-IEPA resonance is rather broad. The short T_2^* of this resonance in vivo does not allow a finer sampling of the spectrum without ramifications for the SNR. At present, the optimum spectral sampling interval is 0.23 ppm/point, which is coarse. Clearly, this is an aspect of the work that needs improvement.

For construction of the pH_e map from the in vivo data, the chemical shift of the H2 resonance of IEPA was determined using a center of gravity (COG) calculation (23) over the titratable chemical shift range for this proton. The calculation was weighted by the shape of the titration curve to correct for its non-linearity (24). Over the titratable range of the IEPA C2 proton, the weighting function is the partial derivative of the observed chemical shift with respect to the pH for Eq. [1], and is given by:

$$\frac{\partial \delta_{obs}}{\partial pH} = \frac{2.3(\delta_{acid} - \delta_{obs})(\delta_{obs} - \delta_{base})}{(\delta_{acid} - \delta_{base})} \qquad \text{[Eq. 2]}$$

Outside the titratable range, the weighting function is zero. As before, chemical shift values were references to unsuppressed water at 4.7 ppm to correct for susceptibility effects and the calculated pH values were color-encoded. Peaks lower than 10% of the maximum IEPA intensity were discarded. Results are shown in Fig. 5.

The intensity of the H2-IEPA resonance is the largest in the center of the tumor (Fig. 5a). Since tumor perfusion is generally worse in the center of a tumor than in the periphery, one would expect to find a higher concentration of IEPA in the periphery of the tumor compared with the center. However, the observed intensity distribution is likely to be caused by the application of the Hanning filter to the raw data. This filter reduces the signal intensity at the edges of the FOV, to reduce ringing artifacts. As a result, data in the center of the FOV appear to be at a higher intensity.

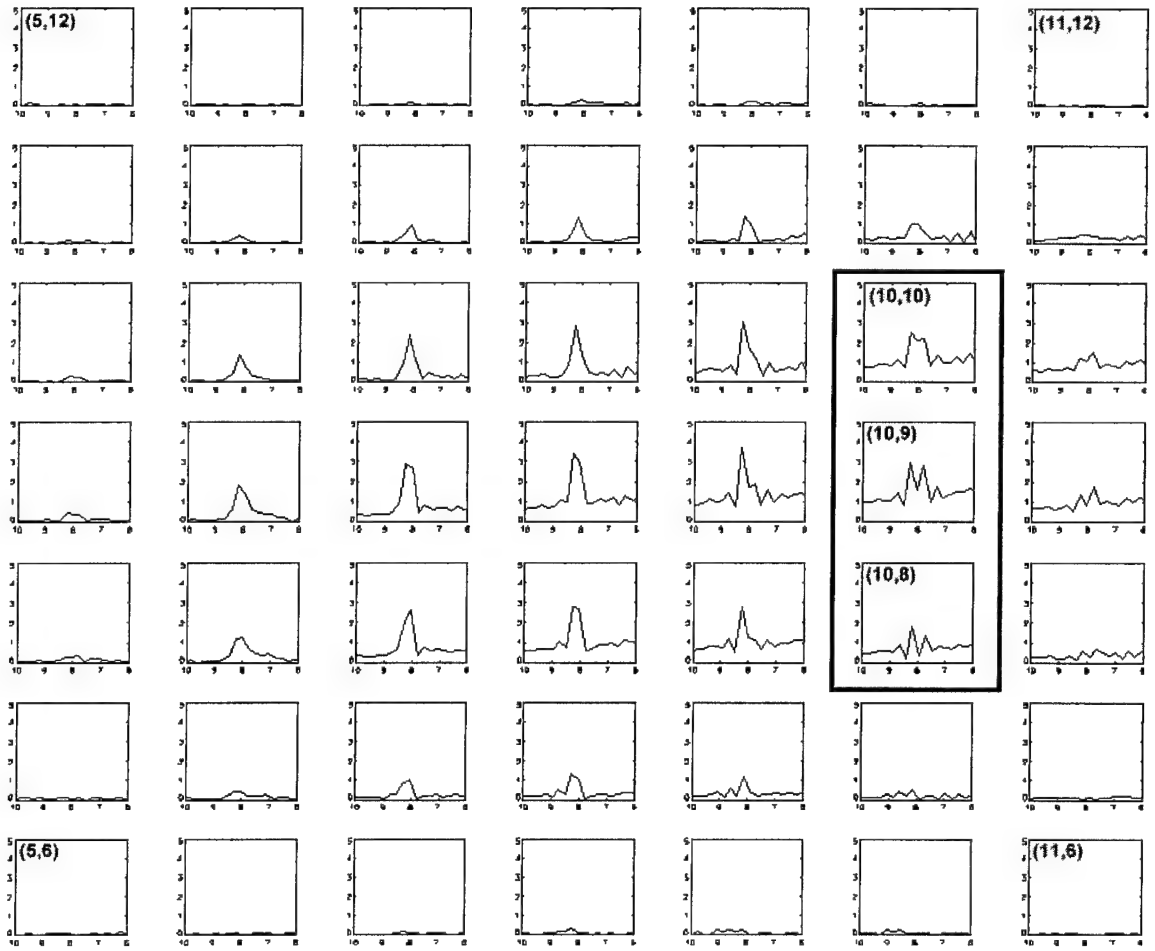

FIG. 4. Array of 7 × 7 in vivo ^{1}H MRSI spectra used for the determination of pH_e in the tumor. The H2-IEPA resonance is clearly visible in the majority of the spectra. The displayed chemical shift range is 10–6 ppm. Note that for these spectra, the voxel size is 2 × 2 mm^2. For construction of the pH_e map, data were interpolated in *k*-space to yield a voxel size of 1 mm^2. The boxed spectra, [10,8], [10,9], and [10,10] are discussed in detail in the text.

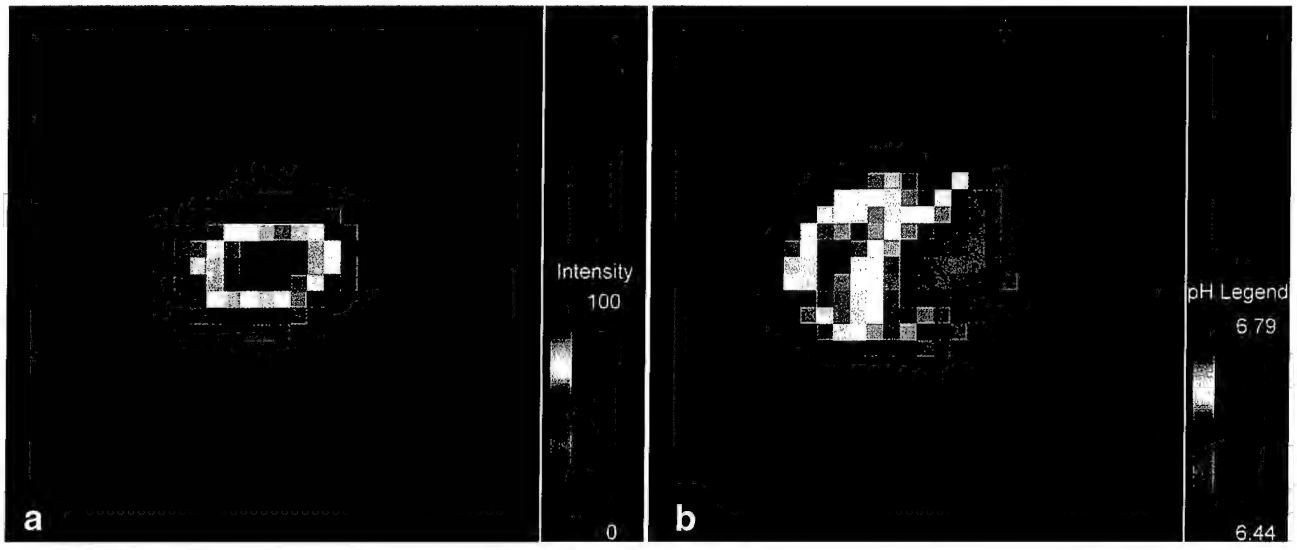

FIG. 5. **a:** Intensity map of the H2-resonance of IEPA in a coronal slice through an MDA^{mb}-435 tumor. **b:** Corresponding pH_e map. In both the intensity and pH_e map, the pixel size is 1 mm^2.

As expected, the data show a good correlation between the signal intensity distribution and the extent of the pH_e map (cf. Fig. 5a and b). Across the tumor, the observed extracellular pH in the tumor is heterogeneous and acidic ($6.44 < pH_e < 6.79$), with a volume average pH_e of 6.64 ± 0.07. This is in good agreement with previous studies (13). Furthermore, it is seen that there are several discrete areas of fairly homogeneous pH_e within the tumor, with areas between 4 and 9 mm^2 (Fig. 5b). The largest continuous area within the tumor appears to have an average pH_e of 6.6, as read from the legend.

Error Analysis

The pH ranges as reported in Figs. 3b and 5b have associated errors resulting from artifacts in the measurement technique. The errors associated with the calibration of the pH_e are relatively small (see above), so that the measurement technique proposed above has two remaining sources of error to be considered. First, the COG method used in determining the peak position will have an accuracy dependent on the linewidth and SNR of the peak under observation. Second, signal modulation due to the PSF, an inherent source of error in any MRSI measurement (21), will cause signals to "bleed" into adjacent voxels. This voxel bleed artifact depends on the intensity and chemical shift differences existing between adjacent voxels. Intensity differences may be caused by changes in the IEPA relaxation times with pH or by differences in IEPA concentration between adjacent voxels. Chemical shift differences between voxels may be caused by pH_e differences. These sources of error will be described in more detail below.

Accuracy of the COG Method

To study the accuracy of the COG method for determination of pH from our spectra, we simulated C2 IEPA resonances for pH values 6.0, 6.5, 7.0, and 7.5, with a spectral resolution of 0.23 ppm/point. Resonances were simulated with different linewidths as defined by the full width at half-maximum (FWHM). Gaussian noise was added to the IEPA resonance to yield SNRs of approximately 20, 10, and 5. The pH as determined by the COG method was compared with the pH as entered into the simulation and the absolute error gives a measure of the accuracy of the COG method in determining the pH. Results are shown in Fig. 6.

The error in the reported pH increases with decreasing SNR, for all linewidths, as expected. Furthermore, the pH is reported more accurately near the pK_a of the C2 IEPA proton, which is 6.49. This is due to the nonlinearity of the titration curve.

It is also observed that the error in the reported pH increases as the H2-IEPA resonance linewidth decreases (see Fig. 6a and 6c). This is directly related to the spectral resolution in the simulated data (0.23 ppm/point). As peaks narrow, the lines are defined by fewer and fewer points, and with the FWHM approaching the spectral resolution, the determination of the position of the maximum peak intensity by the COG method becomes stochastic. However, for reasonable SNRs (>5) and broader peaks (FWHM > 0.16 ppm), as observed in our in vivo spectra, the accuracy of the COG method is better than 0.1 pH units in the range from pH 6.0 to pH 7.0.

Modeling PSF Artifacts

Wang et al (25) have proposed a model to calculate voxel bleed artifacts due to concentration differences alone. Here, we have modified their model to study the combined effects of inhomogeneities in both pH_e and IEPA concentration.

For simulations, an 8×8 grid of IEPA free induction decays (FIDs) was established, with voxel coordinates running from [0,0] to [7,7]. In the descriptions below, voxel [4,4] was used as the "center voxel". Initial simulations demonstrated that the worst contamination occurs in the center voxel when the signal intensity ratio is maximum, i.e., an empty voxel surrounded by voxels of non-zero IEPA concentration. Also, the contamination is worst between nearest neighbor voxels, i.e., the main contributors to the contamination in the center voxel are the 8 voxels immediately surrounding it. These results are in agreement with those of Wang et al (25).

Quantitative estimates of the actual degrees of IEPA concentration and pH_e inhomogeneities in vivo are required before continuing analysis of their effects on the precision of the proposed pH imaging technique.

Estimating IEPA Concentration Inhomogeneity

Since voxel bleed artifacts prevent direct derivation of quantitative information on IEPA concentration inhomogeneity from the MRSI data, studies of the uptake of dimeglumine gadopentetate (Gd-DTPA, Schering, Germany) in MCF-7 tumors were monitored by T_2-weighted imaging as a model for the IEPA concentration distribution. IEPA and Gd-DTPA are comparable in terms of partition coefficient and charge. Both molecules are about the same size, and their charges are -2 for Gd-DTPA (Gd +3, DTPA -5) and 0 to -1 for IEPA (acid group -1, imidazolic nitrogen +0 to +1).

One precontrast ($t = 0$) and 16 Gd-DTPA-enhanced images (17 mm surface coil, FOV 25 mm^2, 128×128 pixels, slice thickness 4 mm) were obtained at regular intervals over the course of 110 min from three consecutive sagittal slices through MCF-7 tumors. Gd-DTPA-enhanced images were subtracted from the precontrast image to yield images of the Gd-DTPA enhancement only, which to a first approximation is linear with Gd-DTPA concentration (26). These subtraction images were rebinned to 16×16 pixels to yield a pixel size of 1.56 mm^2, approximating the 2 mm^2 spatial resolution used when acquiring the IEPA MRSI data. Examples of a high-resolution (128×128) and rebinned (16×16) images of Gd-DTPA enhancement are shown in Fig. 7.

In each of the rebinned subtraction images, 6 pixels were identified that represent the Gd-DTPA distribution in the tumor and, for these 6 pixels, the intensity ratios between nearest neighbors were calculated. The highest and the average nearest neighbor intensity ratios were determined for each image and plotted as a function of time, as shown in Fig. 8. It can be seen that once a steady-state Gd-DTPA concentration has been reached (after 6–8 min), the highest and average intensity ratios stabilize at about 1:3.0 and 1:1.5, respectively. Using these values as a measure of the

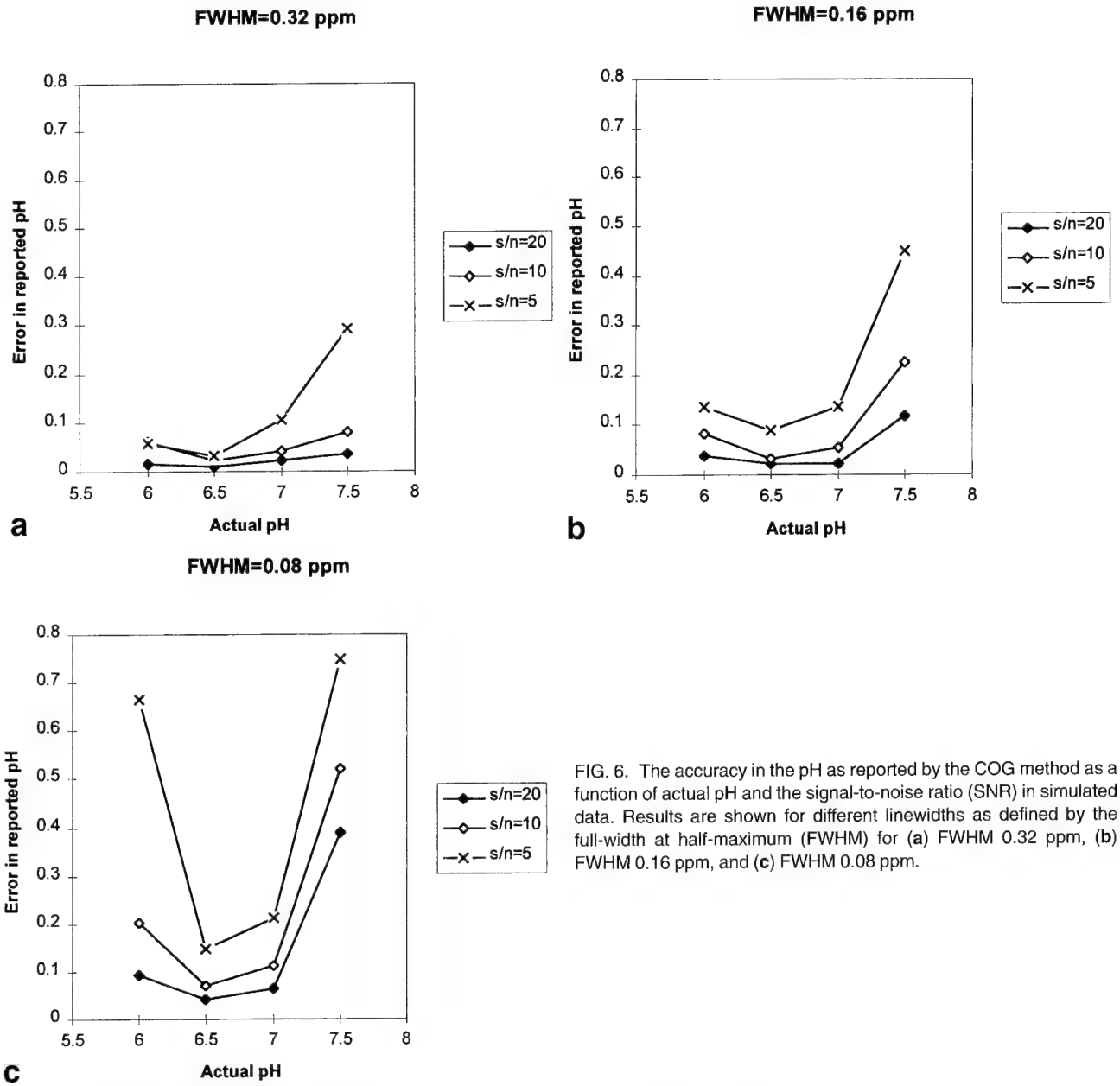

FIG. 6. The accuracy in the pH as reported by the COG method as a function of actual pH and the signal-to-noise ratio (SNR) in simulated data. Results are shown for different linewidths as defined by the full-width at half-maximum (FWHM) for (**a**) FWHM 0.32 ppm, (**b**) FWHM 0.16 ppm, and (**c**) FWHM 0.08 ppm.

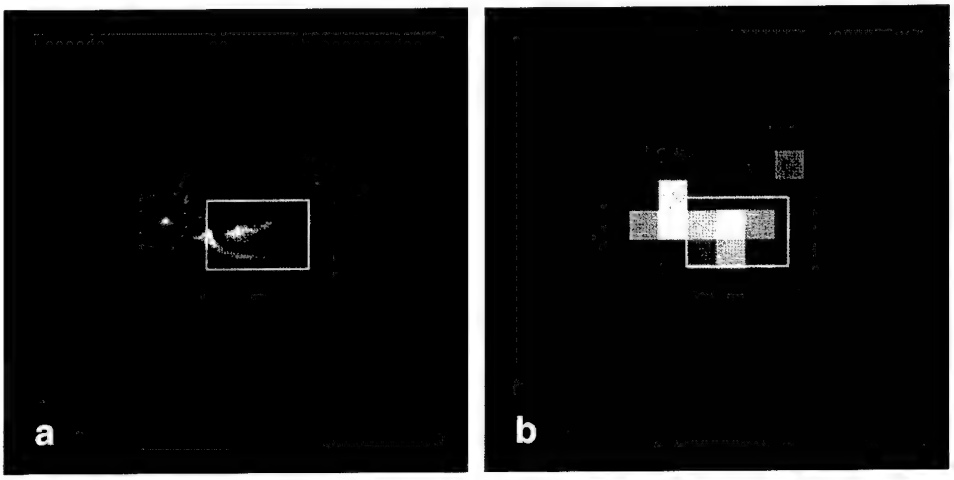

FIG. 7. **a:** High-resolution (128 × 128 pixels) subtraction image of Gd-DTPA uptake in an MCF-7 tumor in vivo. **b:** The same image, rebinned to 16 × 16 pixels. The resulting pixel size (1.56 mm^2) approximates the 2 mm^2 spatial resolution used when acquiring IEPA MRSI data. In both images, the white box indicates the location of the tumor. The six pixels entirely within the tumor in b were used to calculate concentration differences between adjacent voxels.

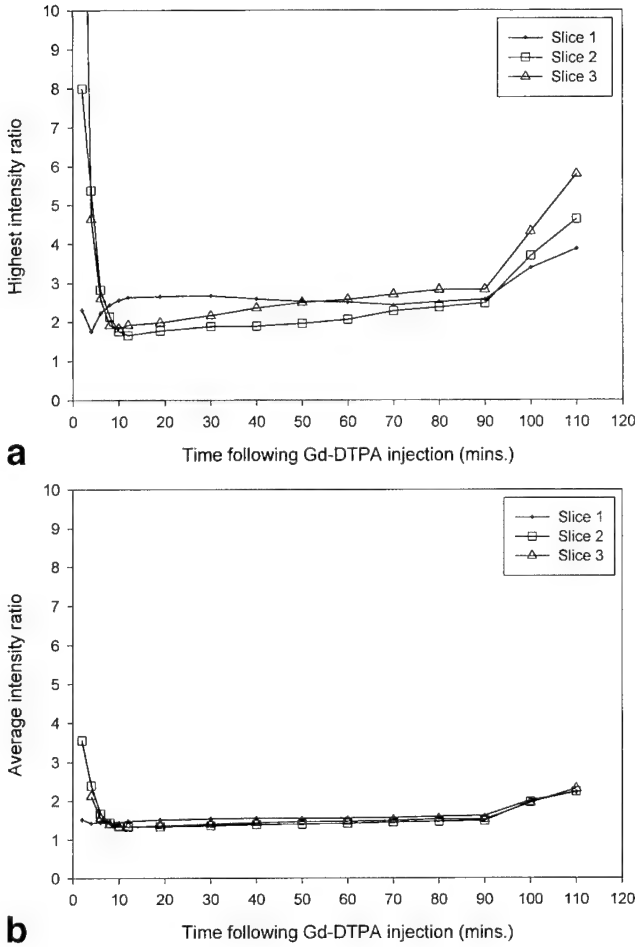

FIG. 8. The nearest neighbor highest (**a**) and average (**b**) intensity ratio as a function of time following Gd-DTPA injection in MCF-7 tumors.

IEPA intensity ratios between adjacent voxels, a simulated IEPA distribution was set up over the previously mentioned grid of 8 × 8 voxels.

Quantifying pH_e Inhomogeneity

Information on the maximum spatial pH_e gradient expected for adjacent voxels in the MRSI data was obtained through the work of Helmlinger et al (27), who reported a 0.7 unit pH_e difference between well-oxygenated (near the blood vessel) and nonoxygenated regions (away from the blood vessel) in tumors, over a distance of 400 μm. This is in good agreement with work by Raghunand et al (13), who found that 85% of tumor pH_e values are within ±0.4 pH units of the mean pH_e. To observe a pH difference of 0.7 pH units between adjacent 16 mm^3 voxels in our MRSI data, it is necessary to have a fully oxygenated voxel (i.e., full of capillaries) immediately next to nonoxygenated voxels (i.e., no capillaries). It would be possible to find completely nonoxygenated voxels in vivo, for example, in necrotic areas. However, since in general tumor cells divide faster than their surrounding vasculature, the presence of a voxel consisting entirely of capillaries would be less likely. Therefore, we have chosen to work with the average pH_e range observed by both Helmlinger et al and Raghunand et al (i.e., 0.4 pH unit), as the maximum pH gradient between adjacent voxels.

Combined Effect of IEPA Concentration and pH_e Inhomogeneity on COG Precision

The maximum pH differences, with signal intensity ratios of either 1:3.0 or 1:1.5, were inserted into the simulation program. The reported pH for the center and surrounding voxels were compared with the actual values. The difference between the actual pH value and the pH value reported by the simulation program expresses the error due to the voxel bleed artifact, as shown in Fig. 9. As expected, when the center voxel is surrounded by more acidic voxels, the reported pH for the center voxel is underestimated and vice versa.

The error in the reported pH for the center voxel over the physiological pH range (6.8–7.6 pH units) is less than 0.15 pH units for a *maximum* intensity ratio of 1:3.0, and less than 0.10 pH units for an *average* intensity ratio of 1:1.5, as shown in Fig. 9. This is an encouraging result for the

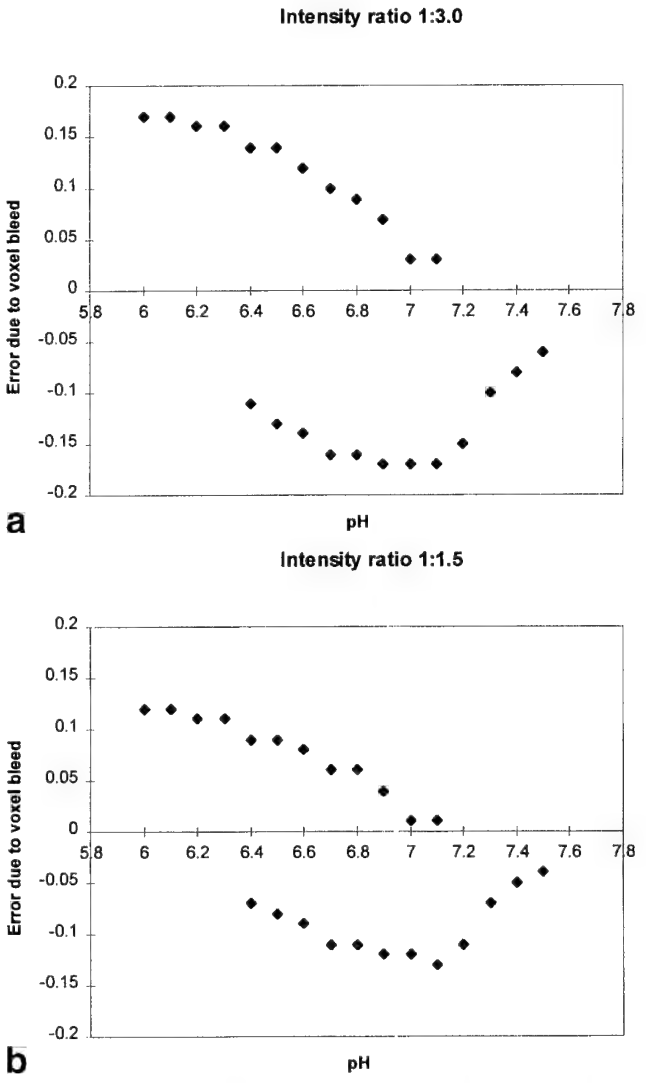

FIG. 9. The error due to the voxel bleed artifact for the center voxel as a function of pH and signal intensity ratio for (**a**) a signal intensity ratio of 1:3.0 and (**b**) 1:1.5.

precision of the proposed technique. Additionally, it must be remembered that these are worst-case scenarios. In practice, it is likely that the pH difference between adjacent voxels is less than 0.4 pH units, thus further reducing the error due to the voxel bleed artifact.

CONCLUSIONS AND FUTURE DIRECTIONS

Using phantom and in vivo data, we have demonstrated the feasibility of imaging extracellular pH using ^{1}H MRSI. The possible sources of error associated with the technique were analyzed in detail. It was found that the COG method leads to an error of <0.1 pH units for broader lines and reasonable SNR. For narrower lines, the poor spectral resolution increasingly reduces this accuracy. From simulations, it was found that artifacts due to voxel bleed in MRSI will introduce a maximum error of 0.1 pH units in the reported pH values. Finally, it was observed that the T_2 of the proposed pH_e indicator is pH dependent. This dependence, its cause, and the effect on reported pH values are currently under investigation.

ACKNOWLEDGMENTS

The authors thank D.C. Shungu, V.P. Chacko, and B. Baggett for their invaluable help with this work. Support from the US Army Breast Cancer Initiative DAMD17–94-J-4368 (to R.J.G.) and DAMD17–96–1-6131 (to Z.M.B.) and grants PB93–0037 (to P.B.) and PB94–011 (to S.C.) is gratefully acknowledged.

REFERENCES

1. Warburg O. On the metabolism of tumors. Cambridge: Cambridge University Press; 1930.
2. Wike-Hooley JL. Haveman J, Reinhold HS. The relevance of tumor pH to the treatment of malignant disease. Radiother Oncol 1984;2:343–366.
3. Gillies RJ, Liu Z, Bhujwalla Z. ^{31}P MRS measurement of extracellular pH of tumor using 3-aminopropylphosphonate. Am J Physiol 1994;267: C195–C203.
4. Negendank W. Studies of human tumors by MRS: a review. NMR Biomed 1992;5:303–324.
5. Griffiths JR. Are cancer cells acidic? Br J Cancer 1991;64:425–427.
6. Raghunand N, He X, van Sluis R, Bhujwalla ZM, Gillies RJ. Plasmalemmal pH gradients in drug-sensitive and drug-resistant MCF-7 human breast carcinoma tumors measured by ^{31}P MRS. In: Proceedings of the ISMRM 6th Annual Meeting, Sydney, 1998. p 1644.
7. LeBoeuf RA, Kerckaert GA, Aardema MJ, Gibson DP. Multistage neoplastic transformation of Syrian hamster embryo cells cultured at pH 6.70. Cancer Res 1990;50:3722–3729.
8. Morita T, Takeda K, Okumura K. Evaluation of clastogenicity of formic acid, acetic acid and lactic acid on cultured mammalian cells. Mutat Res 1990;240:195–202.
9. Morita T, Nagaki T, Fukuda I, Okumura K. Clastogenicity of low pH to various cultured mammalian cells. Mutat Res 1992;268:297–305.
10. Martínez-Zaguilán R, Seftor EA, Seftor REB, Chu Y-W, Gillies RJ, Hendrix MJC. Acidic pH enhances the invasive behavior of human melanoma cells. Clin Exp Metast 1996;14:176–186.
11. Schlappack OK, Zimmermann A, Hill RP. Glucose starvation and acidosis: effect on experimental metastatic potential, DNA content and MTX resistance of murine tumour cells. Br J Cancer 1991;64:663–670.
12. Gerweck LE, Seetharaman K. Cellular pH gradient in tumor versus normal tissue: potential exploitation for the treatment of cancer. Cancer Res 1996;56:1194–1198.
13. Raghunand N, Altbach MI, Bhujwalla ZM, Gillies RJ. Extracellular pH excursions in drug-sensitive and drug-resistant MCF-7 human breast carcinoma cells: a ^{31}P MRS study. In: Proceedings of the ISMRM 5th Annual Meeting, Vancouver, 1997. p 1096.
14. Brown FF, Campbell ID, Kuchel PW, Rabenstein DL. Human erythrocyte metabolism studies by ^{1}H spin echo NMR. FEBS Lett 1977;82:12–16.
15. Pan JW, Hamm JR, Rothman DL, Shulman RG. Intracellular pH in human skeletal muscle by ^{1}H NMR. Proc Natl Acad Sci USA 1998;85: 7836–7839.
16. Rabenstein DL, Isab AA. Determination of the intracellular pH of intact erythrocytes by 1H NMR spectroscopy. Anal Biochem 1992;121:423–432.
17. Gil S, Zaderenzo P, Cruz F, Cerdán S, Ballesteros P. Imidazol-1-ylalkanoic acids as extrinsic 1H NMR probes for the determination of intracellular pH, extracellular pH and cell volume. Bioorg Med Chem 1994;2:305–314.
18. Gillies RJ, Raghunand N, Bhujwalla ZM, Ballesteros P, Alvarez J, Cerdán S. Measurement of extracellular pH in tumors by ^{1}H MRSI. In: Proceedings of the Proc. ISMRM, 5th Annual Meeting, Vancouver, 1997. p 1099.
19. van Sluis R, Bhujwalla ZM, Raghunand N, Ballesteros P, Alvarez J, Cerdán S, Gillies RJ. Imaging of extracellular pH using ^{1}H MRSI. In: Proceedings of the ISMRM 6th Annual Meeting, Sydney, 1998. p 1642.
20. Shungu DC, Glickson JD. Band-selective spin echoes for in vivo localized ^{1}H NMR spectroscopy. Magn Reson Med 1994;32:277–284.
21. Brown TR. Practical applications of chemical shift imaging, NMR Biomed 1992;5:238–243.
22. Wüthrich K, Wagner G. Nuclear magnetic resonance of labile protons in the basic pancreatic trypsin inhibitor. J Mol Biol 1979;130:1–18.
23. Madden A, Leach MO, Sharp JC, Collins DJ, Easton D. A quantitative analysis of the accuracy of in vivo pH measurements with ^{31}P NMR spectroscopy: assessment of pH measurement methodology. NMR Biomed 1991;4:1–11.
24. Graham RA, Taylor AH, Brown TR. A method for calculating the distribution of pH in tissues and a new source of pH error from the ^{31}P NMR spectrum. Am J Physiol 1994;266:R638–R645.
25. Wang Z, Bolinger L, Subramanian VH, Leigh JS. Errors of Fourier chemical shift imaging and their corrections. J Magn Reson 1991;92: 64–72.
26. Roberts TPL. Physiologic measurements by contrast-enhanced MR imaging: expectations and limitations. J Magn Reson Imaging 1997;7: 82–90.
27. Helmlinger G, Yuan F, Delian M, Jain RK. Interstitial pH and pO_2 gradients in solid tumors in vivo: high-resolution measurements reveal a lack of correlation. Nature Med 1997;3:177–182.

Clin. Exp. Metastasis, 1996, **14**, 176–186

Acidic pH enhances the invasive behavior of human melanoma cells

Raul Martínez-Zaguilán*, Elisabeth A. Seftor†, Richard E. B. Seftor†, Yi-Wen Chu‡, Robert J. Gillies*‡ and Mary J. C. Hendrix†

*Department of *Biochemistry and the ‡Cancer Biology Program, University of Arizona Health Sciences Center, Tucson, AZ, and †Department of Pediatrics, Pediatric Research Institute, St Louis University School of Medicine, St Louis, MO, USA*

(*Received 26 June 1995; accepted in revised form 27 November 1995*)

As a consequence of poor perfusion and elevated acid production, the extracellular pH (pH^{ex}) of tumors is generally acidic. Despite this, most *in vitro* experiments are still performed at the relatively alkaline pH^{ex} of 7.4. This is significant, because slight changes in pH^{ex} can have profound effects on cell phenotype. In this study we examined the effects of mildly acidic conditions on the *in vitro* invasive potential of two human melanoma cell lines: the highly invasive C8161, and poorly invasive A375P. We observed that culturing of either cell line at acidic pH (6.8) caused dramatic increases in both migration and invasion, as measured with the Membrane Invasion Culture System (MICS). This was not due to a direct effect of pH on the invasive machinery, since cells cultured at normal pH (7.4) and tested at acidic pH did not exhibit increased invasive potential. Similarly, cells cultured at acidic pH were more aggressive than control cells when tested at the same medium pH. These data indicate that culturing of cells at mildly acidic pH induces them to become more invasive. Since acid pH will affect the intracellular pH (pH^{in}) and intracellular calcium ($[Ca^{2+}]^{in}$), we examined the effect of these parameters on invasion. While changes in $[Ca^{2+}]^{in}$ were not consistent with invasive potential, the changes in pH^{in} were. While these conditions decrease the overall amount of gelatinases A and B secreted by these cells, there is a consistent and significant increase in the proportion of the activated form of gelatinase B.

Keywords: fluorescence, FURA-2, intracellular Ca^{2+}, intracellular pH, invasion, melanoma, SNARF-1

Introduction

The extracellular pH (pH^{ex}) of tumors is generally more acidic than that of normal tissues [1–3]. This is likely a consequence of a collaboration between elevated aerobic glycolysis and reduced blood flow [4–8]. Despite the acidity of tumors, most *in vitro* assays of tumor cell function are routinely performed at neutral-to-alkaline medium pH [9]. Schlappack *et al.* observed that transient acidosis increased metastatic behavior (colonization) in implanted murine sarcoma and lymphoma cells [10]. While these results strongly suggest a trophic effect of pH on metastasis, the uncertainty of *in vivo* growing conditions make these data difficult to interpret. Several biochemical and physiological processes are important for tumor cells to acquire a metastatic phenotype, such as the transcriptional activation of specific genes, cytoskeleton re-organization, induction of secretion, degradation of basement members and stimulation of cell motility [11–14]. Although evidence supporting a role for pH in this ensemble of activities is largely circumstantial, it is likely that each of these processes is individually pH-sensitive. For instance, activation of proteases, such as cathepsins [15], metalloproteinases [16,17] and serine proteases [14,18], is an important component of the metastatic cascade [19], and each class of proteases is pH-sensitive. The cathepsins are lysosomal enzymes and generally have acidic pH optima [20]. Recently, it has been shown that incubation of cells at low pH induces the redistribution and release of cathepsin B from a series of metastatic human cell lines [21]. Although the metalloproteinases have more alkaline pH optima [22–24], their synthesis

Address correspondence to: M. J. C. Hendrix, Pediatric Research Institute, 3662 Park Avenue, St Louis, MO 63110, USA. Tel: (+1) 314 577 5623; Fax: (+1) 314 268 2748.

can be induced by acidic conditions [25]. Finally, the association of serine proteases with endogenous inhibitors, such as α2-macroglobulin and cell surface receptors, is inhibited with acidic conditions [26,27]. Thus, effects of acidic conditions can either be acute, such as activation of cathepsins or release of serine proteases from inhibition, or the effects can be long term, such as induction of metalloproteinase synthesis.

Cytoskeletal proteins are also likely to be involved in the invasive process. High levels of dual intermediate filament expression, and remarkable changes in cell shape and motility are needed for cell invasion [12–14, 28,29]. Schwartz *et al.* [30] have convincingly demonstrated that changes in cell shape are associated with changes in intracellular pH (pH^{in}). Furthermore, assembly–disassembly of cytoskeletal structures is affected by both pH^{in} and intracellular calcium $[Ca^{2+}]^{in}$ [31,32].

We investigated the effects of pH on $[Ca^{2+}]^{in}$ levels as they relate to melanoma cell invasion. This was undertaken for two reasons. First, changes in pH generally affect $[Ca^{2+}]^{in}$ levels [33]. Second, Ca^{2+} has been implicated to play an important role in the invasive cascade, since factors that mobilize Ca^{2+} will also transcriptionally regulate genes encoding for matrix-degradative enzymes and their modulators, e.g. tissue-type and urokinase-type plasminogen activators [34], metalloproteinases [35,36], and tissue inhibitors of metalloproteinases (TIMPs) [37,38]. Furthermore, the contention that pH and Ca^{2+} affect invasive behavior is circumstantially supported by the ability of kinase C to stimulate invasive behavior in a wide variety of tumor cells [39–44]. Activation of kinase C often leads to an increased pH^{in} [45–50].

Tumor cell invasion is an active process which requires cell locomotion. The directional migration of tumor cells occurs in response to a number of soluble factors [13,51], such as chemoattractants which induce increases in $[Ca^{2+}]^{in}$ in other systems [52,53]. Korczack *et al.* [39] have suggested that the induction of spontaneous metastasis in the murine SP-1 adenocarcinoma xenographs involves increases in $[Ca^{2+}]^{in}$. Most recently, Savarese *et al.* [54] have shown that exposure of A2058 human melanoma cells to collagen IV, a component of the basement membrane extracellular matrix, results in increases in $[Ca^{2+}]^{in}$. Moreover, collagen type IV also increases cell motility in these and other cell types, suggesting that increases in $[Ca^{2+}]^{in}$ and cell motility may be linked [11,12].

This study questions whether variations in pH can affect invasive and migratory behavior of established melanoma cell lines with either low (A375P) or high (C8161) invasive potentials [9]. In order to mimic the *in vivo* conditions, cells were grown for 3 weeks at pH^{ex} of 6.8 [1–3,5,6]. To investigate the effects of these treatments on intracellular ions, we used a fluorescence technique which allows the simultaneous measurement of both pH^{in} and $[Ca^{2+}]^{in}$ [33,55]. The effect of altering these ions on the invasive potential of the cells was evaluated using the Membrane Invasion Culture System (MICS) assay [9,28].

Materials and methods

Cell culture

Poorly invasive (A375P) and highly invasive (C8161) human melanoma cells were cultured as described elsewhere [28]. The A375P human melanoma cell line was a gift from Dr I. J. Fidler (The University of Texas M.D. Anderson Hospital and Tumor Institute, Houston, TX, USA [9]). The highly invasive C8161 melanoma cell line was established from an amelanotic metastasis from a patient at the Arizona Cancer Center (Tucson, AZ, USA [57]). These cells were cultured in Dulbecco's modified Eagle's medium (DMEM; Gibco, Grand Island, NY, USA), supplemented with 10% Nu-Serum (Collaborative Research, Bedford, MA, USA), in a 5% CO_2 atmosphere at 37°C. Cells were grown in T-75 culture flasks and passed bi-weekly at an inoculation density of 2×10^5 cells per 75 cm^2 flask. For experiments involving chronic exposure of cells to either low (pH = 6.8) or normal pH (pH = 7.4), with either low (70 μM) or high (1 mM) Ca^{2+}, cells were grown for 3 weeks before experiments in suspension-modified Eagle's medium (S-MEM), supplemented with 10% Nu-Serum. One of the main differences between S-MEM and DMEM is the presence of low Ca^{2+} in S-MEM whereas DMEM contains 1.8 mM Ca^{2+}. S-MEM contains 2 μM Ca^{2+}-pantothenate. Nu-Serum is a synthetic media which contains 30 μM Ca^{2+}. Thus, we supplemented the S-MEM media with Ca^{2+} to obtain the final concentrations of 70 μM or 1 mM Ca^2, as needed.

Preparation for fluorescence measurements

Cells were prepared for measurements of pH^{in} and $[Ca^{2+}]^{in}$ as described previously [33]. Briefly, cells were inoculated into 60-mm Petri dishes containing 9×22 mm coverslips at a density of 2×10^5 cells/60 mm dish in their growing media, and kept in the 5% CO_2 incubator for 48 h. Two coverslips (with attached cells) were then transferred to a 60-mm Petri dish containing 7 μM SNARF-1/AM and 2 μM Fura-2/AM in cell-suspension buffer (CSB). The CSB contained the following: 0.35 mM Na_2HPO_4, 110 mM NaCl, 0.44 mM

KH_2PO_4, 5.4 mM KCl, 1 mM $MgSO_4$, 1.3 mM $CaCl_2$, 25 mM HEPES, 5 mM glucose, and 2 mM L-glutamine at the desired pH at 37°C. Organic components were added the day of experimentation in order to avoid bacterial contamination. The concentration of HCO_3^- needed to obtain the required pH^{ex} values was estimated as described previously [58]. These cells were incubated with dyes for 30 min at 37°C, under a 5% atmosphere in CSB containing their respective concentrations of HCO_3^- and Ca^{2+}, i.e. low (70 μM) Ca^{2+} or 1 mM Ca^{2+}, at their respective pH^{ex} (6.8 or 7.4). Subsequently, the coverslips were transferred to a 60-mm Petri dish containing CSB without dyes at their respective pH and Ca^{2+} concentrations, and further incubated for 30 min, to allow for complete ester hydrolysis of the dyes. The two coverslips were then placed back-to-back in a holder and put in a cuvette in the spectrofluorometer which is equipped with a flow-through device for sample perfusion. The coverslips were continuously perfused at 3 ml/min with their respective buffers. Sample temperature was maintained by keeping both the water jacket and the perfusion medium at 37°C using a circulator water bath (Lauda model RM 20; Brinkman Instruments, Westbury, NY, USA). These buffers were continuously bubbled with 5% CO_2/95% O_2 to maintain a constant pH^{ex}.

Fluorometric pH^{in} and $[Ca^{2+}]^{in}$ measurements

Simultaneous measurement of pH^{in} and $[Ca^{2+}]^{in}$ was performed as described previously [33]. All fluorescence measurements were performed in an SLM8000C (SLM, Urbana, IL, USA) using 4-nm bandpass slits and an external rhodamine standard as a reference. Data were collected in a continuous acquisition mode in which the emission and excitation modes were alternated as follows: emission at 510 nm with excitation wavelengths of 340, 360 and 380 nm (Fura-2 conditions) followed by excitation at 534 nm with acquisitions of the emissions at 584, 600 and 644 nm (SNARF-1 conditions). The duration of this cycle is 0.266 min and is repeated as often as necessary. Fluorescence data were translated to ASCII format for manipulation and analysis. Ratio values obtained are converted to pH^{in} and $[Ca^{2+}]^{in}$ by commercially available software (Sigmaplot 4.1; Jandel Scientific, San Rafael, CA, USA).

In situ *calibration of ion indicators and data analysis*

The calibration of SNARF-1 was performed as described previously [33,58]. Briefly, attached (SNARF-1 loaded) cells were perfused with high K^+ buffer containing 145 mM KCl, 10 mM MES, 10 mM HEPES and 10 mM BICINE. This buffer was supplemented with 6.8 μM of the K^+/H^+ ionophore nigericin and 2 μM valinomycin, which equilibrates intra- and extracellular pH; i.e. pH^{in} of the cells is equal to pH^{ex}. For these experiments, pH^{ex} was varied from 6.0 to 8.0. From these *in situ* calibration curves we obtained R values at each pH^{ex} studied. We have previously shown that the *in situ* calibration parameters of pH indicators may vary from cell to cell type, and therefore accurate calibrations are needed to assign pH values *in situ* [33,58]. The results from these *in situ* titrations are shown in Figure 1A and B. *In vitro* pH values used for calibration were obtained with a Beckman model 71 pH meter, using a Corning glass combination electrode. The electrode was calibrated at two known temperature controlled pH values using commercially prepared standards from VWR Scientific (San Francisco, CA, USA).

In the case of Fura-2, the Kd_a, R_{max}, and R_{min} of Fura-2 are pH-sensitive [33,55,59,60]. Therefore, these parameters have been corrected by pH as described previously [33,55]. From a number of *in vitro* and *in situ* calibration curves for Fura-2, we have previously determined that the effects of pH on the Fura-2 Kd_a are similar *in situ* and *in vitro*. We have also shown that the Kd_a values are also similar among different cell types. As mentioned earlier, the Fura-2 R_{max} and R_{min} values are also affected by pH [33,55]. The magnitude of these pH effects is similar between *in vitro* and *in situ* data for R_{min}, but not in the case of R_{max}. The reasons for this anomalous behavior of the dye are unknown.

Cell number

Cell number was determined using a dye binding assay, as described previously [61]. Briefly, cells were plated at 3×10^4 in 24-well plates (Flow Labs), and 12 h thereafter cells were washed twice with nominally Ca^{2+}-free, serum-free S-MEM, and further incubated for up to 72 h in S-MEM plus 10% Nu-Serum, containing either low (70 μM) or high (1 mM) Ca^{2+}, at selected pH^{ex} values (i.e. either pH 6.8 or 7.4). After 24, 48 and 72 h in their respective growth media, the medium was removed, and the cells were washed with CSB at 37°C. This procedure allows one to stain only viable cells that remained attached to the plastic well. The cultures were then fixed with 1% glutaraldehyde and stained with 0.1% crystal violet for 20 min, de-stained in running water for 5 min and air dried. Subsequently, the dye was solubilized in 0.2% Triton X-100. The absorbance at 590 nm of this Triton X-100 solution is linearly related to the number of viable cells.

Tumor cell invasion assay

Reliable methods for studying the extent of tumor cell migration and invasion *in vitro* have been presented

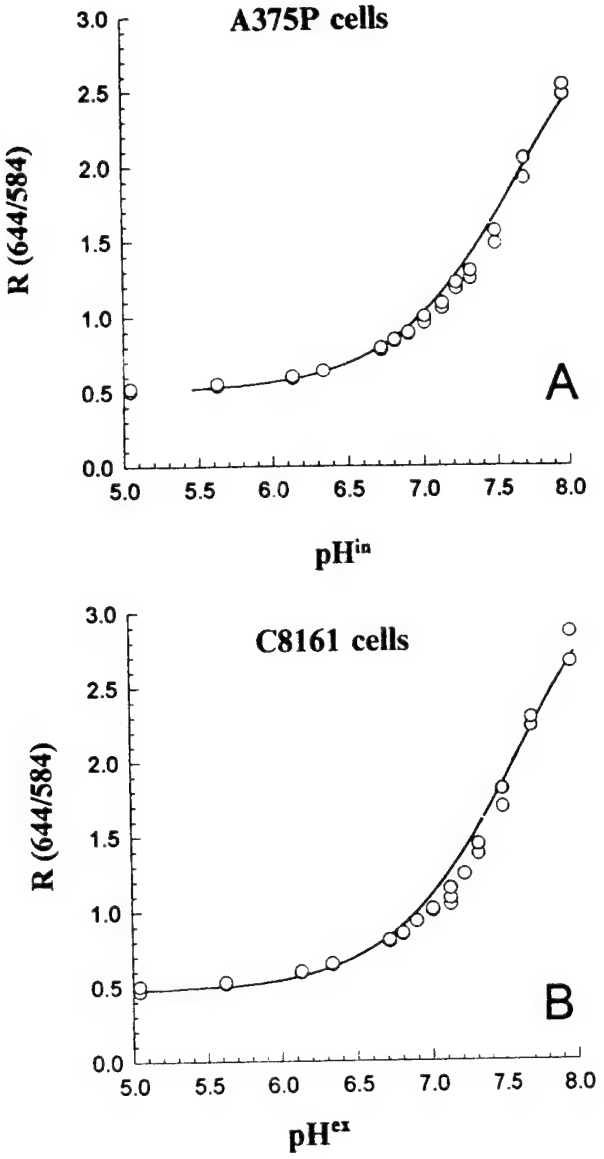

Figure 1. Calibration of SNARF in C8161 and A375P cells. C8161 and A375P cells were grown and prepared for fluorescence. Cells were perfused with high K^+ buffer containing nigericin and valinomycin to collapse the pH gradient. The pH of the perfusing solution was step-wise altered and the fluorescence ratios were collected at discrete pH values. The line represents the best fit using a modified Henderson–Hasselbach relationship using non-linear least squares fitting. See Materials and methods for details.

[9,56]. The ability of tumor cells to invade or penetrate biological matrices in the development of malignant melanoma as well as in other types of metastatic tumors is relevant, since these matrices are present during several steps of the metastatic process such as intravasation, extravasation and dissemination [11–14,51]. The method employed utilized Matrigel-coated (Collaborative Research) polycarbonate filters (Poretics, Livermore, CA, USA) consisting of a reconstituted basement membrane material composed of laminin, type IV collagen, entactin and heparan sulfate proteoglycans, suspended in MICS chambers [9]. This method allows the efficient quantification of invasion of cells through the Matrigel. Briefly, 5×10^4 cells were seeded randomly onto Matrigel-coated polycarbonate filters situated between the upper and lower well plates of each MICS chamber (six upper wells per cell line). Subsequently, the chambers were incubated in a humidified 5% CO_2 modular incubator at 37°C for 48 h, at selected pH values (6.8 and 7.4) in the presence of either low (70 μM) or high (1 mM) Ca^{2+}. At the end of the incubation time, the cells that had penetrated the Matrigel-coated filters were collected, stained, and counted visually [9]. Percent invasion was corrected for proliferation and calculated accordingly:

$$\% \text{ Invasion} = (\text{no. of invading cells/no. of cells seeded}) \times 100.$$

Differences in growth rates can potentially confound results in these experiments. Thus, it is essential to examine the effects of all experimental conditions on the cellular growth rates. A375P and C8161 cells chronically maintained at a pH of 6.8 grow at essentially the same rate as those maintained under control conditions. Thus, differences in invasive behavior measured with the MICS assay reflect differences in invasive behaviors and not differences in growth (data not shown).

Tumor cell motility assay (in vitro)

Unstimulated motility was also determined in MICS chambers containing polycarbonate filters soaked overnight in 0.1% gelatin as described elsewhere [28]. Briefly, 5×10^4 cells grown at various pH values and external Ca^{2+} concentrations were seeded randomly in each upper well (six wells per cell line), allowed to incubate at 37°C for 6 h, and subsequently processed as described above for the invasion assay.

Chemicals

Culture media were obtained from Sigma. Fluorescence ion indicators were purchased from Molecular Probes (Eugene, OR, USA). All other chemicals were obtained from Sigma, unless otherwise noted.

Gel zymography

Cells were cultured at either pH 6.8 or 7.4 for 28 days. After 48 h under serum-free conditions, the medium was removed from cultures containing the same number of cells and centrifuged to remove cells and

debris. One part Laemmli sample buffer minus reductant was added to two parts conditioned medium, and 35 μl were loaded onto a 10% SDS–PAGE gel containing 0.1% gelatin in the resolving gel. After electrophoresis, the gel was washed in 50 mM Tris–HCl (pH 6.8) plus 2.5% Triton X-100 for 30 min, then incubated with Tris–HCl/10 mM $CaCl_2$/0.02% NaN_3 (pH 6.8) for 20 h at 37°C. The gel was stained with Coomassie BBR-250, and destained with 10% acetic acid/10% methanol until destain remained clear.

Data analysis

Student's *t*-test was used for statistical analysis of paired or unpaired samples, as needed.

Results

Effect of pH on invasive behavior

Our first set of functional experiments examined the effect(s) of maintaining cells at pH 6.8 and 7.4 with respect to invasive ability. Figure 2 shows that both poorly invasive A375P and highly invasive C8161 cells maintained at a pH of 6.8 are much more invasive through basement membrane matrixes compared to controls. Of special interest is the observation that A375P cells under pH 6.8 conditions are as invasive as C8161 cells under control conditions. Essentially, there are two differences between the cells at pH 6.8 and at pH 7.4 shown in Figure 2: (1) they are grown at different pH values, and (2) they are tested at different pH values. To determine if the differences in invasion were due to the growth or the incubation pH, we next examined the invasiveness of cells: (a) grown at the same pH and tested under different pH conditions and (b) grown under different pH conditions and tested at the same pH. Accordingly, Figure 3 shows that, in both cell lines grown at pH 7.4, migratory and invasive behavior tested at pH 6.8 is less than or the same as that observed at pH 7.4. This is in direct contrast to the results illustrated in Figure 2, and suggests that low pH induces a change in the cells themselves. This is further supported by the observation that cells chronically grown at pH 6.8 and examined for migratory and invasive potential at a pH of 7.4 consistently demonstrate higher rates of migration and invasion relative to controls, which parallels the data shown in Figure 2 (data not presented). Thus, cells exposed to low pH conditions for 3 weeks migrate

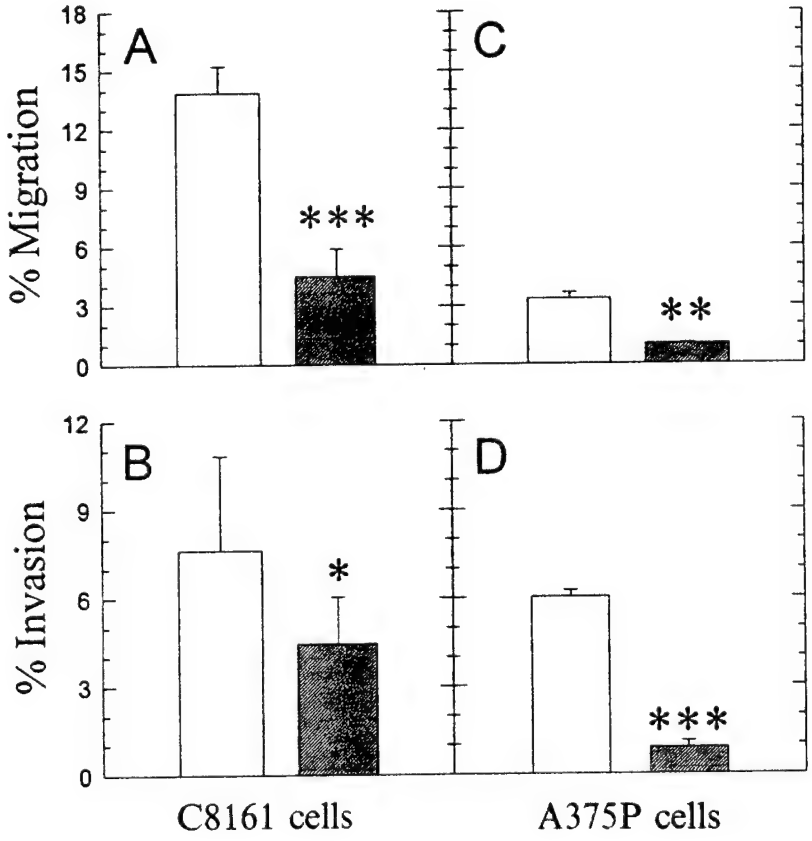

Figure 2. Effect of low pH^{ex} conditions on migration (A,C) and invasion (B,D) in highly invasive C8161 (A,B), and poorly invasive A375P (C,D) human melanoma cells. C8161 and A375P human melanoma cells were chronically grown for 3 weeks in either acidic (pH 6.8, □) or normal (pH 7.4, ▨) conditions (see Materials and methods). Subsequently, cells were transferred to the Membrane Invasion Culture System (MICS) chambers, and the migration and invasion capabilities of these cells were evaluated in their respective media. Data represent the mean ±SEM of three experiments. Statistical analysis was performed using Student's *t*-test: $^{*}P<0.01$; $^{**}P<0.005$; $^{***}P<0.001$.

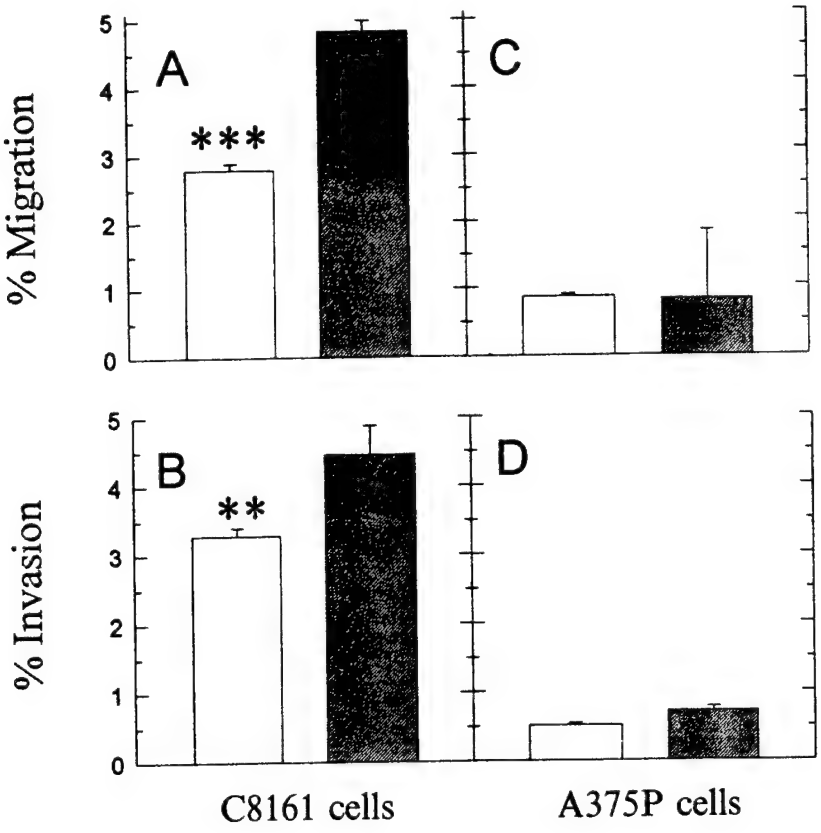

Figure 3. Effect of acute exposure to low pH^{ex} on migration (A,C) and invasion (B,D) in C8161 (A,B) and A375P (C,D) human melanoma cells. C8161 and A375P human melanoma cells which were chronically grown under control (i.e. pH 7.4) conditions were transferred to MICS chambers, and the migration and invasion capabilities of these cells were evaluated at pH 6.8 (□) and pH 7.4 (▨). Data represent mean ±SEM. $^{**}P<0.005$; $^{***}P<0.001$.

and invade at a faster rate, regardless of the pH at which they are tested. It is unclear from these data whether the low pH induced more invasive behavior, or simply selected for more highly invasive cells. However, when we attempted to pre-acclimate cells to a low pH overnight prior to testing migration and invasion, compared to cells which were not pre-acclimated, there were no differences in functional activity (data not presented). This rapid response suggests that low pH induces invasive behavior, rather than selecting for more invasive cells.

Effect of pH on intracellular pH and Ca^{2+}

Since the effects of pH on invasive behavior appear to be mediated via intracellular processes, we investigated whether they might involve changes in pH^{in} and/or $[Ca^{2+}]^{in}$, since both of these parameters are affected by environmental pH. Figure 4 shows the effects of chronic growth at a pH of 6.8 on the pH^{in} and $[Ca^{2+}]^{in}$ values. The resting pH^{in} of control C8161 and A375P cells were similar. As expected, lowering pH^{ex} lowers pH^{in} in both cell types. These effects are identical, whether the C8161 or A375P cells were pre-acclimated to low pH conditions or not (data not shown).

Growth of cells at low pH also led to lower steady-state $[Ca^{2+}]^{in}$ levels in both A375P and C8161 cells. The resting levels of Ca^{2+} were similar in these two cell lines. Incubation of cells at low pH led to lower steady-state Ca^{2+} levels, whether cells were pre-acclimated to pH 6.8 conditions (Figure 4B, D) or not (data not shown). Since both acute and chronic low pH led to lower Ca^{2+} levels, it was unlikely that Ca^{2+} could be responsible for the increased invasive potential, since the effect of pH on invasive potential was observed in only the chronic and not the acute case (cf. Figures 2 and 3). To test this more directly, we reduced cellular Ca^{2+} levels by growing cells in medium with reduced Ca^{2+} levels (see Materials and methods). As shown in Figures 5B and D, growing and testing cells in 70 μM Ca^{2+} caused a significant reduction of Ca^{2+} in C8161 cells and less of a reduction in A375P cells. However, incubating C8161 or A375P cells under reduced Ca^{2+} conditions had no effect on their invasive behaviors (data not shown). Thus, the effects of pH on invasive behaviors is not mediated via changes in $[Ca^{2+}]^{in}$ levels.

Effect of pH on gelatinolytic activity

One of the mechanisms underlying tumor cell invasion is the release of matrix-degrading metalloproteinases, including gelatinases A and B [62–65]. Figure 6 demonstrates that there is less gelatinase A and B

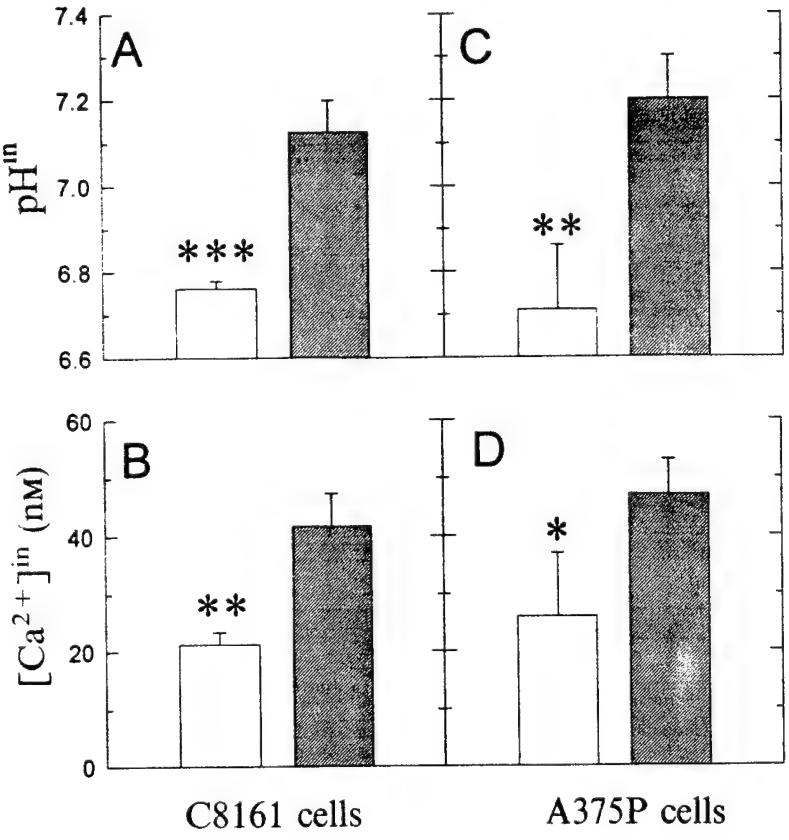

Figure 4. Simultaneous measurement of pH^{in} and $[Ca^{2+}]^{in}$ in C8161 (A,B) and A375P (C,D) melanoma cells chronically grown at low (6.8, □) or high (7.4, ▨) pH. Cells were plated onto coverslips in growth media at pH 6.8 or 7.4 and cultured in a humidified atmosphere for a subsequent 72 h. Cells were then co-loaded with SNARF-1 and Fura-2 to simultaneously measure pH^{in} and $[Ca^{2+}]^{in}$, respectively [33]. After 30 min of dye loading, cells were transferred to CSB at the appropriate pH^{ex} and incubated for a further 30 min to allow for complete hydrolysis of the dye. Subsequently, cells were transferred to the fluorometer cuvette and perfused with CSB at the appropriate pH^{ex}. Data represent the mean ±SD of nine independent determinations. $*P<0.01$; $**P<0.005$; $***P<0.001$.

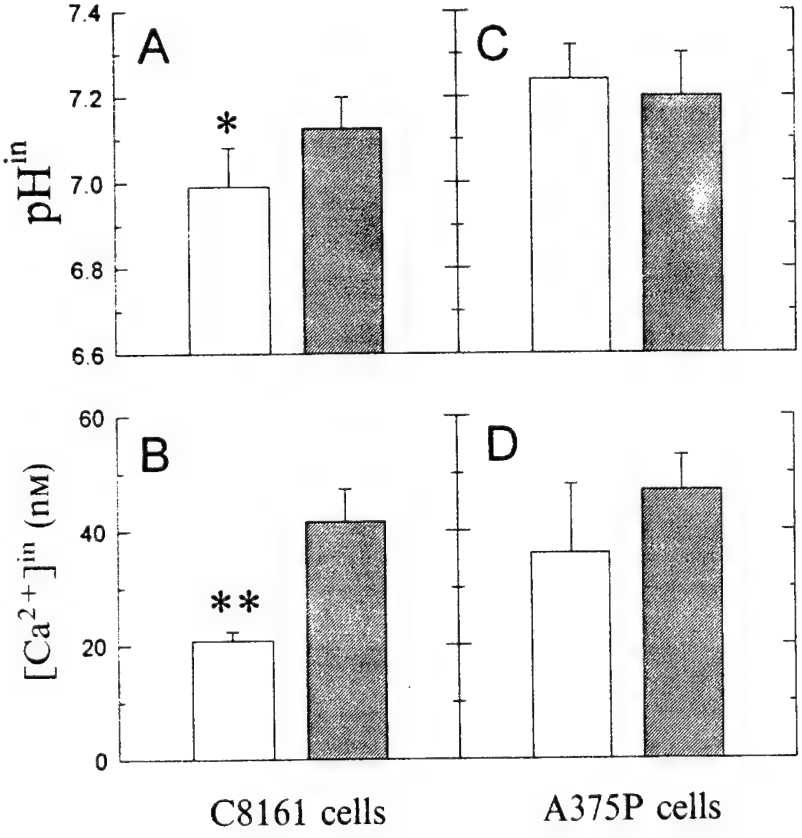

Figure 5. Simultaneous measurement of pH^{in} and $[Ca^{2+}]^{in}$ in C8161 (A,B) and A375P (C,D) melanoma cells at low (70 μM, □) or high (1.0 mM, ▨) Ca^{2+}. Cells were plated onto coverslips in growth media at pH 7.4 and cultured in a humidified atmosphere for a subsequent 72 h. Cells were then co-loaded with SNARF-1 and Fura-2 as described for Figure 4. After 30 min of dye loading, cells were transferred to CSB containing either 70 μM or 1.0 mM Ca^{2+} and incubated for a further 30 min to allow for complete hydrolysis of the dye. Subsequently, cells were transferred to the fluorometer cuvette and perfused with CSB containing either 70 μM or 1.0 mM Ca^{2+} and pH^{in} and $[Ca^{2+}]^{in}$ were determined as described in Materials and methods. Data represent the mean ±SEM of nine independent determinations. $*P<0.01$; $**P<0.005$.

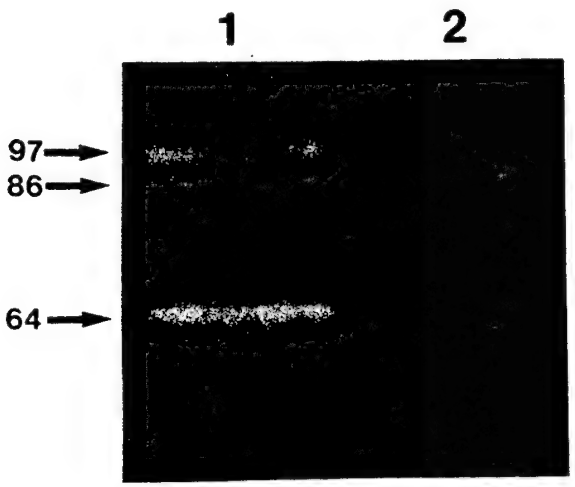

Figure 6. Zymogram of media from C8161 cells grown at pH 7.4 (lane 1) or 6.8 (lane 2). Conditioned medium from the same number of cells was prepared as described in Materials and methods and analysed by gelatin zymography. Cleared zones represent gelatinolytic activity and molecular weights are given in kDa. The relative amounts of these proteins was determined by densitometry. For lane 1 (pH 7.4), the densitometric value obtained for progelatinase A (64 kDa) was arbitrarily set to 1.00 which resulted in active gelatinase B (86 kDa) equaling 0.66 and progelatinase B (97 kDa), equaling 0.85. The values for lane 2 (pH 6.8) normalized against progelatinase A (64 kDa) are 1.00, 0.78 (86 kDa) and 0.65 (97 kDa).

activity in serum-free conditioned medium from C8161 cells grown chronically at pH 6.8 (lane 2) compared to cells grown chronically at pH 7.4 (lane 1). However, while media from cells grown at pH 7.4 contain gelatinolytic activity associated with both pro- and active gelatinase B (97 and 86 kDa, respectively, as seen using this gel system, and verified by Western blot analysis; data not shown; see also [25]), media from cells grown at pH 6.8 contain gelatinase B activity predominantly associated with its active form. Gelatinase A activity appears to be predominantly due to the progelatinase A form of this enzyme (64 kDa as seen on this gel system, and verified by Western blot analysis; data not shown; see also [25]), whether the cells are grown at pH 6.8 or pH 7.4. Moreover, all zymography was normalized based on cell number, medium volume and time of incubation.

Discussion

The ability of tumor cells to migrate and invade through extracellular matrix barriers is a critical function with respect to the acquisition of the metastatic phenotype. Our study examined one aspect of the metastatic cascade, i.e. the effect(s) of pH on the migratory and invasive potential of tumor cells. Specifically, our hypothesis is that the mildly acidic pH generally found in a tumor mass stimulates a more metastatic phenotype, either directly or indirectly, through the stimulation of migratory or invasive behavior.

The above data indicate that incubation of cells at low pH induces more aggressive invasive behavior. This is not a direct trophic effect of pH on the invasive machinery, since acutely lowering pH actually decreases invasive behavior in these cells. These results are consistent with those from Schlappack *et al.*, who observed that culturing murine sarcoma and melanoma cells for 24–48 h at pH 6.5 increased their *in vivo* colonization potential [10]. Their results were observed even if the treated cells were allowed to recover at normal pH for 24–48 h. Similarly, we observed that invasive behavior was increased in acid-treated cells, regardless of the pH at which they were tested. Thus, low pH treatment increases the invasive potential of murine or human melanoma cells by mechanisms which are incompletely understood. Further corroboration of our observations can be found in a study by Kato *et al.* [25], in which B16F10 murine melanoma cells incubated in an acidic medium demonstrated increased migratory ability through type IV collagen gels compared with cells grown at a neutral medium. This effect of pH is not mediated by changes in $[Ca^{2+}]^{in}$, since there is no difference in Ca^{2+} levels between highly and poorly invasive cells, and direct alterations in Ca^{2+} did not affect migration or invasion. However, these results do not rule out the possibility that long-term alterations in Ca^{2+} might be an important mediator of the response.

Low pH does not appear to be merely selective for more invasive cells, since significant increases in migration and invasion are observed with pretreatments as short as 12 h. Thus, low pH induces some aspect of the invasive phenotype. Synthesis of metalloproteinases [25] and transcription of both glucose-regulated proteins [66] and heat shock proteins [67] are inducible by low pH conditions. Although our results did not show an increase in the overall amount of extracellular gelatinolytic activity from cells grown at low pH, there was a significant change in the relative amount of active gelatinase B in these cells that is more conducive to the invasive phenotype. In fact, higher levels of extracellularly active gelatinases A and B were also observed in the human cell lines A-549 and HT 1080, grown under pH 6.8 conditions, and a 103 kDa gelatinase was induced in murine melanoma cell lines grown under acidic

culture conditions [25]. Furthermore, growth at low pH will also spontaneously induce tumorigenic transformation in primary Syrian hamster embryo cells [68]. Thus, by inducing specific proteins and activities, low pH might favor the transient expression of invasive behavior, or additionally, by favoring mutagenesis, it might lead to permanent alterations in cell behavior. These possibilities are currently being tested.

In summary, incubation of human melanoma cells under pH conditions observed in tumors *in vivo* induces them to become more invasive and migratory. This induction is not due to a direct effect of pH on the invasive machinery, but likely involves the induction or activation of specific gene products which augment the invasive phenotype in a multi-step process.

Acknowledgements

The authors would like to thank Ms Gloria M. Martinez and Ms Gudalupe Torres for their technical assistance, and Dr C. George Ray for his scientific suggestions and editorial advice. Supported by US Army Breast Cancer Initiative grant DAMD17-94-J-4368 (to RJG) and NIH grant RO1-CA59702 (to MJCH).

References

1. Wike-Hooley JL, Haveman J and Reinhold HS, 1991, The relevance of tumour pH to the treatment of malignant disease. *Radiother Oncol*, **2**, 343–66.
2. Griffiths JR, 1991, Are cancer cells acidic? *Br J Cancer*, **64**, 425–7.
3. Gillies RJ, Liu Z and Bhujwalla ZM, 1994, ^{31}P NMR measurement of extracellular pH *in situ* using 3-aminopropylphosphonate. *Am J Physiol*, **267** (Cell Physiology 36), C195–C203.
4. Warburg O 1926. *Über den Stoffwechsel der Tumoren*. Cambridge University Press.
5. Sevick EM and Jain RK, 1988, Blood flow and venous pH of tissue-isolated Walker 256 carcinoma during hyperglycemia. *Cancer Res*, **48**, 1201–7.
6. Vaupel P, Kallinowski F and Okunieff P, 1989, Blood flow, oxygen and nutrient supply, and metabolic microenvironment. *Cancer Res*, **49**, 6449–65.
7. Stolk JA, Bhujwalla ZM, Blackband SJ, Shungu DC, Wehrle JP and Glickson JD, 1991, Quantitative *in vivo* measurement of blood flow in RIF-1 tumors by ^{1}H/^{2}H NMR spectroscopy. *Proc 10th Ann Mtg Soc Magn Reson Med*, p. 984.
8. Bhujwalla ZM, Tozer GM, Feld SB, Maxwell RJ and Griffiths JR, 1990, Energy metabolism of RIF-1 tumors following hydralazine. *Radiother Oncol*, **19**, 281–91.
9. Hendrix MJC, Seftor EA, Seftor REB and Fidler IJ, 1987, A simple quantitative assay for studying the invasive potential of high and low human metastatic variants. *Cancer Lett*, **38**, 137–47.
10. Schlappack OK, Zimmermann A and Hill RP, 1991, Glucose starvation and acidosis: effect on experimental metastasic potential, DNA content and MTX resistance of murine tumour cells. *Int J Cancer*, **64**, 663–70.
11. Stetler-Stevenson WG, 1990, Type IV collagenases in tumor invasion and metastasis. *Cancer Metastasis Rev*, **9**, 289–303.
12. Nicolson GL, 1992, Paracrine/autocrine growth mechanisms in tumor metastasis. *Oncol Res*, **4**, 389–99.
13. Miller FR and Heppner GH, 1990, Cellular interactions in metastasis. *Cancer Metastasis Rev*, **9**, 21–34.
14. Fidler IJ, 1991, Cancer metastasis. *Br Med Bull*, **47**, 157–77.
15. Lah TT, Kokalj-Kunovar M, Strukelj B, *et al.* 1992, Stefins and lysosomal cathepsins B, L and D in human breast carcinoma. *Int J Cancer*, **50**, 36–44.
16. Matrisian LM, 1992, The matrix-degrading metalloproteinases. *Bioessays*, **14**, 455–63.
17. Tryggvason K, Hoyhtya M and Pyke C, 1993, Type IV collagenases in invasive tumors. *Breast Canc Res Treat*, **24**, 209–18.
18. Vassalli J-D, Sappino AP and Belin D, 1991, The plasminogen activator/plasmin system. *J Clin Invest*, **88**, 1067–72.
19. Vassalli J-D and Pepper MS, 1994, Membrane proteases in focus. *Nature*, **370**, 14–15.
20. Morisset M, Capony F and Rochefort H, 1986, The 52-kDa estrogen-induced protein secreted by MCF-7 cells is a lysosomal acidic protease. *Biochim Biophys Res Commun*, **138**, 102–9.
21. Rozhin J, Sameni M, Siegler G and Sloane BF, 1994, Pericellular pH affects distribution and secretion of cathepsin B in malignant cells. *Cancer Res*, **54**, 6517–25.
22. Kramer MD, Robinson P, Vlodavsky I, *et al.* 1985, Characterization of an extracellular matrix-degrading protease derived from a highly metastatic tumor cell line. *Eur J Cancer Clin Oncol*, **21**, 307–16.
23. Ishihara A, Nabeshima K and Koono M, 1986, Partial purification and characterization of serum protease from tumor-bearing rats which cleaves type IV collagen. *Invasion & Metastasis*, **6**, 225–45.
24. Slivka SR and Loskutoff DJ, 1991, Platelets stimulate endothelial cells to synthesize type 1 plasminogen activator inhibitor. Evaluation of the role of transforming growth factor beta. *Blood*, **77**, 1013–19.
25. Kato Y, Nakayama Y, Umeda M and Miyazaki K, 1992, Induction of 103-kDa gelatinase/type IV collagenase by acidic culture conditions in mouse metastatic melanoma cell lines. *J Biol Chem*, **267**, 11424–30.
26. Baker MS, Liang XM and Doe, WF, 1992, Occupancy of the cancer cell urokinase receptor (uPAR): effects of acid elution and exogenous uPA on cell surface urokinase (uPA). *Biochim Biophys Acta*, **1117**, 143–52.
27. Uchino T, Sakurai Y, Nishigai M, *et al.* 1993, Isolation and characterization of a novel serine proteinase complexed with alpha 2-macroglobulin from porcine gastric mucosa. *J Biol Chem*, **268**, 527–33.
28. Hendrix MJC, Seftor EA, Chu Y-W, *et al.* 1992, Coexpression of vimentin and keratins by human melanoma tumor cells: correlation with invasive and metastasic potential. *J Natl Cancer Inst*, **84**, 165–74.
29. Chu Y-W, Duffy JJ, Seftor REB, Nagle, RB and Hendrix MJC, 1991, Transfection of a deleted CK18 cDNA into a

highly metastatic melanoma cell line decreases the invasive potential. *Clin Biotech*, **3**, 27–33.
30. Schwartz MA, Both G and Lechene C, 1989, Effect of cell spreading on cytoplasmic pH in normal and transformed fibroblasts. *Proc Natl Acad Sci USA*, **86**, 4525–9.
31. Stossel TP, 1989, From signal to pseudopod. How cells control cytoplasmic actin assembly. *J Biol Chem*, **264**, 18261–4.
32. Soifer D, 1986, Dynamic aspects of microtubule biology. *Ann N Y Acad Sci*, **466**, 1–978.
33. Martínez-Zaguilán R, Martinez GM, Lattanzio F and Gillies RJ, 1991, Simultaneous measurement of intracellular pH and Ca^{2+} using the fluorescence of SNARF-1 and Fura-2. *Am J Physiol*, **260**, C297–C307.
34. Degen DL, Estensen RD, Nagamine Y and Reich E, 1985, Induction and desensitization of plasminogen activator gene expression by tumor promoters. *J Biol Chem*, **260**, 12426–33.
35. Angel P, Baumann I, Stein B, Delius H, Rahmsdorf HJ and Herrlich P, 1987, 12-O-Tetradecanoyld-phorbol-13-acetate induction of the human collagenase gene is mediated by an inducible enhancer element located in the 5'-flanking region. *Molec Cell Biol*, **7**, 2256–66.
36. Frisch SM, Clark EJ and Werb Z, 1987, Coordinate regulation of stromelysin and collagenase genes determined with cDNA probes. *Proc Natl Acad Sci, USA*, **84**, 2600–4.
37. Edwards DR, Waterhouse P, Holman LM and Denhardt DT, 1986, A growth factor-inducible gene (16C8) in mouse fibroblasts is homologous to human tissue inhibitor of metalloproteinases. *Nucl Acid Res*, **14**, 8863–78.
38. Murphy G and Reynolds JJ, 1985, Biosynthesis of tissue inhibitor of metalloproteinases by human fibroblasts in culture. Stimulation by 12-O-tetradecanoylphorbol 13-acetate and interleukin-1 in parallel with collagenase. *J Biol Chem*, **260**, 3079–83.
39. Korczak B, Whale C and Kerbel RS, 1989. Possible involvement of Ca^{2+} mobilization and protein kinase C induction of spontaneous metastasis by mouse mammary adenocarcinoma cells. *Cancer Res*, **49**, 2597–602.
40. Brinckerhoff CE, Plucinska I, Sheldon L and O'Connor GT, 1986, Half-life of synovial cell collagenase mRNA is modulated by phorbol myristate acetate but not by *all-trans*-retinoic acid or dexamethasone. *Biochemistry*, **25**, 6378–84.
41. Takenaga K and Takahashi K, 1986, Effects of 12-O-tetradecanoylphorbol-13-acetate on adhesiveness and lung-colonization ability of Lewis lung carcinoma cells. *Cancer Res*, **40**, 375–80.
42. Gopalakrishna R and Barsky SH, 1988, Tumor-promoter induced membrane-bound kinase C regulates hematogenous metastasis. *Proc Natl Acad Sci, USA*, **85**, 612–16.
43. Whitfield JF, Durkin JP, Franks DJ, *et al.*1987, Calcium, cyclic AMP and protein kinase C: partners in mitogenesis. *Cancer Metastasis Rev*, **5**, 205–50.
44. Barbero MC, Garcia M, Almena A and Alino SF, 1991, Correlation between secretion pattern and metastatic potential from drug-treated 3LL tumor cells line. *Cell Molec Biol*, **37**, 501–8.
45. Moolenaar WH, 1986, Effects of growth factors on intracellular pH regulation. *Ann Rev Physiol*, **48**, 363–76.
46. Berridge MJ, 1987, Inositol triphosphate and diacylglycerol: two interacting second messengers. *Ann Rev Biochem*, **56**, 156–93.
47. Vincentini LM and Villarreal ML, 1986, Inositol phosphate turnover, cytosolic Ca^{2+} and pH: putative signals for the control of cell growth. *Life Sci*, **38**, 2269–76.
48. Rozengurt E, 1986, Early signals in the mitogenic response. *Science*, **234**, 161–6.
49. Hesketh TR, Moore JP, Morris JDH, *et al.*, 1985, A common sequence of calcium and pH signals in the mitogenic stimulation of eukaryotic cells. *Nature*, **313**, 481–4.
50. Gillies RJ, Martinez R, Sneider JM and Hoyer PB, 1989, Sphingosine inhibits phorbol 12-myristate 13-acetate-, but not serum-induced, activation of Na^+/H^+ exchange in mammalian cells. *J Cell Physiol*, **139**, 125–30.
51. Mareel MM, Van Roy FM and De Baetselier P, 1990, The invasive phenotype. *Cancer Metastasis Rev*, **9**, 45–62.
52. Marks PW and Maxfield FR, 1990, Transient increases in cytosolic free calcium appear to be required for the migration of adheren Ca^{2+} trt human neutrophils. *J Cell Biol*, **110**, 43–52.
53. Milne JL and Coukell MB, 1991, A transport system associated with the plasma membrane of *Dictyostelium discoideum is* activated by different chemoattractant receptors. *J Cell Biol*, **112**, 103–10.
54. Savarese DM, Russell JT, Fatatis A and Liotta LA, 1992, Type IV collagen stimulates an increase in intracellular calcium. Potential role in tumor cell motility. *J Biol Chem*, **267**, 21928–35.
55. Martínez-Zaguilán R, 1992, Measurements of intracellular Ca^{2+} and pH^{in} in cultured cells by fluorescence spectroscopy. In: Watson, RR, ed. In Vitro *Methods of Toxicology*. Boca Raton, FL: CRC Press, pp. 217–36.
56. Kleinman HK, McGarvey ML, Liotta LA, *et al.*, 1982, Isolation and characterization of type IV procollagen, laminin and heparan sulfate proteoglycan from the EHS sarcoma. *Biochemistry*, **21**, 6188–93.
57. Bregman MD, Peters E, Sander D and Meyskens FL Jr, 1983, Dexamethasone, prostaglandin A, and retinoic acid modulation of murine and human melanoma cells grown in soft agar. *J Natl Cancer Inst*, **71**, 927–32.
58. Gillies RJ, Martinez-Zaguilan R, Martinez GM, Serrano R and Perona R, 1990, Tumorigenic 3T3 cells maintain an alkaline intracellular pH under physiological conditions. *Proc Natl Acad Sci, USA*, **87**, 7414–18.
59. Lattanzio FA, 1990, The effects of pH and temperature on fluorescent calcium indicators as determined with chelex-100 and EDTA buffer systems. *Biochem Biophys Res Commun*, **171**, 102–8.
60. Wiegmann TB, Welling LW, Beatty DM, Howard DE, Vamos S and Morris, SJ, 1993, Simultaneous imaging of intracellular [Ca^{2+}] and pH in single MDCK and glomerular epithelial cells. *Am J Physiol*, **265**, C1184–C1190.
61. Gillies RJ, Didier N and Denton M, 1986, Determination of cell number in monolayer cultures. *Analyt Biochem*, **159**, 109–13.
62. Matrisian LM, 1990, Metalloproteinases and their inhibitors in matrix remodeling. *Trends Genetics*, **6**, 121–5.
63. Woessner JF, 1991, Matrix metalloproteinases and their inhibitors in connective tissue remodeling. *FASEB J*, **5**, 2145–54.

64. Duffy MJ, 1992, The role of proteolytic enzymes in cancer invasion and metastasis. *Clin Exp Metastasis*, **10**, 145–55.
65. Seftor REB, 1994, Electrophoretic analysis of proteins associated with tumor cell invasion. *Electrophoresis*, **15**, 454–62.
66. Khandjian EW, 1990, Acidic extracellular environment induces only a subset of heat-shock proteins in primary mouse kidney cell cultures. *Biochem Cell Biol*, **68**, 804–7.
67. Mosser DD, Kotzbauer PT, Sarge KD and Morimoto RI, 1990, *In vitro* activation of heat shock transcription factor DNA-binding by calcium and biochemical conditions that affect protein conformation. *Proc Natl Acad Sci, USA*, **87**, 3748–52.
68. LeBoeuf RA, Kerckaert GA, Aardema MJ and Gibson DP, 1990, Multistage neoplastic transformation of Syrian hamster embryo cells cultured at pH 6.7. *Cancer Res*, **50**, 3722–9.

JOURNAL OF CELLULAR PHYSIOLOGY 176:196–205 (1998)

Distinct Regulation of pH^{in} and $[Ca^{2+}]^{in}$ in Human Melanoma Cells With Different Metastatic Potential

RAUL MARTÍNEZ-ZAGUILÁN,[1]* GLORIA M. MARTINEZ,[1] ARACELI GOMEZ,[2] MARY J.C. HENDRIX,[3] AND ROBERT J. GILLIES[2]

[1]*Department of Physiology, Texas Tech University Health Sciences Center, Lubbock, Texas*
[2]*Department of Biochemistry, University of Arizona Health Sciences Center, Tucson, Arizona*
[3]*Department of Anatomy, Iowa Cancer Center, University of Iowa, Iowa City, Iowa*

We investigated whether alterations in the mechanisms involved in intracellular pH (pH^{in}) and intracellular calcium ($[Ca^{2+}]^{in}$) homeostasis are associated with the metastatic potential of poorly (A375P) and highly (C8161) metastatic human melanoma cells. We monitored pH^{in} and $[Ca^{2+}]^{in}$ simultaneously, using the fluorescence of SNARF-1 and Fura-2, respectively. Our results indicated that steady-state pH^{in} and $[Ca^{2+}]^{in}$ between these cell types were not significantly different. Treatment of cells with NH_4Cl resulted in larger pH^{in} increases in highly than in poorly metastatic cells, suggesting that C8161 cells have a lower H^+ buffering capacity than A375P. NH_4Cl treatment also increased $[Ca^{2+}]^{in}$ only in C8161 cells. To determine if the changes in $[Ca^{2+}]^{in}$ triggered by NH_4Cl treatment were due to alterations in either H^+- or Ca^{2+}-buffering capacity, cells were treated with the Ca^{2+}-ionophore 4Br-A23187, to alter $[Ca^{2+}]^{in}$. The magnitude of the ionophore-induced $[Ca^{2+}]^{in}$ increase was slightly greater in C8161 cells than in A375P. Moreover, A375P cells recover from the ionophore-induced $[Ca^{2+}]^{in}$ load, whereas C8161 cells did not, suggesting that A375P may exhibit distinct $[Ca^{2+}]^{in}$ regulatory mechanisms than C8161 cells, to recover from Ca^{2+} loads. Removal of extracellular Ca^{2+} ($[Ca^{2+}]^{ex}$) decreased $[Ca^{2+}]^{in}$ in both cell types at the same extent. Ionophore treatment in the absence of $[Ca^{2+}]^{ex}$ transiently increased $[Ca^{2+}]^{in}$ in C8161, but not in A375P cells. Endoplasmic reticulum (ER) Ca^{2+}-ATPase inhibitors such as cyclopiazonic acid (CPA) and thapsigargin (TG) increased steady-state $[Ca^{2+}]^{in}$ only in C8161 cells. Together, these data suggest that the contribution of intracellular Ca^{2+} stores for $[Ca^{2+}]^{in}$ homeostasis is greater in highly than in poorly metastatic cells. Bafilomycin treatment, to inhibit V-type H^+-ATPases, corroborated our previous results that V-H^+-ATPases are functionally expressed at the plasma membranes of highly metastatic, but not in poorly metastatic cells (Martínez-Zaguilán et al., 1993). Collectively, these data suggest that distinct pH^{in} and $[Ca^{2+}]^{in}$ regulatory mechanisms are present in poorly and highly metastatic human melanoma cells. J. Cell. Physiol. 176:196–205, 1998.

A role for intracellular pH (pH^{in}) and intracellular calcium ($[Ca^{2+}]^{in}$ in the regulation of cellular functions has been contemplated for several decades (for reviews, see Roos and Boron, 1981; Busa, 1986; Carafoli, 1987; Pietrobon et al., 1990; Gillies et al., 1992). With the advent of several sophisticated techniques to measure pH^{in} and $[Ca^{2+}]^{in}$ (Roos and Boron, 1981; Tsien, 1989; Martínez-Zaguilán et al., 1991; Gillies, 1992), our understanding of the role of these ions in many cellular processes (e.g., cell growth, exocytosis, and motility), has increased (Roos and Boron, 1981; Busa, 1986; Pietrobon et al., 1990; Gillies et al., 1992). Regarding their role in cell growth, tumorigenesis, and metastasis, many interesting dilemmas still remain. These difficulties arise by the fact that there is an interrelation between these two ions, so that alterations in either

Abbreviations: $[Ca^{2+}]^{in}$ intracellular calcium; CSB, cell suspension buffer; Fura-2, 5-oxazolecarboxylic acid, 2-(6-(bis(carboxymethyl) amino)-5-(2-(2-bis(carboxymethyl)amino)-5-methylphenoxy-2-benzofuranyl); HEPES, N-2-hydroxyethylpiperazine-N′-2-ethanesulfonic acid; pH^{cyt}, cytoplasmic pH; pH^{ex}, extracellular pH; pH^{in}, intracellular pH; R, ratio; R_{max}, maximum ratio; R_{min}, minimum ratio; SNARF-1, 5′(and 6′′)-carboxy-10-dimethylamino-3-hydroxy-spyro-[7H benzo[c]xanthene-7,1′(3′H)-isobenzofuran]3′-one; X-AM, acetoxymethylester; Kda, dissociation constant.

Contract grant sponsor: U.S. Army Breast Cancer Initiative; Contract grant number: DAMD17-94-J-4368; Contract grant sponsor: NIH; Contract grant number: RO1-CA59702.

*Correspondence to: Raul Martínez-Zaguilán, Department of Physiology, Texas Tech University Health Sciences Center, 3601 4th Street, Lubbock, Texas 79430. E-mail phyrmz@ttuhsc.edu

Received 3 May 1996; Accepted 19 December 1997

one can lead to changes in the other. Furthermore, the role for pH^{in} and $[Ca^{2+}]^{in}$ in proliferation may be distinct from its effects in tumorigenicity and metastasis. Metastasis is a multistage process (reviewed in Mareel et al., 1990; Fidler, 1991), and therefore, it is possible that each stage may have a distinct $pH^{in}/[Ca^{2+}]^{in}$ optimum. Increasing the probability of any single stage, by holding its $pH^{in}/[Ca^{2+}]^{in}$ at its optimum, will increase the probability of the overall process. A number of processes are affected by changes on $pH^{in}/[Ca^{2+}]^{in}$ of physiological magnitude, e.g., glycolysis, protein synthesis, DNA synthesis, gene expression, exocytosis, secretion, assembly-disassembly of cytoskeleton proteins, and enzymatic activities (for reviews, see Roos and Boron, 1981; Busa, 1986; Carafoli, 1987; Frelin et al., 1988; Pietrobon et al., 1990; Gillies et al., 1992). We have recently shown that there were no significant differences in the steady-state levels of pH^{in} and $[Ca^{2+}]^{in}$ in cells with either low or high metastatic potential (Martínez-Zaguilán et al., 1996a). However, a number of studies have provided indirect evidence that alterations in the levels of these two ions are relevant in the acquisition of the metastatic phenotype (Takenaga and Takahashi, 1986; Whitfield et al., 1987; Korczak et al., 1989; Schlappack et al., 1991). In this study we further investigated whether these cells maintain pH^{in} and $[Ca^{2+}]^{in}$ using distinct regulatory mechanisms, albeit maintaining similar steady-state levels in these two ions.

Cytoplasmic pH of mammalian cells is mainly regulated by Na^+/H^+ exchange and HCO_3^--based transport mechanisms (Roos and Boron, 1981; Frelin et al., 1988; Gillies et al., 1992). In most eukaryotic cells, these systems collaborate to maintain pH^{in} within a window of values that are permissive for growth and function. In some specialized cells such as kidney cells, gastric cells, hepatocytes, macrophages, and osteoclasts, a plasma membrane H^+-ATPase has been implicated in pH^{in} regulation (reviewed in Gillies et al., 1992). It is notable that these cells are very dynamic in terms of acid secretion, and at least in two of them, i.e., osteoclasts and macrophages, the H^+-ATPase is a Vacuolar(V)-type H^+-ATPase (Swallow et al., 1990; Vaananen et al., 1990). These latter two cell types also exhibit characteristics of invasive cells. We have also observed the functional expression of V-type H^+-ATPase at the plasma membrane of some human tumor cells (Martínez-Zaguilán et al., 1993). Some of these are highly metastatic tumor cells (Martínez-Zaguilán et al., 1993). It is therefore possible that functional expression of a V-type H^+-ATPase may be relevant for invasion and metastasis.

Steady-state $[Ca^{2+}]^{in}$ levels in most cells are determined by the relative rates of Ca^{2+} entry and Ca^{2+} extrusion (Carafoli, 1987; Orchard and Kentish, 1990; Pietrobon, 1990). Ca^{2+} entry into the cytosolic compartment generally occurs through well-regulated Ca^{2+} channels in the plasma membrane (PM) or IP_3-gated release from the endoplasmic reticulum (ER). Ca^{2+} extrusion from the cytosolic compartment occurs via PM- and ER-localized Ca^{2+}-ATPases (Carafoli, 1987). Ca^{2+}-binding proteins (CaBP) can also play a prominent role in regulating $[Ca^{2+}]^{in}$ homeostasis (Carafoli, 1987). In some cells, transmembrane Ca^{2+} movement can also occur via Na^+/Ca^{2+} exchange (Orchrad and Kentish, 1990). All of these systems are susceptible to pH regulation. High intracellular pH (pH^{in}) inhibits both PM- and ER-Ca^{2+}-ATPases, and favors the open state of Ca^{2+}-channels (Dixon and Haynes, 1990; Lytton et al., 1992). Thus by these mechanisms, high pH^{in} would promote increases in $[Ca^{2+}]^{in}$. Conversely, high pH^{in} might decrease the Kd_a of CaBP for Ca^{2+}, and could decrease the forward direction of the Na^+/Ca^{2+} exchanger, so that these effects would promote a decrease in $[Ca^{2+}]^{in}$ (Orchrad and Kentish, 1990). In addition, variations in extracellular pH (pH^{ex}) can alter the activity of pH^{in} regulatory mechanisms (Roos and Boron, 1981; Gillies and Martínez-Zaguilán, 1991; Gillies et al., 1992). Moreover, variations in $[Ca^{2+}]^{in}$ can also modulate the activity of Na^+/H^+ exchange and induce the insertion of V-H^+-ATPases into the plasma membrane (Van Adelsberg and Al-Awqati, 1986; Vincentini and Villereal, 1986; Martínez-Zaguilán et al., 1991).

In this study, we use human melanoma cells with various degrees of metastatic potential: C8161 cells are highly metastatic, whereas A375P cells have a low metastatic potential. As controls, we use C8161 cells transfected with a cytokeratin deletion mutant (C8161-d1070). The resultant transfected cells are nonmetastatic (Chu et al., 1991). We also include C8161 cells transfected with the neomycin resistant construct alone (Neo-C8161). These cells are as metastatic as the parental cell line (Chu et al., 1991). The pH^{in} and $[Ca^{2+}]^{in}$ were monitored simultaneously using the fluorescence of SNARF-1 and Fura-2, respectively. This approach is needed since the dissociation constant and maximum and minimum fluorescence ratios of Fura-2 used to determine $[Ca^{2+}]^{in}$ are sensitive to pH (Lattanzio, 1990; Martínez-Zaguilán et al., 1991; Vorndran et al., 1995; Martínez-Zaguilán et al., 1996b). Therefore, concurrent pH^{in} or $[Ca^{2+}]^{in}$ measurements allow the pH-correction of the Fura-2 parameters (Martínez-Zaguilán et al., 1991; Martínez-Zaguilán et al., 1996b). Our results indicated that highly metastatic cells exhibited a lower H^+- and Ca^{2+}-buffering capacity than poorly metastatic cells, when exposed to NH_4Cl or the Ca^{2+}-ionophore A23187. These protocols were used to increase pH^{in} or $[Ca^{2+}]^{in}$, respectively. $[Ca^{2+}]^{ex}$ removal resulted in larger $[Ca^{2+}]^{in}$ decreases in both cell types. The magnitude of the $[Ca^{2+}]^{in}$ decrease, however, was not statistically different. In the absence of $[Ca^{2+}]^{ex}$, A23187 transiently increased $[Ca^{2+}]^{in}$ in C8161 cells without significant $[Ca^{2+}]^{in}$ changes in A375P cells. We also determined that treatment of cells with ER-Ca^{2+}-ATPase inhibitors resulted in increases in steady-state $[Ca^{2+}]^{in}$ in highly metastatic, but not in poorly metastatic cells. Moreover, the functional expression of V-H^+-ATPases is only observed in highly metastatic cells. These data suggest that there are distinct pH^{in} and $[Ca^{2+}]^{in}$ regulatory mechanisms in cells with different degrees of metastatic potential.

MATERIALS AND METHODS

Cell culture and preparation of cells for simultaneous measurements of pH^{in} and $[Ca^{2+}]^{in}$ by fluorescence

Poorly metastatic (A375P) and highly metastatic (C8161) human melanoma cells were cultured as described elsewhere (Martínez-Zaguilán et al., 1996a). The A375P human melanoma cell line was a gift from I.J. Fidler (University of Texas, M.D. Anderson Hospi-

tal and Tumor Institute, Houston, TX). The highly metastatic C8161 melanoma cell line was established from an amelanotic metastasis from a patient at the Arizona Cancer Center (Tucson, AZ). These cells were grown at pH^{ex} 7.4 in Dulbecco's Modified Eagle Media (DMEM) supplemented with 10% Nu serum. The culture of C8161-d1070 and Neo-C8161 cells was performed as previously described (Chu et al., 1991).

The procedures for the simultaneous measurements pH^{in} and $[Ca^{2+}]^{in}$ using the fluorescence of SNARF-1 and Fura-2, respectively, has been previously described (Martínez-Zaguilán et al., 1991). Briefly, cells were inoculated into 60-mm petri dishes containing 9 × 22-mm coverslips at a density of 2×10^5 cells/60 mm dish in their growing media, in the 5% CO_2 incubator for 48 h. Two coverslips (with attached cells) were then transferred to a 60-mm petri dish containing 7 μM SNARF-1/AM and 2 μM Fura-2/AM in cell-suspension buffer (CSB) and incubated for 30 min at 37°C. The acetoxymethyl ester (AM) forms of these dyes are lipophilic and cell permeant. Cellular esterases cleave the ester groups of the dyes in the cytosol, leaving the relatively impermeant free acid form of the dye and preventing leakage of the dye out of the cell or accumulation in intracellular organelles (Tsien, 1989). Following the 30-min incubation, the coverslips were transferred to a 60-mm petri dish containing CSB without dyes and further incubated for 30 min to allow for complete ester hydrolysis of the dyes. The two coverslips were then placed back-to-back in a holder and put in a cuvette in the spectrofluorometer, which is equipped with a flow-through device for buffer perfusion. The coverslips were continuously perfused at 3 ml/min with their respective buffers. Temperature was maintained by keeping both the water jacket and the perfusion medium at 37°C using a circulator water bath (Lauda model RM 20, Brinkman Instruments, Westbury, NY). In situ calibration curves for pH^{in} and $[Ca^{2+}]^{in}$ were performed as described previously (Martínez-Zaguilán et al., 1991, 1996a). Since the Kd, R_{max} and R_{min} of Fura-2 are affected by pH, estimation of $[Ca^{2+}]^{in}$ was performed using pH-corrected parameters (Martínez-Zaguilán et al., 1991, 1996a,b).

Fluorescence measurements

All fluorescence measurements were performed in a temperature controlled cuvette housed in an SLM8000C (SLM, Urbana, IL), at 37°C, under ambient CO_2, using 4-nm bandpass slits and an external rhodamine standard as a reference.

Buffers and chemicals

Cell suspension buffer (CSB) contained: 0.35 mM Na_2HPO_4, 110 mM NaCl, 0.44 mM KH_2PO_4, 5.4 mM KCl, 1 mM $MgSO_4$, 1.3 mM $CaCl_2$, 25 mM HEPES, 5 mM glucose, and 2 mM L-glutamine at a pH of 7.15 at 37°C. Organic components were added the day of experimentation in order to avoid bacterial contamination. Na^+-free CSB contained 110 mM Na-gluconate in lieu of NaCl. Fluoroprobes were obtained from Molecular Probes (Eugene, OR). Unless otherwise stated, all other chemicals were obtained from Sigma Chemical (St. Louis, MO).

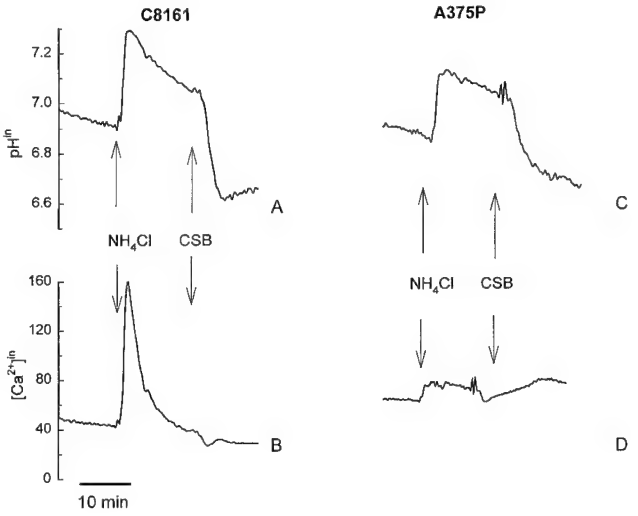

Fig. 1. Effect of NH_4Cl treatment on (pH^{in}) and $[Ca^{2+}]^{in}$ in highly metastatic C8161 (**A,B**) and poorly metastatic A375P (**C,D**) human melanoma cells. Cells were plated onto coverslips for experiments in DMEM supplemented with 10% Nu-serum, as described previously (Martínez-Zaguilán et al., 1996a). After 72 hr in culture under these conditions, cells were co-loaded with SNARF-1 and Fura-2 to simultaneously measure pH^{in} and $[Ca^{2+}]^{in}$, respectively (Martínez-Zaguilán et al., 1991). After 30 min of dye loading, cells were transferred to CSB, at a pH^{ex} 7.15 and pre-incubated for 30 min to allow for complete hydrolysis of the dye. Subsequently, cells were transferred to the fluorometer cuvette and perfused with HCO_3^--free CSB, pH^{ex} 7.15. At the time indicated, the perfusate was exchanged for one containing 25 mM NH_4Cl in HCO_3^--free CSB. Subsequently, the perfusate was exchanged for HCO_3^--free CSB (arrows). Data are representative of 10 experiments.

Data analysis

The student t-test was used for statistical analysis of paired or unpaired samples, as needed.

RESULTS

Highly metastatic cells exhibit a much lower H^+- and Ca^{2+}-buffering capacities than poorly metastatic cells

As shown in Figure 1, there are no differences in the resting pH^{in} and $[Ca^{2+}]^{in}$ between highly metastatic and poorly metastatic melanoma cells (pH values 7.07 ± 0.09 and 7.1 ± 0.08; $[Ca^{2+}]^{in}$ values 48 ± 12 nM and 43 ± 7 nM in C8161 versus A375P cells, respectively; n = 35). This is in agreement with our previous work (Martínez-Zaguilán et al., 1996a). In order to study whether distinct pH^{in} and $[Ca^{2+}]^{in}$ regulatory mechanisms exist in cells with different degrees of metastatic potential, we performed maneuvers that would result in increase in pH^{in}, such as treatment of cells with NH_4Cl or changes in $[Ca^{2+}]^{in}$ using either the Ca^{2+}-ionophore A23187, or removal of $[Ca^{2+}]^{ex}$ followed by A23187 treatment to elicit release of Ca^{2+} from intracellular stores.

In the first set of experiments shown in Figure 1, cells were initially perfused with HCO_3^--free CSB at $pH^{ex} = 7.15$. Once steady-state pH^{in} and $[Ca^{2+}]^{in}$ were reached, perfusate was exchanged for one containing 25 mM NH_4Cl. This results in a rapid alkalinization of the cytosol because the uncharged specie (NH_3) rapidly crosses the plasma membrane and, once inside, picks

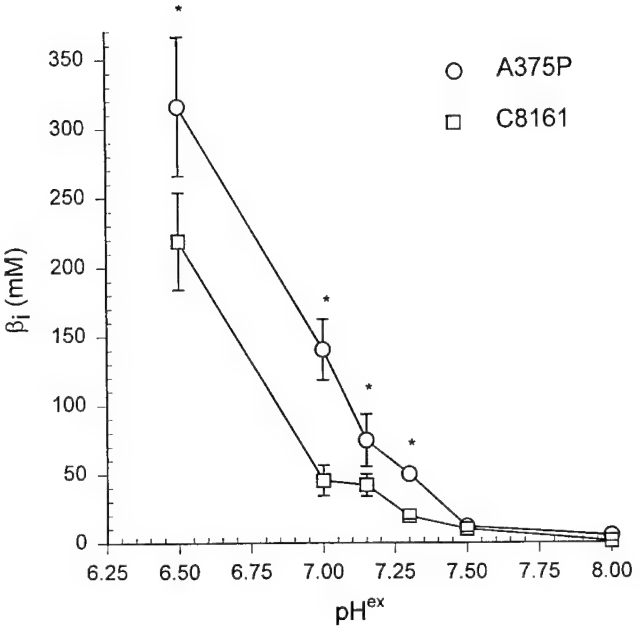

Fig. 2. Intrinsic H^+ buffering capacity (β_i) as a function of pH^{ex} in highly metastatic C8161 and poorly metastatic A375P human melanoma cells. The estimation of β_i was performed from a number of experiments similar to those shown in Figure 1, except that experiments were performed at various pH^{ex} values. *$P < 0.05$ A375P vs. C8161 cells, otherwise differences are not significant.

up a H^+ to form NH_4^+. After 5 min, the perfusate is exchanged by NH_4Cl-free buffer. Under these conditions, NH_3 leaves out the cell rapidly, thus leaving a H^+ behind, i.e., acidifying the cytosol (Roos and Boron, 1981; Gillies and Martínez-Zaguilán, 1991). As shown in Figure 1, the magnitude of the pH^{in} increase upon addition of NH_4Cl (i.e., ΔpH^{in}, which corresponds to the difference in pH^{in} between steady-state pH^{in} and the pH^{in} value at the zenith of the NH_4Cl-induced alkalinization) is larger in C8161 than in A375P (ΔpH^{in} = 0.427 ± 0.044, n = 10 for C8161; and 0.25 ± 0.045, n = 10 for A375P; $P < 0.05$; Fig. 1A,C). The magnitude of these differences is significantly larger at more acidic pH^{ex} values (i.e., $pH^{ex} = 6.25$) than at more alkaline pH^{ex} values (i.e., $pH^{ex} > 7.3$). From a large number of experiments similar to this, performed at various pH^{ex}'s (i.e., 6.5, 7.7.15. 7.5, and 8.0), we have determined that the H^+ buffering capacity (β_i) decreases with increasing pH^{ex} in both C8161 and A375P cells, respectively (Fig. 2). The estimated β_i value in C8161 cells is lower than that determined in A375P cells at pH^{ex} values ≤ 7.25. Differences in H^+ buffering capacity may reflect differences in pH^{in} regulatory mechanisms in these cell types. Indeed, we have previously shown that C8161 cells exhibit V-type H^+-ATPase on their plasma membranes, whereas A375P cells do not (Martínez-Zaguilán, et al., 1993). Moreover, addition of NH_4Cl result in large increases in $[Ca^{2+}]^{in}$ in C8161 cells ($\Delta[Ca^{2+}]^{in}$ = 112 ± 30 nM, where $\Delta[Ca^{2+}]^{in}$ is the difference between steady-state $[Ca^{2+}]^{in}$ and the $[Ca^{2+}]^{in}$ value at the peak; Fig. 1B, Table 1). Similar increases in $[Ca^{2+}]^{in}$ upon NH_4Cl treatment were observed in Neo-C8161 cells. In contrast, the poorly metastatic A375P melanoma cells respond with only minor increases in $[Ca^{2+}]^{in}$, regardless of either the pH^{ex} or the concentration of NH_4Cl used ($\Delta[Ca^{2+}]^{in}$ = 14 ± 8 nM at pH^{ex} = 7.15; Fig. 1D; Table 1, data not shown). Likewise, treatment of C8161-d1070 with NH_4Cl did result in increases in pH^{in} without significant changes in $[Ca^{2+}]^{in}$ (Table 1, data not shown). The differences between poorly (A375P) and highly (C8161 cells) in regards to the magnitude of the $[Ca^{2+}]^{in}$ change following NH_4Cl change were statistically significant ($P < 0.05$).

Since pH can affect the Kd_a of Ca^{2+}-binding proteins (CaBP), it is then possible that the increase in $[Ca^{2+}]^{in}$ triggered by NH_4Cl in C8161 (and Neo-C8161) cells might be due to the fact that these cells have a lower H^+-buffering capacity than A375P cells; thus the effects of pH on CaBP would be larger. To determine whether the observed increases in $[Ca^{2+}]^{in}$ in C8161 cells upon NH_4Cl treatment is due to differences in Ca^{2+} buffering capacity, we treated these cells with the nonfluorescent Ca^{2+} ionophore 4Br-23187, to induce a $[Ca^{2+}]^{in}$ load (Fig. 3). Figure 3D indicates that treatment of A375P cells with 1 μM A23187 results in a rapid transient increase in $[Ca^{2+}]^{in}$ ($\Delta[Ca^{2+}]^{in}$ peak = 31 ± 7 nM, n = 8), which is followed by a $[Ca^{2+}]^{in}$ recovery to the initial resting levels with a $t_{1/2}$ of 3.9 ± 0.5 min (Fig. 3D). In contrast, treatment of highly metastatic C8161 cells with 1 μM A23187 results in a rapid increase in $[Ca^{2+}]^{in}$ ($\Delta[Ca^{2+}]^{in}$ peak = 35 ± 9 nM, n = 8). Moreover, unlike A375P cells, the resultant increase in $[Ca^{2+}]^{in}$ is sustained and remains elevated during the time frame of these experiments (Fig. 3B). Similarly, treatment of Neo-C8161 cells with A23187 resulted in sustained increases in $[Ca^{2+}]^{in}$ (Table 1, data not shown). These data suggest that A375P cells may exhibit distinct mechanisms than highly metastatic C8161 cells to cope with $[Ca^{2+}]^{in}$ loads.

Since most cells recover from Ca^{2+} loads through the activity of Ca^{2+}-ATPases or Na^+/Ca^{2+} exchanger, we then investigated whether differences in any of these mechanisms could explain the differences in the kinetics of the $[Ca^{2+}]^{in}$ recovery observed in these cell types. In several cell types, including nonmuscle cells, the Na^+/Ca^{2+} exchanger plays a prominent role in $[Ca^{2+}]^{in}$ homeostasis (reviewed in Carafoli, 1987; Sage et al., 1991). Whether this activity determines the differences in $[Ca^{2+}]^{in}$ recovery observed between highly and poorly metastatic cells was therefore investigated by acutely removing Na^+ from the medium to produce an increase in $[Ca^{2+}]^{in}$ by reversing the exchanger. Although the experiment is simple, the interpretation of the data is not straightforward because removal of Na^+ generally results in a decrease in pH^{in} due to reversal of the usual direction of the ubiquitous Na^+/H^+ exchanger (Orchrad and Kentish, 1990; Lax et al., 1994). Under these conditions, more protons are available to bind to Fura-2 and affect its fluorescence (Martínez-Zaguilán et al., 1991, 1996b). This could result in misinterpretation of the data (Martínez-Zaguilán et al., 1994). Therefore, corrections for pH effects on Fura-2 should be made with simultaneous measurements of pH^{in} and $[Ca^{2+}]^{in}$. Once these corrections for H^+ binding on Fura-2 were made, we determined that there were no changes in $[Ca^{2+}]^{in}$ in any of the cell lines tested (data not shown). These data indicate that poorly and highly metastatic cells lack Na^+/Ca^{2+} exchanger activity, since if present, Na^+

TABLE 1. Summary of results

Parameter	Metastatic		Non-metastatic	
	C8161	Neo-C8161	A375P	C8161-d1070
		pH^{in} regulation		
pH^{in}	same	same	same	low
bafilomycin sensitivity	high[1]	high[1]	poor[2]	poor
Na^+ removal sensitivity	low[3]	low	high[4]	high
pH^{in} recovery in Na^+-free (NH_4Cl experiment)	yes	yes	no	no
		$[Ca^{2+}]^{in}$ regulation		
$[Ca^{2+}]^{in}$	same	same	same	low
NH_4Cl treatment	↑↑ $[Ca^{2+}]^{in}$	↑↑ $[Ca^{2+}]^{in}$	minor ↑	no change
Cyclopiazonic acid	↑↑ $[Ca^{2+}]^{in}$	↑↑ $[Ca^{2+}]^{in}$	no changes	no change
Thapsigargin	↑ $[Ca^{2+}]^{in}$	↑ $[Ca^{2+}]^{in}$	no changes	no change

[1]bafilomycin sensitivity high is > 0.1 pH unit decrease.
[2]bafilomycin sensitivity low is < 0.05 pH unit decrease.
[3]Na^+-removal sensitivity low is < 0.2 pH unit.
[4]Na^+ removal sensitivity high is > 0.3 pH unit decrease.

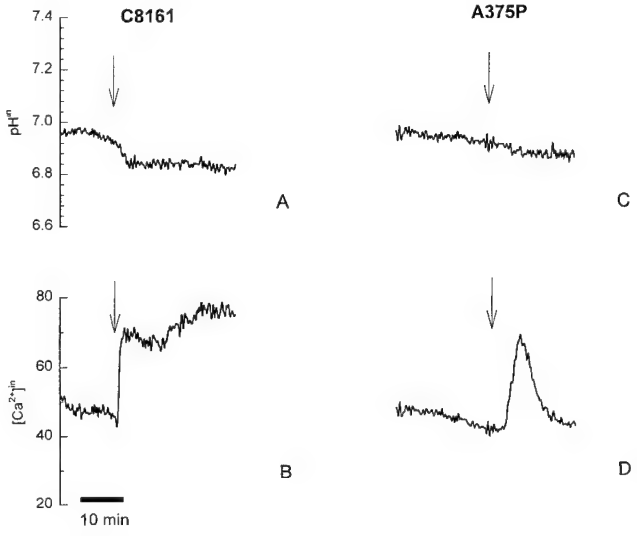

Fig. 3. Effect of the Ca^{2+} ionophore, 4Br-A23187, on pH^{in} and $[Ca^{2+}]^{in}$ in highly metastatic C8161 (**A,B**) and poorly metastatic A375P (**C,D**) human melanoma cells. Cells were handled as described in Figure 1 and co-loaded with SNARF-1 and Fura-2 to simultaneously measure pH^{in} and $[Ca^{2+}]^{in}$, respectively. Perfusion begun with HCO_3^--free CSB, pH^{ex} 7.15. At the time indicated, the perfusate was exchanged for one containing 1 μM 4Br-A23187 in HCO_3^--free CSB (arrows). Data are representative of eight experiments.

removal should reverse its direction, and increase $[Ca^{2+}]^{in}$. There was, however, a decrease in pH^{in} following Na^+ removal that was likely due to reversal of the Na^+/H^+ exchanger. The magnitude of the pH_{in} decrease was larger in A375P than in C8161 cells (vide infra).

To evaluate whether the different kinetics in the $[Ca^{2+}]^{in}$ recovery after A23187-treatment between poorly and highly metastatic cells is due to expression of distinct $[Ca^{2+}]^{in}$ regulatory mechanisms, we decided to use well-known ER-Ca^{2+}-ATPase inhibitors such as cyclopiazonic acid (CPA) and thapsigargin (TG; Seidler et al., 1989, Martínez-Zaguilán and Wesson, 1996c). Figure 4 shows that addition of CPA, an ER Ca^{2+}-ATPase inhibitor, results in a transient increase in $[Ca^{2+}]^{in}$ in C8161 cells (cf. Fig. 4B). Similar behavior regarding $[Ca^{2+}]^{in}$ increases following CPA treatment were observed in Neo-C8161 cells (Table 1, data not shown). This is in contrast to A375P cells, where CPA treatment does not result in changes in $[Ca^{2+}]^{in}$ (Fig. 4E). The lack of sensitivity to either CPA- or NH_4Cl-treatment in terms of increases in steady-state $[Ca^{2+}]^{in}$ have been also observed in the nonmetastatic C8161-d1070 cells transfected with a cytokeratin mutant (Fig. 4D). It is worthwhile to mention that C8161-d1070 not only have a decrease in their metastatic potential, but also exhibit a much lower steady-state pH^{in} and $[Ca^{2+}]^{in}$, when compared to their highly metastatic counterpart (Fig. 4). Thus these cells have also altered pH^{in} and $[Ca^{2+}]^{in}$ regulatory mechanisms. The distinct effect of CPA on $[Ca^{2+}]^{in}$ in these cells with various metastatic potentials may be due to several factors including: (1) the presence of a CPA-insensitive Ca^{2+}-ATPase in A375P and C8161-d1070 cells, (2) distinct contribution of intracellular stores to $[Ca^{2+}]^{in}$ homeostasis, or (3) the presence of distinct Ca^{2+} regulatory mechanisms. To test further for differences in sensitivity of these cells to Ca^{2+}-ATPase inhibitors, we then use TG, another ER-Ca^{2+}-ATPase inhibitor (Thastrup et al., 1990). Our results indicated that neither A375P nor C8161-d1070 cells responded with increases in steady-state $[Ca^{2+}]^{in}$ upon TG-treatment. In contrast, C8161 cells responded with minor increases in steady-state $[Ca^{2+}]^{in}$ upon TG treatment (Table 1, data not shown). A similar trend of response was observed in Neo-C8161 cells (Table 1, data not shown). The observation that C8161 (and Neo-C8161) cells responded with increases in $[Ca^{2+}]^{in}$ upon CPA treatment and (albeit to less extent) to TG, suggest that there are differences in $[Ca^{2+}]^{in}$ regulatory mechanisms between poorly metastatic and highly metastatic cells.

To evaluate the relative contribution of intracellular stores to $[Ca^{2+}]^{in}$ homeostasis in relation to Ca^{2+} fluxes from the extracellular milieu, we removed extracellular Ca^{2+} ($[Ca^{2+}]^{ex}$). We reasoned that if transmembrane

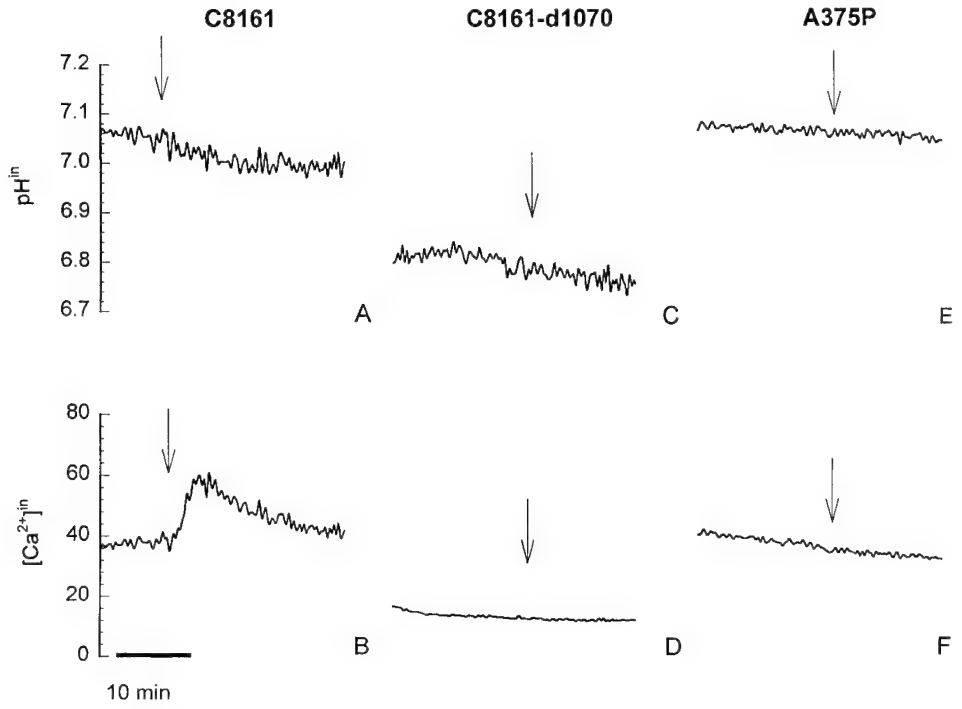

Fig. 4. Inhibition of Ca^{2+}-ATPase with cyclopiazonic acid (CPA) results in increases in $[Ca^{2+}]^{in}$ only in the highly metastatic C8161 (**A,B**) human melanoma cell line. Cells were handled as described in Figure 1. C8161-d1070 cells (**C,D**) were obtained by transfection of C8161 cells with a gene that encodes for a cytokeratin deleted at the carboxyl terminus domain. These transfected cells are nonmetastatic (Chu et al., 1991). Poorly metastatic A375P human melanoma cells are shown in **E** and **F**. Simultaneous measurements of pH^{in} and $[Ca^{2+}]^{in}$ were performed as described previously (Martínez-Zaguilán et al., 1991). Cells were perfused with HCO_3^--free CSB, pH^{ex} 7.15. At the time indicated, the perfusate was exchanged for one containing 10 μM CPA (arrows). Data is representative of 10 experiments for each cell type.

Ca^{2+} fluxes are relevant for maintenance of steady-state $[Ca^{2+}]^{in}$, this maneuver should result in cell type-dependent decreases in $[Ca^{2+}]^{in}$. As shown in Figure 5, removal of $[Ca^{2+}]^{ex}$ resulted in a rapid decrease in $[Ca^{2+}]^{in}$ in both cell types ($\Delta[Ca^{2+}]^{in}$ decrease from baseline: C8161 = -31.8 ± 1.8 nM (n = 9); and A375P = -30.2 ± 2.9 (n = 8). The magnitude of the $[Ca^{2+}]^{in}$ decrease between these cell types were not significantly different. We interpret these data to suggest that Ca^{2+} efflux is similar in both cell types. Treatment of these cells with 4Br-A23187 in the absence of $[Ca^{2+}]^{ex}$, resulted in transient increases in $[Ca^{2+}]^{in}$, which were significantly greater in C8161 than in A375P cells ($\Delta[Ca^{2+}]^{in}$ increase from baseline in the absence of $[Ca^{2+}]^{ex}$ was 11.8 ± 1.9 nM, n = 9; and 2.4 ± 0.8 nM (n = 8) for C8161 and A375P cells, respectively; $P < 0.05$). Because the magnitude of the $[Ca^{2+}]^{in}$ increase following A23187 treatment in the absence of $[Ca^{2+}]^{ex}$ was larger in C8161 than in A375P cells, we interpret these data to suggest that the Ca^{2+} from intracellular stores is readily mobilizable in C8161 than in A375P cells. An alternative explanation is that the intracellular Ca^{2+} stores are distinct in C8161 than in A375P cells.

Since there are no differences in the resting pH^{in} of poorly metastatic (A375P) and highly metastatic (C8161) melanoma cells, the question that remains is how to explain the differences in H^+-buffering capacities between these cells. A possibly explanation is that nonetheless there are no differences in steady-state pH^{in} between highly and poorly metastatic cells, they may exhibit distinct pH^{in} regulatory mechanisms. For example, they may express a lower number and/or activity of Na^+/H^+ exchangers, or increased number of alternative systems to extrude H^+. Indeed, we have previously shown that the highly metastatic C8161 human melanoma cells exhibit V-type H^+-ATPase at their plasma membranes, whereas the poorly metastatic melanoma cell line A375P do not (Martínez-Zaguilán et al., 1993). These data are supported by the observation that treatment of these cells with bafilomycin A_1 (a V-type H^+-ATPase inhibitor), decreases pH^{in} by ca. 0.1 pH unit in highly metastatic C8161 cells, whereas poorly metastatic A375P cells did not respond with significant pH^{in} changes (Fig. 6A). Moreover, Na^+-removal experiments performed in human melanoma cells indicated that resting pH^{in} decreases by 0.3 pH unit in poorly metastatic A375P cells, whereas smaller decreases in pH^{in} of 0.2 pH unit are observed in the highly metastatic C8161 cells (pH^{in} decrease from 7.06 ± 0.06 to 6.86 ± 0.04 in C8161; and from 7.09 ± 0.05 to 6.79 ± 0.045 in A375P; $P < 0.05$; Fig. 6B). Since the magnitude of the acidification upon Na^+-removal is significantly larger in the poorly metastatic A375P cells than in highly metastatic C8161 cells, this suggests that they may use either a larger number and/or a higher activity of the Na^+/H^+ exchanger to maintain pH^{in} homeostasis than highly metastatic cells. The magnitude of the decrease in pH^{in} upon Na^+-removal is relevant, especially because these experiments were performed in the ab-

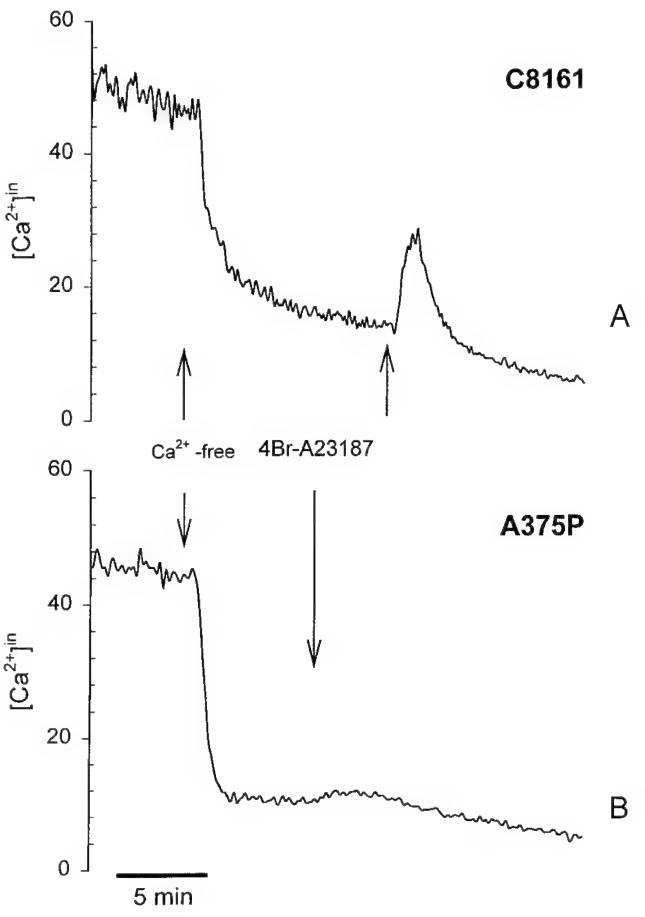

Fig. 5. Effect of $[Ca^{2+}]^{ex}$ removal and 4Br-A23187 treatment on $[Ca^{2+}]^{in}$ in highly metastatic (**A**) C8161 and poorly metastatic (**B**) A375P human melanoma cells. Cells were handled as described in Figure 3, except that at the time indicated (first arrow), media was exchanged for one lacking Ca^{2+} (supplemented with 1 mM EGTA). At the second arrow, perfusate was exchanged for one containing 1 μM 4Br-A23187, in a Ca^{2+} free buffer. Data are representative of nine and eight experiments performed in C8161 and A375P cells, respectively.

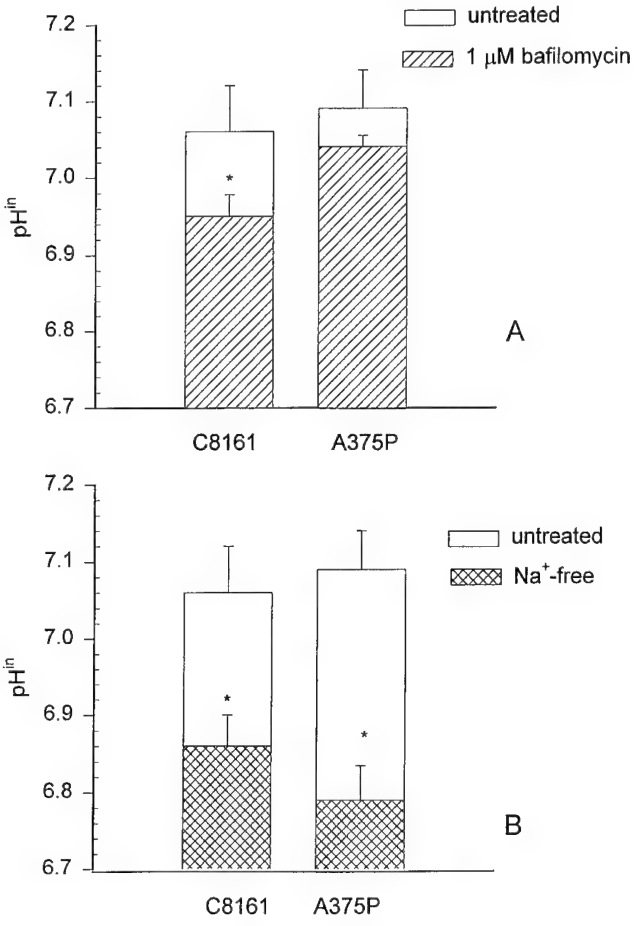

Fig. 6. Effect of bafilomycin, a V-type H^+-ATPase inhibitor (**A**), and Na^+-removal (**B**), on pH^{in} in highly metastatic C8161 and poorly metastatic A375P melanoma cells. Cells were grown onto coverslips and loaded with SNARF-1 to measure pH^{in}, as previously described (Martínez-Zaguilán et al., 1993). Subsequently, cells were transferred to the fluorometer cuvette and perfusate begun with HCO_3^--free CSB at a $pH^{ex} = 7.15$. Once steady-state pH^{in} was reached, perfusate was exchanged for one containing 1 μM bafilomycin A_1, a V-type H^+-ATPase inhibitor (A). Alternatively, perfusate was exchanged for a Na^+- and HCO_3^--free CSB at a $pH^{ex} = 7.15$. Na^+ was substituted with N-Methyl glucamine to maintain osmotic equilibrium (B). The newly resting pH after either bafilomycin addition or Na^+-removal was obtained once equilibrium was established, typically after 5 min. Data represents the mean ± S.D. of seven experiments for each condition. $^*P < 0.05$ for the following conditions: (a) bafilomycin treated versus untreated C8161 cells; (b) magnitude of the pH^{in} decrease following Na^+ removal in both A375P and C8161 cells; (c) magnitude of the acidification following Na^+ removal is significantly larger in A375P than in C8161 cells. There were no significant differences in neither steady-state pH^{in} between C8161 and A375P cells, or following bafilomycin treatment in A375P cells.

sence of HCO_3^-, so that HCO_3^--based transport mechanisms that are ubiquitous did not contribute to pH^{in} regulation (Roos and Boron, 1981; Frelin et al., 1988; Gillies et al., 1992). Therefore, under these conditions, the resting pH^{in} is maintained mainly by the activity of the Na^+/H^+ exchanger in A375P cells, and by the combined activities of the V-H^+-ATPase and the Na^+/H^+ exchanger in the highly metastatic C8161 cells.

DISCUSSION

Using simultaneous pH^{in} and $[Ca^{2+}]^{in}$ measurements, we show that the steady-state levels of these ions are similar between poorly (A375P) and highly (C8161) metastatic melanoma cells. However, there are differences in H^+- and Ca^{2+}-buffering capacities among cells with different degrees of metastatic potential. We hypothesize that these differences can be explained by expression of distinct pH^{in} and $[Ca^{2+}]^{in}$ regulatory mechanisms. Since changes in pH^{in} and $[Ca^{2+}]^{in}$ have been implicated in changes in cell motility, it is of relevance that the cells with a higher degree of invasion and motility (Martínez-Zaguilán et al., 1996a), are cells that exhibit the lower buffering capacities to these ions. Rapid ionic changes may provide a selective advantage to metastatic cells, so that invasion can ensue. Evidence for the presence of different mechanisms of $[Ca^{2+}]^{in}$ homeostasis in highly metastatic cells derive from the observation that an increase in pH^{in} triggered by NH_4Cl increases $[Ca^{2+}]^{in}$ only in highly metastatic cells, but has no effect on $[Ca^{2+}]^{in}$ in nonmetastatic, or poorly metastatic cells. In some cell types, an increase

in pH^{in} can induce $[Ca^{2+}]^{in}$ increases (Siffert and Akkerman, 1987; Lax et al., 1994; Martínez-Zaguilán et al., 1994). Such effects of pH^{in} on $[Ca^{2+}]^{in}$ can be explained by its effects on Ca^{2+} channels (i.e., opening Ca^{2+} channels; Orchrad and Kentish, 1990), or by inhibition of either the PM- or ER-Ca^{2+}-ATPase (Carafoli, 1987; Dixon and Haynes, 1990; Lytton et al., 1992). Further evidence for the existence of distinct $[Ca^{2+}]^{in}$ regulatory mechanisms in highly metastatic cells derive from our studies using ER-Ca^{2+}-ATPase inhibitors such as CPA and TG. Cyclopiazonic acid, and albeit to less extent TG, induce transient increases in $[Ca^{2+}]^{in}$ only in metastatic cells without affecting $[Ca^{2+}]^{in}$ in poorly or nonmetastatic cells (cf. Fig 4). Poorly metastatic A375P cells and the nonmetastatic C8161-d1070 did not responded to either CPA or TG with increases in steady-state $[Ca^{2+}]^{in}$. We and others have already shown that in other cell types, TG and CPA can induce several patterns of $[Ca^{2+}]^{in}$ response: transient increases (Wegner et al., 1994; Martínez-Zaguilán et al., 1994); sustained $[Ca^{2+}]^{in}$ increases (Martínez-Zaguilán et al., 1994; Lien et al., 1995); or no effects on steady-state $[Ca^{2+}]^{in}$ levels (Lax et al., 1994; Martinez et al., 1994). These various responses are cell type specific and they seem to be also related to the metabolic status of the cell (Martinez et al., 1994; Lien et al., 1995; Wang et al., 1995; see Martínez-Zaguilán and Wesson, 1996c, for a review). We have also suggested that the degree of responsiveness of cells to ER-Ca^{2+}-ATPase inhibitors is related to the coupling of glycolysis to the activity of Ca^{2+} pumps (reviewed in Martínez-Zaguilán and Wesson, 1996c). Thus it is possible that highly metastatic cells (which are more glycolytic than non metastatic cells) responded with increases in $[Ca^{2+}]^{in}$ upon CPA treatment, because the coupling of glycolysis to the activity of Ca^{2+}-ATPase is different than in nonmetastatic cells.

Because maintenance of $[Ca^{2+}]^{in}$ is strictly controlled by the equilibrium between Ca^{2+} influx pathways (across the plasma membrane) and Ca^{2+} release from intracellular stores, we have performed experiments using Ca^{2+} free buffer, to obtain some insight into the relevance of transmembrane Ca^{2+} influx/efflux pathways for $[Ca^{2+}]^{in}$ homeostasis in poorly and highly metastatic cells. Our data indicated that removal of $[Ca^{2+}]^{ex}$ resulted in similar decreases in $[Ca^{2+}]^{in}$ in both A375P and C8161 cells. We interpret these data to suggest that Ca^{2+} efflux is similar between A375P and C8161 cells. Since A23187 treatment in the absence of $[Ca^{2+}]^{ex}$ elicit significant transient $[Ca^{2+}]^{in}$ increases only in C8161 cells, these data suggest that their intracellular stores have either more mobilizable Ca^{2+} or that Ca^{2+} is more loosely bound than in A375P cells, i.e., C8161 cells have a lower Ca^{2+} buffering capacity. These data should be contrasted with that from A375P cells, where treatment with A23187, in the absence of $[Ca^{2+}]^{ex}$, does not significantly change $[Ca^{2+}]^{in}$, suggesting that their intracellular Ca^{2+} stores either bind this ion more tightly (i.e., A375P cells have a higher Ca^{2+} buffering capacity), or that their Ca^{2+} stores are more readily depleted than in C8161 cells. Further studies are needed to address these possibilities.

A higher glycolytic activity would result in enhanced production of H^+ equivalents. We have recently shown that acidic pH enhanced the metastatic potential of poorly and highly metastatic melanoma cells (Martínez-Zaguilán et al., 1996a). However, highly metastatic C8161 cells that have been transfected with a deletion cytokeratin mutant (C8161-d1070) exhibit not only a lost in their metastatic potential (Chu et al., 1991), but also a much lower steady-state pH^{in} and $[Ca^{2+}]^{in}$, when compared to their highly metastatic phenotype (cf. Fig 4). Therefore, it is unlikely that the sole difference in steady-state levels of intracellular H^+ or Ca^{2+} determine metastatic potential. Moreover, C8161-d1070 cells have also altered pH^{in} and $[Ca^{2+}]^{in}$ regulatory mechanisms. These alterations have some similarity to those observed in poorly metastatic A375P cells. Unlike C8161 cells, neither C8161-d1070 nor A375P cells responded with increases in $[Ca^{2+}]^{in}$ upon CPA-, TG-, or NH_4Cl-treatment (Fig. 4, Table 1). Therefore, our data suggest that alterations in pH^{in} and $[Ca^{2+}]^{in}$ regulatory mechanisms, and not in the steady-state levels of these ions, are relevant for the increase in metastatic potential.

It has been shown that the degree of invasiveness of tumor cells correlates positively with the levels of expression of dual intermediate filaments (Ben-ze'ev et al., 1986; Trask et al., 1990; Hendrix et al., 1992; Chu et al., 1996). Therefore, the possibility exists that intermediate filaments may be relevant for the proper membrane recycling mechanisms and that its overexpression may lead to mis-targeting and/or increase in the number of functional V-type H^+-ATPases at the plasma membrane in highly metastatic cells. Highly metastatic C8161 melanoma cells express plasmalemmal V-H^+-ATPase activity (Martínez-Zaguilán et al., 1993). In addition, higher levels of dual intermediate filament expression may be linked to the increased ability of metastatic cells to undergo deformation in the microcirculation, since cell deformability is another important factor that allows tumor cells to invade other tissues (reviewed in Fidler, 1990; Mareel et al., 1990; Starkley, 1990). This assertion is further supported by the observation that drugs that disrupt the cytoskeletal organization decreased the metastatic potential in melanoma cells (Hart et al., 1980; Ben-ze'ev et al., 1986). The mechanisms by which altered expression of dual intermediate filament suppress the metastatic potential are unknown. However, it has been suggested that intermediate filaments can act as signal transducers, delivering information from the extracellular matrix to the nucleus (Goldaman et al., 1986), and that the extracellular matrix can regulate gene expression (McDonald, 1989). It is therefore possible that, in addition to their architectural role in maintaining cell shape, dual intermediate filament may play a role in controlling cell adhesion and penetration of extracellular matrices, possibly through effects on pH^{in} and $[Ca^{2+}]^{in}$. Changes in cell shape are also associated with changes in pH^{in} and possibly $[Ca^{2+}]^{in}$ (Schwartz et al., 1989). As mentioned earlier, transfection of highly metastatic cells (C8161) with a mutated cytokeratin gene (C8161-d1070) to impair the proper functioning of intermediate filaments result in cells that are nonmetastatic and have altered $[Ca^{2+}]^{in}$ and pH^{in} regulatory mechanisms that resemble those found in poorly metastatic cells. We have also performed experiments in C8161-d1070 cells in order to evaluate whether these

cells express plasmalemmal V-H^+-ATPase and have determined that these cells are unable to recover from acid loads in the absence of Na^+, under experimental conditions where both the parental cell line (C8161) and the Neo-C8161 cells do recover. It is worthwhile to mention that A375P cells do not express plasmalemmal V-H^+-ATPase activity either. This suggest that dynamic assembly-disassembly of cytoskeleton proteins may be relevant in the process of metastasis, since it may allow the insertion of V-H^+-ATPases to the plasma membrane.

We do not believe that constant pH^{in} and $[Ca^{2+}]^{in}$ are required for metastasis. We favor the hypothesis that alterations in the metastatic potential require rapid changes in pH^{in} and $[Ca^{2+}]^{in}$. A need for rapid changes in pH^{in} and $[Ca^{2+}]^{in}$ during migration/invasion is justified since both of these ions have been implicated in the regulation of the dynamic assembly-disassembly of cytoskeleton proteins (Soifer, 1986; Stossel, 1989). These changes in cell shape and motility also involve a transition of the cytoplasmic environment from a gel state (gelation) to a sol state (solation) in the leading edge. These transitions gel-sol can also be regulated by changes in pH^{in} and $[Ca^{2+}]^{in}$. Thus we can envision a model where active association-dissociation of cytoskeleton proteins occur while sol-gel transitions in the cytoplasm modulate the force of the contraction. In support of a dual model, Giuliano and Taylor (1990) have shown that stimulation of serum-deprived cells with growth factors that are likely to induce changes in pH^{in} and $[Ca^{2+}]^{in}$ resulted in shortening of stress fibers by decreasing the gel state of the cytoplasm. Moreover, treatment of cells with cytochalasin D or B also result in a decrease in the gel state of the cytoplasm both in vitro and in situ (Kolega et al., 1991; Janson et al., 1993). These effects were also associated with disassembly of microfilaments. Therefore, we hypothesize that distinct pH^{in} and $[Ca^{2+}]^{in}$ regulatory mechanisms that allow rapid transitions in these ions are relevant for the increase in metastatic potential. We also hypothesize that the insertion of V-H^+-ATPases at the plasma membranes and altered regulation of ER-Ca^{2+}-ATPases are important elements in the acquisition of the metastatic phenotype.

ACKNOWLEDGMENTS

The authors acknowledge Dr. Yi-Wen Chu for providing us with C8161-d1070 and Neo-C8161 cells and Elisabeth Seftor for her valuable help.

LITERATURE CITED

Ben-ze'ev, A., Zoller, M., and Raz, A. (1986) Differential expression of intermediate filaments in metastasic and nonmetastasic variants of the BSp73 tumor. Cancer Res., *46:*785–790.

Busa, W.B. (1986) Mechanisms and consequences of pH-mediated cell regulation. Ann. Rev. Physiol., *48:*389–402.

Carafoli, E. (1987) Intracellular calcium homeostasis. Ann. Rev. Biochem., *56:*395–433.

Chu, Y.-W., Duffy, J.J., Seftor, R.E.B., Nagle, R.B., and Hendrix, M.J.C. (1991) Transfection of a deleted CK18 cDNA into a highly metastasic melanoma cell line decreases the invasive potential. Clin. Biotech., *3:*27–33.

Chu, Y.-W., Seftor, E.A., Romer, L.H., and Hendrix, M.J.C. (1996) Experimental coexpression of vimentin and keratin intermediate filaments in human melanoma cells augments motility. Am. J. Pathol., *148:*63–69.

Dixon, D.A., and Haynes, D.H. (1990) The pH dependence of the cardiac sarcolemmal Ca^{2+}-transporting ATPase: Evidence that the Ca^{2+} translocator bears a doubly negative charge. Biochim. Biophys. Acta, *1029:*274–284.

Fidler, I.J. (1991) Cancer metastasis. Br. Med. Bull., *47:*157–177.

Frelin, C., Vigne, P., Ladoux, A., and Lazdunski, M. (1988) The regulation of the intracellular pH in cells from vertebrates. Eur. J. Biochem., *174:*3–14.

Gillies, R.J. (1992) Nuclear magnetic resonance and its application to physiological problems. Ann. Rev. Physiol., *54:*733–748.

Gillies, R.J., and Martínez-Zaguilán, R. (1991) Regulation of intracellular pH in Balb/c-3T3 cells: Bicarbonate raises pH via $NaHCO_3$/HCl exchange and attenuates the activation of Na^+/H^+ exchange by serum. J. Biol. Chem., *266:*1551–1556.

Gillies, R.J., Martínez-Zaguilán, R., Peterson, E.P., and Perona, R. (1992) The role of intracellular pH in mammalian cell proliferation. Cell. Physiol. Biochem., *2:*159–179.

Giuliano, K.A., and Taylor, D.L. (1990) Formation, transport, contraction, and disassembly of stress fibers in fibroblasts. Cell Motil. and Cytoskeleton, *16:*14–21.

Goldaman, R.D., Goldman, A.E., and Green, K.J. (1986) Intermediate filament networks: organization and possible functions of a diverse group of cytoskeletal elements. J. Cell Sci., *5:*69–97.

Hart, I.R., Raz, A., and Fidler, I.J. (1980) Effect of cytoskeleton-disrupting agents on the metastasic behaviour of melanoma cells. J. Natl. Cancer Inst., *64:*891–899.

Hendrix, J.C., Seftor, E.A., Chu, Y.-W., Seftor, R.E.B., Nagle, R.B., McDaniel, K.M., Leong, S.P.L., Yohem, K.H., Leibovitz, A.M., Meyskens, F.L., Conaway, D.H., Welch, D.R., Liotta, L.A., and Stetler-Stevenson, W. (1992) Coexpression of vimentin and keratins by human melanoma tumor cells: correlation with invasive and metastasic potential. J. Natl. Cancer Inst., *84:*165–174.

Janson, L.W., and Taylor, D.L. (1993) In vitro models of tail contraction and cytoplasmic streaming in amoeboid cells. J. Cell Biol., *123:*345–356.

Kolega, J., Janson, L.W., and Taylor, D.L. (1991) The role of solation-contraction coupling in regulating stress fiber dynamics in nonmuscle cells. J. Cell Biol., *114:*993–1003.

Korczak, B., Whale, C., and Kerbel, R.S. (1989) Possible involvement of Ca^{2+} mobilization and protein kinase C induction of spontaneous metastasis by mouse mammary adenocarcinoma cells. Cancer Res., *49:*2597–2602.

Lattanzio, F.A. (1990) The effects of pH and temperature on fluorescent calcium indicators as determined with chelex-100 and EDTA buffer systems. Biochem. Biophys. Res. Commun., *171:*102–108.

Lax, D., Martínez-Zaguilán, R., and Gillies, R.J. (1994) Furazolidone increases thapsigargin sensitive Ca^{2+}-ATPase in chick cardiac myocytes. Am. J. Physiol. (Heart and Circ. Physiol., 36), *267:*H734–H741.

Lien, H.H., Wang, X., Gillies, R.J., and Martínez-Zaguilán, R. (1995) Modulation of intracellular free calcium by glucose in madin-darby canine kidney cells: Role of endoplasmic reticulum Ca^{2+}-ATPase. Am. J. Physiol. (Renal Fluid and Electrolyte Physiol), *268:*F671–F679.

Lytton, J., Westin, M., Burk, S.E., Shull, G.E., and McLennan, D.H. (1992) Functional comparisons between isoforms of the sarcoplasmic or endoplasmic reticulum family of calcium pumps. J. Biol. Chem., *267:*14483–14489.

Mareel, M.M., Van Roy, F.M., and De Baetselier, P. (1990) The invasive phenotype. Cancer Metastasis Rev., *9:*45–62.

Martinez, G.M., Martínez-Zaguilán, R., and Gillies, R.J. (1994) Effect of glucose on pH^{in} and $[Ca^{2+}]^{in}$ in NIH-3T3 cells transfected with the yeast P-type H^+-ATPase. J. Cell Physiol., *161:*129–141.

Martínez-Zaguilán, R., Martinez, G.M., Lattanzio, F., and Gillies, R.J. (1991) Simultaneous measurement of intracellular pH and Ca^{2+} using the fluorescence of SNARF-1 and Fura-2. Am. J. Physiol. (Cell Physiol., 29), *260:*C297–C307.

Martínez-Zaguilán, R., Lynch, R.M., Martinez, G.M., and Gillies, R.J. (1993) Vacuolar-type H^+-ATPases are functionally expressed in plasma membranes of human tumor cells. Am. J. Physiol. (Cell Physiol., 34), *265:*C1015–C1029.

Martínez-Zaguilán, R., Wegner, J., Gillies, R.J., and Hoyer, P. (1994) Differential regulation of Ca^{2+} homeostasis in ovine large and small luteal cells. Endocrinology, *135:*2099–2108.

Martínez-Zaguilán, R., Seftor, E.A., Seftor, R., Chu, Y.W., Hendrix, M.J.C., and Gillies, R.J. (1996a) Acidic pH enhances the invasive behavior of human melanoma cells. Clin. Exptl. Metastasis, *14:*176–186.

Martínez-Zaguilán, R., Gurule, and Lynch, R.M. (1996b) Simultaneous measurement of calcium and pH in insulin secreting cell lines by fluorescence spectral imaging. Am. J. Physiol. (Cell Physiol., 39), *270:*C1438–C1446.

Martínez-Zaguilán, R., and Wesson, D.E. (1996c) Regulation of endo-

plasmic reticulum (ER)-Ca^{2+}-ATPase by glycolysis in eukaryotic cells. Min. Electrolyte Metab., *22:*318–335.

McDonald, J.A. (1989) Matrix regulation of cell shape and gene expression. Curr. Opin. Cell Biol., *1:*995–999.

Miller, F.R., and Heppner, G.H. (1990) Cellular interactions in metastasis. Cancer Metastasis Rev., *9:*21–34.

Orchrad, C.H., and Kentish, J.C. (1990) Effects of changes of pH on the contractile function of cardiac muscle. Am. J. Physiol. (Cell Physiol.), *258:*C967–C981.

Pietrobon, D., DiVirgilio, F., and Pozzan, T. (1990) Structural and functional aspects of calcium homeostasis in eukaryotic cells. Eur. J. Biochem., *193:*599–622.

Roos, A., and Boron, W.F. (1981) Intracellular pH. Physiol. Rev., *61:*296–434.

Sage, S.O., van Breemen, C., and Cannell, M.B. (1991) Sodium-calcium exchange in cultured bovine pulmonary artery endothelial cells. J. Physiol., *440:*569–580.

Schlappack, O.K., Zimmermann, A., and Hill, R.P. (1991) Glucose starvation and acidosis: Effect on experimental metastasic potential, DNA content and MTX resistance of murine tumour cells. Int. J. Cancer, *64:*663–670.

Schwartz, M.A., Both, G., and Lechene, C. (1989) Effect of cell spreading on cytoplasmic pH in normal and transformed fibroblasts. Proc. Natl. Acad. Sci. USA, *86:*4525–4529.

Seidler, N.W., Jona, I., Vegh, M., and Martonosi, A. (1989) Cyclopiazonic acid is a specific inhibitor of the Ca^{2+}-ATPase of sarcoplasmic reticulum. J. Biol. Chem., *264:*17816–17823.

Siffert, W., and Akkermann, J.W.N. (1987) Activation of sodium-proton exchange is a prerequisite for Ca^{2+} mobilization in human platelets. Nature (London), *325:*456–458.

Soifer, D. (1986) Dynamic aspects of microtubule biology. Ann. N.Y. Acad. Sci., *466:*1–978.

Starkley, J.R. (1990) Cell-matrix interactions during tumor invasion. Cancer Metastasis Rev., *9:*113–123.

Stossel, T.P. (1989) From signal to pseudopod: How cells control cytoplasmic actin assembly. J. Biol. Chem., *264:*18261–18264.

Swallow, C.J., Grinstein, S., and Rotstein, O.D. (1990) A vacuolar type H^+-ATPase regulates cytoplasmic pH in murine macrophages. J. Biol. Chem., *265:*7645–7654.

Takenaga, K., and Takahashi, K. (1986) Effects of 12-O-tetradecanoylphorbol-13-acetate on adhesiveness and lung-colonization ability of Lewis lung carcinoma cells. Cancer Res., *40:*375–380.

Thastrup, O., Cullen, P.J., Drobak, B.K., Hanley, M.R., and Dawson, A.P. (1990) Thapsigargin, a tumor promoter, discharges intracellular Ca^{2+} stores by specific inhibition of the endoplasmic reticulum Ca^{2+}-ATPase. Proc. Natl. Acad. Sci. USA, *87:*2466–2470.

Trask, D.K., Band, V., Zajchowski, D.A., Yaswen, P., Suh, T., and Sager, R. (1990) Keratins as markers that distinguish normal and tumor-derived mammary epithelial cells. Proc. Natl. Acad. Sci., USA., *87:*2319–2323.

Tsien, R.Y. (1989) Fluorescent indicators of ion concentration. Meth. Cell Biol., *10:*127–1156.

Vaananen, H.K., Karhukorpi, E.-K., Sunquist, K., Wallmark, B., Roinine, I., Hentune, T., Tuukkanen, J., and Lakkakorpi, P. (1990) Evidence for the presence of H^+-ATPase type in the ruffled borders of osteoclasts. J. Cell Biol., *111:*1305–1311.

Van Adelsberg, J., and Al-Awqati, Q. (1986) Regulation of cell pH by Ca^{2+}-mediated exocytotic insertion of H^+-ATPases. J. Cell Biol., *102:*1638–1645.

Vincentini, L.M., Villarreal, M.L. (1986) Inositol phosphate turnover, cytosolic Ca^{2+} and pH: putative signals for the control of cell growth. Life Sci., *38:*2269–2276.

Vorndran, C., Minta, A., and Poenie, M. (1995) New fluorescent calcium indicators designed for cytosolic retention or measuring calcium near membranes. Biophys. J., *69:*2112–2124.

Wang, X., Lien, Y.-H.H., Gillies, R.J., and Martínez-Zaguilán, R. (1995) Glucose decreases intracellular calcium ($[Ca^{2+}]^{in}$) and pH (pH^{in}) in cultured rat vascular smooth muscle cells: Role of Ca^{2+}-ATPase. Cell. Physiol. Biochem., *5:*299–312.

Whitfield, J.F., Durkin, J.P., Franks, D.J., Kleine, L.P., Raptis, L., Rixon, R.H., Sikorska, M., and Walker, P.R. (1987) Calcium, cyclic AMP and protein kinase C: partners in mitogenesis. Cancer Metastasis Rev., *5:*205–250.

Wegner, J.A., Martínez-Zaguilán, R., Gillies, R.J., and Hoyer, P.B. (1994) Prostaglandin $F_{2\alpha}$ releases calcium from a thapsigargin-sensitive pool in ovine large luteal cells. Am. J. Physiol. (Endocrinol. Metab., 29), *266:*E50–E56.

Magnetic Resonance in Medicine 41:897–903 (1999)

Nm23-Transfected MDA-MB-435 Human Breast Carcinoma Cells Form Tumors With Altered Phospholipid Metabolism and pH: A ^{31}P Nuclear Magnetic Resonance Study In Vivo and In Vitro

Zaver M. Bhujwalla,[1]* Eric O. Aboagye,[1] Robert J. Gillies,[2] V.P. Chacko,[1] Charmaine E. Mendola,[3] and Joseph M. Backer[3]

Nm23 genes are involved in the control of the metastatic potential of breast carcinoma cells. To understand the impact of nm23 genes on tumor physiology and metabolism, a ^{31}P nuclear magnetic resonance (NMR) spectroscopic study was performed on tumors formed in the mammary fat pad of severe combined immunodeficiency mice by MDA-MB-435 human breast carcinoma cells transfected with cDNA encoding wild type nm23-H1 and nm23-H2 proteins. Tumors formed by MDA-MB-435 cells transfected with vector alone were used as controls. All transgene tumors exhibited significantly higher levels of phosphodiester (PDE) compounds relative to phosphomonoester (PME) compounds in vivo compared with control tumors. Similar differences in PDE and PME also were observed for spectra obtained from cells growing in culture. Intracellular pH was significantly lower and extracellular pH was significantly higher for transgene tumors compared with control tumors. Histologic analysis of lung sections confirmed reductions in incidence, number, and size of metastatic nodules for animals bearing transgene tumors. These results suggest that nm23 genes may affect suppression of metastasis through phospholipid-mediated signaling and cellular pH regulation. Magn Reson Med 41:897–903, 1999. © **1999 Wiley-Liss, Inc.**

Key words: human breast carcinoma metastasis; nonmetastatic 23 transfection; phospholipid metabolism and pH; ^{31}P nuclear magnetic resonance spectroscopy

The ability of solid tumors to metastasize and establish colonies at distant sites is one of the most life-threatening aspects of cancer. Despite continuing advances in the molecular characterization of events promoting metastasis, little impact has been made on therapy or survival for patients with advanced metastatic tumors (1). This is due partly to the lack of identifiable targets against which to design antineoplastic agents to control the metastatic spread of cancer. Multinuclear magnetic resonance (multi-NMR) methods have a unique role to play in answering this challenge by providing an understanding of the biochemical and physiologic mechanisms involved in invasion and metastasis. Such an understanding can identify rational targets for therapy.

Recently it was shown that the nm23 (nonmetastatic) gene is related to suppression of metastasis; the metastasis suppression function of the nm23 gene was proposed on the basis of correlation and transfection studies in murine and human systems (2,3). Two highly homologous and evolutionary conserved nm23 genes, nm23–1 and nm23–2, have been identified in rodents (4,5), and two nm23 genes (nm23-H1 and nm23-H2) have been identified in humans (6,7). The two murine nm23 genomic DNAs have been cloned and sequenced (8,9). The human nm23-H1 and nm23-H2 genes have been localized to chromosome 17q21 (10,11). These genes encode 17-kDa proteins identified as nucleoside diphosphate kinase A (NDPK A) and NDPK B, which form homomers and heteromers. In addition, NDPK B displays an increasing list of other activities that apparently are unrelated to its catalytic functions (4). However, the cellular mechanisms by which the nm23 protein suppresses metastatic phenotypic expression is still unknown. In the current study, we have used ^{31}P NMR spectroscopy to study metabolic and physiologic characteristics of tumors induced in severe combined immunodeficiency (SCID) mice by MDA-MB-435 human breast carcinoma cells transfected with wild type cDNA of nm23-H1 and nm23-H2 and demonstrated that nm23 transfection alters phospholipid metabolism and pH in these breast tumors. Histologic analysis of lung sections from tumor-bearing animals was performed to confirm decreases in metastatic behavior of these breast tumors following transfection with nm23-H1 and nm23-H2. These studies have provided further understanding of the cellular functions of nm23 and of the mechanisms of action of nm23–1 and nm23–2 genes and their role in metastatic dissemination of tumor cells.

MATERIALS AND METHODS

Coding sequences of normal nm23-H1 and nm23-H2 proteins were cloned into the eucaryotic expression vector pβalPstNeo under control of a constitutive HCMV promoter (11,12). The vector contains an neo resistance gene under control of a simian virus 24 (SV40) promoter. MDA-MB-435 breast carcinoma cells were transfected with nm23 constructs by using a Lipofectin kit (BRL-Life Technologies, Inc., Gaithersburg, MD), and selection of trans-

[1]Oncology Section-Division of Magnetic Resonance Research, Department of Radiology, The Johns Hopkins University School of Medicine, Baltimore, Maryland.

[2]Department of Biochemistry, University of Arizona, Tucson, Arizona.

[3]Department of Microbiology and Immunology, New York Medical College, Valhalla, New York.

Grant sponsor: USAMRMC; Grant numbers: DAMD17–96–1-6131, DAMD17–94–4368, CA58881–03, and DAMD17–96–6078.

Charmaine E. Mendola is currently at the Department of Pharmacology, UMDNJ-R.W. Johnson Medical School, Piscataway, NJ 08854.

*Correspondence to: Zaver M. Bhujwalla, Department of Radiology, The Johns Hopkins University School of Medicine, Room 208C Traylor Building, 720 Rutland Avenue, Baltimore, MD 21205. E-mail: zaver@mri.jhu.edu

Received 28 September 1998; revised 16 December 1998; accepted 26 December 1998.

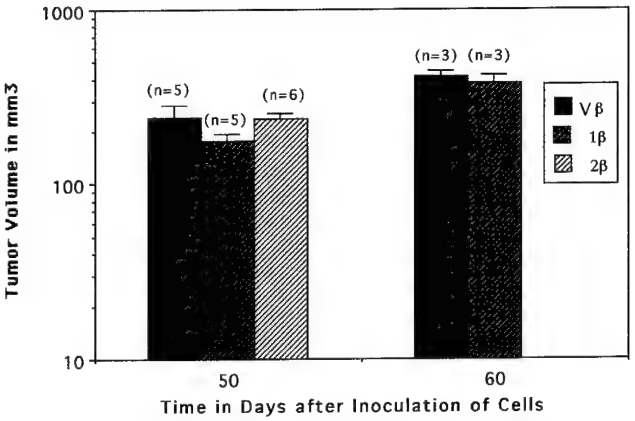

FIG. 1. Tumor volumes following inoculation of identical cell numbers (10^6 cells in 0.05 ml of Hank's balanced salt solution) in the mammary fat pad for the groups of animals used in the study. Bars represent ± 1 standard error of the mean (S.E.M.).

fected clones was performed in the presence 800 μg/ml G418. Nm23-transfected pooled clones of MDA-MB-435 were then transfected with p1Zsp-βgluc (puro), a mammalian expression vector containing bacterial β-glucuronidase under control of a constitutive HCMV promoter and puromycin-resistance gene under control of an SV40 promoter (gift from Dr. T. Jones, Lederle Laboratories). Selection of clones expressing bacterial β-glucuronidase was performed in the presence of 0.375 μg/ml puromycin and 800 μg/ml G418. Pooled clones of double-transfected cells named MDA-MB-435-Vβ, MDA-MB-453–1β, and MDA-MB-435–2β (for vector/β-glucuronidase, nm23-H1/β-glucuronidase, and nm23-H2/β-glucuronidase transfections, respectively) were maintained in the presence of 0.375 μg/ml puromycin and 200 μg/ml G418 in Dulbecco's minimum essential medium (Sigma Ltd., St. Louis, MO) containing 10% fetal bovine serum (Sigma Ltd.). Presence of transgenes was confirmed by polymerase chain reaction (PCR) analysis, Western blot analysis, and staining with 5-bromo-4-chloro-3-indol 1 glucuronide (X-glu). Cell doubling times were determined by counting cells plated in 10 mm Petri dishes (three plates per cell line) using a hemocytomter. Cells were counted 48 hr after plating 5×10^4 cells per Petri dish. Cell doubling times were approximately 1.5–2.5 days, with no significant differences between the cell lines. Mean values ± 1 standard error of the mean (S.E.M.) for the three lines were as follows: 2.3 days ± 0.4 (MDA-MB-435-Vβ), 1.5 days ± 0.1 (MDA-MB-435–1β), and 2.4 days ± 0.6 (MDA-MB-435–2β).

MDA-MB-435-Vβ, MDA-MB-435–1β, and MDA-MB-435–2β cells were inoculated in the upper left thoracic mammary fat pad of SCID mice, and 10^6 cells were inoculated in 0.05 ml of Hank's balanced salt solution (Sigma Ltd.). The experimental protocol was approved by the Institutional Animal Care and Use Committee. Mice were anesthetized with ketamine (50 mg/kg; Aveco Ltd.) and acepromazine (5 mg/kg; Aveco Ltd.). Tumor volumes, which were measured just prior to performing the ^{31}P NMR spectroscopic studies, were calculated from caliper measurements of tumor axes (a,b,c) by using the equation for an elliptical volume $(\pi/6)abc$. Volumes used in this study were of the order of 300 mm^3.

^{31}P NMR spectroscopic studies were performed on a GE CSI 4.7 T instrument (General Electric, Fremont, CA) equipped with shielded gradients. Spectra were obtained with home-built solenoidal coils fitted around the tumor. Because the coil design allowed the probe to be tuned to the proton frequency for shimming, proton images were acquired with the coil to ascertain that only the tumor (and skin) was in the sensitive volume of the coil. Animal body temperature was maintained at 37°C by heat generated

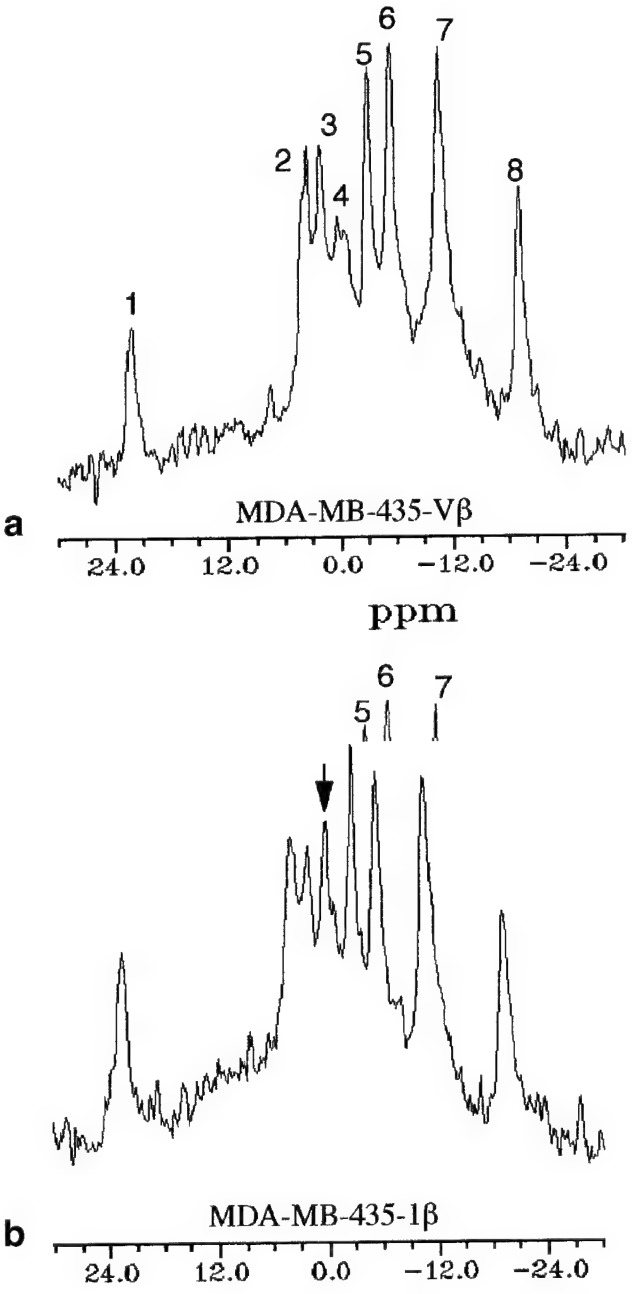

FIG. 2. Representative fully relaxed ^{31}P nuclear magnetic resonance (NMR) spectra obtained from an MDA-MB-435-Vβ tumor (**a**) and from an MDA-MB-435–1β tumor (**b**). Peak assignments are 1) 3-aminopropylphosphonate (3-APP); 2) phosphomonoester (PME); 3) inorganic phosphate (Pi); 4) phosphodiester (PDE); 5) phosphocreatine (PCr); 6) γ-nucleoside triphosphate (NTP); 7) α-NTP (set to −10 ppm); and 8) β-NTP.

from a pad circulating with warm water. For the ^{31}P NMR studies, mice were injected intraperitoneally with a solution of the extracellular pH marker 3-aminopropylphosphonate (3-APP; Sigma Ltd.) administered in a volume of 0.2 ml saline (480 mg/kg) following anesthetization. Fully relaxed ^{31}P NMR spectra were obtained by using a 45° flip angle with 64 scans, a repetition of 5 sec, and a sweep width (SW) of 10000 Hz. Parameters were determined from two spectra obtained per tumor. NMR examinations were completed within 20 min. Extracellular pH (pHe) was obtained from the chemical shift of 3-APP (13), and intracellular pH (pHi) was obtained from the chemical shift of inorganic phosphate (Pi) (14) from the endogenous reference α-nucleoside triphosphate (NTP) set to −7.57 ppm. pHe was calculated from the relationship $pH = 6.91 + \log [(\delta_{3\text{-APP}} - 21.11)/(24.30 - \delta_{3\text{-APP}})]$, and pHi was calculated from the relationship $pH = 6.66 + \log [(\delta_{Pi} - 0.65)/(3.11 - \delta_{Pi})]$. Data sets were processed by using an exponential line-broadening factor of 22 Hz. Peak areas were determined in the time domain by using an in-house, nonlinear, least-squares, curve-fitting routine for MR data analysis written by Dr. D.C. Shungu.

High-resolution spectra of perchloric acid (PCA) extracts from tumors and cell lines were obtained to resolve the components of the peak in the phosphodiester (PDE) and the phosphomonoester (PME) regions. Mice were anesthetized, and tumors were excised and immediately freeze clamped. Neutralized PCA extracts of tumors were lyophilized and resuspended in D_2O. High-resolution ^{31}P NMR spectra of tumor extracts were acquired at 11.7 T (MSL-500 spectrometer; Bruker) with a 10-mm high-resolution probe. Spectra were acquired with a 45° flip angle, an SW of 8000 Hz, a repetition time of 5 sec, a block size of 4 K, and 3600 scans.

PCA extracts were obtained from equal numbers of cells for all of the lines used in the study. Cell volumes of the lines were identical. Cells from approximately eight flasks with similar confluency for each cell line were trypsinized, and the action of trypsin was blocked with ice-cold growth medium. Cells were fed approximately 3 hr prior to trypsinization. Cells were washed twice with cold 0.9% NaCl solution and extracted with ice-cold 8% (volume/volume) PCA. The supernatant was neutralized (with 3 M K_2CO_3/1 M KOH), lyophilized, and resuspended in D_2O. Phosphorus spectra of the extracts were obtained at 11.7 T with a 10-mm high-resolution probe. Spectral acquisition parameters were 45° flip angle, SW = 8000 Hz, 5 sec repetition time, 4 K block size, and scans = 32000–128000.

Lungs from tumor-bearing animals were excised at the end of the NMR experiments and fixed in 10% buffered formalin. Three 5-μm-thick, paraffin-embedded sections were obtained from each pair of lungs and stained with hematoxylin and eosin. Lung sections were examined under an optical microscope and evaluated for incidence, number, and size of metastatic nodules.

Statistical analysis of the data was performed by using StatView II software (version 1.04; Abacus Concepts, Inc., Berkeley, CA). One factorial analysis of variance (ANOVA) was used to evaluate the statistical significance of the in vivo data.

RESULTS

All of the cell lines were tumorigenic in SCID mice, with a latent period of 5–6 weeks. Growth rates for control and transgene tumors were similar, with a volume-doubling time of 10–14 days. Tumor volumes for groups of animals inoculated at the same time are shown in Figure 1. These data demonstrate the absence of any significant differences in growth rate or "silent interval" following inoculation of the different cell lines in the mammary fat pad.

The most striking difference between ^{31}P NMR spectra of control (Fig. 2a) and transgene tumors (Fig. 2b) was a marked increase of the peak in the PDE region relative to the PME region in spectra of transgene tumors. The components of the PME region were identified as the membrane precursors phosphocholine (PC) and phosphoethanolamine (PE), and those of the PDE region were identified as the membrane breakdown products glycerophosphocholine (GPC) and glycerophosphoethanolamine (GPE). These components were identified from the high-resolution ^{31}P NMR spectra of tumor extracts by using the spectral assignments of Evanochko et al. (15). Elevation of the PDE peak relative to the PME peak was observed consistently for all transgene tumors but not for MDA-MB-435-Vβ control tumors. An example of a high-resolution spectrum obtained from PCA extracts of MDA-MB-435–1β tumors

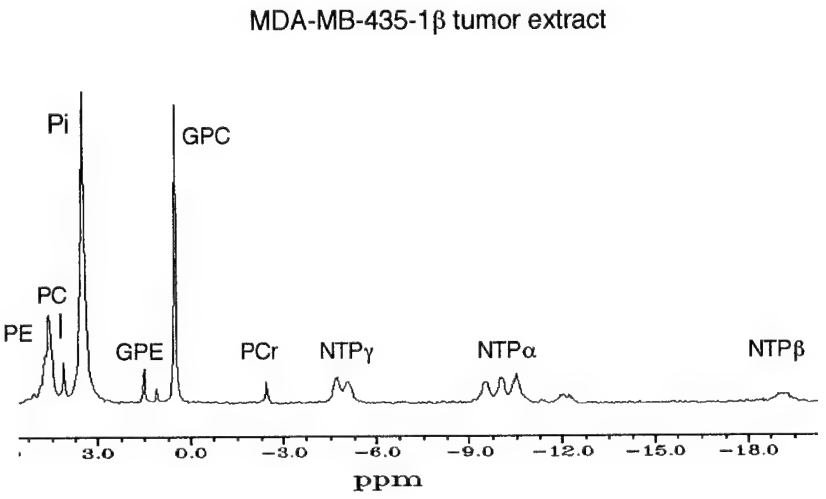

FIG. 3. High-resolution ^{31}P NMR spectrum from MDA-MB-435–1β tumor extract (obtained from three pooled tumors). Spectral acquisition parameters for in vivo tumors and extract are detailed in Materials and Methods. GPC, glycerophosphocholine; GPE, glycerophosphoethanolamine; PC, phosphocholine; PE, phosphoethanolamine.

Table 1
Nuclear Magnetic Resonance Parameters and Tumor Volumes Obtained From In Vivo Tumors Derived From Control and Transgene MDA-MD-435 Cells

Solid tumor type	Transfection and nm23 levels	Tumor volume (mm^3)	PDE/PME = [GPE + GPC] / [PE + PC]	pHi	pHe
Control MDA-MB-435-Vβ (n = 7)	Vector/β-glucuronidase transfection (low nm23-H1, H2)	324 ± 42	0.60 ± 0.05	7.37 ± 0.07	6.8 ± 0.11
Transgene MDA-MB-435-1β (n = 6)	nm23-H1/β-glucuronidase transfection (high nm23-H1)	311 ± 45	1.45 ± 0.24*	7.16 ± 0.05*	7.17 ± 0.1*
Transgene MDA-MB-435-2β (n = 6)	nm23-H2/β-glucuronidase transfection (high nm23-H2)	255 ± 19	1.36 ± 0.14*	7.15 ± 0.06*	7.09 ± 0.08*

*Ninety-five percent confidence limit ($P < 0.05$), analysis of variance, Fisher's protected least significant difference test. Values represent mean ± 1 standard error of the mean; n represents number of animals for each group; PDE, phosphodiester; PME, phosphomonoester; GPE, glycerophosphoethanolamine; GPC, glycerophosphocholine; PE, phosphoethanolamine; PC, phosphocholine; pHi, intracellular pH; pHe, extracellular pH.

with the corresponding peak assignments is shown in Figure 3.

The in vivo results for all of the animals in the study are summarized in Table 1 and show that the PDE/PME ratio was significantly higher for the transgene tumors compared with control tumors. Significant differences in pHi and pHe also were detected for the transgene tumors. pHi was significantly lower, whereas pHe was significantly higher for nm23-H1- and nm23-H2-transfected tumors compared with those derived from cells transfected with vector only (Table 1). No significant differences in NTP/Pi were detected between the cell lines.

^{31}P NMR high-resolution spectra of isolated cell extracts obtained from cells growing in tissue culture flasks for each of the transfected cell lines and the control cell line are shown in Figure 4. PDE/PME ratios obtained from cell extracts are summarized in Table 2. Observations made in vivo also were apparent in the spectra of cell extracts, suggesting that differences in PME and PDE peaks for the transgene tumors are due to intrinsic cellular properties arising from transfection of cells with nm23 rather than in vivo physiologic effects related to tumor vascularization or the fraction of necrosis.

For the evaluation of metastasis, we analyzed the lungs of five animals bearing MDA-MB-435-Vβ tumors and six animals with MDA-MB-435–1β tumors. Because the two nm23 genes (nm23-H1 and nm23-H2) are 88% to 90% identical in their amino acid sequences, respectively, we analyzed the lungs of two randomly picked animals with MDA-MB-435–2β tumors that showed no evidence of lung metastasis. Data from micrcoscopic analysis of the lung specimens obtained from tumor bearing mice are presented in Table 3. Lungs obtained from animals bearing transgene tumors showed a reduction in the incidence as well as the number and size of metastatic nodules compared with control tumors (Fig. 5).

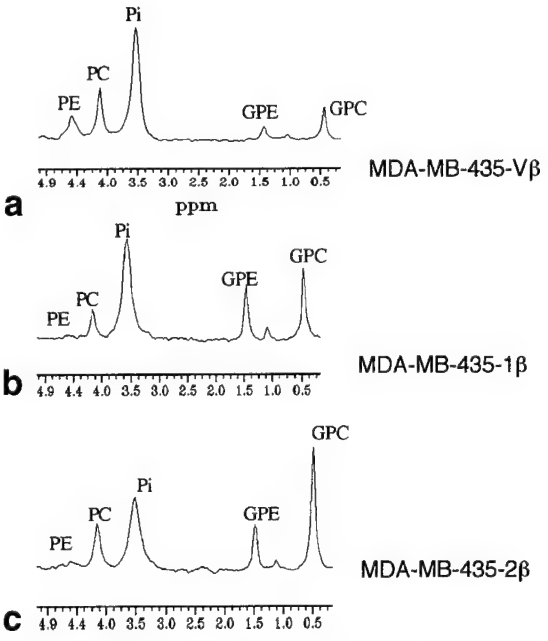

FIG. 4. High-resolution ^{31}P NMR spectra of cells from MDA-MB-435-Vβ (**a**), MDA-MB-435–1β (**b**), and MDA-MB-435–2β (**c**) cell lines maintained in tissue culture flasks. Spectra are expanded to focus on the phospholipid region. Spectral acquisition parameters are detailed in Materials and Methods.

DISCUSSION

The metastatic cascade is a complex phenomenon. To establish metastatic colonies at a site distant from the primary tumor, a cancer cell should pass successfully through the following stages: invasion, intravasation, arrest of cancer cells, extravasation, and, finally, neovascular-

Table 2
Phosphodiester/Phosphomonoester Ratios of Control and Transgene Cells

Tumor cell type	Transfection and nm23 levels	(PDE/PME) = [GPE + GPC][a] / [PE + PC]
Control MDA-MB-435-Vβ	Vector/β-glucuronidase transfection (low nm23-H1, 2)	0.53
Transgene MDA-MB-435-1β	nm23-H1/β-glucuronidase transfection (high nm23-H1)	1.96
Transgene MDA-MB-435-2β	nm23-H2/β-glucuronidase transfection (high nm23-H2)	1.7

[a]Values obtained from eight flasks per cell line. Cells were obtained from a total of eight T-150 flasks for each cell line.

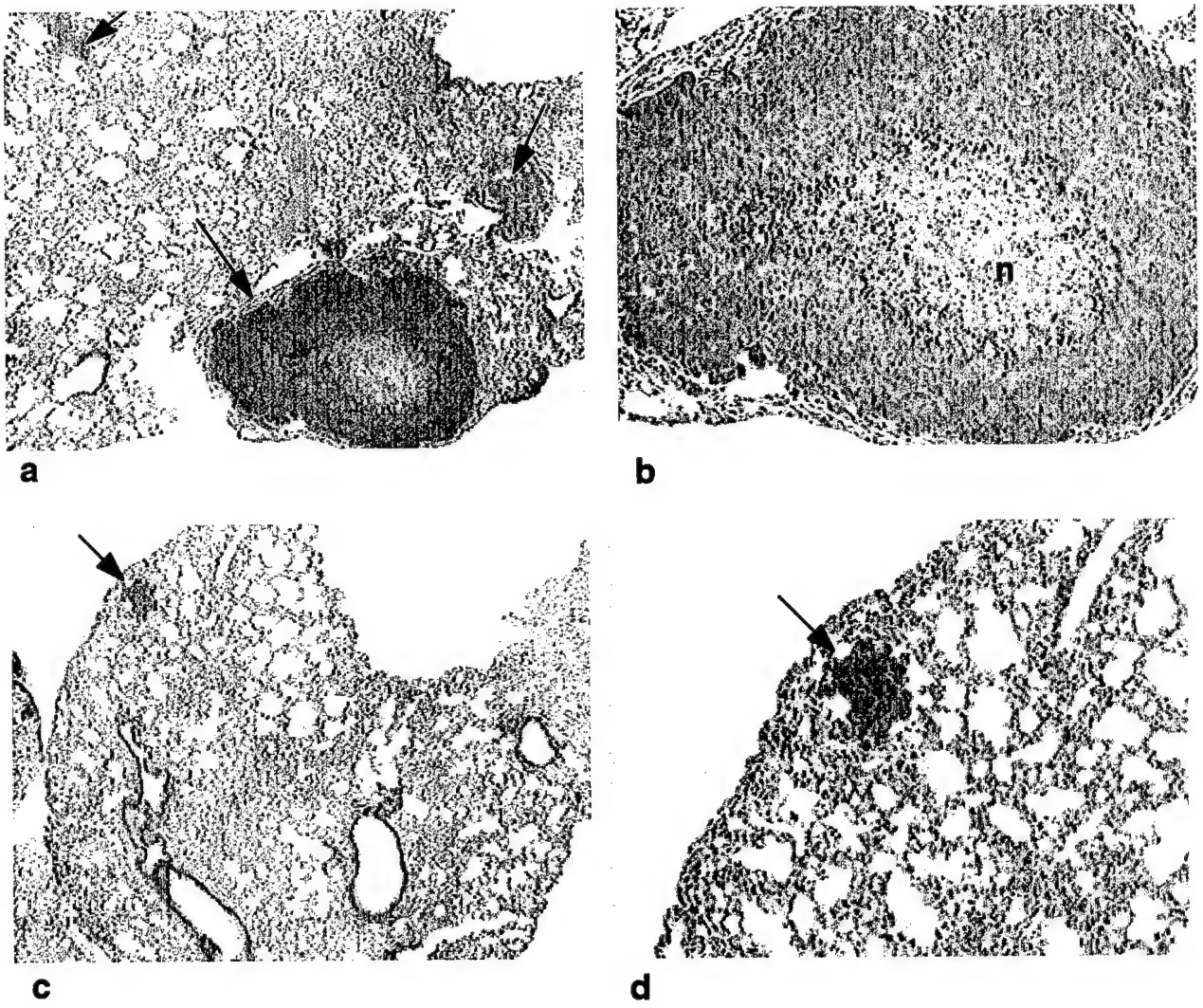

FIG. 5. Photomicrographs demonstrating the marked differences in metastatic nodules in lung sections obtained from mice bearing MDA-MB-435-Vβ and MDA-MB-435–1β tumors. **a,b:** Low- and high-power photomicrographs, respectively, from lung sections obtained from a mouse with an MDA-MB-435-Vβ tumor. **c,d:** Low- and high-power photomicrographs, respectively, from lung sections obtained from a mouse with an MDA-MB-435–1β tumor. Metastatic nodules are marked by arrows, and n denotes a region of necrosis in the metastatic nodule shown in b. No nodules were observed in lung sections that were examined for mice bearing MDA-MB-435–2β tumors.

ization. Attenuation of metastasis may occur at any of these stages. Histologic analyses of lung sections from tumor-bearing animals demonstrated that control tumors and transgene tumors formed by derivatives of MDA-MB-435 human breast carcinoma cells transfected with nm23 constructs showed different metastatic potential. ^{31}P NMR spectra of primary tumors in SCID mice revealed significant differences in the phospholipid composition, pHi, and pHe of control and transgene tumors. Because transgene tumors were formed by pooled, transfected cells, these alterations were not due to properties of individual clones. These differences in ^{31}P NMR spectra have provided an insight into how the loss of the nm23 gene induces metabolic and physiologic alterations that may facilitate metastatic dissemination.

Transgene tumors in vivo formed by wild type forms of nm23-H1 and nm23-H2 exhibited a significantly higher amount of PDE relative to PME levels compared with control tumors. These differences in phospholipid metabo-

Table 3
Incidence, Number, and Size of Metastatic Nodules Detected in Histologic Sections Obtained from Lungs of Tumor-Bearing Animals

Tumor type	Incidence of metastatic nodules[a]	Number of metastatic nodules averaged for all animals	Range of sizes of metastatic nodules
Control MDA-MB-435-Vβ	5/5	20	50–3000 μm[b]
Transgene MDA-MB-435-1β	4/6	2	50–700 μm[c]
Transgene MDA-MB-435-2β	0/2	0	—

[a]Number of animals with lungs containing metastatic nodules/number of animals with lungs examined (three histologic sections were analyzed for each lung specimen).
[b]Mean nodule diameter averaged over all the sections was 800 μm.
[c]Only one nodule was 700 μm in diameter. The remaining nodules were less than 100 μm in diameter.

Biochemical Pharmacology, Vol. 57, pp. 1037–1046, 1999.

ISSN 0006-2952/99/$–see front matter
PII S0006-2952(99)00022-2

pH and Drug Resistance. I. Functional Expression of Plasmalemmal V-type H^+-ATPase in Drug-Resistant Human Breast Carcinoma Cell Lines

Raul Martínez-Zaguilán, Natarajan Raghunand, Ronald M. Lynch, William Bellamy, Gloria M. Martinez, Bertha Rojas, Douglas Smith, William S. Dalton† and Robert J. Gillies‡*

Departments of Biochemistry, Physiology, Pathology and Pharmacology, University of Arizona Health Sciences Center, Tucson, AZ 85724-5042, U.S.A.

ABSTRACT. A major obstacle for the effective treatment of cancer is the phenomenon of multidrug resistance (MDR) exhibited by many tumor cells. Many, but not all, MDR cells exhibit membrane-associated P-glycoprotein (P-gp), a drug efflux pump. However, most mechanisms of MDR are complex, employing P-gp in combination with other, ill-defined activities. Altered cytosolic pH (pH_i) has been implicated to play a role in drug resistance. In the current study, we investigated mechanisms of pH_i regulation in drug-sensitive (MCF-7/S) and drug-resistant human breast cancer cells. Of the drug-resistant lines, one contained P-gp (MCF-7/DOX; also referred to as MCF-7/D40) and one did not (MCF-7/MITOX). The resting steady-state pH_i was similar in the three cell lines. In addition, in all the cell lines, HCO_3^- slightly acidified pH_i and increased the rates of pH_i recovery after an acid load, indicating the presence of anion exchanger (AE) activity. These data indicate that neither Na^+/H^+ exchange nor AE is differentially expressed in these cell lines. The presence of plasma membrane vacuolar-type H^+-ATPase (pmV-ATPase) activity in these cell lines was then investigated. In the absence of Na^+ and HCO_3^-, MCF-7/S cells did not recover from acid loads, whereas MCF-7/MITOX and MCF-7/DOX cells did. Furthermore, recovery of pH_i was inhibited by bafilomycin A_1 and NBD-Cl, potent V-ATPase inhibitors. Attempts to localize V-ATPase immunocytochemically at the plasma membranes of these cells were unsuccessful, indicating that V-ATPase is not statically resident at the plasma membrane. Consistent with this was the observation that release of endosomally trapped dextran was more rapid in the drug-resistant, compared with the drug-sensitive cells. Furthermore, the drug-resistant cells entrapped doxorubicin into intracellular vesicles whereas the drug-sensitive cells did not. Hence, it is hypothesized that the measured pmV-ATPase activity in the drug-resistant cells is a consequence of rapid endomembrane turnover. The potential impact of this behavior on drug resistance is examined in a companion manuscript. BIOCHEM PHARMACOL 57;9:1037–1046, 1999.

KEY WORDS. MDR; P-glycoprotein; H^+-ATPase; SNARF-1; intracellular pH; MCF-7; cancer cells; vacuolar pH

A major barrier for the effective treatment of cancer is the phenomenon of MDR§ exhibited by tumor cells [1, 2]. While some mechanisms of resistance allow cells to survive exposure to a single agent, the phenomenon of MDR confers upon cells the ability to withstand exposure to lethal doses of many structurally unrelated antineoplastic agents. Drugs commonly involved in MDR are generally natural products or their derivatives, e.g. anthracyclines, *Vinca* alkaloids, epipodophyllotoxins, and actinomycin D (reviewed in Ref. 3). Many of these are weak bases, such as the anthracycline derivatives MITOX and DOX, and their distribution thus would be affected by pH gradients (see Ref. 4). A common feature of MDR cells is a net decrease in the intracellular accumulation of drugs. MDR has been strongly linked to the overexpression of membrane-associated drug efflux pumps, P-gp or multidrug resistance-associated proteins (MRP) [5].

Alterations in pH_i homeostasis also have been implicated in drug resistance. MDR cells are sometimes observed with a more alkaline pH_i than their drug-sensitive counterparts, yet this observation is inconsistent, indicating that

* Current address: Department of Physiology, Texas Tech University Health Sciences Center, 3601 4th St., Lubbock, TX 79430.

† Current address: Moffitt Cancer Center, 12902 Magnolia Drive, Tampa, FL 33612.

‡ Corresponding author: Dr. Robert J. Gillies, Department of Biochemistry, University of Arizona Health Sciences Center, 1501 N. Campbell Ave., Tucson, AZ 85724-5042. Tel. (520) 626-5050; FAX (520) 626-5051; E-mail: Gillies@u.arizona.edu

§ *Abbreviations*: AE, anion exchanger; AM, acetoxymethyl ester; CPB, cell perfusion buffer; DOX, doxorubicin; MDR, multidrug resistant/resistance; MITOX, mitoxantrone; NHE, Na^+/H^+ exchange; P-gp, P-glycoprotein; pH_e, extracellular pH; pH_i, cytosolic pH; pH_v, endosomal/lysosomal pH; R, ratio; R_{max}, maximum ratio; R_{min}, minimum ratio; and SNARF-1, carboxy-seminaphthorhodafluor-1.

Received 20 November 1997; accepted 28 September 1998.

other processes must be involved [6–12]. The pH_i of mammalian cells is mainly regulated by the collaboration between Na^+/H^+ exchange and HCO_3^--based transport mechanisms (reviewed in Refs. 13 and 14). In some specialized cells such as kidney cells, gastric cells, hepatocytes, macrophages, and osteoclasts, vacuolar (V)-type H^+-ATPase activity has been demonstrated at the plasma membrane (pmV-ATPase) [15, 16]. Additionally, some human tumor cells also exhibit pmV-ATPase activity [17], and this pump is overexpressed in some MDR cells [18, 19]. A functional role for pmV-ATPase activity in tumor cells is not yet known.

In this study, we investigated the mechanisms of pH regulation in drug-sensitive and drug-resistant human breast cancer cell lines. The MCF-7 line was used as the experimental model because a number of clones derived from the parental cell line are available with various degrees and different mechanisms of drug resistance [20]. The parental drug-sensitive MCF-7 cell line (MCF-7/S) was used along with P-gp-negative mitoxantrone-resistant (MCF-7/MITOX) cells or P-gp-positive doxorubicin-resistant (MCF-7/DOX; also referred to as MCF-7/D40) cells. Although these cell lines were independently derived via stepwise increases in the concentration of each drug, respectively, each cell line exhibits a significant amount of cross-resistance [20].

The current experiments involved measurements of pH_i using the fluorescence of SNARF-1 [21, 22]. Additionally, pH regulation of these same cell lines has been examined in tumors *in vivo* [23]. Consistent with other tumors, the pH_e of all three cell lines decreased as a function of increased tumor size. The pH_i of the drug-sensitive tumors decreased concomitant with the decrease in pH_e, such that the pH gradient (ΔpH) remained constant. In contrast, the pH_i of the drug-resistant tumors remained constant, leading to an increase in the ΔpH with increasing tumor size. Thus, there are differences in the regulation of pH_i *in vivo* between the current drug-resistant and drug-sensitive tumor cell lines.

MATERIALS AND METHODS

Buffers and Chemicals

CPB contained the following: 0.35 mM Na_2HPO_4, 110 mM NaCl, 0.44 mM KH_2PO_4, 5.4 mM KCl, 1 mM $MgSO_4$, 1.3 mM $CaCl_2$, 25 mM HEPES, 5 mM glucose, and 2 mM L-glutamine at a pH of 7.15 at 37°. When required, CPB was supplemented with $NaHCO_3$. Organic components were added the day of experimentation in order to avoid bacterial contamination. The fluorescence ion indicators SNARF-1 and coumarin-dextran were purchased from Molecular Probes. DOX was obtained from Adria Laboratories; MITOX was from Lederle/Cyanamid. All other chemicals were obtained from the Sigma Chemical Co., unless otherwise noted.

Cell Culture

The MCF-7 parental cell line was obtained from the American Type Culture Collection, and were cultured as described previously [20]. Cells were grown in T-75 culture flasks and passed bi-weekly at an inoculation density of 2×10^5 cells/75-cm^2 flask. The cells were cultured in RPMI 1640 medium, supplemented with 10% Nu-serum (Collaborative Research), 10 mM HEPES (Organic Chemicals), 24 mM $NaHCO_3$, 0.1% (v/v) penicillin, 0.1% streptomycin, and 0.1% L-glutamine (GIBCO), pH 7.4, at 37°. These cells were maintained in a 5% CO_2 atmosphere at 37°. Selection of MITOX- or DOX-resistant cell lines was achieved as described previously [20]. Briefly, the parental MCF-7 cell line was exposed to either DOX or MITOX at initial concentrations of 1×10^{-8} M. Fresh drug was added three times per week. As allowed by cell growth, the concentration of each drug was slowly increased in a multiple-step procedure, over a period of several months (*ca.* 30 months to reach a maximum concentration of 4×10^{-7} M, representing a 40-fold increase and full development of the DOX-resistant variant). The MITOX-resistant cell line was selected in a similar fashion by increasing the MITOX concentration from 1×10^{-8} M to 8×10^{-8} M, over a period of 6 months. These cell lines have been fully characterized for growth characteristics, P-gp, chromosome analysis, and drug influx/efflux [20]. These cells are chronically cultured in media containing the highest indicated concentration of their respective drug.

Fluorometric pH_i Measurements

pH_i was determined by the fluorescence of SNARF-1, as described previously [22]. Briefly, cells were inoculated into 60-mm Petri dishes containing 9 × 22-mm cover slips at a density of 2×10^5 cells/60-mm dish in their growing medium, in the 5% CO_2 incubator for 48 hr. Two cover slips (with attached cells) were then transferred to a 60-mm Petri dish containing 7 μM SNARF-1(AM) in CPB, pH 7.15, and incubated for 30 min at 37°. The AM form of SNARF-1 is lipophilic and cell-permeant. Cytosolic esterases hydrolyze SNARF-1(AM), trapping the impermeant free acid form of the dye in the cytosol. Following this incubation, the cover slips were transferred to a 60-mm Petri dish containing CPB without dyes and incubated in a 5% CO_2 atmosphere for 30 min, to allow for complete ester hydrolysis of the dyes. The two cover slips were then placed back-to-back in a holder and put in a quartz cuvette in the spectrofluorometer, which is equipped with a flow-through device for sample perfusion. The cover slips were perfused continuously at 3 mL/min. Sample temperature was maintained by keeping both the water jacket and the perfusion medium at 37° using a circulating water bath (Lauda model RM 20, Brinkmann Instruments).

All fluorescence measurements were performed in an SLM8000C fluorometer (SLM) using 4-nm bandpass slits and an external rhodamine standard as a reference. Data

TABLE 1. ***In vitro*** **and** ***in situ*** **calibration parameters for fluorescent dyes**

	pK_a	R_{min}	R_{max}	S_{f2}/S_{b2}
SNARF				
In vitro	7.61 ± 0.08	0.46 ± 0.01	3.63 ± 0.35	0.82 ± 0.06
MCF-7/S	7.83 ± 0.10	0.45 ± 0.01	2.50 ± 0.27	0.82 ± 0.06
MCF-7/DOX	7.60 ± 0.08	0.49 ± 0.01	2.08 ± 0.17	0.89 ± 0.05
MCF-7/MITOX	7.68 ± 0.16	0.44 ± 0.01	2.13 ± 0.16	0.92 ± 0.05
Coumarin-dextran				
In vitro	6.70 ± 0.02	0.010 ± 0.002	6.05 ± 0.02	

Valure are means ± SD from calibrations performed using at least 15 different pH values.

were collected in a continuous acquisition mode in which the excitation and emission modes were alternated as follows: excitation at 534 nm with acquisitions of the emissions at 584, 600, and 644 nm (SNARF-1 conditions). The duration of this cycle was 0.109 min, and it was repeated as often as necessary. Fluorescence data were translated to ASCII format for manipulation and analysis. Ratio values obtained were converted to pH_i by the following equation:

$$pH = pK_a + \log(S_{f2}/S_{b2}) + \log[(R - R_{min})/(R_{max} - R)] \quad (1)$$

where R_{min} and R_{max} represent the 644/584 ratios of the fully protonated and fully deprotonated SNARF-1, respectively. S_{f2} and S_{b2} are the fluorescence values at 584 nm for the deprotonated and protonated forms of the dye, respectively. These are used to correct for the ion sensitivity of the denominator wavelength [22].

Measurement of Endosomal/Lysosomal and Cytosolic pH by Fluorescence

Endosomal/lysosomal and cytosolic pH were measured simultaneously using the fluorescence of 7-hydroxycoumarin conjugated to 70-kDa dextran (coumarin-dextran) and SNARF-1, respectively. Cultures on coverslips were incubated with 0.05 mg/mL of coumarin-dextran for 2–3 hr, which loads both the endosomal and lysosomal compartments to steady state. Then cells were loaded with 0.007 mM SNARF-1(AM) (*vide supra*) for 30 min, followed by 30 min in dye-free buffer to complete ester hydrolysis at 37°. Under these loading conditions, the coumarin-dextran is localized to the endosomes and lysosomes (the E-L compartment) and the de-esterified SNARF-1 is localized to the cytosol [17].

Fluorescence measurements were carried out as above, except that data were collected by sequential acquisition at excitation wavelengths of 352, 370, and 402 nm at an emission wavelength of 448 nm (coumarin-dextran conditions), followed by excitation at 534 nm, collected at emissions of 584, 600, and 644 nm (SNARF-1 conditions). Cycles were repeated every 13.3 sec. For coumarin-dextran, the ratio of fluorescence at excitations of 352 and 402 nm is pH-sensitive, whereas fluorescence at 370 nm is not (isoexcitation point). For SNARF-1, fluorescence at emissions of 584 and 644 nm is pH-sensitive, whereas fluorescence at 600 nm is not (isoemissive point). The ratio values were converted to pH values using standard calibration curves. These conditions were also used to monitor the release of dye (see below). pH recovery rates following an ammonium prepulse were measured as the slope (dpH/dt) between 5 and 8 min following the switch to NH_4Cl-free buffer. This time was chosen to represent the initial phase of pH recovery at a time after all ammonium has left the system. pH_i values during this recovery measurement period were consistently between 6.8 and 7.0.

In Situ *Calibration of Ion Indicators*

We have shown previously that the *in situ* calibration parameters of pH indicators may vary from cell type to cell type, and therefore accurate calibrations are needed to assign pH values *in situ* [22, 24]. The calibration of SNARF-1 was performed as described previously [17]. Briefly, attached (SNARF-1 loaded) cells were perfused with their corresponding high K^+ buffer plus a 6.8 μM concentration of the K^+/H^+ ionophore nigericin and 2 μM valinomycin, which elicits equilibration of cytosolic and extracellular pH, i.e. pH_i of the cells is equal to pH_e. For these experiments, pH_e was varied from pH 6.0 to 8.0. From these *in situ* calibration curves one can obtain R values at each pH_e studied. Equation (1) was then solved iteratively using nonlinear least-squares analysis (MINSQ, MicroMath Scientific Software), yielding values of R_{max}, R_{min}, and pK_a for the dye. *In vitro* and *in situ* calibration curves yielded the parameters shown in Table 1. pH_v was estimated from *in vitro* calibration curves and not from *in situ* calibration parameters due to the uncertainty of equilibration of extracellular K^+ with the lysosomal/endosomal compartments. *In vitro* pH values used for calibration were obtained with a Beckman model 71 pH meter, using a Corning glass combination electrode. The electrode was calibrated at two known temperature-controlled pH values, using commercially prepared standards from VWR Scientific.

Measurement of Endosomal Turnover Rates by Dye Release

To estimate endosomal turnover rates, cells on coverslips were incubated with coumarin-dextran as above for 2 hr at 37°. Following this incubation, two coverslips were placed back-to-back in the cuvette, and data were acquired at an emission wavelength of 448 nm and excitation wavelengths of 352, 370, and 402 nm. Then perfusion was begun with CPB. The fluorescence at 370-nm excitation was taken to represent dye concentration, since it is pH-insensitive. The decline in 370-nm fluorescence followed a double exponential curve, with the initial decay from washing adventitial dye off the surface of the cells, and the second component representing release of dye from recycling endosomes. The first component was complete within 5 min of perfusion. Hence, the time-dependent decrease in fluorescence was fit to a single exponential curve beginning 5 min after the start of perfusion. These data were obtained from all three cell lines, as well as from two negative controls: MCF-7/MITOX cells at 4° and MCF-7/MITOX cells in the presence of 0.05 mM Colcemid.

Immunocytochemistry

Cells were fixed in 4% filtered paraformaldehyde, and unreacted fixative was quenched with 25 mM glycine. Then the cells were permeabilized with 0.05% saponin for 15 min. Next the cells were incubated with a 1:10,000 dilution of Mab Fl3.2, which recognizes subunit B of the human V-type H^+-ATPase [25]. This antibody was a gift from M. Forgac, Tufts University. After staining with primary antibody for 45 min, cells were washed, and then incubated with fluorescein-conjugated anti-mouse antibody for an additional 45 min. After washing, the coverslips were mounted on microscope slides with *p*-phenylenediamine dissolved in glycerol, and sealed. Images were obtained on an Olympus IMT-2 epifluorescence microscope equipped with achromatic lenses and a liquid-cooled Photometrics CCD camera with a Tektronics (TEK-512) 512 × 512 pixel chip. Images were captured using Photometrics PMIS imaging software running on a 80486 computer with 32 Mb RAM. Image processing was performed using a Silicon Graphics Personal IRIS for image and graphics analysis and Silicon Graphics IRIS INDIGO 3000xs for computation. To image in three dimensions, the cell image was aligned in the camera field, and the image was viewed through emission filters selected for the fluorophores of interest. A computer controlled the microscope focus and the shutter of a camera. A magnetic eddy current position sensor provided precise information to the computer regarding the relative position of the objective from the sample. A series of images were collected at planes of focus minimally spaced 0.25 μm apart. Images from different focal planes through the cell were deconvolved in three dimensions using a point-spread function to provide information regarding each object in all planes of focus [26].

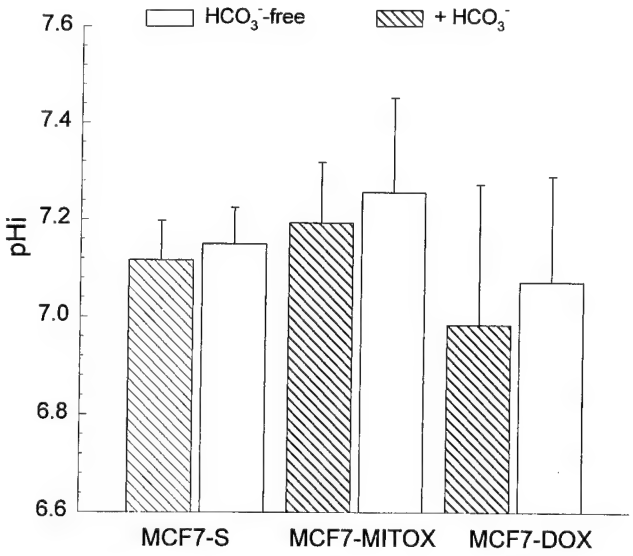

FIG. 1. Steady-state pH_i in MCF-7/S, MCF-7/MITOX, and MCF-7/DOX cell lines, in the presence and absence of HCO_3^-. Cells were grown onto cover slips for 72 hr before experiments. Thereafter, two cover slips containing cells (at subconfluence) were loaded with SNARF-1 and prepared for fluorescence experiments as described in Materials and Methods. Subsequently, two cover slips were placed (back-to-back) into a holder/perfusion device as described previously [22]. Cells were perfused continuously with CPB at a rate of 3 mL/min, and steady-state pH_i was measured. Data represent the means ± SD of nine independent measurements.

DOX Localization by Confocal Microscopy

MCF-7 cells exposed to DOX were visualized using a Zeiss model 210 confocal microscope equipped with a HeNe laser. Cells were seeded onto sterile glass coverslips at a density of 1×10^6 cells/coverslip and allowed to attach overnight prior to drug exposure. The coverslips were then placed into a modified Dvorak-Stotler controlled-environment culture chamber (Nicholson Precision Instruments, Inc.) maintained at 37° and exposed to 1 μM doxorubicin for 30 min.

RESULTS

Steady-State pH_i, Bicarbonate Transport, and Sodium-Proton Exchange

The pH_i values of drug-sensitive (MCF-7/S) and drug-resistant (MCF-7/MITOX, MCF-7/DOX) human breast carcinoma cell lines were determined under conditions where the HCO_3^--based transporting mechanisms are either inactive (absence of HCO_3^-) or active (presence of HCO_3^-). Cells were perfused in the cuvette at a rate of 3 mL/min with CPB in the presence or absence of HCO_3^- at a pH_e of 7.15. This pH_e was used because it best approximates the pH_e experienced *in vivo* [23]. As shown in Fig. 1, the steady-state pH_i of all three cell lines was higher in the absence of HCO_3^-. Furthermore, the differences in steady-state pH_i between the three cell lines were not significant, either in the presence or absence of HCO_3^-. Therefore,

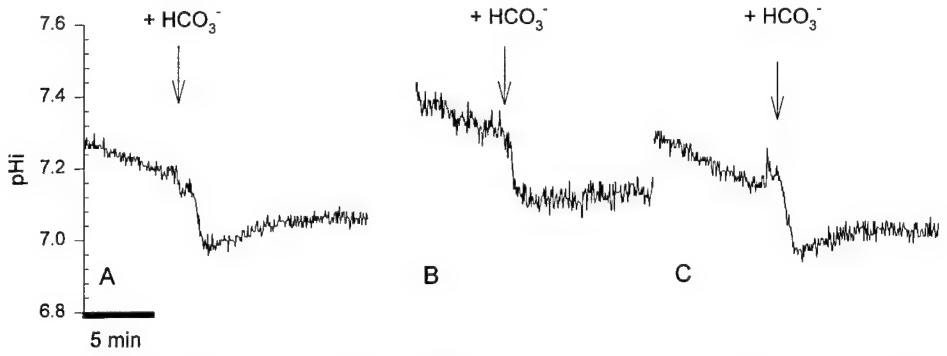

FIG. 2. Effect of HCO_3^- on pH_i in MCF-7/S (A), MCF-7/MITOX (B), and MCF-7/DOX (C) cell lines. Cells were handled as described for Fig. 1. Perfusion was begun with HCO_3^--free CPB. At the time indicated (arrow), the perfusate was exchanged for CPB containing HCO_3^-. Data are representative of five independent experiments for each cell line.

differences in steady-state pH_i cannot explain the differences in drug-sensitivity exhibited by these cell lines. Although HCO_3^- did not affect the pH_i significantly, it is still possible that HCO_3^--based H^+ transporting mechanisms participate in pH_i regulation in these cell types [27, 28].

The activity of HCO_3^- transporting mechanisms vis-à-vis the MDR phenotype was then examined. Figure 2 shows that addition of HCO_3^- to HCO_3^--depleted cells uniformly resulted in a rapid decrease in pH_i of *ca.* 0.2 pH units in all cell types. The magnitude of this decrease was not different among the three cell lines (cf. Fig. 2, A, B, and C). These data indicate that all three of these cell lines express comparable levels of a HCO_3^-/Cl^- exchanger of the AE family that works to acidify the cytosol. This was confirmed by monitoring the rate of pH_i recovery from an NH_4Cl-induced acid load in the presence and absence of HCO_3^- [13]. As shown in Fig. 3, the rate of pH_i recovery after an acid load was similar in all three cell lines, whether or not HCO_3^- was present (solid lines) or absent (dotted lines). In the absence of HCO_3^-, the predominant pH-regulatory mechanism was presumed to be Na^+/H^+ exchange (NHE-1). As shown in these figures, the rate of recovery in the presence of HCO_3^- was much greater, compared with its absence, indicating that AE is much more active in these cell lines, compared with NHE-1. Results from a number of similar experiments are presented in Table 2, and indicate that neither NHE activity nor AE activity was associated with the MDR phenotype.

Vacuolar (V)-type H$^+$-ATPase Activity at the Plasma Membrane of Drug-Resistant Cell Lines

Neither Na^+/H^+ exchange nor HCO_3^--based transporting mechanisms are related to MDR in this system. A third type of pH-regulatory activity has been observed in some tumor cells, viz. plasmalemmal vacuolar-type H^+-ATPase (pmV-ATPase) activity. To measure pmV-ATPase activity, acid loading experiments were performed in the absence of both HCO_3^- and Na^+ to inactivate both AE and NHE. Acid loads were given at a pH_e of 8.0 in order to prevent the nadir of pH_i following NH_4Cl washout from going below 6.8, where pmV-ATPase activities are reduced [17]. As shown in Fig. 4A, under these conditions MCF-7/S cells did

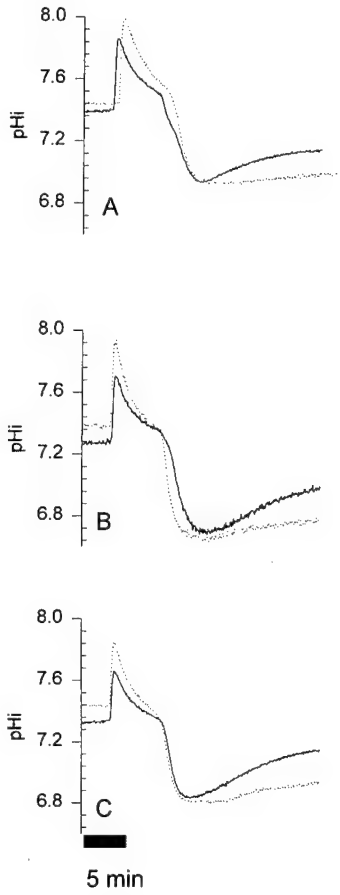

FIG. 3. Effect of NH_4Cl on pH_i in the absence and presence of HCO_3^-. MCF-7/S (A), MCF-7/MITOX (B), and MCF-7/DOX (C) cells were handled as described in the legend to Fig. 1. Cells were perfused with CPB in the absence (dotted lines) or presence (solid lines) of HCO_3^-. After 3 min, perfusate was exchanged for one containing NH_4Cl in normal or HCO_3^--free CPB, respectively. Five minutes later, perfusate was exchanged back to the original CPB (NH_4Cl-free). Data are representative of six independent experiments for each cell line.

TABLE 2. Summary of results: Rates of pH_i recovery

Condition	dpH/dt (10^{-3} pH unit/min) MCF-7/S	MCF-7/DOX	MCF-7/MITOX
HCO_3^--free + Na^+	6.65 ± 2.1 (6)	8.6 ± 2.9 (6)	10.7 ± 4.8 (6)
HCO_3^- + Na^+	25.1 ± 7.3 (6)	26.5 ± 5.1 (6)	28.5 ± 6.8 (6)
HCO_3^- & Na^+-free	2.45 ± 3.3 (9)	27.4 ± 9.4 (9)	24.1 ± 7.8 (9)
+ Bafilomycin A, 1 μM	NA	−2.8 ± 1.4 (3)	−5.3 ± 3.6 (4)
+ NBD-Cl 50 μM	NA	−7.7 ± 2.5 (6)	−10.3 ± 4.5 (6)

Values are means ± SEM of the number of experiments indicated in parentheses. dpH/dt was obtained from a plot of dpH versus time between 5 and 8 min following removal of 10 mM NH_4Cl.
NA = not applicable

not recover from NH_4Cl-induced acid loads, whereas the drug-resistant cell lines MCF-7/MITOX and MCF-7/DOX did. As explained in Materials and Methods, pH_i recovery rates in experiments such as the ones shown in Fig. 4A were measured as the slope (dpH/dt) between 5 and 8 minutes following the switch to NH_4Cl-free buffer. From a number of experiments similar to those shown in Fig. 4A, we have estimated that the rates of pH_i recovery are slightly faster in MCF-7/DOX than in MCF-7/MITOX cells, yet these differences were not significant (Table 2). The pH_i recovery was mediated via V-H^+-ATPase, since it was inhibited by bafilomycin A_1 and NBD-Cl (panels B and C of Fig. 4, Table 2). These observations indicate that pmV-ATPase activity is functionally expressed in both P-gp-positive and P-gp-negative drug-resistant cell lines, and not in the drug-sensitive cell line.

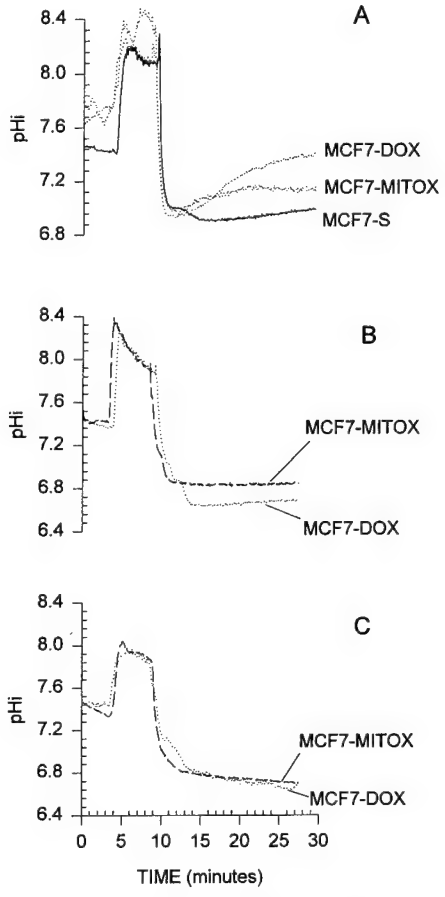

FIG. 4. (A) pH_i recovery in the absence of Na^+ and HCO_3^-. MCF-7/S, MCF-7/MITOX, and MCF-7/DOX cells were handled as described in the legend of Fig. 1. Cells were perfused for 3 min with HCO_3^--free CPB at pH_e = 8.0. Thereafter, perfusate was exchanged for CPB supplemented with 10 mM NH_4Cl, and continuously perfused for 5 min. At the end of this period of time, perfusate was exchanged for HCO_3^-- and Na^+-free CPB. (B) Effect of bafilomycin A_1 on pH_i recovery. Cells were handled as described in (A), except that the buffers contained 1 μM bafilomycin A_1 from beginning to end of the experiment. (C) Effect of NBD-Cl on pH_i recovery. Cells were handled as described in (B), except that 50 μM NBD-Cl was used instead of bafilomycin A_1.

Steady-State pH_v in Drug-Sensitive and Drug-Resistant Cell Lines

The presence of plasmalemmal V-H^+-ATPase at the plasma membranes in MDR cells, but not in sensitive cells, might be due to overexpression of V-H^+-ATPases and/or mistargeting. Previous studies by Ma and Center [19] have shown that the C-subunit of V-H^+-ATPase is overexpressed in human leukemia cells expressing the MDR phenotype. If V-ATPase were overexpressed, it might alter the steady-state pH of the endosomes or lysosomes (pH_v). Fig. 5B shows that the steady-state pH_v was not different between sensitive and resistant cell lines. Moreover, Fig. 5A shows that addition of NH_4Cl did not affect the endosomal/lysosomal compartment, suggesting that the H^+-buffering capacities in these entities are extremely high. Previous studies have shown that the "active" H^+-buffering capacity in endosomes/lysosomes is cell-type dependent and can be as high as 2.75 M H^+/pH unit [17]. These data suggest that neither the pH_v nor the H^+-buffering capacity of the endosomal/lysosomal compartments can explain the MDR phenotype.

Immunocytochemistry using monoclonal or polyclonal antibodies against the "B" subunit of V-ATPase has failed to show localization of V-ATPase at the plasma membrane, although numerous intracellular structures are labeled (e.g. Fig. 6). These data were obtained regardless of how the cells were prepared on coverslips (i.e. with fibronectin, with serum, at low or high density). These data are also consistent with those obtained from metastatic C8161 melanoma

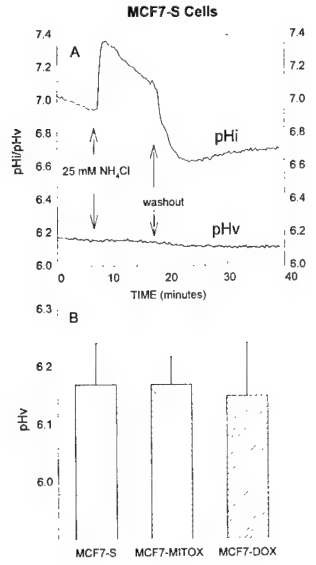

FIG. 5. (A) Effect of NH_4Cl on endosomal/lysosomal pH (pH_v) and cytosolic pH (pH_i) in MCF-7/S cells. Cells were co-loaded with SNARF-1 and coumarin-dextran, as described in Materials and Methods. Coverslips containing cells were transferred to the fluorometer cuvette, and perfusion was begun with HCO_3^--free CPB, at a pH_c of 7.15. At the time indicated, perfusate was exchanged for one containing 10 mM NH_4Cl. Data are representative of six experiments. (B) Steady-state pH_v. MCF-7/S, MCF-7/MITOX, and MCF-7/DOX cells were co-loaded with SNARF-1 and coumarin-dextran, and their pH_i and pH_v were monitored as in (A). Steady-state pH_v was measured during the first 6 min of the experiment. Data represent the means ± SD of six independent experiments.

FIG. 6. Immunocytochemistry of MCF-7/DOX cells labeled with V-ATPase antibody. MCF-7/DOX cells were grown on coverslips, fixed and stained with monoclonal antibody Fl3.2, which recognizes the "B" subunit of V-ATPase. This figure is representative of dozens of experiments under a variety of conditions, varying serum, growth status, fibronectin, and pH. MCF-7/MITOX and MCF-7/S cells showed similar staining patterns.

cells (unpublished observations), and they indicate that V-ATPase is not statically resident at the plasma membrane. Thus, the measured V-ATPase activity (i.e. H^+ extrusion in the absence of Na^+ and HCO_3^-) might result from the dynamic exocytosis of acidic vesicles and not the static residence of V-ATPase pumps at the cell surface.

Endosomal Turnover in Drug-Sensitive and Drug-Resistant Cells

Endosomal turnover was investigated by monitoring the release of endosomally trapped coumarin-dextran. Coumarin-dextran has an acidic pK_a, two pH-sensitive wavelengths (352 and 402 nm), and a pH-insensitive isoexcitation wavelength (370 nm). In these experiments, cells on coverslips were allowed to endocytose coumarin-dextran for 2–3 hr, after which they were placed in the cuvette and perfused with CPB while monitoring fluorescence at pH-sensitive and -insensitive wavelengths. Figure 7A illustrates the fluorescence at all three wavelengths prior to and during perfusion of MCF-7 cells loaded with coumarin-dextran. As shown in this figure, there was a dramatic drop in fluorescence in all three wavelengths within 1 min of the beginning of perfusions (arrow). Following this initial drop, the fluorescence at the isoemissive wavelength (370 nm) declined slowly, whereas the fluorescence intensities of the other wavelengths changed more rapidly, indicating that the pH of the environment of the dye was changing with kinetics distinct from the drop in dye concentration. The rate of decline in isoemissive fluorescence at 370 nm 10 min after the start of perfusion was taken to represent the rate at which dye is exocytosed from the endosomal/lysosomal store. This interpretation is supported by the observation that dye release was inhibited by low temperature (4°) and by 0.05 to 0.1 μM Colcemid (T and C, respectively, in Fig. 7C). Dye was released more rapidly from the drug-resistant cells. This is shown in Fig. 7B, which plots the fluorescence as a function of time in MITOX-resistant and -sensitive cells. The compiled data are shown in Fig. 7C, which shows a significantly ($P < 0.005$) higher rate of dye leakage from MITOX- (M) and DOX- (D) resistant cells compared with the parental drug-sensitive (S) cells.

DOX Sequestration in Vesicles in Drug-Resistant Cells

DOX is endogenously fluorescent. When this drug was incubated with MCF-7/DOX or MCF-7/MITOX cells, it was excluded from the nucleus and sequestered in cytoplasmic vesicles (e.g. Fig. 8). This pattern persisted for approximately 1 hr, after which time, drug was expelled completely from the cells. This is in contrast to the pattern observed in MCF-7/S cells, which stained uniformly throughout the cytoplasm and the nucleus (data not shown). *In toto*, these observations prompt the hypothesis

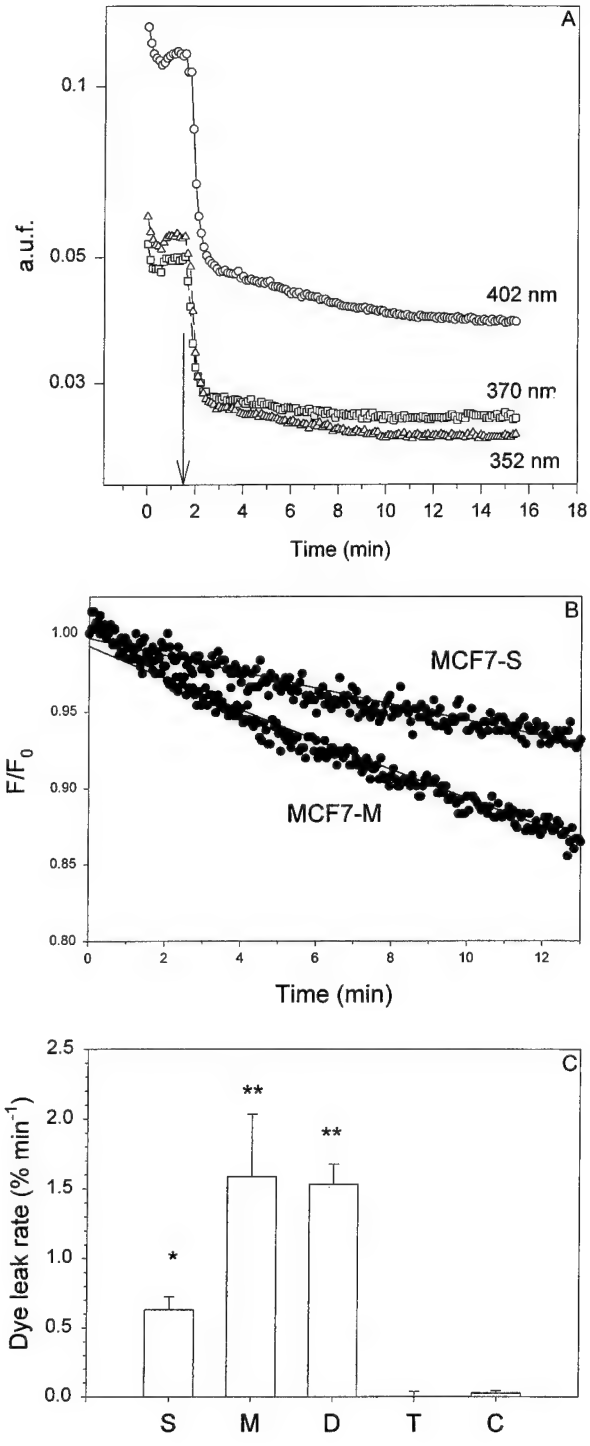

FIG. 7. (A) Fluorescence of coumarin-dextran during fluorophore-free perfusion. MCF-7/DOX cells were loaded for 2 hr with coumarin-dextran as described in Materials and Methods, after which time they were placed in a fluorometer cuvette, and fluorescence was monitored sequentially at excitation wavelengths of 352, 370, and 402 nm. Perfusion with fluorophore-free CPB was begun at 90 sec (arrow). Note that data are plotted semi-logarithmically and that fluorescence values at all three wavelengths decreased to different degrees. (B) Exocytosis in MCF-7/S and MCF-7/MITOX cells. Data were obtained as in (A) from MCF-7/S and MCF-7/MITOX cells. Time = 0 was set to 10 min after the beginning of perfusion, and all subsequent fluorescence values (F) were normalized to the value at this time (F_0). Dots indicate raw data, and lines represent the fitted first-order exponential slopes. (C) Leak rate. Data were obtained as in (A) from MCF-7/sec(S), MCF-7/MITOX (M), and MCF-7/DOX (D) cells, as well as from MCF-7/MITOX cells perfused with CPB at 4° (T) or in the presence of 50 μM Colcemid (C). Data (means ± SD) were from a minimum of three (T, C) and a maximum of 18 (S, M, D) independent measurements per condition. Leak rate is expressed as percent per minute, determined from time constants of first-order exponential fits to data as in (B). For S, $P < 0.005$ relative to all others (*). For M and D, $P < 0.001$ relative to negative controls (T, C), and $P < 0.005$ relative to S (**).

that weakly basic chemotherapeutic drugs are sequestered in a recycling acidic vesicle compartment and thus are removed rapidly from the cytosol. The implications of this are investigated in the companion manuscript [4].

DISCUSSION

Steady-State pH_i in MDR and Sensitive Cells

It has been suggested that reduced intracellular accumulation of drugs could be due to alkaline-inside pH gradients. For example, the pH_i of Chinese hamster ovary (CHO) cells resistant to colchicine (CH^RC5 cells) and that of Chinese hamster lung (CHL) cells resistant to actinomycin

FIG. 8. DOX localization by confocal microscopy. Intracellular distribution of DOX in MCF-7/DOX cells incubated in the presence of 1 μM DOX for 30 min at 37° (see text for details).

D (DC3F-ADX) is approximately 0.15 pH units higher than their parental (i.e. drug-sensitive) cell lines [9]. A trend of higher pH_i with increasing degrees of MDR also has been shown in a series of human lung tumor cell lines [10] and breast cancer cells [29]. Moreover, Roepe [30] has also shown that increased steady-state levels of chemotherapeutic drug efflux from MDR myeloma cells were correlated with intracellular alkalinization. In the same cell lines as in the current study, we have observed that the pH gradient *in vivo* is larger for the drug-resistant lines compared with the drug-sensitive lines, only at large tumor volumes [23]. Consistent with this, data from the current study indicate that, at a pH_c of 7.15, there were no significant differences in steady-state pH_i between drug-sensitive (MCF-7/S) and drug-resistant (MCF-7/DOX or MCF-7/MITOX) cell lines, regardless of the presence or absence of HCO_3^- (Fig. 1). Similarly, a lack of correlation between MDR and pH_i has been shown in MCF-7/S and Adriamycin-resistant MCF-7 cell lines [6] and in a series of sensitive and MDR human lung carcinoma cells [7]. Moreover, neither human HeLa-Pur^{RII} cells resistant to puromycin nor KB-Cl human cells resistant to colchicine exhibit a higher pH_i when compared with their sensitive parental cell lines [9]. Furthermore, Altenberg *et al.* [8] have shown that acute changes in intra- or extracellular pH do not affect P-gp-dependent drug efflux in MDR cell lines. Therefore, MDR can occur in cells with low, normal, or high pH_i. The reasons for these apparent discrepancies are unclear. It is unlikely that the lack or presence of correlation of MDR with pH_i is due to different experimental conditions but rather to the existence of multiple mechanisms of MDR. For example, Soto *et al.* [11] have found that P-gp-overexpressing murine leukemia cell lines do not have elevated pH_i, whereas P-gp negative drug-resistant cells have elevated pH_i compared with the parental drug-sensitive L1210 cell line. These data suggest that both elevated pH_i and P-gp can contribute to drug resistance in these cell lines. In the present study, we found no differences in steady-state pH_i between cells that express P-gp (MCF-7/DOX) and cells that do not (MCF-7/MITOX and MCF-7/S). This is in contrast to Roepe *et al.* [12], who observed a decrease in AE activity (and elevated pH_i) with increased P-gp transfection copy number. Differences in the activity of NHE or AE are unlikely to be related to drug resistance in the current system. Differences in NHE activity are unlikely to be involved in the MDR phenotype since, in the presence of Na^+ and in the absence of HCO_3^-, both the steady-state pH_i and the rates of pH_i recovery from acid loads were similar between drug-resistant (MCF-7/DOX and MCF-7/MITOX) and drug-sensitive (MCF-7/S) cell lines (Figs. 2 and 3). Previous studies have suggested that the differences in steady-state pH_i observed in some MDR cells could be explained by differences in the activity of NHE, since pH_i recovery was suppressed by amiloride [9]. However, those experiments were performed using the pH indicator BCECF, whose fluorescence is quenched by amiloride [27]. Thus, it is possible that the suppression of the pH_i recovery upon amiloride treatment was artifactual. This suggestion is further supported by the observation that amiloride does not reverse MDR [9]. Furthermore, the magnitude of the pH_i decrease induced by amiloride does not correlate with the degree of reversal of the MDR phenotype in a series of colon carcinoma cells with various degrees of MDR but low P-gp expression [31]. Although the mRNA encoding human NHE is overexpressed in MDR cells, the level of overexpression does not correlate with the relative drug resistance or steady-state pH_i [12].

V-type H^+-ATPase Activity in Drug-Resistant Cells

Two of the main pH_i regulatory mechanisms (Na^+/H^+ exchange and HCO_3^--based H^+-transporting mechanisms) are not different among the MCF-7/S, MCF-7/MITOX, and MCF-7/DOX cell lines. However, the drug-resistant cells express V-H^+-ATPase activity in their plasma membranes, whereas the sensitive cells do not. Previous studies have shown that the subunit C of the V-ATPase is overexpressed in HL60 cells resistant to DOX or vincristine [19]. Similar to the current system, one of the resistant lines (HL60/Vinc) exhibits high levels of P-gp, whereas the other (HL60/Adr) does not [18].

MDR and Intracellular Compartments

The current study showed a lack of staining for V-ATPase at the plasma membrane in all cell lines (Fig. 6, for example) and a higher rate of exocytosis in the cell lines exhibiting pmV-ATPase activity (Fig. 7, panels A–C). These observations suggest a role for rapid endomembrane recycling in drug-resistance. This is addressed theoretically in the companion manuscript [4]. Additionally, there is much evidence in the literature to suggest a role of intracellular compartments in resistance to chemotherapeutic drugs. Many anticancer drugs are weak bases or molecules whose binding to cellular structures is pH dependent (e.g. MITOX and DOX have pK_a values of 7.5 and 8.3, respectively). Accumulation of these drugs within cells thus will be affected by transmembrane pH gradients. Thus, if the endosomal/lysosomal pH (pH_v) were more acidic (e.g. by overexpression of V-H^+-ATPases), it would tend to enhance the accumulation of drugs in any of these compartments and reduce drug accumulation in the cytosol or nucleus. This does not seem to be the case in the present system, since the pH_v was not different between drug-sensitive and drug resistant cell lines (Fig. 5). Nevertheless, DOX and daunomycin rapidly accumulate within acidic compartments, and accumulation can be stimulated by raising pH_i [32]. Thus, the current data suggest that acidic vesicles accumulate drugs and are recycled rapidly, resulting in extrusion of drugs and H^+ from the cells. Hence, the apparent activity of V-ATPase at the plasma membrane is an epiphenomenon of rapid endomembrane recycling.

This work was supported by US Army Breast Cancer Initiative Grant DAMD17–94-J-4368.

References

1. Juranka PF, Zastawny RL and Ling V, P-glycoprotein: Multidrug-resistance and a superfamily of membrane-associated transport proteins. *FASEB J* **3:** 2583–2592, 1989.
2. Roninson IB, Molecular mechanism of multidrug resistance in tumor cells. *Clin Physiol Biochem* **5:** 140–151, 1987.
3. Moscow JA and Cowan KH, Multidrug resistance. *J Natl Cancer Inst* **80:** 14–20, 1988.
4. Raghunand N, Martínez-Zaguilán R, Wright SH and Gillies RJ, pH and drug resistance. II. Turnover of acidic vesicles and resistance to weakly basic chemotherapeutic drugs. *Biochem Pharmacol* **57**: 1047–1058, 1999.
5. Gottesman MM and Pastan I, Biochemistry of multidrug resistance mediated by the multidrug transporter. *Annu Rev Biochem* **62:** 385–427, 1993.
6. Lyon RC, Cohen JS, Faustino PJ, Megnin F and Myers CE, Glucose metabolism in drug-sensitive and drug-resistant human breast cancer cells monitored by magnetic resonance spectroscopy. *Cancer Res* **48:** 870–877, 1988.
7. Versantvoort CH, Broxterman HJ, Feller N, Dekker H and Kuiper CMLJ, Probing daunorubicin accumulation defects in non-P-glycoprotein expressing multidrug-resistant cell lines using digitonin. *Int J Cancer* **50:** 906–911, 1992.
8. Altenberg GA, Young G, Horton JK, Glass D, Belli JA and Reuss L, Changes in intra- or extracellular pH do not mediate P-glycoprotein-dependent multidrug resistance. *Proc Natl Acad Sci USA* **90:** 9735–9738, 1993.
9. Boscoboinik D, Gupta RS and Epand RM, Investigation of the relationship between altered intracellular pH and multidrug resistance in mammalian cells. *Br J Cancer* **61:** 568–572, 1990.
10. Keizer HG and Joenje H, Increased cytosolic pH in multidrug resistance human lung tumor cells: Effect of verapamil. *J Natl Cancer Inst* **81:** 706–709, 1989.
11. Soto F, Planells-Cases R, Canaves JM, Ferrer-Montiel AV, Aleu J, Gamarro F, Castanys S, Gonzalez-Ros JM and Ferragut JA, Possible coexistence of two independent mechanisms contributing to anthracycline resistance in leukaemia P388 cells. *Eur J Cancer* **29A:** 2144–2150, 1993.
12. Roepe PD, Wei LY, Cruz J and Carlson D, Lower electrical membrane potential and altered pH_i homeostasis in multidrug-resistant (MDR) cells: Further characterization of a series of MDR cell lines expressing different levels of P-glycoprotein. *Biochemistry* **32:** 11042–11056, 1993.
13. Roos A and Boron WF, Intracellular pH. *Physiol Rev* **61:** 296–434, 1981.
14. Gillies RJ, Martínez-Zaguilán R, Peterson EP and Perona R, The role of intracellular pH in mammalian cell proliferation. *Cell Physiol Biochem* **2:** 159–179, 1992.
15. Swallow CJ, Grinstein S and Rotstein OD, A vacuolar type H^+-ATPase regulates cytoplasmic pH in murine macrophages. *J Biol Chem* **265:** 7645–7654, 1990.
16. Vaananen HK, Karhukorpi E-K, Sunquist K, Wallmark B, Roinine I, Hentune T, Tuukkanen J and Lakkakorpi P, Evidence for the presence of H^+-ATPase types in the ruffled borders of osteoclasts. *J Cell Biol* **111:** 1305–1311, 1990.
17. Martínez-Zaguilán R, Lynch RM, Martinez GM and Gillies RJ, Vacuolar-type H^+-ATPases are functionally expressed in plasma membranes of human tumor cells. *Am J Physiol* **265:** C1015–C1029, 1993.
18. Marquardt D and Center MS, Involvement of vacuolar H^+-adenosine triphosphatase activity in multidrug resistance in HL60 cells. *J Natl Cancer Inst* **83:** 1098–1102, 1991.
19. Ma L and Center MS, The gene encoding vacuolar H^+-ATPase subunit C is overexpressed in multidrug-resistant HL60 cells. *Biochem Biophys Res Commun* **182:** 675–681, 1992.
20. Taylor CW, Dalton WS, Parrish PR, Gleason MC, Bellany WT, Thompson FH, Roe DJ and Trent JM, Different mechanisms of decreased drug accumulation in doxorubicin and mitoxantrone resistant variants of the MCF7 human breast cancer cell line. *Br J Cancer* **63:** 923–929, 1991.
21. Gillies RJ and Martínez-Zaguilán R, Regulation of intracellular pH in Balb/c-3T3 cells: Bicarbonate raises pH via $NaHCO_3$/HCl exchange and attenuates the activation of Na^+/H^+ exchange by serum. *J Biol Chem* **266:** 1551–1556, 1991.
22. Martínez-Zaguilán R, Martinez GM, Lattanzio F and Gillies RJ, Simultaneous measurement of intracellular pH and Ca^{2+} using the fluorescence of SNARF-1 and Fura-2. *Am J Physiol* **260:** C297–C307, 1991.
23. Raghunand N, Altbach MI, van Sluis R, Baggett B, Taylor CW, Bhujwalla ZM and Gillies RJ, Plasmalemmal pH-gradients in drug-sensitive and drug-resistant MCF-7 human breast carcinoma xenografts measured by ^{31}P magnetic resonance spectroscopy. *Biochem Pharmacol* **57**: 309–312, 1999.
24. Gillies RJ, Martínez-Zaguilán R, Martinez GM, Serrano R and Perona R, Tumorigenic 3T3 cells maintain an alkaline intracellular pH under physiological conditions. *Proc Natl Acad Sci USA* **87:** 7414–7418, 1990.
25. Puopolo K, Kumamoto C, Adachi I, Magner R and Forgac M, Differential expression of the "B" subunit of the vacuolar H^+-ATPase in bovine tissues. *J Biol Chem* **267:** 3696–3706, 1992.
26. Carrington WA, Lynch RM, Moore EDW, Isenberg G, Fogarty KE and Fay FS, Superresolution three-dimensional images of fluorescence in cells with minimal light exposure. *Science* **268:** 1483–1487, 1995.
27. Sanchez-Armass S, Martínez-Zaguilán R, Martinez GM and Gillies RJ, Regulation of pH on rat brain synaptosomes. I. Role of sodium, bicarbonate, and potassium. *J Neurophysiol* **71:** 2236–2247, 1994.
28. Martinez-Zaguilan R, Gillies RJ and Sanchez-Armass S, Regulation of pH in rat brain synaptosomes. II. Role of Cl^-. *J Neurophysiol* **71:** 2249–2257, 1994.
29. Altan N, Chen Y, Schindler M and Simon SM, Defective acidification in human breast tumor cells and implications for chemotherapy. *J Exp Med* **187:** 1583–1598, 1998.
30. Roepe PD, Analysis of the steady-state and initial rate of doxorubicin efflux from a series of multidrug-resistant cells expressing different levels of P-glycoprotein. *Biochemistry* **31:** 12555–12564, 1992.
31. Hamilton G, Cosentini EP, Teleky B, Koperna T, Zacheri J, Riegler M, Feil W, Schiessel R and Wenzi E, The multidrug-resistance modifiers verapamil, cyclosporine A and tamoxifen induce an intracellular acidification in colon carcinoma cell lines *in vitro*. *Anticancer Res* **13:** 2059–2063, 1993.
32. Simon S, Roy D and Schindler M, Intracellular pH and the control of multidrug resistance. *Proc Natl Acad Sci USA* **91:** 1128–1132, 1994.

Biochemical Pharmacology, Vol. 57, pp. 1047–1058, 1999.

ISSN 0006-2952/99/$–see front matter
PII S0006-2952(99)00021-0

pH and Drug Resistance. II. Turnover of Acidic Vesicles and Resistance to Weakly Basic Chemotherapeutic Drugs

Natarajan Raghunand, Raul Martínez-Zaguilán, Stephen H. Wright and Robert J. Gillies†*

Departments of Biochemistry and Physiology, University of Arizona Health Sciences Center, Tucson, AZ 85724-5042, U.S.A.

ABSTRACT. Resistance to chemotherapeutic agents is a major cause of treatment failure in patients with cancer. The primary mechanism leading to a multidrug-resistant phenotype is assumed to be plasma-membrane localized overexpression of drug efflux transporters, such as P-glycoprotein (P-gp). However, acidic intracellular organelles can also participate in resistance to chemotherapeutic drugs. In this study, we investigated, both experimentally and theoretically, the effect of acidic vesicle turnover on drug resistance. We have developed a general model to account for multiple mechanisms of resistance to weakly basic organic cations, e.g. anthracyclines and *Vinca* alkaloids. The model predicts that lower cytosolic concentrations of drugs can be achieved through a combination of high endosomal turnover rates, a low endosomal pH, and an alkaline-inside pH gradient between cytosol and the extracellular fluid. Measured values for these parameters have been inserted into the model. Computations using conservative values of all parameters indicate that turnover of acidic vesicles can be an important contributor to the drug-resistant phenotype, especially if vesicles contain an active uptake system, such as H^+/cation exchange. Even conservative estimates of organic cation-proton antiport activity would be sufficient to make endosomal drug extrusion a potent mechanism of resistance to weakly basic drugs. The effectiveness of such a drug export mechanism would be comparable to drug extrusion via drug pumps such as P-gp. Thus, turnover of acidic vesicles can be an important factor in chemoresistance, especially in cells that do not overexpress plasma membrane-bound drug pumps like P-glycoprotein. BIOCHEM PHARMACOL **57**;9: 1047–1058, 1999. © 1999 Elsevier Science Inc.

KEY WORDS. multidrug resistance; mathematical model; compartmentation; organic cation transport; exocytosis; vacuolar-type H^+-ATPase

Acquired resistance to chemotherapeutic agents is a major cause of treatment failure in patients with cancer [1]. In classic multidrug resistance, cells exhibit resistance to a wide range of structurally unrelated cytostatic drugs of primarily natural origin, such as anthracyclines, *Vinca* alkaloids, and epipodophyllotoxins [2]. MDR‡ cell lines have been obtained either from resistant tumors or from drug-sensitive cell lines that have been adapted in culture to progressively higher concentrations of the drug [3]. A majority of drug-resistant cells overexpress a variety of membrane proteins, the commonest among them being P-gp, a 170- to 180-kDa plasma membrane glycoprotein [4]. In addition, an MRP has been cloned from a multidrug-resistant, doxorubicin-selected cell line that did not overexpress P-gp [5]. Transfection with cDNA encoding P-gp [6, 7] or MRP [8] induces multidrug resistance in drug-sensitive cell lines. Drug-resistant cells also have been reported to overexpress vesicular proteins, such as vacuolar H^+-ATPase [9, 10] and LRP [11, 12].

To be multidrug-resistant, cells are thought to have one or both of the following features: (i) lower intracellular drug concentration [1], possibly in conjunction with compartmentation of the drug away from the site of drug action (the nucleus) [13], and/or (ii) altered susceptibility to the drug and increased repair mechanisms [14, 15]. A lower intracellular concentration of drug may be obtained by a decreased rate of uptake of drug [16, 17] or an enhanced efflux of drug from the cell. In the most widely accepted hypothesis for MDR, P-gp acts as a plasmalemmal ATP-dependent "drug pump" to extrude drug molecules from the cell (reviewed in Ref. 4). P-gp-mediated drug transport is saturable [18] and capable of acting against a concentration gradient of its substrate [19]. Molinari *et al.* [20] have

* Current address: Department of Physiology, Texas Tech University Health Sciences Center, 3601 4th St., Lubbock, TX 79430.

†Corresponding author: Dr. Robert J. Gillies, Department of Biochemistry, University of Arizona Health Sciences Center, 1501 N. Campbell Ave., Tucson, AZ 85724-5042. Tel. (520) 626-5050; FAX (520) 626-5051; E-mail: Gillies@u.arizona.edu

‡*Abbreviations:* 3-APP, 3-aminopropylphosphonate; LRP, lung resistance-Associated protein; MDR, multidrug resistance/resistant; MR, magnetic resonance; MRP, multidrug resistance-associated protein; P-gp, P-glycoprotein; pH_e, extracellular pH; pH_i, cytosolic pH; pH_v, endosomal/lysosomal pH; and SNARF-1, carboxy-seminaphthorhodafluor-1.

Received 20 November 1997; accepted 28 September 1998.

presented evidence that, in addition to being present on the plasma membrane, P-gp is also present in the Golgi apparatus of several MDR cells. There have also been an increasing number of reports of MDR cells that do not overexpress P-gp [21–23]. Daunorubicin efflux against a concentration gradient has been observed in non-small-cell lung carcinoma cells that were multidrug-resistant, but that did not overexpress P-gp, suggesting that a multidrug transporter different from P-gp is functional in these cells [24]. One such transporter could be the MRP, an ATP-binding cassette-containing transporter overexpressed in some MDR cell lines. MRP confers MDR properties on cells transfected with MRP expression vectors [25]. However, MRP is thought to be an anion transporter [25], and drugs such as anthracyclines and *Vinca* alkaloids are cations.

An alternative, yet non-exclusive, explanation for achieving lowered intracellular drug concentrations involves drug molecules being transported to and trapped in acidic vesicles, from where they are extruded from the cell by exocytosis. Sehested *et al.* [26] have reported observing greatly enhanced rates of endocytosis in Ehrlich ascites tumor cells resistant to daunorubicin, compared with their drug-sensitive parent cell line. The same authors report a 3- to 4-fold increase in endosomal volume, endosomal surface area, and number of endosomes in daunorubicin-resistant P388 leukemic cells, as compared with drug-sensitive P388 cells [27]. Sognier *et al.* [28] reported the development of a Chinese hamster cell line highly resistant to doxorubicin whose increased drug resistance seems to result not from increased P-gp expression or activity, but from a greatly increased number of endocytic vesicles as compared with the parent LZ-8 cell line. Seidel *et al.* [29] have studied the subcellular localization of daunorubicin in drug-sensitive and drug-resistant EPG85–257 gastric carcinoma cells and have found that while the drug rapidly accumulates in the nuclei of the sensitive cells, resistant cells redistribute the drug from the nucleus to perinuclear vesicles, which subsequently move to the cell periphery. The major vault protein LRP has also been hypothesized to be involved in vesicle-related extrusion of drug molecules away from cell nuclei [12].

Other evidence for the involvement of acidic vesicles in the phenomenon of MDR links vesicle alkalinization with diminished resistance to drugs. Dubowchik *et al.* [30] have found that some imidazole compounds, in addition to raising lysosomal pH, also reversed drug resistance in a doxorubicin-resistant human colon carcinoma cell line, HCT116-VM46. Sehested *et al.* [31] have employed the carboxylic ionophores monensin and nigericin, as well as exogenous amines, to raise intravesicular pH and disrupt vesicular traffic, and have found a concomitant inhibition of the MDR phenotype in daunorubicin-resistant Ehrlich ascites tumor cells. Schindler and co-workers [32] have found a similar re-sensitization of drug-resistant MCF-7adr cells upon disruption of vesicular acidification with nigericin and monensin. In this context, it is interesting that some MDR cells overexpress a subunit of the vacuolar-type H^+-ATPase (V-ATPase) [9], the proton pump responsible for vesicle acidification. In a companion manuscript [10], we report that plasma-membrane V-ATPase activity and increased rates of endosomal turnover occurred in MDR human breast carcinoma cells.

It is therefore likely that some MDR cell lines transport drug molecules from their cytosol into acidic vesicles and expel the drug by exocytosis. There is also evidence that these vesicles may be predominantly perinuclear in location, possibly affording greater protection to the nucleus [33]. Drug uptake into these vesicles can be achieved either with the activity of P-gp [34], or by the combined activity of V-type H^+-ATPase-driven acidification and an organic cation/proton antiporter. The low pH in the vesicles would cause the typical weak-base drug molecule to exist in its charged, protonated form, possibly causing it to be "trapped" in the vesicle due to the low permeability of the charged molecule to the vesicular membrane [35]. In this study, we investigated, mathematically, the efficacy of these proposed mechanisms of MDR.

MATERIALS AND METHODS

Cell Culture

Primary human tumorigenic and non-tumor cells were obtained from the Arizona Cancer Center. These have been characterized previously with respect to colony formation in soft agar, lactic acid production rates, karyotype, P-gp content, invasiveness, and expression of plasmalemmal V-type H^+-ATPase activity [36]. Established cell lines were obtained from the American Type Culture Collection or the Michigan Cancer Foundation. MCF-7 cells resistant to mitoxantrone (MCF-7/MITOX) and doxorubicin (MCF-7/D40) were generated by sequential culturing in increased concentrations of mitoxantrone and doxorubicin, respectively [21]. MCF-7/D40 cells overexpress P-gp, whereas MCF-7/MITOX cells do not [21]. Human primary cells from ACC included non-tumor fibroblasts from esophagus and foreskin. All cells were cultured in Dulbecco's modified Eagle's medium (DMEM, Gibco) supplemented with 10% Nu-serum (Collaborative Research) in a 5% CO_2 atmosphere at 37°. Cells were grown in T-75 tissue culture flasks and passed bi-weekly at an inoculation density of 2×10^5 cells/flask. For fluorescence measurements, cells were inoculated at 5×10^4 cells/60-mm Petri dish containing sterile glass coverslips (9 × 22 mm) and grown to subconfluency.

Measurement of Endosomal/Lysosomal and Cytosolic pH by Fluorescence

Endosomal and cytosolic pH were measured simultaneously using the fluorescence of 7-hydroxycoumarin conjugated to 70-kDa dextran (coumarin-dextran) and SNARF-1, respectively. Both dyes were obtained from Molecular Probes. Cultures on coverslips were incubated with 0.05 mg/mL of coumarin-dextran for 12–16 hr, after which time cells were

loaded with a 0.007 mM concentration of the acetoxymethyl ester form of SNARF-1 [SNARF-1(AM)] for 30 min, followed by a 30-min incubation in dye-free buffer to complete ester hydrolysis at 37°. Under these loading conditions, the coumarin-dextran is localized to the endosomes and lysosomes (the E–L compartment), and the de-esterified SNARF-1 is localized to the cytosol [36].

Fluorescence measurements were carried out in a temperature-controlled coverslip perfusion unit housed in an SLM-8000C spectrofluorometer (SLM Instruments) using 4-nm slits and an external rhodamine standard. Cells were perfused with Hanks' balanced salt solution supplemented with 1 mM glutamine and 2 mM glucose (HBSS-G). For simultaneous measurement of cytosolic and endosomal/lysosomal pH, data were collected by sequential acquisition at excitation wavelengths of 352, 370, and 402 nm at an emission wavelength of 448 nm (coumarin-dextran conditions), followed by excitation at 534 nm, collected at emissions of 584, 600, and 644 nm (SNARF-1 conditions). Cycles were repeated every 13.3 sec. For coumarin-dextran, the ratio of fluorescence at excitations of 352 and 402 nm is pH-sensitive, whereas fluorescence at 370 is not (isoexcitation point). For SNARF-1, the ratio of fluorescence at emissions of 584 and 644 nm is pH-sensitive, whereas fluorescence at 600 nm is not (isoemissive point). These ratio values were converted to pH values using standard calibration curves, as described by Martínez–Zaguilán *et al.* [36].

Cells and Animals Used for Tumor Growth

Severe combined immune deficient (SCID) mice were obtained from the University of Arizona SCID mouse resource. MCF-7/MITOX cells were implanted in the mammary fat pads of 6- to 7-week-old female SCID mice as a suspension of 2×10^6 cells in a total volume of 0.05 mL of Matrigel (Collaborative Research) diluted to 50% with Hanks' balanced salt solution. 17β-Estradiol pellets (0.72 mg, 60-day release, Innovative Research of America) were implanted subcutaneously on the backs of the mice by means of a 12-gauge trochar (Innovative Research) 2 days prior to tumor inoculation.

Preparation of Mice for NMR Spectroscopy

Tumors were allowed to grow for 3–8 weeks to volumes of 150-1500 mm^3, as estimated by external morphometry. Prior to MR spectroscopy, the mice were anesthetized with a combination of ketamine (72 mg/kg), xylazine (6 mg/kg), and acepromazine (6 mg/kg). A 3/4 inch, 24-G catheter (Elf Sanofi Inc.) connected to a 1 m long, 1.58 mm i.d. polyethylene tube (Becton Dickinson) was inserted into the intraperitoneal cavity of the anesthetized animal. The mouse was then immobilized on a home-built probe with a coil tunable to ^1H or ^{31}P. A solution of 3-APP (0.1 to 0.3 mL, 128 mg/mL, pH 7.4) could be injected into the mouse at the appropriate time via the i.p. catheter. This permitted the acquisition of spectra from the tumor before and after administration of 3-APP without changing the position of the animal within the magnet.

Localized In Vivo *MR Spectroscopy*

All *in vivo* measurements were performed at 4.7 T on a Bruker Biospec MR spectrometer/imager with a maximum gradient strength of 14 G/cm, using a home-built probe and solenoid coil tunable to ^1H or ^{31}P. Unlocalized ^{31}P spectra were acquired using 20–45° pulses with repetition times of 500-1000 msec. Volume-selective ^{31}P MR spectra were acquired using either VSEL, an implementation of the PRESS sequence provided by Bruker Medizintechnik, or the ISIS sequence, as previously described [37]. VSEL spectra were acquired using 764-μsec slice-selective Hemetian radiofrequency (rf) pulses (corresponding to 80 ppm in the ^{31}P spectrum), an echo time of 11.0 msec, and a repetition time of 1200 msec. ISIS spectra were acquired with adiabatic slice-selective and excitation pulses repeated every 10–12 sec. In all cases, a dwell time of 62.5 μsec was employed, and 8192 data points were collected. Transients were averaged for 10–30 min. Time-domain data were processed by exponential multiplication with a line broadening factor of 5–15 Hz, followed by Fourier transformation. The chemical shifts of 3-APP and inorganic phosphate were used to measure the extracellular and cytosolic pH values, respectively, as previously described [37–39].

Modeling the Effect of Vesicle Turnover on Drug Resistance

Our model is based upon drug molecules partitioned between four compartments: the extracellular medium, the cytosol, the perinuclear region and nucleus, and the endosomal/exocytotic vesicles (Fig. 1). Equations, discussed below, describe the flux of drug molecules between these pools. Calculations are made assuming that: (i) all cells are perfect spheres of identical geometry, (ii) endosomes are clustered in the perinuclear region, (iii) diffusional movement of the uncharged drug across a membrane is described by Fick's Law, and (iv) diffusional movement of the charged drug across a membrane is described by the constant electric field (Goldman) equation [40].

Binding of drug molecules to membranes or macromolecules is not taken into account. It is assumed that the equilibrium between free drug and drug bound with DNA and lipids is fast, and concentration of bound drug can be fully explained by partition with free drug.

FLUX OF DRUG INTO THE CYTOSOL. The flux of uncharged molecules entering the cytosol via the plasma membrane is described as a Fickian diffusion process:

$$J_{D,1} = P_{D,c}(C_{De} - C_{D1})S_{cell} \quad (1)$$

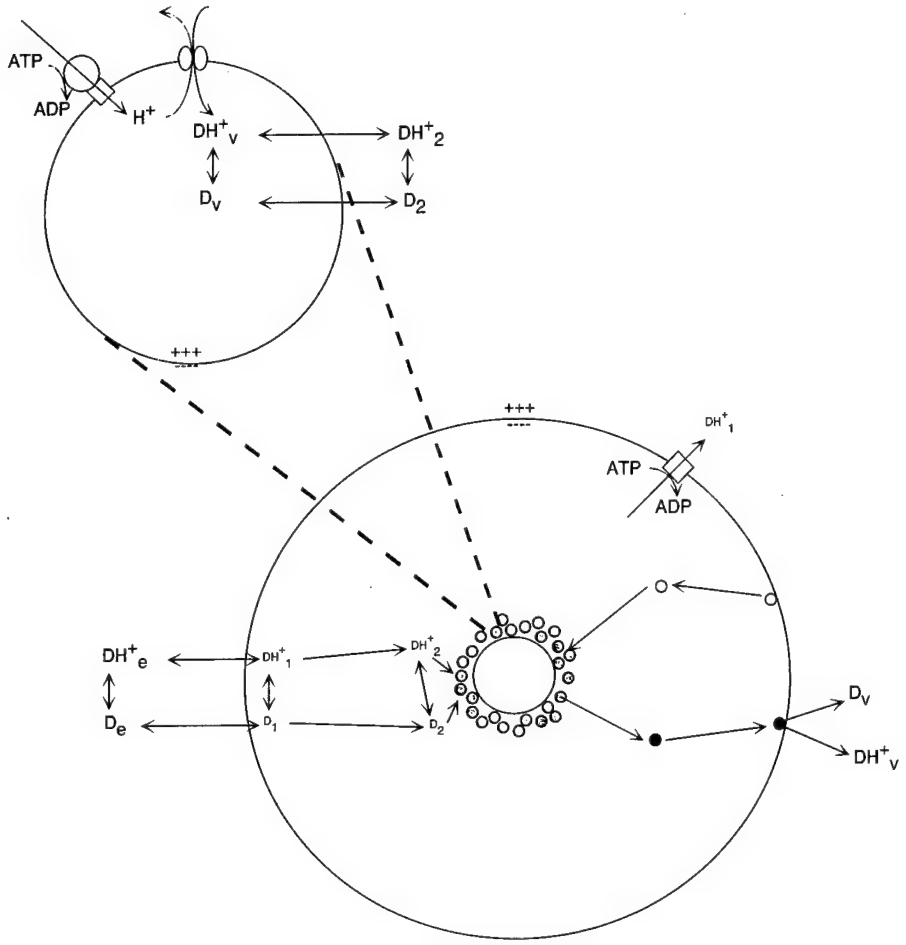

FIG. 1. Four-compartment model of drug distribution in the cell. Compartments include extracellular medium, cytosol, perinuclear region and nucleus, and endosomal/exocytotic vesicles. P-gp-mediated active transport of the drug may occur at the plasma membrane. In addition, protonated drug molecules may also be transported into endosomes by an organic cation/H^+ antiporter.

where $J_{D,1}$ stands for the molar diffusional flux of uncharged drug entering the cytosol from the extracellular medium, $P_{D,c}$ stands for the permeability of the uncharged drug to the plasma membrane, C_{De} and $C_{D,1}$ stand for the concentration of the uncharged molecule at the external and internal faces of the plasma membrane, respectively, and S_{cell} is the surface area of the plasma membrane. The amount of drug entering the cell by fluid phase endocytosis would be negligible compared with that entering by diffusion across the plasma membrane (data not shown). This term was therefore neglected in the model.

Charged drug molecules are taken to cross the plasma membrane passively, and by active transport of charged drug molecules out of the cytosol by a pump or exchanger. The passive flux of charged molecules entering the cytosol via the plasma membrane is described by the constant electric-field equation [40], whereas active transport out of the cytosol was taken to occur as per the kinetics described by Spoelstra *et al.* [41]. Thus, an equation of the following form describes the *net* movement of charged drug molecules into the cytosol:

$$J_{DH,1} = P_{DH,c}\left(\frac{\Delta\psi_{mc}F}{RT}\right) \cdot \left(\frac{C_{DHe} - C_{DH1}\exp\left(\frac{\Delta\psi_{mc}F}{RT}\right)}{\exp\left(\frac{\Delta\psi_{mc}F}{RT}\right) - 1}\right) S_{cell} - \frac{V_P[C_{DH1}]^h}{K_m^h + [C_{DH1}]^h} \quad (2)$$

where $J_{DH,1}$ represents the net molar flux of protonated drug entering the cytosol through the plasma membrane: positive for net inward flux, and negative for net outward flux. $P_{DH,c}$ is the permeability of the charged drug molecule to the plasma membrane; $\Delta\psi_{mc}$ is the plasma membrane potential ($\psi_{in} - \psi_{out}$); F is Faraday's constant; R is the gas constant; T is the absolute temperature (Kelvin); C_{DHe} and C_{DH1} are the concentrations of the protonated drug at the external and internal faces of the plasma membrane, respectively; V_P is the maximal velocity of the plasmalemmal drug efflux pump (mol/sec/cell); K_m is the Michaelis–

Menten constant for this process; and h is the Hill coefficient for binding of drug molecules to the transporter.

FREE DIFFUSION OF DRUG MOLECULES ACROSS THE CYTOSOL. In our model, drug molecules need not be homogeneously distributed in the cytosol. Instead, there can be an inwardly-directed concentration gradient from the plasma membrane toward the perinuclear region. $J_{D,2}$ and $J_{DH,2}$, the fluxes across the cytosol of the unprotonated and protonated drug molecules, respectively, represent a process of free diffusion (see Appendix):

$$J_{DH,2} = \frac{4\pi\, D_{DH}\, R_c R_P (C_{DH1} - C_{DH2})}{R_c - R_P} \tag{3}$$

$$J_{D,2} = \frac{4\pi\, D_D R_c R_P (C_{D1} - C_{D2})}{R_c - R_P} \tag{4}$$

Here, R_c is the radius of the cell; R_P is the radius of the perinuclear region; C_{D2} and C_{DH2} are the concentrations of unprotonated and protonated drug molecules at the radius R_P; and D_D and D_{DH} are the diffusivities of unprotonated and protonated drug molecules in the cytosol.

DIFFUSION OF DRUG MOLECULES INTO THE PERINUCLEAR REGION. There have been numerous reports in the literature of MDR cells displaying diminished nuclear drug accumulation [13, 42, 43], and drug sequestration in perinuclear vesicles with very little nuclear drug accumulation [33]. We have therefore modeled a situation where most of the endosomes are clustered in the perinuclear region. Drug molecules are transported from the perinuclear region into vesicles, which then move to the plasma membrane and expel the drug by exocytosis. Since the nuclear drug concentration is set by the concentration of drug around the nucleus, this transport of drug out of the perinuclear region would result in lowered nuclear drug levels at steady state. Because the positions of the endosomes in the perinuclear region will change continuously over time, the concentration of drug at any point in the region, even at steady state, will be changing constantly. The volume-averaged concentration of drug in the region, however, will not change at steady state. We have therefore modeled the perinuclear region as a region of uniform drug distribution. Thus, at steady state, the concentration of unprotonated and protonated drug molecules in the nucleus and perinuclear region will equal their concentrations at radius $r = R_P$, C_{D2} and C_{DH2}.

PASSIVE FLUX OF DRUG (MOLES/TIME) INTO ENDOSOMES. Passive movement of uncharged molecules into endosomes can be described by:

$$J_{D,3} = P_{D,v}\,(C_{D1} - C_{Dv}) S_{endo} N_{endo} \tag{5}$$

where $J_{D,3}$ is the net molar flux of uncharged drug into all the endosomes from the perinuclear region; $P_{D,v}$ stands for the permeability of the uncharged drug molecule to the endosomal membrane; C_{Dv} is the concentration of the uncharged molecule in the endosomes; S_{endo} is the surface area of a single endosome; and N_{endo} is the total number of endosomes per cell.

TRANSPORT OF PROTONATED DRUG INTO ENDOSOMES. Protonated drug may be transported across the endosomal membrane either along its electrochemical gradient, or by active transport. This active transport could be ATP dependent, as is the case with P-gp [44]. Izquierdo *et al.* [12] have hypothesized that LRP, the major vault protein, may have a transport function and may be involved in drug resistance by vesicular extrusion of drug molecules from the cell. Active transport of organic cations into endosomes may also be driven by the proton-gradient across the endosomal membrane [45, 46]. This is also an energy-dependent mechanism for drug transport into the endosomes, since the H^+ gradient across the endosomal membrane is maintained by V-type H^+-ATPases [47]. The characteristics of endosomal organic cation/H^+ exchange in the kidney and liver are the same as those measured in plasma membrane vesicles from these tissues [48–52]. Based on these studies, we have assumed the following equation to describe the dependence of transporter kinetics on $C_{DH,2}$ and vesicular pH:

$$v_{DH,v} = \frac{V_T\,[C_{DH2}][H^+]_v}{(k_{DH} + [C_{DH2}])(k_H + [H^+]_v)} \tag{6}$$

where V_T = the maximum transport rate (mol DH^+ transported/time/cell); k_{DH} = the apparent Michaelis constant of the transporter for protonated drug; k_H = the apparent Michaelis constant of the transporter for protons; and $[H^+]_v$ = the free H^+ concentration in the endosomes.

Combined with diffusive flux, the movement of charged molecules into endosomes is described by:

$$J_{DH,3} = P_{DH,v}\left(\frac{\Delta\psi_{mv}F}{RT}\right) \cdot \left(\frac{C_{DHv} - C_{DH2}\exp\left(\frac{-\Delta\psi_{mv}F}{RT}\right)}{\exp\left(\frac{-\Delta\psi_{mv}F}{RT}\right) - 1}\right) S_{endo}N_{endo} + \frac{V_T\,[C_{DH2}][10^{-pH_v}]}{k_{DH} + [C_{DH2}](k_H + [10^{-pH_v}])} \tag{7}$$

where $J_{DH,3}$ is the net molar flux of protonated drug entering all the endosomes; $P_{DH,v}$ stands for the permeability of the charged drug molecule to the endosomal membrane; $\Delta\psi_{mv}$ is the endosomal membrane potential ($\psi_{in} - \psi_{out}$); and C_{DHv} is the concentration of the protonated drug in the endosomes.

TABLE 1. Parameters used in model calculations

Symbol	Parameter	High	Low	References
pH_e	Extracellular pH	7.5	6.5	38
pH_i	Cytosolic pH	6.5	7.5	
pH_v	Endosomal /lysosomal pH	4.5	6.5	10, 46, 53, 54
T_{vc}	Rate of exocytosis (% endosomal vol.min^{-1})	10	0	10, 26
pK_a	Acid dissociation constant of the drug	9.5	7.5	55, 56
P_D	Permeability of uncharged drug ($\times 10^{-7}$ m/sec)	2.5	7.5	41, 57, 58
P_{DH}	Permeability of charged drug (rel. to P_D)	0.001	0.005	
D_D, D_{DH}	Diffusion coefficients of drug ($\times 10^{-10}$ m^2/sec)	1	5	59, 60
$\Delta\psi_{mc}$	Plasma membrane potential (mV)	−30	−80	61
$\Delta\psi_{mv}$	Endosomal membrane potential (mV)	+10	+100	
N_{endo}	Number of endosomes	50	200	27
d_{cell}	Diameter of the cell (μm)	20	10	
$V_{endo} \cdot N_{endo}$	Total endosomal volume, relative to cell volume	0.02	0.005	27
	Ratio, (perinuclear + nuclear)/cell volume	0.1	0.25	
k_{DH}	K_d of drug from cation/H^+ antiporter (μM)	1	10	49, 51
k_H	K_d of protons from cation/H^+ antiporter (M)	10^{-8}	10^{-7}	48
C_T	Initial extracellular drug concentration (μM)	1	10	21, 62
V_T	V_{max} cation/H^+ antiporter (10^{-18} mol/cell/sec)	7.5	1.0	48–52
V_P	V_{max}, P-glycoprotein (10^{-18} mol/cell/sec)	3.5	0	41
K_m	Michaelis-Menten constant for P-gp (μM)	1	5	41, 63
h	Hill coefficient for binding of drug to P-gp	1	2	41, 63

STEADY–STATE REQUIREMENTS. All parameters are modeled to determine steady-state values. Therefore, we have the following flux balance equations:

$$J_{D,1} + J_{DH,1} = J_{D,2} + J_{DH,2} \tag{8}$$

$$J_{D,2} + J_{DH,2} = J_{D,3} + J_{DH,3} \tag{9}$$

The flux into the endosomes = flux of drug out of the cell by exocytosis. Therefore,

$$J_{D,3} + J_{DH,3} = (C_{Dv} + C_{DHv})T_{vc}V_{endo}N_{endo} \tag{10}$$

where V_{endo} is the volume of a single endosome, and T_{vc} is the fractional endosomal volume exocytosed per unit time (the "turnover rate").

EQUILIBRIUM REQUIREMENTS. The equilibrium between unprotonated and protonated drug molecules is taken to be instantaneous. We therefore have the following equations:

$$C_{De} = C_{DHe} \cdot 10^{(pH_e - pK_a)} \tag{11}$$

$$C_{D1} = C_{DH1} \cdot 10^{(pH_c - pK_a)} \tag{12}$$

$$C_{D2} = C_{DH2} \cdot 10^{(pH_c - pK_a)} \tag{13}$$

$$C_{Dv} = C_{DHv} \cdot 10^{(pH_v - pK_a)} \tag{14}$$

OVERALL CONSERVATION OF DRUG. There must be a conservation of drug mass over the extracellular medium, the cytosol, and the endosomes. Since the extracellular space dominates all other volumes, we have:

$$C_{De} + C_{DHe} \approx C_T \tag{15}$$

where C_T is the total extracellular concentration of the drug. Equations 1–5 and 7–15 may be solved simultaneously once we have set values for all the parameters involved. Solutions to the model were calculated using Mathcad 5.0 (Mathsoft Inc.), and parameter values are shown in Table 1.

RESULTS

Selection of Parameters

The model describing the role of endosomal turnover in drug resistance includes several parameters, listed in Table 1. Physiologically reasonable ranges for these parameters are available in the literature, and the extremes of these ranges are presented in the table as either "low" or "high." Low values represent those extremes that contribute the least toward active efflux of the drug from the cell. This is an important point because, with so many parameters, it would be simple to choose high parameter combinations that yield maximal drug resistance yet are physiologically unreasonable. Hence, the most rigorous test of the model would employ only low values. To determine which parameters are most important to the model, we calculated the steady-state nuclear drug concentration (relative to the extracellular) in cells with all parameters set to their low values, and then iteratively determined the effects of altering single parameters. In this way, the principal components of the model could be readily determined.

One of the most important effects of pH on drug concentration ratio is the intra- to extracellular pH gradient. It can be shown that weakly basic chemotherapeutic agents will partition away from the cytosol [35, 64] simply

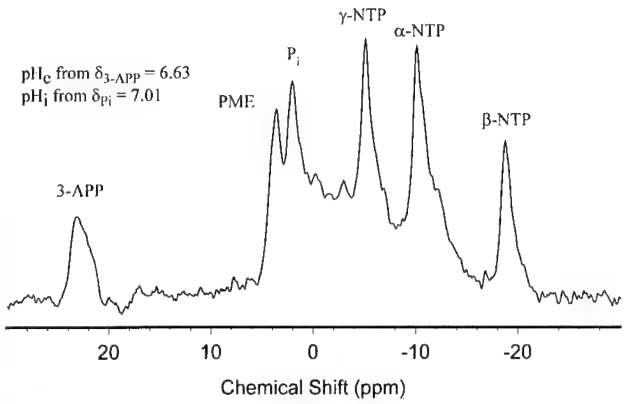

FIG. 2. ^{31}P MR spectrum acquired from a 974-mm^3 tumor of MCF-7/MITOX cells growing in the mammary fat pad of a severe combined immune deficient (SCID) mouse. An exponential line-broadening factor of 15 Hz was applied to the time-domain signal prior to Fourier transformation. P$_i$, inorganic phosphate; NTP, nucleoside triphosphates; PME, phosphomonoesters. The extracellular and cytosolic pH values reported in the figure were determined from the chemical shift of 3-APP and P$_i$, respectively.

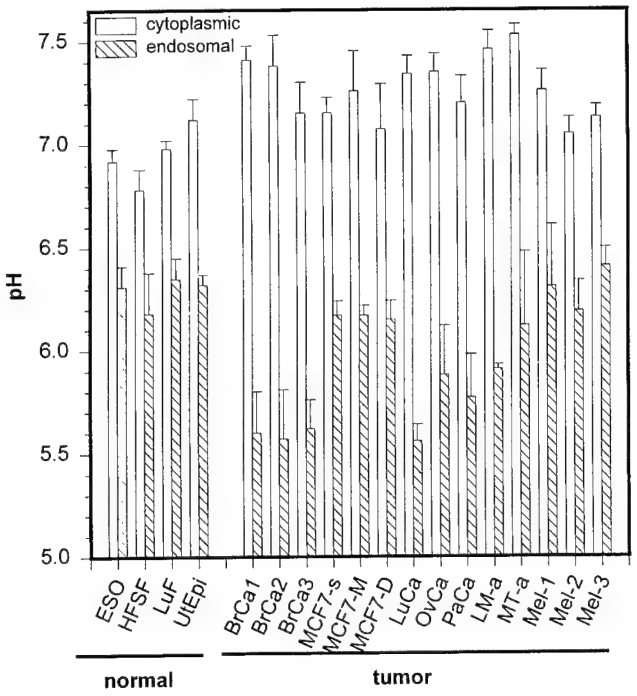

FIG. 4. Endosomal/lysosomal and cytosolic pH in human normal and tumor cells. Compartment pH values were measured using the pH-dependent fluorescent dyes coumarin-dextran and SNARF-1, respectively. Normal cells include esophageal (ESO), foreskin (HFSF), and lung (LuF) fibroblasts and uterine epithelial (UtEpi) cells. Tumor cells include breast (BrCa), lung (LuCa), ovarian (OvCa), and pancreatic (PaCa) carcinomas, leiomyo (LM) and mesothelial (MT) sarcomas, and melanomas (Mel). Data represent means ± SEM with a minimum of five independent measurements.

because the extracellular pH of tumors is acidic [38, 39, 65, 66]. The extracellular pH in solid tumors is typically 0.3 to 0.4 pH units more acidic than the cytoplasmic pH. Fig. 2 illustrates a ^{31}P MR spectrum of MCF-7/MITOX breast carcinoma cells, which are idiotypically resistant, *in vivo* and *in vitro*, to mitoxantrone, a weak base chemotherapeutic drug. As shown in this spectrum, the extracellular pH (pH$_c$) is 6.63 and the cytosolic pH (pH$_i$) is 7.01, as measured from the resonance frequencies of exogenous 3-APP and endogenous inorganic phosphate, respectively. These data are similar to those measured in other tumors of similar size [38, 39, 65, 66] and indicate that ΔpH values of up to +0.38 are observed in tumors *in vivo*. Fig. 3 illustrates the effect of varying extracellular pH on the nuclear-to-extracellular drug ratio with all other parameters set to their low values, including no endosomal turnover. As expected, the steady-state drug distribution followed the cytosolic-extracellular pH gradient (ΔpH), with a ratio of ~1.0 at a ΔpH of 0.0, and a ratio of 0.35 to 0.4 at a ΔpH of +0.5 (alkaline inside). Thus, a ΔpH of +0.38 would lead to a nuclear-to-extracellular drug ratio of *ca.* 0.4, even in the absence of endosomal turnover. This phenomenon of "physiological resistance" will be additive to the effects of endosomal sequestration and turnover investigated in the current study, since it will reduce the amount of drug presented to the surface of the endosome.

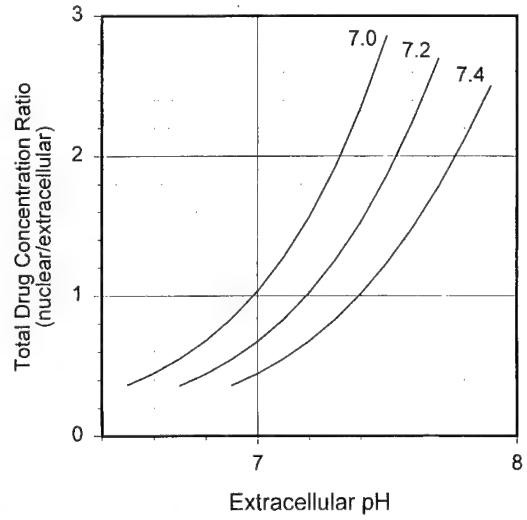

FIG. 3. Drug ratios affected by extracellular pH. Predicted nuclear/extracellular drug concentrations are shown at three different cytosolic pH values (7.0, 7.2, and 7.4) as a function of extracellular pH, for a drug of pK$_a$ 8.25. These data were calculated according to coupled equations, as described in the text, in the absence of endosomal turnover.

Two additional parameters that most markedly affect the efficacy of endosome-mediated drug extrusion are the endosomal pH and turnover rates. These have been measured in breast cancer cells with fluorescence [10]. To assess the generality of these values, we have extended these measurements to other cell lines. Fig. 4 illustrates the pH$_v$ and pH$_i$ values in a series of primary and established human tumor cell lines measured using the pH-dependent fluorescent dyes, coumarin-dextran and SNARF-1, respectively. As shown in this figure, the pH$_v$ of all carcinomas taken together (x-Ca) was 5.72 ± 0.04. Interestingly, the pH$_v$ of

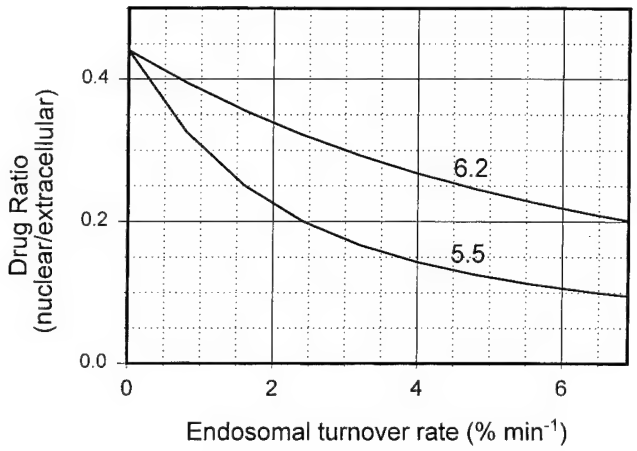

FIG. 5. Effects of endosomal turnover rates and endosomal pH on the nuclear drug concentration. Predicted nuclear/extracellular drug concentrations are shown at two endosomal pH values (5.5 and 6.2) as a function of endosomal turnover rate. These data were calculated according to coupled equations, as described in the text, with the "low" values for parameters from Table 1 except for: pH_e = 6.7, pH_i = 7.1, and drug pK_a = 8.25.

the MCF-7 series of breast cancer cells studied in the companion manuscript [10] was higher than that of the other breast cancer cells in this study (cf. BrCa vs MCF-7). These differences are correlated with metastatic potential, since the other breast cancer cell lines were highly metastatic, whereas MCF-7 cells are non-metastatic. The pH_v of the melanoma cells (Mel) was higher, 6.28 ± 0.12, and that of the sarcomas (LM-a, MT-a) was intermediate, 6.01 ± 0.09. The pH_v of normal cells was similar to that of melanomas, i.e. 6.27 ± 0.06. Other researchers have measured endosomal and late endosomal pH values of 4.5 to 6.5 [46, 53, 54]. Thus, the pH_v of 5.5 to 6.2 seen here is a physiologically reasonable range.

Endosomal turnover rates in the MCF-7 breast cancer cells of the companion study [10] were 0.59 to 1.58% min^{-1}. Endosomal turnover rates have been measured in other cell lines by other methods. For instance, labeling cells *in situ* with antibody against an extracellular epitope of V-ATPase yielded uptake time constants of 6.7% min^{-1} for C8161 melanoma cells (data not shown). Other researchers have measured values for endosomal turnover of up to 10% min^{-1} [26]. Thus, a physiologically reasonable range of values for endosomal turnover rates is 0.6 to 6.0% min^{-1}.

Figure 5 shows the effects of endosomal pH and endosomal turnover rate on the drug ratios, using a drug pK_a = 8.25 (daunorubicin), a pH_e of 6.7, a pH_i of 7.1, and low values for all remaining parameters. These data show that, at physiological endosomal pH values (5.5 to 6.2) and endosomal turnover rates (0.6 to 6.0% min^{-1}), the drug concentration in the cytoplasm will be 10–45% that of the extracellular environment. Thus, turnover of acidic vesicles can contribute to a significant lowering of steady-state concentrations of weakly basic drugs.

Drug pK_a and Mediated Transport of Drug into Endosomes

Two other interrelated parameters were revealed to be important in the endosome-mediated drug export during analyses: the activity of a mediated drug transport system and the drug pK_a. The rates of the organic cation/H^+ antiporter activity used in this simulation are modeled after those found in kidney brush border membrane vesicles and are conservatively within the physiologically reasonable range [48, 49, 51]. It is assumed that the driving force for this reaction is the activity of intravesicular H^+, provided by V-type H^+-ATPase. Since these antiporters act on the charged form of the drug, the pK_a of the drug molecule will affect the efficiency of the transport. Fig. 6 illustrates the effects of drug pK_a and transporter activity (V_T) on the perinuclear drug concentration. In Fig. 6A, these were calculated with the values pH_e = 6.7, pH_i = 7.1, pH_v = 5.75, endosomal turnover rate of 5.0%/min, and low values for all other parameters. It can be seen that this mechanism of drug efflux from the cell is strongly influenced by the acid dissociation constant of the drug, because a higher proportion is present in its charged form. Fig. 6B illustrates the influence of endosomal turnover rate on this carrier-mediated process with values for parameters pH_e = 6.7, pH_i = 7.1, pH_v = 5.75, pK_a = 8.25, and low values for other parameters. It is noteworthy that, if the transporter is inactive, there is no reduction in the perinuclear drug concentration even at the highest rates of endosomal turnover. This is seen from similar values of the y-intercept for all turnover rates. This illustrates that an endosomal pH gradient alone is not sufficient to make increased rates of exocytosis an effective mechanism of drug resistance. Equally, even at the highest transporter activity, there is no reduction in perinuclear drug concentration in the absence of vesicular turnover. Thus, both transport of drug into endosomes and turnover of the vesicles are required for reducing perinuclear concentrations of the drug. Note that, even with modest transport rates and rates of endosomal turnover, there are significant decreases in the perinuclear drug concentration.

Comparison with P-gp Activity at the Plasma Membrane

P-gp is thought to act at the plasma membrane, although it has also been detected in intracellular organelles [20]. Figure 7 shows the effect of increasing P-gp activity (at the plasma membrane) upon the cytosolic drug concentration, for drugs of different pK_a values. These calculations were made with pH_e = 6.7, pH_i = 7.1, pH_v = 5.75, endosomal turnover rate of 5.0%/min, V_T = 0.0, Hill coefficient h = 1, and low values for all other parameters. V_P, the plasma-membrane pump activity, was chosen to be in the same range of values as V_T in Fig. 6A. A comparison with Fig. 6A revealed that for equal maximal activities, a drug pump located at the plasma membrane was slightly more effective

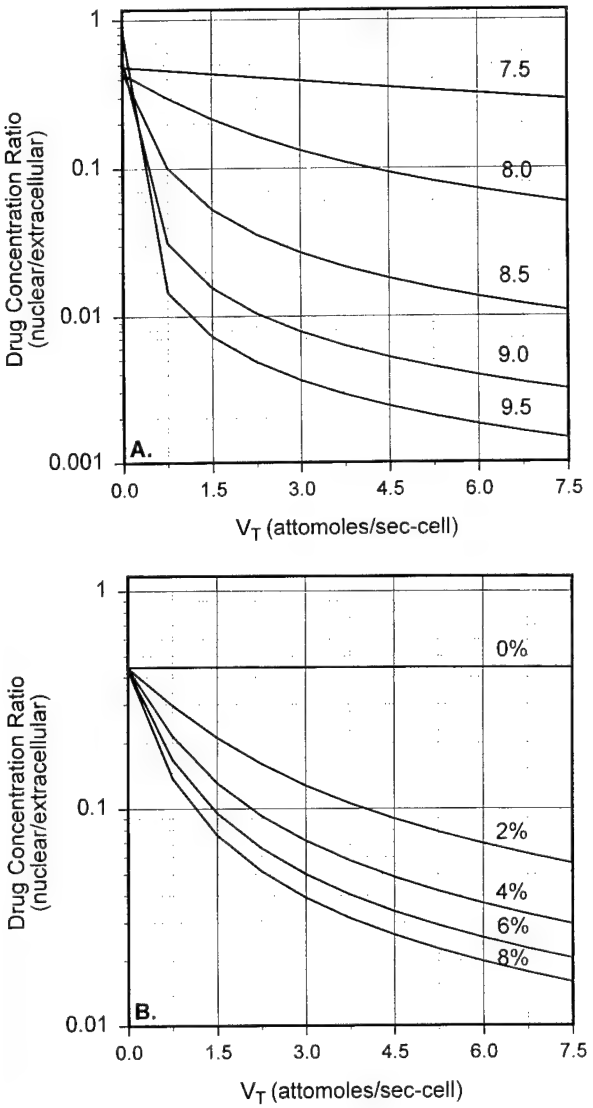

FIG. 6. Effects of endosomal transporter activity (V_T) on drug ratios. (A) Effects of drug pK_a and endosomal organic cation/H^+ antiporter activity (V_T) on the nuclear drug concentration. Model calculations were made with pH_c = 6.7, pH_i = 7.1, pH_v = 5.75, endosomal turnover rate = 5%/min, and "low" values for other parameters from Table 1. (B) Effects of endosomal turnover rate and endosomal organic cation/H^+ antiporter activity (V_T) on the nuclear drug concentration. Model calculations were made with pH_c = 6.7, pH_i = 7.1, pH_v = 5.75, drug pK_a = 8.25, and "low" values For other parameters from Table 1.

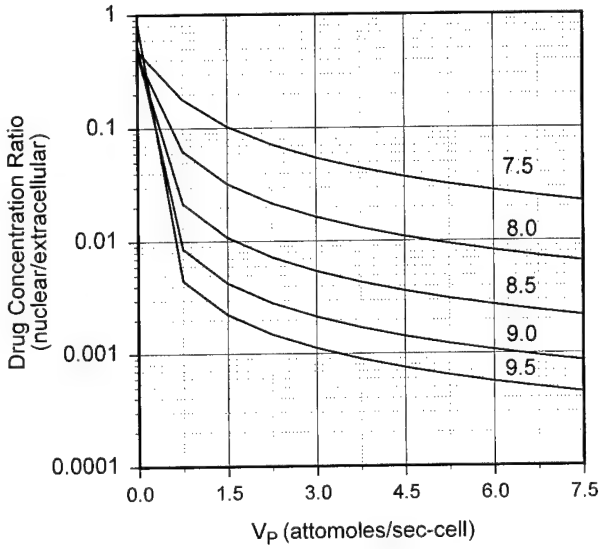

FIG. 7. Effects of plasmalemmal transporter activity (V_P) on drug ratios. Effects of drug pK_a and plasmalemmal drug pump activity (V_P) on the nuclear drug concentration. Model calculations were made with pH_c = 6.7, pH_i = 7.1, pH_v = 5.75, endosomal turnover rate = 5%/min, V_T = 0, and "low" values for other parameters from Table 1.

at reducing the nuclear concentration of a weak-base drug than a pump located at the endosomal membrane. However, this was only true if the drug did not display cooperative binding with the plasmalemmal drug transporter (h = 1). We also determined that for more basic drug molecules (higher pK_a), the difference in efficiencies between the two mechanisms narrowed considerably. Furthermore, it can be seen that in conjunction with high rates of endosomal turnover, an endosomal drug transporter can produce reductions in nuclear drug concentrations comparable to those produced by a plasma-membrane bound drug transporter. Indeed, with a conservative value of h = 2, the effectiveness of the plasmalemmal transporter at maintaining a low nuclear drug concentration was inferior to that of an endosomal drug transporter (calculations not shown).

Membrane Potentials

A correlation has been made by some groups between a less negative plasma membrane potential and increased drug resistance [61, 67, 68]. Agents that reverse MDR, e.g. verapamil and cyclosporin A, have been shown to reduce the plasma membrane potential of the resistant cells [67]. In our model, a more negative plasma membrane potential resulted in a small lowering of the perinuclear-to-extracellular drug ratio, but a more positive endosomal membrane potential did not have a noticeable effect on the drug ratio, for values above 10 mV.

Endosomal Clustering in the Perinuclear Region

When the perinuclear region was modeled to include the entire cell, the perinuclear-to-extracellular drug concentration ratios were 10–15% higher than the drug ratios resulting with endosomal clustering in a perinuclear region comprising only 25% of the cell volume. Thus, clustering of the endosomes in the perinuclear region results in an enhancement of their protective effect. The values assumed for diffusivities in the cytosol of the charged and uncharged drug molecules (Table 1) were at the high end of values reported for other molecules in the cytosol [59, 60]. Lower values of diffusivities would enhance the protective effect of

drug-sequestering acidic vesicles clustered around the nucleus.

DISCUSSION

Our data, both theoretical and experimental, indicate that a combination of low endosomal pH, high endosomal turnover rate, and active transport of drug molecules into endosomes, can effectively reduce perinuclear drug concentrations, yielding a drug-resistant phenotype. The activity of endosome-mediated drug resistance is slightly lower than that produced by equal activities of a plasmalemmal drug pump, but the difference narrows for weak-base drugs with more alkaline acid-dissociation constants or with cooperative binding of drug to the plasmalemmal transporter.

Demant *et al.* [69] have published a mathematical model simulating the effects of plasma membrane P-gp activity, transmembrane pH gradient, and endosomal turnover on the cytosolic concentration of drug molecules, and have concluded that for exocytotic extrusion of drug molecules to be an effective mechanism of MDR, unrealistically high rates of endosomal turnover and/or unrealistically low endosomal pH values would be needed. They have concluded therefore that endosomal turnover-mediated drug extrusion does not contribute to multidrug resistance. In their model, only the uncharged form of the drug molecule was taken to cross (passively or actively) any membrane. Our data are in complete agreement. The y-intercepts of panels A and B of Fig. 6 show that, in the absence of active transport of charged species into the endosomes, there is only a modest reduction of 40–50% in the levels of drug in the nucleus. In this study, we have chosen to also consider the movements of charged drug molecules, and have determined that this makes a significant difference. Moreover, we have chosen to consider vesicles that are located primarily in the perinuclear region.

It appears from our model that some form of active transport is required for a reduction in the cytosolic/perinuclear drug concentration with respect to the extracellular drug concentration at steady state. Simple alterations in cytosolic pH or number and volume of endosomes, in the absence of active transport, do not lower the nuclear drug concentration to therapeutically significant levels (i.e. $< 10\%$). Model calculations reveal that for cells that do not overexpress P-gp, an organic cation/H^+ antiporter located at the endosomal membrane can, in conjunction with physiologically reasonable rates of turnover of the acidic vesicles, substantially reduce the drug concentration in the perinuclear region. Computations using physiologically reasonable values for all model parameters illustrate that cells can lower cytosolic concentrations of weak base drugs through a combination of mechanisms including: (i) active transport of the drug into the endosomes, (ii) increased endosomal turnover rates, (iii) decreased endosomal pH, and (iv) increased plasma membrane pH gradient. Such a mechanism of drug export could be important to multidrug-resistant cells not overexpressing plasma membrane-bound drug pumps like P-gp.

This work was supported by the US Army Breast Cancer Research Program, Grant DAMD17–94-J-4368 (N.R, R.J.G.) and NIH DK49222 (S.H.W.).

References

1. Nielsen D and Skovsgaard T, P-glycoprotein as multidrug transporter: A critical review of current multidrug resistant cell lines. *Biochim Biophys Acta* **1139:** 169–183, 1992.
2. Dalton WS, Is p-glycoprotein a potential target for reversing clinical drug resistance? *Curr Opin Oncol* **6:** 595–600, 1994.
3. Clynes M, Cellular models for multiple drug resistance in cancer. *In Vitro Cell Dev Biol* **29A:** 171–179, 1993.
4. Gottesman MM and Pastan I, Biochemistry of multidrug resistance mediated by the multidrug transporter. *Annu Rev Biochem* **62:** 385–427, 1993.
5. Cole SPC, Bhardwaj G, Gerlach JH, Mackie JE, Grant CE, Almquist KC, Stewart AJ, Kurz EU, Duncan AMV and Deeley RG, Overexpression of a transporter gene in a multidrug-resistant human lung cancer cell line. *Science* **258:** 1650–1658, 1992.
6. Pastan I, Gottesman MM, Ueda K, Lovelace E, Rutherford AV and Willingham MC, A retrovirus carrying an MDR1 cDNA confers multidrug resistance and polarized expression of P-glycoprotein in MDCK cells. *Proc Natl Acad Sci USA* **85:** 4486–4498, 1988.
7. Ueda K, Cardarelli C, Gottesman MM and Pastan I, Expression of a full-length cDNA for the human "*MDR1*" gene confers resistance to colchicine, doxorubicin and vinblastine. *Proc Natl Acad Sci USA* **84:** 3004–3008, 1987.
8. Grant CE, Valdimarsson G, Hipfner DR, Almquist KC, Cole SPC and Deeley RG, Overexpression of multidrug resistance-associated protein (MRP) increases resistance to natural product drugs. *Cancer Res* **54:** 357–361, 1994.
9. Ma L and Center MS, The gene encoding vacuolar H^+-ATPase subunit C is overexpressed in multidrug-resistant HL60 cells. *Biochem Biophys Res Commun* **182:** 675–681, 1992.
10. Martínez-Zaguilán R, Raghunand N, Lynch RM, Bellamy W, Martinez GM, Rojas B, Smith D, Dalton WS and Gillies RJ, pH and drug resistance. I. Functional expression of plasmalemmal V-type H^+-ATPase in drug-resistant human breast carcinoma cell lines. *Biochem Pharmacol* **57:** 1037–1046, 1999.
11. Scheper RJ, Broxterman HJ, Sceffer GL, Kaaijk P, Dalton WS, van Heijningen THM, van Kalken CK, Slovak ML, de Vries EGE, van der Valk P, Meijer CJLM and Pinedo HM, Overexpression of a M_r 110,000 vesicular protein in non-P-glycoprotein-mediated multidrug resistance. *Cancer Res* **53:** 1475–1479, 1993.
12. Izquierdo MA, Scheffer GL, Flens MJ, Schroeijers AB, van der Valk P and Scheper RJ, Major vault protein LRP-related multidrug resistance. *Eur J Cancer* **32A:** 979–984, 1996.
13. Schuurhuis GJ, Broxterman HJ, de Lange JHM, Pinedo HM, van Heijningen TMH, Kuiper CM, Scheffer GL, Scheper RJ, van Kalken CK, Baak JPA and Lankelma J, Early multidrug resistance, defined by changes in intracellular doxorubicin distribution, independent of P-glycoprotein. *Br J Cancer* **64:** 857–861, 1991.
14. De Isabella P, Capranico G and Zunino F, The role of topoisomerase II in drug resistance. *Life Sci* **48:** 2195–2205, 1991.
15. Klohs WD, Steinkampf RW, Leopold WR and Fry DW,

Potentiation of adriamycin, trimetrexate and an AMSA analog (CI-921) cytotoxicities by amiodarone and reserpine in multidrug resistant P388 cells. *Proc Am Assoc Cancer Res* **28:** 298–302, 1987.
16. Klohs WD, Steinkampf RW, Havlick MJ and Jackson RJ, Resistance to anthrapyrazoles and anthracyclines in multidrug-resistant P388 murine leukemia cells: Reversal by calcium channel blockers and calmodulin antagonists. *Cancer Res* **46:** 4352–4356, 1986.
17. Klohs WD, Steinkampf RW, Besserer JA and Fry DW, Cross resistance of pleiotropically drug resistant P388 leukemia cells to the lipophilic antifolates trimetrexate and BW 301U. *Cancer Lett* **31:** 253–260, 1986.
18. Spoelstra EC, Dekker H, Schuurhuis GJ, Broxterman HJ and Lankelma J, P-glycoprotein drug efflux pump involved in the mechanisms of intrinsic drug resistance in various colon cancer cell lines. *Biochem Pharmacol* **41:** 349–359, 1991.
19. Ruetz S and Gros P, A mechanism For P-glycoprotein action in multidrug resistance: Are we there yet? *Trends Pharmacol Sci* **15:** 260–263, 1994.
20. Molinari A, Cianfriglia M, Meschini S, Calcabrini A and Arancia G, P-glycoprotein expression in the Golgi apparatus of multidrug-resistant cells. *Int J Cancer* **59:** 789–795, 1994.
21. Taylor CW, Dalton WS, Parrish PR, Gleason MC, Bellamy WT, Thompson FH, Roe DJ and Trent JM, Different mechanisms of decreased drug accumulation in doxorubicin and mitoxantrone resistant variants of the MCF7 human breast cancer cell line. *Br J Cancer* **63:** 923–929, 1991.
22. Dalton WS, Cress AE, Alberts DS and Trent JM, Cytogenetic and phenotypic analysis of a human colon carcinoma cell line resistant to mitoxantrone. *Cancer Res* **48:** 1882–1888, 1988.
23. Harker WG, Slade DL, Dalton WS, Meltzer PS and Trent JM, Multidrug resistance in mitoxantrone-selected HL-60 leukemia cells in the absence of P-glycoprotein overexpression. *Cancer Res* **49:** 4542–4549, 1989.
24. Mulder HS, Lankelma J, Dekker H, Broxterman HJ and Pinedo HM, Daunorubicin efflux against a concentration gradient in non-P-glycoprotein multidrug-resistant lung-cancer cells. *Int J Cancer* **59:** 275–281, 1994.
25. Leier I, Jedlitschky G, Buchholz U, Cole SPC, Deeley RG and Keppler D, The *MRP* gene encodes an ATP-dependent export pump for leukotriene C_4 and structurally related conjugates. *J Biol Chem* **269:** 27807–27810, 1994.
26. Sehested M, Skovsgaard T, van Deurs B and Winther-Neilsen H, Increase in nonspecific adsorptive endocytosis in anthracycline- and vinca alkaloid-resistant Ehrlich ascites tumor cell lines. *J Natl Cancer Inst* **78:** 171–179, 1987.
27. Sehested M, Skovsgaard T, van Deurs B and Winther-Neilson H, Increased plasma membrane traffic in daunorubicin resistant P388 leukemic cells: Effect of daunorubicin and verapamil. *Br J Cancer* **56:** 747–751, 1987.
28. Sognier MA, Zhang Y, Eberle RL, Sweet KM, Altenberg GA and Belli JA, Sequestration of doxorubicin in vesicles in a multidrug-resistant cell line (LZ-100). *Biochem Pharmacol* **48:** 391–401, 1994.
29. Seidel A, Hasmann M, Loser R, Bunge A, Schaefer B, Herzig I, Steidtmann K and Dietel M, Intracellular localization, vesicular accumulation and kinetics of daunorubicin in sensitive and drug-resistant gastric carcinoma EPG85–257 cells. *Virchows Arch* **426:** 249–256, 1995.
30. Dubowchik GM, Padilla L, Edinger K and Firestone RA, Reversal of doxorubicin resistance and catalytic neutralization of lysosomes by a lipophilic imidazole. *Biochim Biophys Acta* **1191:** 103–108, 1994.
31. Sehested M, Skovsgaard T and Roed H, The carboxylic ionophore monensin inhibits active drug efflux and modulates *in vitro* resistance in daunorubicin resistant Ehrlich ascites tumor cells. *Biochem Pharmacol* **37:** 3305–3310, 1988.
32. Schindler M, Grabski S, Hoff E and Simon SM, Defective pH regulation of acidic compartments in human breast cancer cells (MCF-7) is normalized in adriamycin-resistant cells (MCF-7adr). *Biochemistry* **35:** 2811–2817, 1996.
33. Gervasoni JE Jr, Fields SZ, Krishna S, Baker MA, Rosado M, Thuraisamy K, Hindenburg AA and Taub RN, Subcellular distribution of daunorubicin in P-glycoprotein-positive and -negative drug-resistant cell lines using laser-assisted confocal microscopy. *Cancer Res* **51:** 4955–4963, 1991.
34. Klohs WD and Steinkampf RW, The effect of lysosomatropic agents and secretory inhibitors on anthracycline retention and activity in multiple drug-resistant cells. *Mol Pharmacol* **34:** 180–185, 1988.
35. Simon SM and Schindler M, Cell biological mechanisms of multidrug resistance in tumors. *Proc Natl Acad Sci USA* **91:** 3497–3504, 1994.
36. Martínez-Zaguilán R, Lynch RM, Martinez GM and Gillies RJ, Vacuolar-type H^+-ATPases are functionally expressed in plasma membranes of human tumor cells. *Am J Physiol* **265:** C1015–C1029, 1993.
37. Raghunand N, Altbach MI, van Sluis R, Baggett B, Taylor CW, Bhujwalla ZM and Gillies RJ, Plasmalemmal pH-gradients in drug-sensitive and drug-resistant MCF-7 human breast carcinoma xenografts measured by ^{31}P magnetic resonance spectroscopy. *Biochem Pharmacol* **57**: 309–312, 1999.
38. Gillies RJ, Liu Z and Bhujwalla Z, ^{31}P-MRS measurements of extracellular pH of tumors using 3-aminopropylphosphonate. *Am J Physiol* **267:** C195–C203, 1994.
39. McCoy CL, Parkins CS, Chaplin DJ, Griffiths JR, Rodrigues LM and Stubbs M, The effect of blood flow modification on intra- and extracellular pH measured by ^{31}P magnetic resonance spectroscopy in murine tumors. *Br J Cancer* **72:** 905–911, 1995.
40. Goldman DE, Potential, impedance, and rectification in membranes. *J Gen Physiol* **27:** 37–60, 1943.
41. Spoelstra EC, Westerhoff HV, Dekker H and Lankelma J, Kinetics of daunorubicin transport by P-glycoprotein of intact cancer cells. *Eur J Biochem* **207:** 567–579, 1992.
42. Toffoli G, Simone F, Gigante M and Boiocchi M, Comparison of mechanisms responsible for resistance to idarubicin and daunorubicin in multidrug resistant LoVo cell lines. *Biochem Pharmacol* **48:** 1871–1881, 1994.
43. Slapak CA, Mizunuma N and Kufe DW, Expression of the multidrug resistance associated protein and P-glycoprotein in doxorubicin-selected human myeloid leukemia cells. *Blood* **84:** 3113–3121, 1994.
44. Schlemmer SR and Sirotnak FM, Functional studies of P-glycoprotein in inside-out plasma membrane vesicles derived from murine erythroleukemia cells overexpressing MDR3. *J Biol Chem* **269:** 31059–31066, 1994.
45. Pritchard JB, Sykes DB, Walden R and Miller DS, ATP-dependent transport of tetraethylammonium by endosomes isolated from rat renal cortex. *Am J Physiol* **266:** F966–F976, 1994.
46. Van Dyke RW, Faber ED and Meijer DKF, Sequestration of organic cations by acidified hepatic endocytic vesicles and implications for biliary excretion. *J Pharmacol Exp Ther* **261:** 1–11, 1992.
47. Forgac M, Structure, function and regulation of the coated vesicle V-ATPase. *J Exp Biol* **172:** 155–169, 1992.
48. Wright SH and Wunz TM, Mechanism of *cis-* and *trans*-substrate interactions at the tetraethylammonium/H^+ exchanger of rabbit renal brush-border membrane vesicles. *J Biol Chem* **263:** 19494–19497, 1988.
49. Ayer Lazaruk KD and Wright SH, MPP^+ is transported by the TEA^+-H^+ exchanger of renal brush-border membrane vesicles. *Am J Physiol* **258:** F597–F605, 1990.
50. Moseley RH, Jarose SM and Permoad P, Organic cation

transport by rat liver plasma membrane vesicles: Studies With tetraethylammonium. *Am J Physiol* **263:** G775–G785, 1992.
51. Wright SH, Wunz TM and Wunz TP, Structure and interaction of inhibitors with the TEA/H^+ exchanger of rabbit renal brush border membranes. *Pflugers Arch* **429:** 313–324, 1995.
52. Moseley RH and Van Dyke RW, Organic cation transport by rat liver lysosomes. *Am J Physiol* **268:** G480–G486, 1995.
53. Murphy RF, Powers S and Cantor CR, Endosome pH measured in single cells by dual fluorescence flow cytometry: Rapid acidification of insulin to pH 6. *J Cell Biol* **98:** 1757–1762, 1984.
54. Fuchs R, Male P and Mellman I, Acidification and ion permeabilities of highly purified rat liver endosomes. *J Biol Chem* **264:** 2212–2220, 1989.
55. Skovsgaard T and Nissen NI, Membrane transport of anthracyclines. *Pharmacol Ther* **18:** 293–311, 1982.
56. Dalmark M, Characteristics of doxorubicin transport in human red blood cells. *Scand J Clin Lab Invest* **41:** 633–639, 1981.
57. Dalmark M and Hoffman EK, Doxorubicin (Adriamycin) transport in Ehrlich ascites tumour cells: Comparison with transport in human red blood cells. *Scand J Clin Lab Invest* **43:** 241–248, 1983.
58. Dordal MS, Winter JN and Atkinson AJ Jr, Kinetic analysis of P-glycoprotein-mediated doxorubicin efflux. *J Pharmacol Exp Ther* **263:** 762–766, 1992.
59. Hubley MJ, Rosanske RC and Moerland TS, Diffusion coefficients of ATP and creatine phosphate in isolated muscle: Pulsed gradient ^{31}P NMR of small biological samples. *NMR Biomed* **8:** 72–78, 1995.
60. Tanner JE, Intracellular diffusion of water. *Arch Biochem Biophys* **224:** 416–428, 1993.
61. Roepe PD, Wei LY, Cruz J and Carlson D, Lower electrical membrane potential and altered pH_i homeostasis in multidrug-resistant (MDR) cells: Further characterization of a series of MDR cell lines expressing different levels of P-glycoprotein. *Biochemistry* **32:** 11042–11056, 1993.
62. Awasthi S, Sharma R, Awasthi YC, Belli JA and Frenkel EP, The relationship of doxorubicin binding to membrane lipids with drug resistance. *Cancer Lett* **63:** 109–116, 1992.
63. Guiral M, Viratelle O, Westerhoff HV and Lankelma J, Cooperative P-glycoprotein mediated daunorubicin transport into DNA-loaded plasma membrane vesicles. *FEBS Lett* **346:** 141–145, 1994.
64. Wadkins RM and Roepe PD, Biophysical aspects of P-glycoprotein-mediated multidrug resistance. *Int Rev Cytol* **171:** 121–165, 1997.
65. Bhujwalla ZM, Shungu DC, Chatham JC, Wehrle JP and Glickson JD, Glucose metabolism in RIF-1 tumors After reduction in blood flow: An *In vivo* ^{13}C and ^{31}P NMR study. *Magn Reson Med* **32:** 303–309, 1994.
66. Stubbs M, Rodrigues L, Howe FA, Wang J, Jeong KS, Veech RL and Griffiths JR, Metabolic consequences of a reversed pH gradient in rat tumors. *Cancer Res* **54:** 4011–4016, 1994.
67. Vayuvegula B, Slater L, Meador J and Gupta S, Correction of altered plasma membrane potentials: A possible mechanism of cyclosporin A and verapamil reversal of pleiotropic drug resistance in neoplasia. *Cancer Chemother Pharmacol* **22:** 163–168, 1988.
68. Hasmann M, Valet GK, Tapiero H, Treverrow K and Lampidis T, Membrane potential differences between Adriamycin-sensitive and -resistant cells as measured by flow cytometry. *Biochem Pharmacol* **38:** 305–312, 1989.
69. Demant EJF, Sehested M and Jensen PB, A model for computer simulation of P-glycoprotein and transmembrane ΔpH-mediated anthracycline transport in multidrug-resistant tumor cells. *Biochim Biophys Acta* **1055:** 117–125, 1990.

APPENDIX

Diffusion of drug molecules across the cytosol from radius $(r+\delta r)$ to radius r is described by Fick's law:

$$Ji = Di\left(\frac{\partial Ci(r)}{\partial r}\right)(4\pi r^2)$$

where J_i is the steady-state flux of species i (unprotonated or protonated drug); D_i is the cytosolic diffusion coefficient of species i; and $C_i(r)$ is the radius-dependent steady-state concentration of species i in the cytosol. Integrating both sides of the above equation, we have:

$$\int_{R_c}^{R_P} \frac{dr}{r^2} = \frac{4\pi Di}{J} \int_{C_{i,r=R_c}}^{C_{i,r=R_P}} dCi$$

i.e. the flux of species i from radius R_c to radius R_P is:

$$J_i = \frac{4\pi D_i R_c R_P (C_{i,r=R_c} - C_{i,r=R_P})}{R_c - R_P}$$

Biochemical Pharmacology, Vol. 57, pp. 309–312, 1999.

ISSN 0006-2952/99/$–see front matter
PII S006-2952(98)00306-2

SHORT COMMUNICATION

Plasmalemmal pH-Gradients in Drug-Sensitive and Drug-Resistant MCF-7 Human Breast Carcinoma Xenografts Measured by ^{31}P Magnetic Resonance Spectroscopy

Natarajan Raghunand, Maria I. Altbach,† Robert van Sluis,* Brenda Baggett,* Charles W. Taylor,‡ Zaver M. Bhujwalla§ and Robert J. Gillies*‖*

Departments of *Biochemistry, †Radiology, and ‡Internal Medicine, University of Arizona Health Sciences Center, Tucson, AZ 85724-5042; and §Department of Radiology, Johns Hopkins School of Medicine, Baltimore, MD 21205, U.S.A.

ABSTRACT. ^{31}P Magnetic resonance spectroscopy (MRS) was employed to investigate tumor pH in xenografts of drug-sensitive and drug-resistant MCF-7 human breast carcinoma cells. Measured extracellular pH values were found to be lower than the intracellular pH in all three tumor types investigated. The magnitude of this acid-outside plasmalemmal pH gradient increased with increasing tumor size in tumors of two drug-resistant variants of MCF-7 cells, but not in tumors of the parent (drug-sensitive) cells. The partitioning of weak-base or weak-acid drug molecules across the plasma membrane of a tumor cell is dependent upon the acid-dissociation constant (pK_a) of the drug as well as the plasmalemmal pH gradient. A large acid-outside pH gradient, such as those seen in MCF-7 xenografts, can exert a protective effect on the cell from weak-base drugs such as anthracyclines and *Vinca* alkaloids, which have pK_a values of 7.5 to 9.5. The possibility of enhancing the therapeutic efficacy of weak-base drugs by dietary or metabolic manipulation of the extracellular pH, in order to reduce or reverse the plasmalemmal pH gradient, deserves investigation. BIOCHEM PHARMACOL **57**;3:309–312, 1999. © 1998 Elsevier Science Inc.

KEY WORDS. MCF-7; breast carcinoma; xenograft; tumor pH; ^{31}P magnetic resonance spectroscopy; 3-aminopropylphosphonate

Combination chemotherapy of breast cancer and other cancers usually involves the use of at least one partially ionizable drug species [1]. The partitioning of weak-base or weak-acid drug molecules across the plasma membrane of a tumor cell is dependent upon the pK_a¶ of the drug as well as the plasmalemmal pH gradient. A large acid-outside pH gradient can exert a protective effect upon the cell from weak-base drugs such as anthracyclines and *Vinca* alkaloids, which have pK_a values of 7.5 to 9.5 [2–5]. The pH of tissues, including tumors, has been measured most commonly by the use of microelectrodes [6]. The pH thus measured is generally a combined measurement of the pH of interstitial fluid, and fluid and blood from damaged cells and capillaries. The invasive nature of microelectrodes and the uncertainty as to the nature of the interrogated fluid space complicate their use. In contrast, ^{31}P MRS can be employed to non-invasively, and simultaneously, measure pH_i from the chemical shift of endogenous inorganic phosphate [7] and pH_e from the chemical shift of exogenous 3-APP [8]. We have employed ^{31}P MRS to investigate differences in the steady-state plasmalemmal pH gradients in xenografts of drug-sensitive and drug-resistant MCF-7 human breast carcinoma cells. The pH_e and pH_i of all cell lines decreased with increasing tumor size. However, the (pH_i–pH_e) gradient was observed to increase with increasing tumor size only in tumors of two drug-resistant variants of MCF-7 cells, and not in tumors of the parent (drug-sensitive) cells. Implications of an acid-outside pH gradient for chemotherapy with weak-base drugs are discussed.

MATERIALS AND METHODS

Cells and Animals Used

MCF-7/S cells were obtained from the Michigan Cancer Foundation. MCF-7 cells resistant to mitoxantrone (MCF-7/Mitox) and doxorubicin (MCF-7/D40) were generated by sequential culturing in increased concentrations of mitoxantrone and doxorubicin, respectively [9]. SCID mice were obtained from the University of Arizona SCID mouse resource. Cells were implanted in the mammary fat pads of

‖ Corresponding author: Dr. Robert J. Gillies, Department of Biochemistry, University of Arizona Health Sciences Center, 1501 North Campbell Ave., Tucson, AZ 85724-5042. Tel. (520) 626-5050; FAX (520) 626-2110; E-mail: gillies@u.arizona.edu

¶*Abbreviations:* 3-APP, 3-aminopropylphosphonate; MRS, magnetic resonance spectroscopy; NTP, nucleoside triphosphate; pH_e, extracellular pH; pH_i, intracellular pH; pK_a, acid-dissociation constant; and SCID, severe combined immune-deficient.

Received 3 June 1998; accepted 2 September 1998.

6- to 7-week-old female SCID mice as a suspension of 5×10^6 cells in 0.05 mL of Hanks' balanced salt solution containing 50% Matrigel (Collaborative Research). As these cells are estrogen-dependent, 17β-estradiol pellets (0.25 mg, 21-day release; or 0.75 mg, 60-day release; Innovative Research of America) were implanted subcutaneously in the shoulder region of the mice by means of a 12-gauge trocar (Innovative Research) 2 days prior to tumor inoculation. In the case of the 21-day release pellets, a new pellet was implanted every 3 weeks, as necessary.

In vivo MRS

Tumors were allowed to grow for 3–8 weeks to volumes of 150–1500 mm^3, as estimated by external measurements of the tumor. Tumor volumes were calculated from orthogonal measurements of the external dimensions of tumors using the formula $(\text{width})^2 \times \text{length}/2$ [10]. Prior to MRS, the mice were anesthetized with a combination of ketamine (72 mg/kg), xylazine (6 mg/kg), and acepromazine (6 mg/kg). A 3/4 in., 24-gauge catheter (Elf Sanofi Inc.) connected to a 1.58 mm i.d. polyethylene tube (Becton Dickinson) long enough to extend out of the magnet was inserted into the intraperitoneal cavity of the anesthetized animal. 3-APP was obtained from the Sigma Chemical Co. A solution of 3-APP (0.15 to 0.3 mL, 128 mg/mL, pH 7.4) could be remotely injected into the mouse at the appropriate time before spectroscopy via the i.p. catheter. All *in vivo* measurements were performed at 4.7 Tesla (T) on a Bruker Biospec spectrometer/imager. The mouse was immobilized on a home-built probe, with the whole tumor placed inside a 3-turn solenoid radiofrequency (rf) coil of appropriate diameter—8, 12, or 17 mm—tunable to ^1H or ^{31}P. Body temperature was maintained by a circulating water blanket placed under the immobilized mouse. Unlocalized ^{31}P MR spectra were acquired using 20–45° pulses with repetition times of 500–1000 msec. Volume-selective ^{31}P spectra were acquired using either VSEL, a double-refocused spin-echo implementation of the VOSY pulse sequence [11] provided by Bruker Medizintechnik, or the ISIS sequence [12]. Scout images of the tumors were acquired prior to localized spectroscopy, to guide voxel placement. VSEL spectra were acquired using 764 μsec slice-selective hermitian rf pulses (corresponding to 80 ppm in the ^{31}P MR spectrum), an echo time of 11 msec, and a repetition time of 1200 msec. ISIS spectra were acquired with adiabatic slice-selective and excitation pulses repeated every 10–12 sec, using a gradient strength of 75 mT/m. In all cases, a dwell time of 62.5 μsec was employed, and 8192 data points were collected. Transients were averaged for 10–30 min. The large spectral widths employed resulted in up to a 1-mm difference in the positioning of the voxel containing either α-NTP or 3-APP, and the voxel containing the central frequency. This chemical shift artifact was not corrected for, but voxel sizes and placement were chosen so as to minimize the contribution of signal arising from the mouse body wall, while covering as much of the tumor as possible.

pH Calibration of Spectral Peaks

^{31}P MR time-domain data were processed by exponential multiplication followed by Fourier transformation. Chemical shifts of 3-APP and inorganic phosphate were calibrated to the α peak of NTP (set to −10.05 ppm). Titration curves reported elsewhere for the pH-dependencies of the chemical shifts of 3-APP [13, *] and inorganic phosphate [14] were used to calculate pH_e and pH_i, respectively, from each ^{31}P MR spectrum. The intensity of each 3-APP peak was corrected for the non-linearity of the titration curve prior to assigning a pH value to the chemical shift of the top of the peak [15]. Figure 1 shows a representative ^{31}P MR spectrum of an MCF-7/S tumor obtained using the ISIS sequence.

Statistical Analyses

Tumor pH_e and pH_i were obtained from ^{31}P MR spectra of several MCF-7/S, MCF-7/D40, and MCF-7/Mitox tumors. A linear regression analysis was performed for data sets from each tumor type, in order to determine the nature of the relationship between tumor pH_e (or pH_i) and tumor volume. The values and 95% confidence intervals for the first-order regression parameters were calculated using Sigmastat (Jandel Corp.).

RESULTS AND DISCUSSION

^{31}P MR Spectrum

Figure 1 shows a representative ^{31}P MR spectrum of a 610 mm^3 MCF-7/S tumor, obtained from an $8 \times 8 \times 8$ mm^3 voxel within the tumor. pH_e and pH_i were calculated from the chemical shifts of the 3-APP and inorganic phosphate peaks, respectively, as described in Materials and Methods.

Variation in pH_e and pH_i with Tumor Size

Panels a–c of Fig. 2 display the tumor pH_e and pH_i measured from localized and unlocalized ^{31}P MR spectra of three different tumor types, as a function of tumor volume. Also displayed are the results of first-order linear regression curve fits for each data set. Table 1 shows the values and the 95% confidence intervals for the fitted slopes, obtained from a linear regression analysis of each data set. The data clearly show that tumor pH_e and pH_i decrease with increasing tumor size.

Variation of Plasmalemmal (pH_i–pH_e) Gradient with Tumor Volume

The first-order fitted lines shown in Fig. 2a indicate that for the drug-sensitive MCF-7/S tumors, the magnitude of the

* Raghunand N, Aiken NR, Bhujwalla ZM and Gillies RJ, Measurement of extracellular pH *in vivo* using 3-aminopropylphosphonate: Deconvolution of T_2* effects. In: *Proceedings of the International Society for Magnetic Resonance in Medicine*, Vol. 2, p. 1111, 1996.

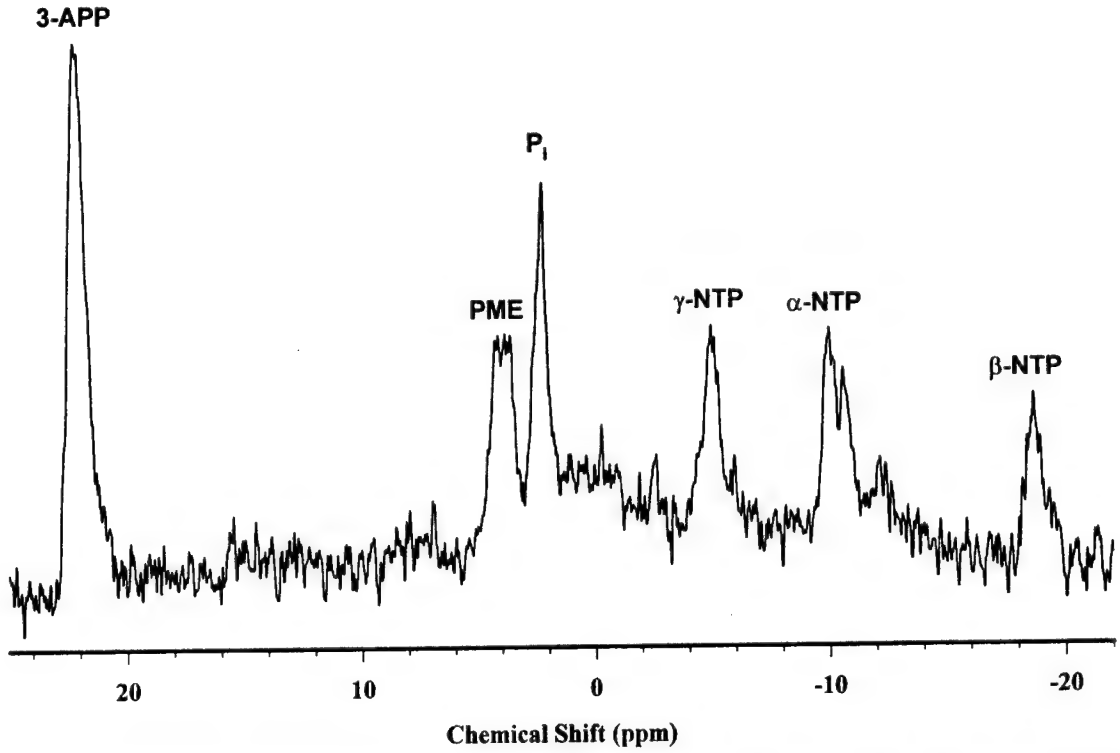

FIG. 1. ^{31}P MR ISIS spectrum acquired from an 8 × 8 × 8 mm^3 voxel placed on a 610 mm^3 MCF-7/S tumor. Adiabatic excitation pulses were used to minimize artifacts arising from non-uniform spatial excitation; 8192 data points were collected over a spectral window of 8000 Hz, from a total of 184 averages with a recycle delay of 10.5 sec. An exponential line-broadening factor of 5 Hz was applied to the time-domain signal prior to Fourier transformation. P_i, inorganic phosphate; NTP, nucleoside triphosphate; and PME, phosphomonoesters. $pH_{3\text{-APP}} = 7.11$, $pH_{Pi} = 7.17$.

(pH_i–pH_e) gradient changed little with increasing tumor volumes. The pH_i dropped concomitantly with the drop in pH_e. The overlapping 95% confidence intervals for the slopes of the pH_e and pH_i data sets for the MCF-7/S tumors (Table 1) verify that the (pH_i–pH_e) gradient was not altered significantly. From panels b and c of Fig. 2, it can be seen that the fitted lines are divergent for the pH_i and pH_e values of MCF-7/D40 and MCF-7/Mitox tumors. Thus, for these tumors, the magnitude of the (pH_i–pH_e) gradient increased as the tumors grew. The 95% confidence intervals for the fitted slopes for the pH_e and pH_i data sets from both MCF-7/D40 and MCF-7/Mitox tumors did not overlap

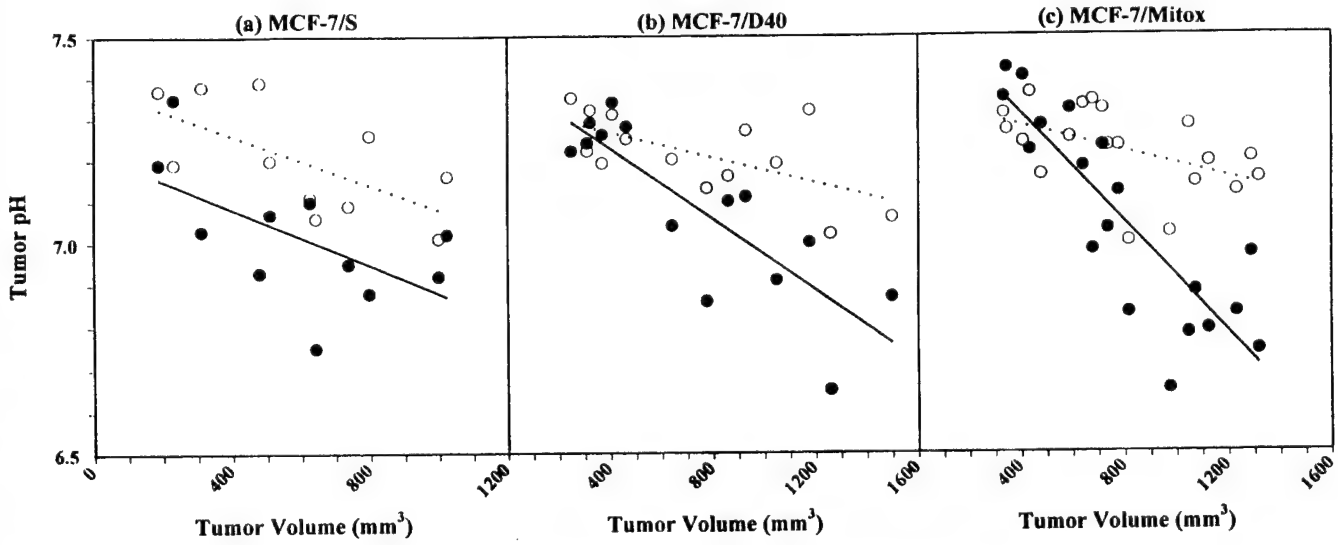

FIG. 2. Variation in pH_i and pH_e with tumor size. (a) MCF-7/S tumors, (b) MCF-7/D40 tumors, and (c) MCF-7/Mitox tumors. Key: (●) pH_e data, (○) pH_i data, (—) pH_e linear regression, and (···) pH_i linear regression.

TABLE 1. Slopes and 95% confidence intervals for the tumor pH versus the tumor volume data sets shown in Fig. 2

Data set	Fitted slope (10^{-4} pH units/mm^3)	95% Confidence interval (10^{-4} pH units/mm^3)
MCF-7/S, pH_e	−3.4	−1.9 to −4.9
MCF-7/S, pH_i	−3.0	−1.8 to −4.2
MCF-7/D40, pH_e	−4.3	−3.5 to −5.0
MCF-7/D40, pH_i	−1.5	−0.98 to −2.1
MCF-7/Mitox, pH_e	−6.6	−5.6 to −7.5
MCF-7/Mitox, pH_i	−1.6	−0.93 to −2.2

(Table 1), indicating that the slopes of the pH_e and pH_i regressions for these two tumor types were significantly different. Furthermore, the pH_e slope for MCF-7/Mitox tumors was significantly steeper than that for MCF-7/D40 tumors.

It is thus clear that (i) a positive (pH_i–pH_e) gradient exists in tumors of all three variants of MCF-7 cells, and (ii) the magnitude of this gradient increases with increasing tumor volume in the two drug-resistant variants, but not the drug-sensitive parent tumor type. A pH gradient in this direction may confer a measure of protection to the tumors from weak-base drugs like doxorubicin and mitoxantrone, by partial exclusion of the drugs from the cytosol [2–5]. This would be a form of "physiological" drug resistance, as distinct from the better characterized "biochemical" drug resistance observed, for example, in cells expressing the P-glycoprotein drug pump (reviewed in Ref. 16). The increased magnitude of the plasmalemmal pH gradient in MCF-7/D40 and MCF-7/Mitox tumors at the larger tumor sizes may partially explain why the large tumors are refractory to drug therapy (unpublished results). While such a pH gradient would seem to favor the use of weak-acid drugs such as chlorambucil, these are not commonly used. The possibility of enhancing the therapeutic efficacy of commonly used weak-base drugs by dietary or metabolic manipulation of pH_e in order to reduce or reverse the plasmalemmal pH gradient deserves investigation.

This work was supported by the U.S. Army Breast Cancer Research Program, Grant DAMD17-94-J-4368

References

1. Taylor CW, Dalton WS, Mosley K, Dorr RT and Salmon SE, Combination chemotherapy with cyclophosphamide, vincristine, adriamycin, and dexamethasone (CVAD) plus oral quinine and verapamil in patients with advanced breast cancer. *Breast Cancer Res Treat* **42:** 7–14, 1997.
2. Tannock IF and Rotin D, Acid pH in tumors and its potential for therapeutic exploitation. *Cancer Res* **49:** 4373–4384, 1989.
3. Roepe PD, Analysis of the steady-state and initial rate of doxorubicin efflux from a series of multidrug-resistant cells expressing different levels of P-glycoprotein. *Biochemistry* **31:** 12555–12564, 1992.
4. Simon S, Roy D and Schindler M, Intracellular pH and the control of multidrug resistance. *Proc Natl Acad Sci USA* **91:** 1128–1132, 1994.
5. Gerweck LE and Seetharaman K, Cellular pH gradient in tumor versus normal tissue: Potential for exploitation for the treatment of cancer. *Cancer Res* **56:** 1194–1198, 1996.
6. Wike-Hooley JL, Haveman J and Reinhold HS, The relevance of tumour pH to the treatment of malignant disease. *Radiother Oncol* **2:** 343–366, 1984.
7. Stubbs M, Bhujwalla ZM, Tozer GM, Rodrigues LM, Maxwell RJ, Morgan R, Howe FA and Griffiths JR, An assessment of ^{31}P MRS as a method of measuring pH in rat tumours. *NMR Biomed* **5:** 351–359, 1992.
8. Gillies RJ, Liu Z and Bhujwalla Z, ^{31}P-MRS measurements of extracellular pH of tumors using 3-aminopropylphosphonate. *Am J Physiol* **267:** C195–C203, 1994.
9. Taylor CW, Dalton WS, Parrish PR, Gleason MC, Bellamy WT, Thompson FH, Roe DJ and Trent JM, Different mechanisms of decreased drug accumulation in doxorubicin and mitoxantrone resistant variants of the MCF7 human breast cancer cell line. *Br J Cancer* **63:** 923–929, 1991.
10. Taetle R, Rosen F, Abramson I, Venditti J and Howell S, Use of nude mouse xenografts as preclinical drug screens: *In vivo* activity of established chemotherapeutic agents against melanoma and ovarian carcinoma xenografts. *Cancer Treat Rep* **71:** 297–304, 1987.
11. Kimmich R and Hoepfel D, Volume-selective multipulse spin-echo spectroscopy. *J Magn Reson* **72:** 379–384, 1987.
12. Ordidge RJ, Bowley RM and McHale G, A general approach to selection of multiple cubic volume elements using the ISIS technique. *Magn Reson Med* **8:** 323–331, 1988.
13. McCoy CL, Parkins CS, Chaplin DJ, Griffiths JR, Rodrigues LM and Stubbs M, The effect of blood flow modification on intra- and extracellular pH measured by ^{31}P magnetic resonance spectroscopy in murine tumors. *Br J Cancer* **72:** 905–911, 1995.
14. Gillies RJ, Alger JR, den Hollander JA and Shulman RG, Intracellular pH measured by NMR: Methods and results. In: *Intracellular pH: Its Measurement, Regulation, and Utilization in Cellular Functions* (Eds. Nuccitelli R and Deamer DW), pp. 79–104. Alan R. Liss, New York, 1982.
15. Graham RA, Taylor AH and Brown TR, A method for calculating the distribution of pH in tissues and a new source of pH error from the ^{31}P-NMR spectrum. *Am J Physiol* **266:** R638–R645, 1994.
16. Gottesman MM and Pastan I, Biochemistry of multidrug resistance mediated by the multidrug transporter. *Annu Rev Biochem* **62:** 385–427, 1993.

British Journal of Cancer (1999) 80(7), 1005–1011

Article no. bjoc.1998.0455

Enhancement of chemotherapy by manipulation of tumour pH

N Raghunand[1,*], X He[1,*], R van Sluis[1], B Mahoney[1], B Baggett[1], CW Taylor[1], G Paine-Murrieta[1], D Roe[1], ZM Bhujwalla[2] and RJ Gillies[1]

[1]Arizona Cancer Center, 1501 N Campbell Avenue, Tucson, AZ 85724-5024, USA; [2]Department of Radiology, Johns Hopkins School of Medicine, Baltimore, MD, USA

Summary The extracellular (interstitial) pH (pHe) of solid tumours is significantly more acidic compared to normal tissues. In-vitro, low pH reduces the uptake of weakly basic chemotherapeutic drugs and, hence, reduces their cytotoxicity. This phenomenon has been postulated to contribute to a 'physiological' resistance to weakly basic drugs in vivo. Doxorubicin is a weak base chemotherapeutic agent that is commonly used in combination chemotherapy to clinically treat breast cancers. This report demonstrates that MCF-7 human breast cancer cells in vitro are more susceptible to doxorubicin toxicity at pH 7.4, compared to pH 6.8. Furthermore ^{31}P-magnetic resonance spectroscopy (MRS) has shown that the pHe of MCF-7 human breast cancer xenografts can be effectively and significantly raised with sodium bicarbonate in drinking water. The bicarbonate-induced extracellular alkalinization leads to significant improvements in the therapeutic effectiveness of doxorubicin against MCF-7 xenografts in vivo. Although physiological resistance to weakly basic chemotherapeutics is well-documented in vitro and in theory, these data represent the first in vivo demonstration of this important phenomenon.

Keywords: doxorubicin; acid-base balance; chemotherapy; MRS; bicarbonate

In the early part of this century, Otto Warburg postulated that tumours were acidic because the rate at which they produced lactic acid was 'remarkable' (Warburg, 1956). Subsequent measurement of pH in a variety of solid tumours with microelectrodes apparently confirmed this hypothesis (Wike-Hooley et al, 1984). It is assumed that microelectrode measurements primarily interrogate extracellular (interstitial) volumes. However, in-vivo ^{31}P magnetic resonance spectroscopy (MRS) of endogenous intracellular inorganic phosphate (Pi) measures an intracellular pH (pHi) which is neutral-to-alkaline in the same or similar tumours (Griffiths, 1991; Negendank, 1992). Thus, the apparent acidity of the extracellular (interstitial) pH (pHe) does not translate to an acidic pHi. Recently, ^{31}P MRS methods have been developed to simultaneously measure the pHi and pHe of tumours using endogenous Pi and exogenous 3-aminopropylphosphonate (3-APP), respectively (Gillies et al, 1994). This method has clearly shown, in a number of solid tumour xenografts, that the pHi of tumour cells is neutral–alkaline, while the pHe of the same tumours is acidic (McCoy et al, 1995; Raghunand et al, 1999a). Thus, solid tumours generally have substantial acid-outside pH gradients.

Acid-outside pH gradients have a number of important sequellae that are germane to cancer, including a theoretically reduced partitioning of weakly basic chemotherapeutic drugs into the relatively alkaline cells. This phenomenon has its basis in the 'ion-trapping' hypothesis wherein weak bases partition into, and are sequestered by, acidic compartments, such as the extracellular fluid (Roos, 1978). This occurs because uncharged, organic free bases are much more permeable than their protonated and charged counterparts and establish equal concentrations on both sides of the membrane (Gillies and Deamer, 1978). Since the ratio of charged–uncharged species increases with lower pH, more total base is found in acidic compartments. This hypothesis is applicable to weakly basic chemotherapeutic drugs, such as doxorubicin (pKa = 7.6), which is one of the most widely prescribed antineoplastic agents used in the treatment of breast cancer (Taylor et al, 1991).

Received 24 August 1998
Revised 3 December 1998
Accepted 7 December 1998

Correspondence to: RJ Gillies

MATERIALS AND METHODS

Cell and tumour growth

MCF-7 cells were obtained from W S Dalton (Arizona Cancer Center) and cultured in RPMI-1640/DMEM (Dulbecco's modified Eagle's medium) supplemented with 10% fetal bovine serum (FBS) (HyClone, Logan, UT, USA). For in vivo culturing, a suspension of 5×10^6 MCF-7 cells in 0.05 ml of Hank's balanced salt solution were implanted in the mammary fat pads of 6- to 7-week-old female severe combined immunodeficient (SCID) mice. Since MCF-7 cells are oestrogen-dependent, 17β-oestradiol pellets (0.72 mg, 60-day release; Innovative Research of America, Sarasota, FL, USA) were subcutaneously implanted in the shoulder region of the mice by means of a 12-gauge trochar (Innovative Research) 2 days prior to tumour inoculation.

Magnetic resonance spectroscopy

Prior to MRS, mice were anaesthetized with a combination of ketamine (72 mg kg^{-1}), xylazine (6 mg kg^{-1}) and acepromazine (6 mg kg^{-1}). A 3/4″, 24-gauge catheter (Elf Sanofi Inc., Overland Park, KS, USA), connected to a 1.58 mm intradermal (i.d.)

*These authors contributed equally to this work.

polyethylene tube (Becton Dickinson, Parsippany, NJ, USA), long enough to extend out of the magnet was inserted into the intraperitoneal (i.p.) cavity of the anaesthetized animal. The mouse was then immobilized on a home-built probe with a coil tunable to ^{1}H or ^{31}P. After shimming the magnet, 3-APP (0.15–0.3 ml, 128 mg ml^{-1}, pH 7.4) was injected into the mouse via the i.p. catheter. Volume-selective ^{31}P spectra were acquired at 4.7 T on a Bruker Biospec with the ISIS sequence (Ordidge et al, 1988) with adiabatic slice-selective and excitation pulses repeated every 10–12 s, using a gradient strength of 75 mT m^{-1}. In all cases, a dwell time of 62.5 μs was employed, and 8192 data points were collected from 184 transients. Scout images of the tumour and surrounding abdominal tissue were obtained each time in order to guide the positioning of the voxel. The large spectral widths employed resulted in up to a 1 mm difference in the positioning of the voxel containing either α-NTP or 3-APP, and the voxel containing the central frequency. This chemical shift artefact was not corrected for, but voxel sizes and placement were chosen so as to minimize the contribution of signal arising from the mouse body wall, while covering as much of the tumour as possible.

Measurement of intracellular pH in vitro

Intracellular pH (pHi) was measured in vitro using the fluorescent dye, SNARF-1, as described previously (Martinez-Zaguilan et al, 1991). Briefly, MCF-7 cells were grown onto 9 × 22 mm glass coverslips, washed three times with buffer A (1.3 mM calcium chloride, 1 mM magnesium sulphate, 5.4 mM potassium chloride, 0.44 mM KH_2PO_4, 110 mM sodium chloride, 0.35 mM NaH_2PO_4, 5 mM glucose, 2 mM glutamine and 5 mM HEPES, 5 mM MES, 10 mM sodium hydrogen carbonate ($NaHCO_3$) at a pH of 7.15 at 37°C and subsequently incubated for 30 min at 37°C, in a 5% carbon dioxide atmosphere with 3 ml of buffer A containing 10 μM acetoxymethylester SNARF-1 (Molecular Probes, Eugene, OR, USA). This was followed by a second incubation in buffer A for 45 min to allow for complete hydrolysis of the dye. Coverslips were then placed in a holder/perfusion device and inserted into a fluorometer cuvette and fluorescence measurements were acquired at an excitation of 534 nm with the emission sequentially sampled at 584 and 644 nm in an SLM8000C (SLM, Urbana, IL, USA). The ratio (R) of fluorescence intensities of emissions at 584 and 644 nm was converted to pHi values using the equation: $pH = 7.38 + \log_{10} 0.822 + \log_{10} [(R - 0.458)/(1.928 - R)]$. Data are presented as mean ± s.e.m. of six independent measurements.

Doxorubicin uptake and cytotoxicity in vitro

MCF-7 cells were grown to confluence in 6-well plates at which time the cells were incubated in DMEM/F12 containing 20 mM HEPES, 20 mM MES, 10% FBS and 0.208 μCi per well of ^{14}C doxorubicin (Amersham) for 30 min at 37°C in a 5% carbon dioxide atmosphere at pH of 6.8 and 7.4 respectively. After the incubation, the plates were placed on ice and washed five times with ice-cold HBSS, followed by extraction with 1.0 ml of 0.1 N NaOH for 1 h at 4°C. Samples were divided into equal aliquots for determination of protein content using the Bradford assay (Bio-Rad), and radioactivity using liquid scintillation counting.

Cytotoxicity was determined as previously described (Gillies et al, 1986). Briefly, cells were grown to log phase in 96-well plates and medium was exchanged for one at either pH 6.8 or 7.4 containing the indicated concentrations of doxorubicin. Medium pH was buffered using non-volatile buffers (10 mM MES, 20 mM HEPES and 10 mM TRICINE) in combination with bicarbonate concentrations that were adjusted to be in equilibrium with 5% ambient carbon dioxide. Twenty-four hours later, regular growth medium was replaced and cells allowed to grow a subsequent 72 h, after which time they were fixed and stained with crystal violet for determination of cell number.

Table 1 Theoretical and measured enhancement of doxorubicin uptake caused by increasing extracellular pH in vitro and in vivo

In vitro	Low pHe	High pHe
Extracellular pH	6.8	7.4
Intracellular pH (*n*)	7.05 ± 0.06 (22)	7.20 ± 0.07 (5)
Theoretical ratio	0.69 ± 0.07	1.36 ± 0.17
Theoretical enhancement		1.97 ± 0.45
Doxorubicin uptake (*n*)	65.1 ± 2.7 (6)	166.9 ± 9.1 (6)
Uptake enhancement		2.56 ± 0.25
EC_{50} (μM)	0.27	0.12
Toxicity enhancement		2.25
In vivo	**Control**	**+ $NaHCO_3$**
pHe (800 mm^3 tumour)	6.99 ± 0.11	7.84 ± 0.13
pHi (800 mm^3 tumour)	7.15 ± 0.08	7.39 ± 0.13
pH gradient	+0.16	−0.45
Theoretical ratio	0.6	1.6
Theoretical enhancement		2.5

Table 2 Tumour growth statistics

	A	B	C	D
No. mice	17	13	12	13
T–C (d to 300 mm^3)	–	–	15	22
T/C (%)	–	–	0.47	0.29
Growth rate (d^{-1})	0.206	0.215	0.156	0.092
Standard deviation	0.094	0.060	0.067	0.047
P vs group A	–	0.732	0.031	0.002
P vs group B	0.732	–	0.027	0.001
P vs group C	0.031	0.027	–	0.008
P vs group D	0.002	0.001	0.008	–

Calculation of theoretical drug distributions

Cytoplasmic–extracellular drug ratios were calculated at the steady-state using methods described previously (Roos, 1978; Raghunand et al, 1999*b*). Briefly, the ratio of protonated (charged) to deprotonated (uncharged) doxorubicin were calculated from the Henderson–Hasselbach equation in both intracellular and extracellular compartments using the pHi and pHe, respectively, and a drug pKa of 7.6. The concentration of the uncharged specie was set to 1.0 on both sides of the membrane and the total concentration was calculated as the sum of (charged + uncharged). Data were expressed as a ratio of intra- to extracellular concentrations. Enhancement was calculated as the ratio at high pH, relative to that at low pH.

Tumour growth statistics

Tumour size was measured with calipers and calculated as: $[(\text{width})^2 \times \text{length}]/2$. Data were linearized by converting volumes (in mm^3) to their cube roots. The least squares regression line of

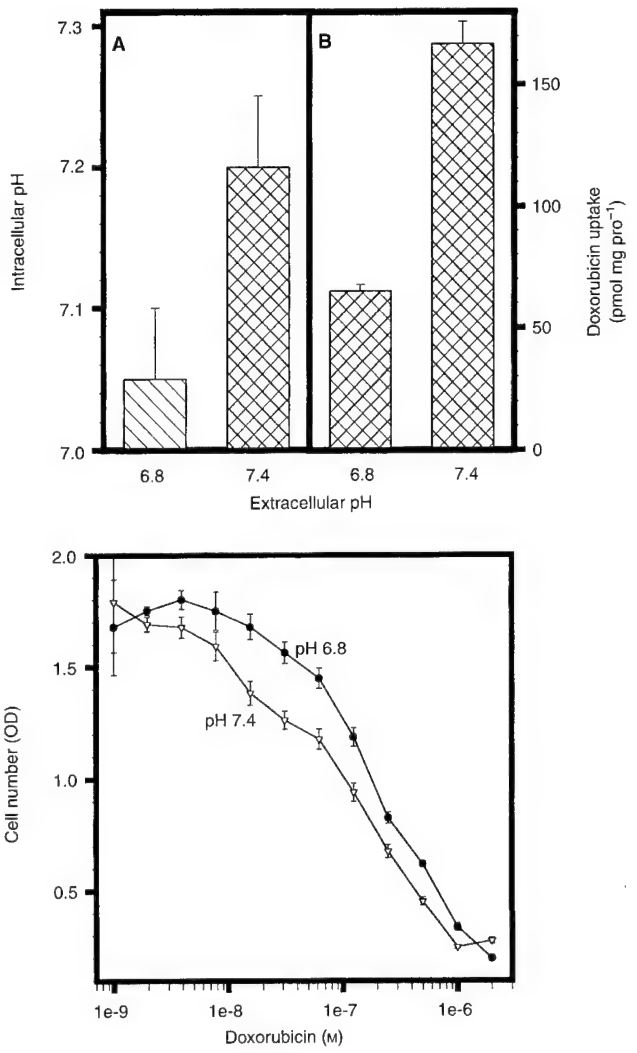

Figure 1 In vitro effects of pH on doxorubicin chemotherapy. (**A**) Intracellular pH of MCF-7 cells in-vitro. MCF-7 cells grown on coverslips were loaded with SNARF-1 fluorescent dye and the intracellular pH was measured as described in Methods. (**B**) Doxorubicin levels in MCF-7 cells as a function of pHe. MCF-7 cells were incubated with ^{14}C doxorubicin for 30 min at medium pH of 6.8 or 7.4, after which time cells were washed and radioactivity determined (see Methods). Data are expressed as pmol mg protein^{-1}. (**C**) Cytotoxicity of doxorubicin as a function of pHe. MCF-7 cells were grown in 96-well plates to sub-confluence, at which time they were treated with doxorubicin at the indicated concentrations. Ninety-six hours later, media were removed and remaining cell numbers were determined by crystal violet staining, as described previously (Gillies et al, 1986). Data are shown for MCF-7 cells at pH 6.8 and 7.4. OD, optical density

the cube root volumes from day 9 onward were fit for each mouse with non-zero tumour growth. Three-way analyses of variance were used to examine the effect of different experiments, injection (doxorubicin vs saline), and water (plain vs bicarbonate). The differences between experiments were not significant ($P = 0.767$) and, hence, data from all experiments were pooled for further two-way analyses of variance. Tumour cell log kill was calculated from the equation $[(T–C)/3.32T_d]$, where T and C are the number of days it took for treated and control groups, respectively, to reach 1000 mm^3. T_d is the exponential doubling time of the treated group (Corbett et al, 1982). T/C was calculated as the ratio of the median volumes of treated and control groups on day 20. T/C < 44% is considered significant by the Division of Cancer Treatment (National Cancer Institute), while a T/C value of < 10% (DN-2 level activity) is considered highly significant.

RESULTS

pH affects doxorubicin distribution and cytotoxicity in vitro

Solid tumours generally exhibit pHe values of 6.7–6.8 (Wike-Hooley et al, 1984; Griffiths, 1991; Gillies et al, 1994; McCoy et al, 1995; Raghunand et al, 1999*a*). In vitro, MCF-7 cells at medium pH values of 6.8 and 7.4 have pHi values of 7.05 ± 0.06 and 7.20 ± 0.07, respectively, as measured with fluorescence (Figure 1A). Thus, according to theory (see Methods), the pH gradient of +0.25 at pHe = 6.8 will yield an intracellular–extracellular doxorubicin ratio of 0.69 ± 0.07, whereas at pHe = 7.4, the ratio will be 1.36 ± 0.17 (Table 1). Hence, there will be a 1.97 ± 0.45-fold enhancement of the steady-state intracellular drug concentration as pHe is raised from 6.8 to 7.4. The empirical steady-state levels of ^{14}C doxorubicin in MCF-7 cells at medium pH values of 6.8 and 7.4 show a 2.56 ± 0.25-fold enhancement (Figure 1B), which is in good agreement with theory.

The difference in intracellular levels of doxorubicin between low and high pHe values should give rise to differences in cytotoxicity. Figure 1C shows that, following a 24-h treatment, the EC_{50} of doxorubicin in MCF-7 cells is 0.27 μm at pH 6.8, compared to 0.12 μm at pH 7.4. One-hour treatments with doxorubicin yielded essentially the same results, although both EC_{50} values were higher. Similar data for doxorubicin have been reported elsewhere (Tannock and Rotin, 1989; Simon and Schindler, 1994). In the current study, the 2.25-fold enhancement of doxorubicin cytotoxicity at pH 7.4 compared to pH 6.8 is similar in magnitude to both theory and the empirical doxorubicin distribution ratio (cf. Table 1). Thus, the enhanced cytotoxicity at high pHe is likely due to increased partitioning of doxorubicin into cells.

Bicarbonate raises pHe in vivo

While there is substantial evidence that doxorubicin is more effective at higher pHe, this phenomenon is of limited utility unless the pHe of tumours can be manipulated in vivo. For the current experiments, pHe was raised via sodium bicarbonate-induced metabolic alkalosis. However, the addition of bicarbonate could have important negative sequelae, since it is osmotically active and could cause hypernatraemia. To determine the maximum tolerated doses of bicarbonate, eight different cohorts of SCID mice were given $NaHCO_3$-supplemented water to drink ad libitum. Bicarbonate concentrations ranged from 0 to 250 mM. Animal weights and water consumption were monitored daily. For bicarbonate concentrations up to 225 mM, weight gain and subjective parameters (e.g. grooming behaviour and activity) were unaffected compared to water controls for up to 9 weeks (data not shown). In a separate experiment, animals were given 200 mM $NaHCO_3$ ad lib. Four to 10 days following commencement of bicarbonate therapy, pHi and pHe were measured using ^{31}P MRS. A representative ^{31}P spectrum from an untreated MCF-7 cell tumour is shown in Figure 2A. In this Figure, the pHe measured by 3-APP is 6.57 and the pHi measured by Pi is 6.95. Figure 2B shows the region containing the 3-APP resonance from a representative ^{31}P MRS spectrum of

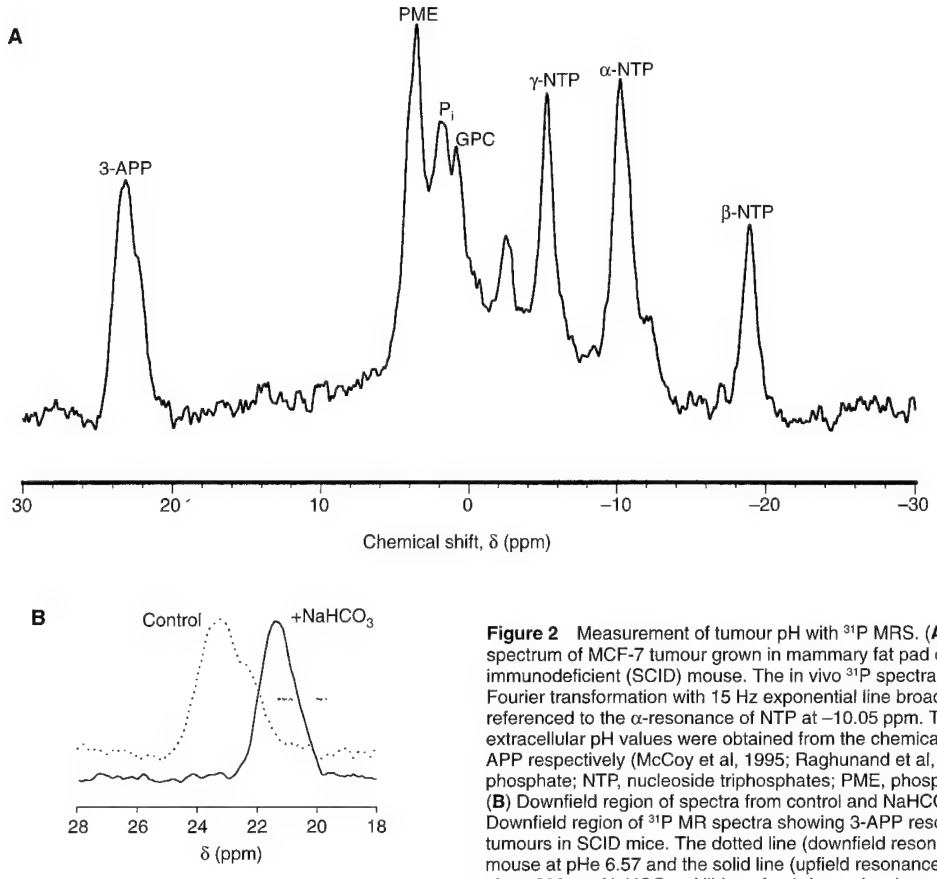

Figure 2 Measurement of tumour pH with ^{31}P MRS. (**A**) In vivo ^{31}P NMR spectrum of MCF-7 tumour grown in mammary fat pad of severe combined immunodeficient (SCID) mouse. The in vivo ^{31}P spectra were processed by Fourier transformation with 15 Hz exponential line broadening and referenced to the α-resonance of NTP at –10.05 ppm. The intra and extracellular pH values were obtained from the chemical shifts of Pi and 3-APP respectively (McCoy et al, 1995; Raghunand et al, 1999*a*). Pi, inorganic phosphate; NTP, nucleoside triphosphates; PME, phosphomonoesters. (**B**) Downfield region of spectra from control and $NaHCO_3$-treated mice. Downfield region of ^{31}P MR spectra showing 3-APP resonance from MCF-7 tumours in SCID mice. The dotted line (downfield resonance) is from control mouse at pHe 6.57 and the solid line (upfield resonance) is from mouse given 200 mM $NaHCO_3$ ad libitum for 4 days, showing a pHe of 7.72. Acquisition conditions were identical to those in Figure 1A

MCF-7 tumours obtained 4 days following substitution of drinking water with 200 mM $NaHCO_3$. Note the shift in the position of the 3-APP resonance relative to controls indicating a significant alkalinization of pHe. All other resonances (Pi, PME, ATP) were statistically indistinguishable from the controls. In this example, the measured pHe was 7.72. Thus, $NaHCO_3$ can significantly increase pHe.

Results from all of the MRS-based pH measurements are shown in Figure 3A, expressed as a function of tumour size. Note that in untreated MCF-7 tumours (triangles), the pHe (open) and pHi (closed) decrease with approximately the same slope with increasing tumour size. Thus, the pH gradient is relatively constant at 0.22 ± 0.09 pH unit, consistent with previous reports (Raghunand et al, 1999*a*). In animals supplemented with HCO_3^-, the measured pHe values (open circles) are significantly higher than the measured pHi values (closed circles). This is significantly different than the pHe and pHi of control animals. The direction of the plasmalemmal (in–out) pH gradient is shown by arrows in the Figure and it is clear that the direction is reversed in all $NaHCO_3$-treated animals, compared to controls. The pHe reported by the 3-APP resonance in $NaHCO_3$-treated tumours is high, 7.84 ± 0.13 pH unit. The pHi values in the same animals were 7.39 ± 0.12. The imprecision in both the pHe and pHi measurements are likely higher due to these values being near the alkaline extreme of the titration curves for both 3-APP and Pi respectively. Nevertheless, the data clearly show that chronic bicarbonate therapy effectively alkalinizes the pHe in vivo, generating an (in–out) ΔpH of approximately – 0.45 pH unit, compared to a ΔpH of + 0.20 in untreated animals.

Bicarbonate chemosensitizes tumour xenografts in vivo

According to the measured pH gradients, the theoretical cytosolic–extracellular drug ratio should be 1.6 in bicarbonate-treated animals, and 0.6 in controls, leading to a 2.5-fold increase in doxorubicin sensitivity (Table 1). To test this, MCF-7 tumours were grown in the mammary fat pads of 6-week-old female SCID mice, to sizes of 50–200 mm^3, and were forcibly randomized according to tumour size into four groups.

Groups A and C were given normal water ad libitum, while the water given to groups B and D was supplemented with 200 mM $NaHCO_3$. The start of the bicarbonate treatment was designated as day 1. On days 3, 7 and 11, animals in groups C and D were injected i.p. with doxorubicin while animals in groups A and B ($n = 10$ each) received saline injections of the same volume, as per established protocols (Paine-Murrieta et al, 1997). The maximum tolerated dose (MTD) of SCID mice for doxorubicin under this regimen is a cumulative 6.7 mg kg^{-1} (Paine-Murrieta et al, 1997). Initial experiments used three doses of doxorubicin at 2.0 mg kg^{-1} (cohorts C_1/D_1) and this was reduced in later experiments to three doses at 1.6 mg kg^{-1} (cohorts C_2/D_2) to reduce morbidity. In all

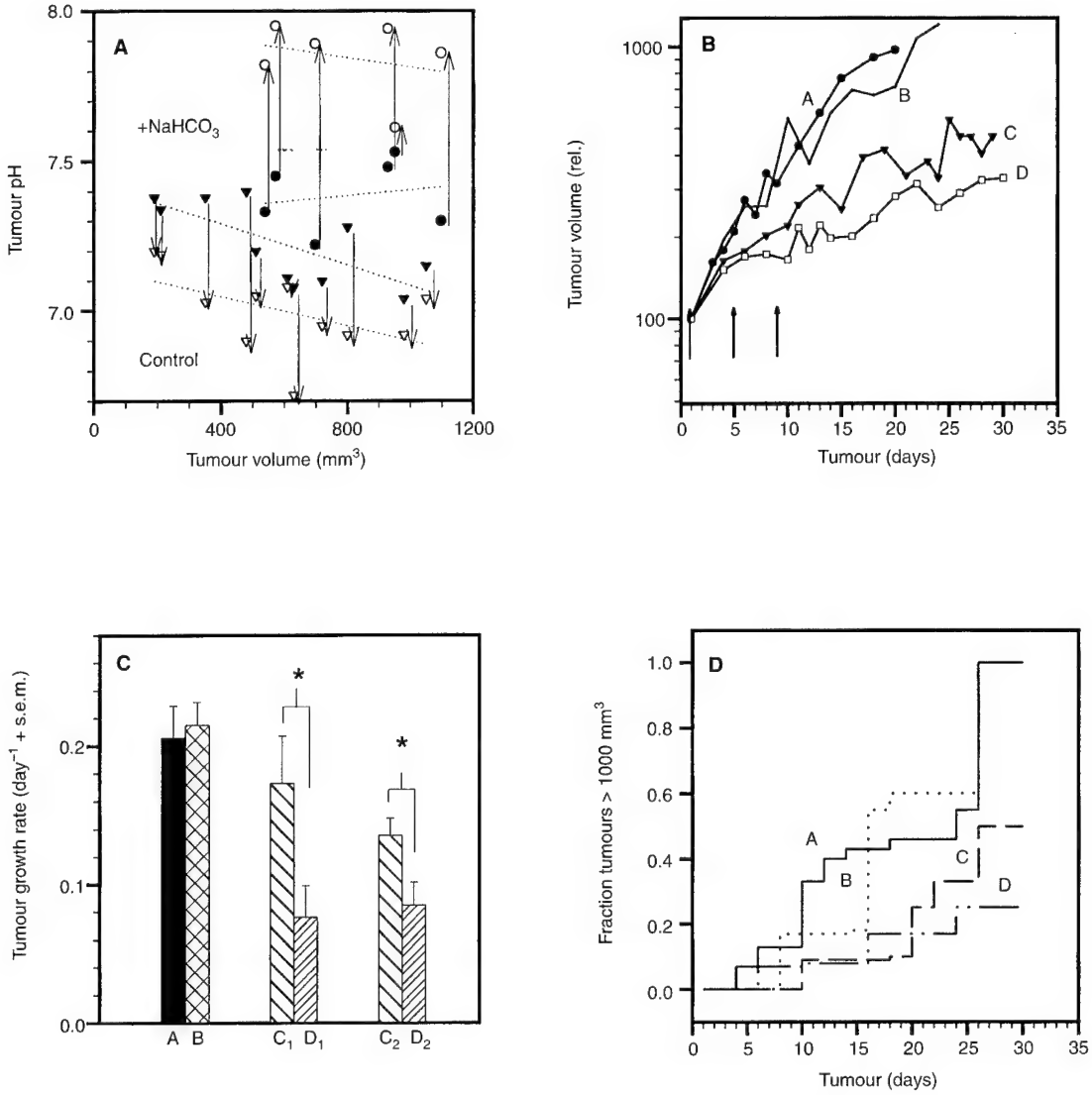

Figure 3 In vivo effects of combination chemotherapy. (**A**) pHi and pHe of MCF-7 tumours in control (triangles) and bicarbonate-treated (circles) mice. pHi and pHe values were measured using ^{31}P MRS, as described for Figure 1. These pHe data were collected 4–10 days following commencement of bicarbonate therapy. Closed symbols represent the intracellular pH values, measured with Pi, and the open symbols represent extracellular pH values, measured with 3-APP. Arrows indicate the direction of the intra- to extracellular gradient, and dotted lines represent independent linear regressions of the four data sets. (**B**) Tumour volumes as a function of time. MCF-7 tumours were grown in SCID mice to volumes of 50–200 mm^3, after which time they were randomized into four cohorts (A–D). Beginning on day 1, cohorts A and C received drinking water, whereas cohorts B and D received 200 mM $NaHCO_3$. On days 1, 5 and 9, animals of cohorts C and D were injected i.p. with doxorubicin (arrows), whereas animals from cohorts A and B were injected with saline. On day 15, animals of cohorts B and D were placed back on drinking water. For the purpose of display, tumour volumes were normalized to 100% on day 4. Data points represent the pooled means of 3–16 measurements at each time point from all experiments. (**C**) Specific growth rates. The rate of increase in tumour size was determined between days 9 and 15 for each animal by linear regression and expressed as fraction of surviving mice per day individual tumour. The illustrated data represent the mean ± standard deviation of these data sets binned by cohort. The cohorts were as described in Figure 3B, except that cohorts C_1/D_1 and C_2/D_2 were separated since they received doxorubicin at 2.0 and 1.6 mg kg^{-1} respectively. *Indicates values were significantly different ($P < 0.03$) by Student's *t*-test. (**D**) Individual tumour growth curves. Percent of total tumours in a cohort greater than 1000 mm^3 are plotted as a function of time since beginning of experiments. Cohorts are as described for Figure 3B

experiments, the incidence of morbidity following drug treatment was identical between groups C and D. In parallel experiments, three doses of i.p. doxorubicin at 2.0 mg kg^{-1} on days 1, 5 and 9 gave no evidence of vesication upon day 10 necropsy. Tumour volumes and animal weights were monitored every 2–3 days. For graphing purposes, tumour volumes for each mouse were normalized to day 1. As shown in Figure 3B, doxorubicin has a significant effect on the tumour growth rate, and this effect is greater in animals co-treated with bicarbonate. For statistical analyses, normalized data were used to calculate specific tumour growth rates for each tumour, from day 9 onward. The means of these normalized tumour growth rates are shown in Figure 3C. Regardless of dose, the tumour growth rate was significantly ($P \leq 0.03$) slower in the bicarbonate plus doxorubicin groups (D_1, D_2), compared to the doxorubicin alone groups (C_1, C_2) (Table 2). Furthermore, bicarbonate alone had no significant effect on the growth rate ($P > 0.4$, A vs B). Table 2 also shows that the tumour growth delays (T–C) were 15 and 22 days at 300 mm^3 for groups C and D respectively. However, since the slopes of the growth curves diverge, the T–C increased with time, and thus cannot be used to

reliably calculate log cell kill. The T/C values calculated at day 20 were 0.47 (751/1571) and 0.29 (458/1571) for groups C and D respectively. A modified (Kaplan–Meier type) survival plot showing the fraction of remaining animals with small (< 1000 mm^3) tumours is shown in Figure 3D. These data show that animals receiving doxorubicin plus bicarbonate take significantly longer to develop larger tumours compared to the other groups.

DISCUSSION

These data indicate that raising pHe increased the cytotoxic effectiveness of doxorubicin both in vitro and in vivo. In-vitro, raising the pHe from 6.8 to 7.4 resulted in a 2.25-fold enhancement of cytotoxicity and a 2.56-fold increase in intracellular doxorubicin concentrations. These data compared well to the 1.97-fold enhancement predicted from the calculated difference in doxorubicin distributions (Table 1). It is possible that the larger enhancement observed empirically, relative to theory, is due to sequestration of doxorubicin in acidic vesicles, which was not accounted for in the theoretical calculations (Altan et al, 1998; Raghunand et al, 1999*b*).

In vivo, in the SCID mouse–MCF7 tumour model system used here, the data clearly show that $NaHCO_3$ effectively raises the pHe for extended periods of time. Prolonged treatments with bicarbonate in drinking water did not have significant effects on animal well-being.

Nevertheless, for bicarbonate therapy to have clinical utility, the minimum required treatment time needs to be determined. Previous protocols involving bicarbonate treatment of humans have primarily been developed to counteract acidosis caused by exercise or renal failure (Passfall et al, 1997; Verbitsky et al, 1997). A problem in these protocols is poor patient compliance, with chronic bicarbonate ingestion. Clinical metabolic alkalinization with bicarbonate will be most successful if it is administered acutely, viz. shortly prior to the time of chemotherapy. Hence, experiments are underway to determine the time course of alkalinization and whether acute, intermittent alkalinization is as effective, compared to chronic bicarbonate administration.

Combination therapy with bicarbonate and doxorubicin resulted in a significantly lowered tumour growth rate compared to treatment with doxorubicin alone. In SCID mice, as in human patients, doxorubicin alone is not a highly effective cytotoxic agent with much heterogeneity of response. Many workers have used SCID mice to test doxorubicin chemotherapy (Liu et al, 1996; Cesano et al, 1997; Durand and LePard, 1997). However, a recent report indicates that doxorubicin is not effective to treat tumours in SCID mice, due to granulocyte toxicity to the host (Polin et al, 1997). This may be observed in our studies, since the tumour outgrowth did not occur with the same doubling time as the untreated tumours. Consequently, log kill values could not be reliably calculated. However, the T/C value measured at day 20 was 0.29 for group D, compared to 0.47 for group C. T/C < 44% is considered significant by the Division of Cancer Treatment (NCI). Thus, this measure indicates a meaningful boost in therapeutic effectiveness caused by raising the pH with bicarbonate. In other systems, such as sygeneic mice (16/C mammary adenocarcinoma in C3H mice), log kill from doxorubicin can be 2.5–3.0 (T Corbett, personal communication). Hence, experiments are planned using this more responsive mouse system, even though it is not a high connectivity model for human clinical response.

The growth rates resulting from the two different doxorubicin doses were not significantly different (i.e. C_1 vs C_2, D_1 vs D_2). However, the lower doxorubicin dose did reduce the mortality of the treated animals during the course of the experiments. At 2 mg kg^{-1}, half of the animals survived in both groups to day 30. At 1.6 mg kg^{-1}, only one animal from each group (out of eight) did not survive until day 30. It must be noted that doxorubicin-treated animals appeared more distressed than controls. By day 15, animals in groups C and D displayed poor grooming and urinary discharges. By day 30, all animals in group D were experiencing anal discharge as well. This suggests that, in addition to the tumours, bicarbonate also sensitized the intestinal epithelium to doxorubicin cytotoxicity. Since bicarbonate should only have this effect on tissues with low initial pHe, this might indicate that intestinal epithelial cells or colonic crypts have a naturally low pHe. This side-effect of combination bicarbonate–doxorubicin chemotherapy might be avoided with shorter bicarbonate treatment times, more selective alkalinizing agents, or protection of the intestinal epithelium with acid buffers or V-ATPase inhibitors. Despite the qualitatively poorer condition of group D animals, there was no significant difference in their body weights, compared to animals of group C.

Our calculations predict that alkalinization should provide a two- to threefold increase in the therapeutic efficacy of doxorubicin. This is significant, because many current clinical studies indicate that threefold accelerated dosing of doxorubicin is more effective in treating node-positive breast cancers (Bearman et al, 1997). However, doxorubicin has associated cardiotoxicity and there is a significant morbidity associated with accelerated dosing regimens. Thus, if two- to threefold increases in cytosolic doxorubicin could be achieved through manipulation of pH, it is likely that the therapeutic benefits could be realized without the increased morbidity associated with accelerated dosing.

In summary, the current data indicate that the pHe of human breast tumour xenografts is acidic and that this reduces the cytotoxicity of doxorubicin in vitro and in vivo. Tumour pHe can be chronically raised by treatment with sodium bicarbonate in the drinking water of tumour-bearing SCID mice, and this significantly increases the chemotherapeutic efficacy of doxorubicin chemotherapy in vivo.

ACKNOWLEDGEMENTS

The authors would like to thank J-P Galons for helpful discussions, L Celaya for secretarial assistance, and TH Corbett, J Evelhoch and S Salmon for thoughtful evaluations of the manuscript. Support from the US Army Breast Cancer Initiative grants DAMD-17-94-J-4368 (RJG) and DAMD-17-96-1-6131 (ZMB) and NIH RO1-CA23074 is also gratefully acknowledged.

REFERENCES

Altan N, Chen Y, Schindler M and Simon SM (1998) Defective acidification in human breast tumor cells and implications for chemotherapy. *J Exp Med* **187**: 1583–1598

Bearman SI, Overmoyer BA, Bolwell BJ, Taylor CW, Shpall EJ, Cagnoni PJ, Mechling BE, Ronk B, Baron AE, Purdy MH, Ross M and Jones RB (1997) High-dose chemotherapy with autologous peripheral blood progenitor cell support for primary breast cancer in patients with 4–9 involved axillary lymph nodes. *Bone Marrow Transplant* **20**: 931–937

Cesano A, Visonneau S, Rovera G and Santoli (1997) Synergistic effects of adriamycin and TALL-104 cell therapy against a human gastric carcinoma in vivo. *Anticancer Res* **17**: 1887–1892

Corbett TH, Roberts BJ, Trader MW, Laster WR Jr, Griswold DPJ and Schabel FM Jr. (1982) Response of transplantable tumors of mice to anthracenedione derivatives alone and in combination with clinically useful agents. *Cancer Treat Rep* **66**: 1187–1200

Durand RE and LePard NE (1997) Tumour blood flow influences combined radiation and doxorubicin treatments. *Radiother Oncol* **42**: 171–179

Gillies RJ and Deamer DW (1978) Intracellular pH: methods and applications. *Curr Top Bioenergetics* **9**: 63–87

Gillies RJ, Didier N and Denton M (1986) Determination of cell number in monolayer cultures. *Analyt Biochem* **159**: 109–113

Gillies RJ, Liu Z and Bhujwalla Z (1994) ^{31}P-MRS measurements of extracellular pH of tumors using 3-aminopropylphosphonate. *Am J Physiol* 195–203

Griffiths JR (1991) Are cancer cells acidic? *Br J Cancer* **64**: 425–427

Liu C, Lambert JM, Teicher BA, Blattler WA and O'Connor R (1996) Cure of multidrug-resistant human B-cell lymphoma xenografts by combinations of anti-B4-blocked ricin and chemotherapeutic drugs. *Blood* **87**: 3892–3898

Martinez-Zaguilan R, Martinez GM, Lattanzio F and Gillies RJ (1991) Simultaneous measurement of intracellular pH and Ca^{2+} using the fluorescence of SNARF-1 and Fura-2. *Am J Physiol* **260**: C297–C307

McCoy CL, Parkins CS, Chaplin DJ, Griffiths JR, Rodrigues LM and Stubbs M (1995) The effect of blood flow modification on ontra- and extracellular pH measured by 31P magnetic resonance spectroscopy in murine tumours. *Br J Cancer* **72**:

Negendank W (1992) Studies of human tumors by MRS: a review. *NMR Biomed* **5**: 303–324

Ordidge RJ, Bowley RM and McHale G (1988) A general approach to selection of multiple cubic volume elements using the ISIS technique. *Magn Reson Med* **8**: 323–331

Paine-Murrieta GD, Taylor CW, Curtis RA, Lopez MHA, Dorr RT, Johnson CS, Funk CY, Thompson F and Hersh EM (1997) Human tumor models in the severe combined immune deficient (*Scid*) mouse. *Cancer Chemother Pharmacol* **xx**: 1–6

Passfall J, Pai J, Spies KP, Haller H and Luft FC (1997) Effect of water and bicarbonate loading in patients with chronic renal failure. *Clin Nephrol* **47**: 92–98

Polin L, Valeriote F, White K, Panchapor C, Pugh S, Knight J, LoRusso, Hussain M, Liversidge E, Peltier N, Golakoti T, Patterson G, Moore and Corbett TH (1997) Treatment of human prostate tumors PC-3 and TSU-PR1 with standard and investigational agents in SCID mice. *Invest New Drugs* **15**: 99–108

Raghunand N, Altbach MI, Van Sluis R, Baggett B, Taylor CW, Bhujwalla ZM and Gillies RJ (1999*a*) Plasmalemmal pH-gradients in drug-sensitive and drug-resistant MCF-7 human breast carcinoma xenografts measured by 31P MR spectroscopy. *Biopharm Pharmacol* **57**: 309–312

Raghunand N, Martinez-Zaguilan R, Wright SH and Gillies RJ (1999*b*) pH and drug resistance II: turnover of acidic vesicles and resistance to weakly basic chemotherapeutic drugs. *Biochem Pharmacol* **57**: 1047–1058

Roos A (1978) Weak acids, weak bases, and intracellular pH. *Respir Physiol* **33**: 27–30

Simon SM and Schindler M (1994) Cell biological mechanisms of multidrug resistance in tumors. *Proc Natl Acad Sci USA* **91**: 3497–3504

Tannock IF and Rotin D (1989) Acid pH in tumors and its potential for therapeutic exploitation. *Cancer Res* **49**: 4373–4384

Taylor CW, Dalton WS, Parrish PR, Gleason MC, Bellamy WT, Thompson FH, Roe DJ and Trent JM (1991) Different mechanisms of decreased drug accumulation in doxorubicin and mitoxantrone resistant variants of the MCF7 human breast cancer cell line. *Br J Cancer* **63**: 923–929

Verbitsky O, Mizrahi J, Levin M and Isakov E (1997) Effect of ingested sodium bicarbonate on muscle force, fatigue, and recovery. *J Appl Physiol* **83**: 333–337

Warburg O (1956) On the origin of cancer cells. *Science* **123**: 309–314

Wike-Hooley JL, Haveman J and Reinhold HS (1984) The relevance of tumour pH to the treatment of malignant disease. *Radiother Oncol* **2**: 343–366

British Journal of Cancer (1999) **80**(7), 1012–1019

Article no. bjoc.1998.0456

Amphiregulin acts as an autocrine growth factor in two human polarizing colon cancer lines that exhibit domain selective EGF receptor mitogenesis

L Damstrup[1,2], SK Kuwada[3,4], PJ Dempsey[1], CL Brown[1], CJ Hawkey[1], HS Poulsen[2], HS Wiley[3] and RJ Coffey Jr[1]

[1]Departments of Medicine and Cell Biology, Vanderbilt University School of Medicine and Veterans Affairs Medical Center, Nashville, TN 37232, USA; [2]Section for Radiation Biology, University Hospital Copenhagen, Finsen Center 3993, Copenhagen DK-2100, Denmark; [3]Departments of Medicine and Pathology, [4]and Veterans Affairs Medical Center, University of Utah, Salt Lake City, UT 84132, USA

Summary Colonic enterocytes, like many epithelial cells in vivo, are polarized with functionally distinct apical and basolateral membrane domains. The aims of this study were to characterize the endogenous epidermal growth factor (EGF)-like ligands expressed in two polarizing colon cancer cell lines, HCA-7 Colony 29 (HCA-7) and Caco-2, and to examine the effects of cell polarity on EGF receptor-mediated mitogenesis. HCA-7 and Caco-2 cells were grown on plastic, or as a polarized monolayer on Transwell filters. Cell proliferation was measured by ^{3}H-thymidine incorporation and EGF receptor (EGFR) binding was assessed by Scatchard analysis. EGFR ligand expression was determined by Northern blot analysis, reverse transcription polymerase chain reaction, metabolic labelling and confocal microscopy. We found that amphiregulin (AR) was the most abundant EGFR ligand expressed in HCA-7 and Caco-2 cells. AR was localized to the basolateral surface and detected in basolateral-conditioned medium. Basolateral administration of neutralizing AR antibodies significantly reduced basal DNA replication. A single class of high-affinity EGFRs was detected in the basolateral compartment, whereas the apical compartment of polarized cells, and cells cultured on plastic, displayed two classes of receptor affinity. Basolateral administration of transforming growth factor alpha (TGF-α) or an EGFR neutralizing antibody also resulted in a dose-dependent stimulation or attenuation, respectively, of DNA replication. However, no mitogenic response was observed when these agents were added to the apical compartment or to confluent cells cultured on plastic. We conclude that amphiregulin acts as an autocrine growth factor in HCA-7 and Caco-2 cells, and EGFR ligand-induced proliferation is influenced by cellular polarity.

Keywords: EGFR; polarized cells; colon cancer cell lines; ligand and proliferation

Six mammalian ligands have been identified that bind to the epidermal growth factor receptor (EGFR): EGF, transforming growth factor-α (TGF-α), amphiregulin (AR), heparin-binding EGF-like growth factor (HB-EGF), betacellulin (BTC) and epiregulin. These ligands have been shown to mediate various cellular functions, including proliferation, differentiation and migration (Basson et al, 1992, 1994; Amemiya et al, 1994; Chen et al, 1994; Traverse et al, 1994). In epithelial cells cultured as a flat monolayer on plastic, it has been shown that TGF-α and AR can act in an autocrine manner (Culouscou et al, 1992; Johnson et al, 1992; Li et al, 1992; Ziober et al, 1993; Qi et al, 1994). Many epithelial cells in vivo, however, are polarized with spatially restricted apical and basolateral compartments. Certain epithelial cell types, most notably non-transformed canine MDCK-II cells, can be cultured in vitro as a polarized monolayer on semipermeable supports (Transwell filters). It has been shown that EGFRs are restricted to the basolateral compartment of these polarized MDCK cells (Maratos-Flier et al, 1987; Dempsey et al, 1994; Hobert et al, 1995) and it is predicted that basolateral, but not apical, administration of EGFR ligands would elicit biological effects.

Received 3 September 1998
Accepted 15 December 1998

Correspondence to: L Damstrup, Section for Radiation Biology, University Hospital Copenhagen, Finsen Center, 3993, 9, Blegdamsvej, Copenhagen DK-2100, Denmark

The present studies were undertaken to examine EGFR-mediated proliferation in two well-differentiated human colon cancer lines, HCA-7 Colony 29 (HCA-7) and Caco-2, that retain the ability to polarize under their appropriate culture conditions (Kirkland 1985; LeBivic et al, 1991; Coffey et al, 1997). Like MDCK cells, Caco-2 cells have been reported to have EGFRs localized predominantly to the basolateral surface (Bishop et al, 1994). We have compared DNA replication in HCA-7 and Caco-2 cells when cultured as a flat monolayer on plastic, and as a polarized monolayer on Transwell filters. As predicted, TGF-α stimulates mitogenesis when added to the basolateral compartment, but not to the apical compartment or to confluent cells cultured on plastic. Differences in expression of high-affinity EGFRs on different cell substrates used to culture the cells may account for these variations. In addition, conclusive evidence for AR autocrine growth activity is presented for these polarized cells. These results emphasize the biological relevance of studying epithelial cells in vitro in a polarized context.

MATERIALS AND METHODS

Reagents and antibodies

All cell culture reagents were purchased from Gibco Laboratories (Grand Island, NY, USA) and all chemicals were purchased from Sigma Chemical Co. (St Louis, MO, USA), unless otherwise

British Journal of Cancer (1998) 78(5), 606–611

Estimations of intra- and extracellular volume and pH by ^{31}P magnetic resonance spectroscopy: effect of therapy on RIF-1 tumours

ZM Bhujwalla[1], CL McCoy[2], JD Glickson[1]*, RJ Gillies[3] and M Stubbs[2]

[1]Division of NMR Research, Department of Radiology, The Johns Hopkins University School of Medicine, Baltimore, MD 21205, USA;
[2]CRC Biomedical MR Research Group, Division of Biochemistry, St. George's Hospital Medical School, Cranmer Terrace, London SW17 0RE, UK;
[3]Division of Biochemistry, University of Arizona, Tucson, AZ, USA

Summary Quantification of metabolite or drug concentrations in living tissues requires determination of intra- and extracellular volumes. This study demonstrates how this can be achieved non-invasively by ^{31}P magnetic resonance spectroscopy (MRS) employing dimethyl methylphosphonate (DMMP) as a marker of total water space, 3-aminopropylphosphonate (3-APP) as a marker of extracellular space and P_i and 3-APP as markers of intracellular pH (pH_i) and extracellular pH (pH_e) respectively. The MRS measurements of the tumour volumes were validated by classic radiolabelling methods using ^3H_2O and [^{14}C]inulin as markers of total and extracellular space respectively. The extracellular volume fraction measured by radiolabelling of RIF-1 tumours was 23 ± 0.83% (mean ± s.e.m. n = 9), not significantly different ($P > 0.1$) from that found by MRS (27 ± 2.9%, n = 9, London, and 35 ± 6.7, n = 14, Baltimore). In untreated RIF-1 tumours, pH_i was about 0.2 units higher than pH_e ($P < 0.01$). 5-Fluorouracil (5FU) treatment (165 mg kg^{-1}) caused no significant changes in either pH_e or per cent extracellular volume. However significant increases in pH_i 48 h after treatment ($P < 0.01$) correlated with decreased tumour size and improved bioenergetic status [NTP/inorganic phosphate (P_i) ratio]. This study shows the feasibility of an MR method (verified by a 'gold standard') for studying the effects of drug treatment on intra- and extracellular spaces and pH in solid tumours in vivo.

Keywords: ^{31}P magnetic resonance spectroscopy; 5-fluorouracil; pH; phosphonate; volume fraction

Determination of accurate metabolite concentrations is essential to elucidate tumour biochemistry and its relationship to underlying tissue physiology. Understanding the mechanisms that cause biochemical and physiological changes in tumours, particularly in response to treatment (Braunschweiger and Schiffer, 1986; Braunschweiger, 1988), is crucial in the quest to cure cancer. Current magnetic resonance spectroscopy (MRS) techniques for quantification reference the metabolite level to an external reference signal or an internal reference such as water (Thulborn and Ackerman, 1983; Shungu et al, 1992*a*). Changes in signal intensity detected following a therapeutic or physiological intervention (e.g. administration of a cancer drug or modification of tumour blood flow respectively) may be due either to a change in the amount of specific metabolites or to a change in the intracellular volume fraction. A method for measuring non-invasively the intra- and extracellular volume fraction is necessary to distinguish between these possibilities. Here we demonstrate that this can be accomplished by ^{31}P-MRS using dimethyl methylphosphonate (DMMP) and 3-aminopropylphosphonate (3-APP) as markers for total and extracellular water spaces respectively. DMMP is distributed among all the water spaces, whereas 3-APP accesses only the extracellular compartment; both compounds are chemically inert and non-toxic and are, therefore, suitable as compartmental volume indicators (Barry et al, 1993; Clarke et al, 1994; Gillies et al, 1994). Here we have validated this method by comparison with classical radiolabelling methods (^3H_2O and [^{14}C]inulin).

In a ^{1}H-MRS study of RIF-1 tumours responding to 5-fluorouracil (5FU) therapy, a decrease in trimethylamine and lactate signals was detected (Shungu et al, 1992*b*). However, whether these decreases resulted from a decrease in the intracellular quantities of these metabolites or from a change in the intracellular volume fraction is not known, and information on volume fraction would allow us to distinguish between these two possibilities. In addition, distinction between intra- and extracellular compartments is particularly important in pH measurements of normal and tumour tissue. The hydrogen ion (H^+) concentration of the intra- and extracellular milieu can influence drug uptake or repair of cellular damage (Hult and Larson, 1976; Hofer and Mivechi, 1980; Nissen and Tanneberger, 1981). As 3-APP also serves as an indicator of extracellular pH (pH_e) (Gillies et al, 1994) and inorganic phosphate (P_i) is predominantly in the intracellular compartment and is, hence, an endogenous indicator of intracellular pH (pH_i) under most conditions (Stubbs et al, 1992), we have also monitored changes in pH_i and pH_e of RIF-1 tumours following treatment with 5FU. Several agents such as 5FU or radiation are known to induce changes in pH following treatment (Tozer et al, 1989; Li et al, 1991). However, the contribution of the intra- and extracellular compartments to these changes has not been adequately defined.

Received 15 July 1997
Revised 9 March 1998
Accepted 11 March 1998

Correspondence to: M Stubbs

**Current address:* Department of Radiology, The University of Pennsylvania, B1 Stellar-Chance Research Labs, 422 Curie Boulevard, Philadelphia PA 19104-6100, USA.

Hendricks DT, Taylor R, Reed M and Birrer MJ (1997) FHIT gene expression in human ovarian, endometrial, and cervical cancer cell lines. *Cancer Res* **57**: 2112–2115

Kastury K, Baffa R, Druck T, Ohta M, Cotticelli MG, Inoue H, Negrini M, Rugge M, Huang D, Croce CM, Palazzo J and Huebner K (1996) Potential gastrointestinal tumor suppressor locus at the 3p14.2 FRA3B site identified by homozygous deletions in tumor cell lines. *Cancer Res* **56**: 978–983

Kok K, Naylor SL and Buys CH (1997) Deletions of the short arm of chromosome 3 in solid tumors and the search for suppressor genes. *Adv Cancer Res* **71**: 27–92

Lench N, Stanier P and Williamson R (1988) Simple non-invasive method to obtain DNA for gene analysis. *Lancet* **1**: 1356–1358

Lisitsyn NA, Leach FS, Vogelstein B and Wigler MH (1994) Detection of genetic loss in tumors by representational difference analysis. *Cold Spring Harbor Symp Quant Biol* **59**: 585–587

Luan X, Shi G, Zohouri M, Paradee W, Smith DI, Decker HJ and Cannizzaro LA (1997) The FHIT gene is alternatively spliced in normal kidney and renal cell carcinoma. *Oncogene* **15**: 79–86

Man S, Ellis IO, Sibbering M, Blamey RW and Brook JD (1996) High levels of allele loss at the FHIT and ATM genes in non-comedo ductal carcinoma in situ and grade I tubular invasive breast cancers. *Cancer Res* **56**: 5484–5489

Mao L, Fan Y-H, Lotan R and Hong WK (1996) Frequent abnormalities of FHIT, a candidate tumor suppressor gene, in head and neck cancer cell lines. *Cancer Res* **56**: 5128–5131

Melo JV (1996) The diversity of BCR-ABL fusion proteins and their relationship to leukemia phenotype. *Blood* **88**: 2375–2384

Naylor SL, Johnson BE, Minna JD and Sakaguchi AY (1987) Loss of heterozygosity of chromosome 3p markers in small-cell lung cancer. *Nature* **329**: 451–454

Negrini M, Monaco C, Vorechovsky I, Ohta M, Druck T, Baffa R, Huebner K and Croce CM (1996) The FHIT gene at 3p14.2 is abnormal in breast carcinomas. *Cancer Res* **56**: 3173–3179

Ohta M, Inoue H, Cotticelli MG, Kastury K, Baffa R, Palazzo J, Siprashvili Z, Mori M, McCue P, Druck T, Croce CM and Huebner K (1996) The FHIT gene, spanning the chromosome 3p14.2 fragile site and renal carcinoma-associated t(3;8) breakpoint, is abnormal in digestive tract cancers. *Cell* **84**: 587–597

Panagopoulos I, Pandis N, Thelin S, Petersson C, Mertens F, Borg Å, Kristoffersson U, Mitelman F and Åman P (1996) The FHIT and PTPRG genes are deleted in benign proliferative breast disease associated with familial breast cancer and cytogenetic rearrangements of chromosome band 3p14. *Cancer Res* **56**: 4871–4875

Panagopoulos I, Thelin S, Mertens F, Mitelman F and Åman P (1997) Variable FHIT transcripts in non-neoplastic tissues. *Genes Chromosom Cancer* **19**: 215–219

Paradee W, Mullins C, He Z, Glover T, Wilke C, Opalka B, Schutte J and Smith DI (1995) Precise localization of aphidicolin-induced breakpoints on the short arm of human chromosome 3. *Genomics* **27**: 358–361

Sambrook J, Fritsch EF and Maniatis T (eds) (1989) *Molecular Cloning – A Laboratory Manual*. Cold Spring Harbor Laboratory Press: Cold Spring Harbor, New York

Shridhar R, Shridhar V, Wang X, Paradee W, Dugan M, Sarkar F, Wilke C, Glover TW, Vaitkevicius VK and Smith DI (1996) Frequent breakpoints in the 3p14.2 fragile site, FRA3B, in pancreatic tumors. *Cancer Res* **56**: 4347–4350

Sill H, Goldman JM and Cross NCP (1995) Homozygous deletions of the p16 tumor suppressor gene are associated with lymphoid transformation of chronic myeloid leukemia. *Blood* **85**: 2013–2016

Sozzi G, Veronese ML, Negrini M, Baffa R, Cotticelli MG, Inoue H, Tornielli S, Pilotti S, De Gregorio L, Pastorino U, Pierotti MA, Ohta M, Huebner K and Croce CM (1996*a*) The FHIT gene at 3p14.2 is abnormal in lung cancer. *Cell* **85**: 17–26

Sozzi G, Alder H, Tornielli S, Corletto V, Baffa R, Veronese ML, Negrini M, Pilotti S, Pierotti MA, Huebner K and Croce CM (1996*b*) Aberrant FHIT transcripts in Merkel cell carcinoma. *Cancer Res* **56**: 2472–2474

Thiagalingam S, Lisitsyn NA, Hamaguchi M, Wigler MH, Willson JKV, Markowitz SD, Leach FS, Kinzler KW and Vogelstein B (1996) Evaluation of the FHIT gene in colorectal cancers. *Cancer Res* **56**: 2936–2939

Virgilio L, Shuster M, Gollin SM, Veronese ML, Ohta M, Huebner K and Croce CM (1996) FHIT gene alterations in head and neck squamous cell carcinomas. *Proc Natl Acad Sci USA* **93**: 9770–9775

Yanagisawa K, Kondo M, Osada H, Uchida K, Takagi K, Masuda A, Takahashi T and Takahashi T (1996) Molecular analysis of the FHIT gene at 3p14.2 in lung cancer cell lines. *Cancer Res* **56**: 5579–5582

Zbar B, Brauch H, Talmadge C and Linehan M (1987) Loss of alleles of loci on the short arm of chromosome 3 in renal cell carcinoma. *Nature* **327**: 721–724

Zeiger MA, Gnarra JR, Zbar B, Linehan WM and Pass HI (1994) Loss of heterozygosity on the short arm of chromosome 3 in mesothelioma cell lines and solid tumors. *Genes Chromosom Cancer* **11**: 15–20

Zeiger MA, Zbar B, Keiser H, Linehan WM and Gnarra JR (1995) Loss of heterozygosity on the short arm of chromosome 3 in sporadic, von Hippel–Lindau disease-associated, and familial pheochromocytoma. *Genes Chromosom Cancer* **13**: 151–156

Zou T-T, Lei J, Shi Y-Q, Yin J, Wang S, Souza RF, Kong D, Shimada Y, Smolinski KN, Greenwald BD, Abraham JM, Harpaz N and Meltzer SJ (1997) FHIT gene alterations in esophageal cancer and ulcerative colitis (UC). *Oncogene* **15**: 101–105

Table 1 T_1 values obtained for the injection solution and for tumours in vivo

Sample	T_1 3-APP (s)	T_1 DMMP (s)
Injection solution (n = 2)	1.7 ± 0.3	14.3 ± 0.2
Tumours in vivo (n = 3)	6.1 ± 0.2	13.7 ± 0.8

Error bars represent s.e.m.

Table 2 Saturation factors calculated for the repetition times used

Repetition time (s)	Factor *f* where (M = *f*.Mo) for 3-APP	Factor *f* where (M = *f*.Mo) for DMMP
10	0.933	0.786
20	0.987	0.917
30	0.998	0.964

For details and equation see text.

METHODS

The studies were carried out at two different sites: London (St. George's Hospital Medical School) and Baltimore (The Johns Hopkins University School of Medicine). Whereas the fractional volume measurements were made by both the MRS and radiolabelling method in London using separate cohorts of tumours, fractional volume measurements were made by the MRS method only in Baltimore. The pH measurements were made from the MR spectra at both sites, but response to tumour treatment was monitored in Baltimore only.

Animals and tumours

Studies at both sites were performed on RIF-1 tumours grown subcutaneously in the flanks of C3H/HeN mice in either London or Baltimore. The mice in London were fed on Special Diet Services, Rat and Mouse maintenance No. 1 (Lillico, Betchworth, Surrey), whereas in Baltimore mice were fed on Teklad LM-485 Mouse/Rat sterilizable diet (Harlan, Teklad, Madison, WI, USA).

Tumours were grown according to the protocol of Twentyman et al (1980). Tumours were between 300 and 1000 mm^3 when used. Mice were anaesthetized with a combination of ketamine (50 mg kg^{-1}; Aveco) and acepromazine (5 mg kg^{-1}; Aveco) in Baltimore or ketamine (50 mg kg^{-1}; Parke-Davis, UK) and diazepam (25 mg kg^{-1}; Phoenix Pharmaceuticals, UK) in London. They were subsequently injected intraperitoneally with a solution of 3-APP (480 mg kg^{-1}; Sigma) and DMMP (480 µl kg^{-1}; Sigma) administered in a volume of 0.2 ml of saline.

MRS studies

MRS studies were performed on either a GE (Baltimore) or SISCO (London) 4.7-T horizontal magnet, using home-built solenoidal coils (10.5 mm in diameter), which were placed over the tumours with the mice in the supine position. A proton image through the centre of a tumour using the same coil as that used to acquire the ^{31}P spectra demonstrated that there was negligible contribution from tissue outside of the tumour. The mice were placed on a flask or pad containing recirculating warm water to maintain a constant body temperature around 37°C. The same coils were used to obtain spectra of the injection solution (DMMP and 3-APP). As it is known that the T_1 values of phosphonates are longer in solution than in tissue (Clarke et al, 1994), the T_1 values of both 3-APP and DMMP were measured by an inversion recovery sequence in solution and in vivo (Table 1). The spectra of the solution of DMMP and 3-APP (an equal amount of each) were acquired with a single scan, firstly with a 45° pulse and subsequently with a 90° pulse; the time interval between the two spectra was 1 min.

In vivo spectra were acquired with the following parameters: 45° flip angle, recycle time (tr) = 10 or 20 s, number of aquisitions (na) = 64 followed by two partially saturated spectra (tr = 1 s, na = 200 Baltimore only), with a further fully relaxed spectrum (parameters as before). The partially saturated spectra were obtained to confirm the chemical shift positions with improved signal to noise for the pH measurements before and after 5FU treatment. Analysis of the 3-APP and DMMP resonances at both centres was obtained from the mean of two fully relaxed scans (total na = 128). In addition, analysis of 3-APP and DMMP resonances before and after a time interval of 6–7 min ensured that the two compounds were at equilibrium over the time of observation.

A spectrum of the injection solution was obtained before each animal experiment to take into account any evaporation of the

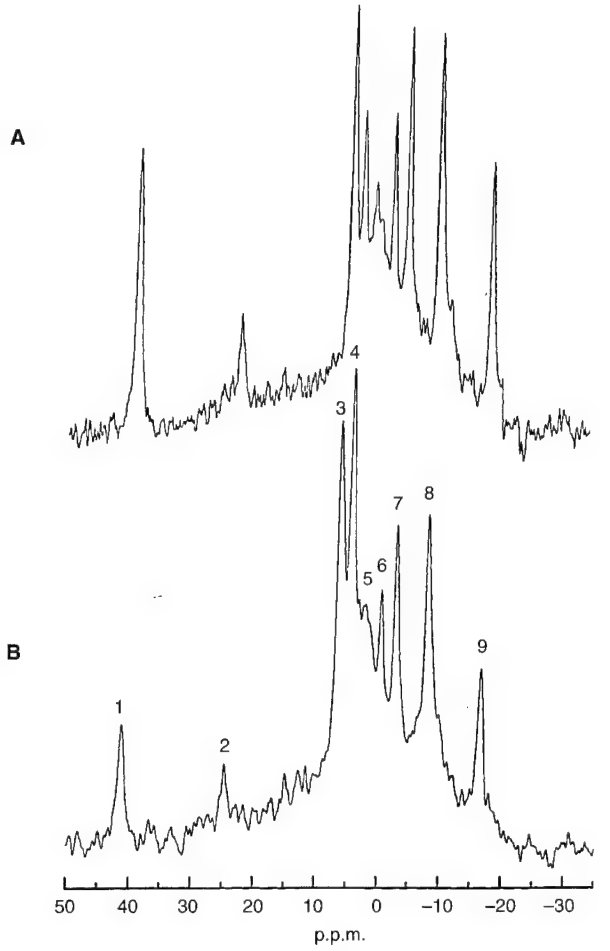

Figure 1 ^{31}P MR-spectra of RIF-1 tumours taken in **A** Baltimore and **B** London. Peak assignments as follows: (1) 3-APP, (2) DMMP, (3) phosphomonoesters, (4) P_i, (5) phosphodiesters, (6) PCr, (7) γ-NTP, (8) α-NTP, (9) β-NTP. For other details see Methods

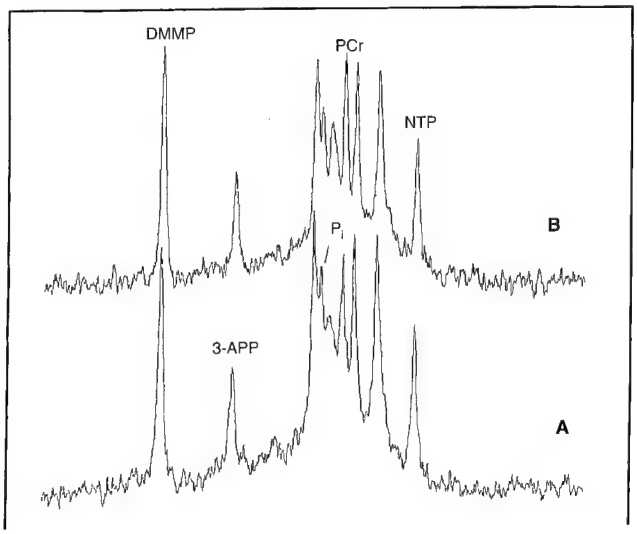

Figure 2 A ^{31}P-MR spectrum obtained from a representative RIF-1 tumour **A** before and **B** 48 h after 165 mg kg^{-1} 5-FU. For acquisition parameters see Methods. Tumour volume was 249 mm^3 on day 0 and regressed to 148 mm^3 by 48 h

solution. These spectra were used to calculate the fractional volumes (see below for details). Additional experiments were performed to ascertain that the rate of clearance of both compounds was similar and that they cleared within 24 h of administration, and this was, indeed, the case.

Data analysis and quantitation

Fully relaxed spectra were used for the quantitative estimation of the fractional volumes, and in-house computer methods were used for quantifying the peaks at both sites. In Baltimore, data sets were processed using an exponential line-broadening factor of 22 Hz. Peak areas were determined in the time domain using an in-house non-linear least squares curve-fitting routine for MR data analysis written by Dr DC Shungu. In London, after 20 Hz line broadening, the MR spectra were analysed using VARPRO, a time domain fitting routine (van der Veen et al, 1988). The DMMP peak area was assumed to be proportional to the amount of DMMP in the sensitive volume of the coil, and equivalent to the total water volume of the tumour (in the sensitive volume of the coil). Analogously, the 3-APP peak resonance area was assumed to be proportional to the amount of 3-APP in the tumour. DMMP and 3-APP resonances in the in vitro spectra were analysed in a similar way.

Using equation 1, the T_1 values measured and a flip angle $\alpha = 45°$, saturation factors were derived for the repetition times used in the study (Table 2) and were taken into account in the data analysis.

$$Mz\,(t) = Mo\,(1\text{-}\exp^{-t/T_1})/(1\text{-}\cos\alpha\exp^{-t/T_1}) \qquad (1)$$

The intra- and extracellular volumes from the MRS data were calculated from the mean of two fully relaxed in vivo spectra and the spectrum of the injection solution (*sol*) as follows:

$$\%\ \text{extracellular space} = Mo(\text{3-APP})/Mo(\text{DMMP})_{\text{in vivo}} \times Mo(\text{DMMP})/Mo(\text{3-APP})_{sol} \times 100$$

pH_i and pH_e measurements

pH_i was calculated from the chemical shift difference between inorganic phosphate (P_i) and α-NTP (an endogenous reference at –7.57 p.p.m. relative to phosphocreatine at 0 p.p.m.), and pH_e was calculated from the chemical shift difference between the 3-APP resonance and α-NTP. The chemical shifts were taken from the maximum resonance of the relevant species. pH_i was calculated from the relationship $pH = 6.66 + \log[\delta Pi - 0.65]/(3.11 - \delta Pi)$, where δ denotes the chemical shift in p.p.m. pH_e was calculated from the relationship $pH = 6.91 - \log[\delta\ \text{3-APP} - 21.11]/(24.3 - \delta\ \text{3-APP})$ (Gillies et al, 1994, see also McCoy et al, 1995). Results are expressed as mean ± 1 s.e.m.

Radiolabelling studies

Extracellular volume was assessed by measuring the distribution of ^3H_2O (as a marker of total cell water) and [^{14}C]inulin (as a marker of extracellular space). Tumours were freeze clamped with liquid nitrogen-cooled tongs 20 min after tail-vein injection of 40 μCi of ^3H_2O and 1 μCi of [^{14}C]inulin (obtained from Amersham International, Amersham, Bucks, UK). The whole tumour was extracted with 6% perchloric acid and neutralized as described in Bergmeyer (1974). Blood plasma was obtained by centrifugation of a whole blood sample taken from the mouse at the time of freeze clamping. The plasma supernatant was deproteinized with 6% perchloric acid. The tumour and plasma samples were subsequently neutralized and counted for radioactivity. Time course measurements showed that equilibration of the label with the body fluids occurred within 20 min. Total water content was measured by comparing ^3H_2O counts in the tissue with those of the plasma (i.e. ^3H_2O c.p.m. per g wet wt/^3H_2O c.p.m. per ml plasma = ml H_2O/g wet wt). Similarly, extracellular volumes were calculated by making comparisons of the ^{14}C inulin distribution between tissue and plasma samples taken at the same time and the results were expressed as a percentage of total cell water (i.e. ml extracellular water/ml total cell water × 100). Extracellular volumes were also measured in a control tissue (liver $n = 7$).

5FU studies

Of the 15 animals studied in Baltimore, eight were treated with 165 mg kg^{-1} 5-FU, with seven acting as controls. Animals were studied by ^{31}P-MRS at 0 and 48 h. None of the animals exhibited any overt signs of toxicity such as loss of weight or appetite; tumour growth in the untreated animals was not affected.

RESULTS

MRS vs radiolabelling measurements of extracellular space

Representative spectra of RIF-1 tumours from both Baltimore and London obtained using similar acquisition parameters are shown in Figure 1. Resonances from endogenous α-, β- and γ-NTP, P_i and a small contribution from PCr are seen, as are resonances from DMMP and 3-APP, administered by i.p. injection. Calculation of the extracellular water content (see Methods) was made from the ^{31}P-MR spectra of RIF-1 tumours (both in Baltimore and London) and from the radiolabelling results (London only). At 23.0 ± 0.83 (mean ± 1 s.e.m.) vs 27 ± 2.9% ($n = 9$) for the radiolabelling and MRS respectively (London), there was no significant difference

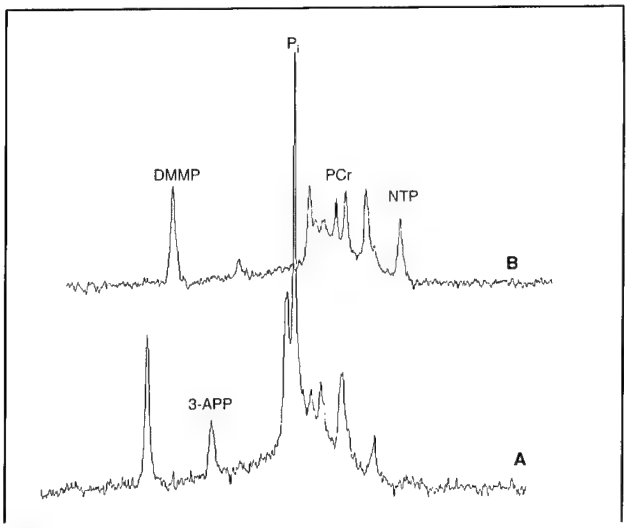

Figure 3 A ^{31}P-MR spectrum obtained from a RIF-1 tumour **A** before and **B** 48 h after 165 mg kg^{-1} of 5-FU, which showed a large increase in both NTP/P_i ratio and in pH_i and pH_e after treatment. For acquistion parameters see Methods. Tumour volume was 500 mm^3 on day 0 and regressed to 300 mm^3 by 48 h

between the two techniques ($P > 0.1$). This compared well with 35 ± 6.7 ($n = 14$) for the MRS method found in Baltimore ($P > 0.1$) compared with either 'gold standard' or London MRS values. From the radiolabelling studies we were able to calculate that the total water content of the tumours was 0.91 ± 0.08 ml g^{-1} wet wt compared with 0.74 ± 0.04 ($n = 8$) in liver. The extracellular space of the tumours was significantly higher than that of livers ($16.6 \pm 0.76\%$, $n = 7$ ($P < 0.0001$) and similar to that found previously in rat tumours (Stubbs et al, 1992).

pH_i and pH_e of RIF-1 tumours

pH values for the untreated set of tumours measured in London gave values for pH_i of 7.06 ± 0.03 ($n = 9$), and pH_e of 6.81 ± 0.07 ($n = 9$), confirming the relatively more acidic extracellular pH found previously (Gillies et al, 1994; McCoy et al, 1995). Both pH_i and pH_e values for the Baltimore tumours were slightly higher; pH_i 7.20 ± 0.04 and pH_e 7.02 ± 0.11 ($n = 14$).

Effect of 5-FU on pH and extracellular volume

^{31}P-MR spectra (Baltimore) obtained from a RIF-1 tumour before and 48 h after 5-FU and representative of most of the tumours studied are shown in Figure 2A and B respectively. The tumour volume had regressed from 249 mm^3 to 148 mm^3 during this time. The NTP/P_i ratio and the pH_i had both increased and a statistical summary of the data are presented in Figure 4. Although pH_i of RIF-1 tumours is usually 7.1–7.2, one tumour demonstrated a dramatic change in both intra- and extracellular pH, which can occur following 5-FU (Figure 3A and B). In this tumour pH_i increased from 6.8 to 7.44, and pH_e increased from 6.8 to 7.24 48 h after 5FU treatment. The overall changes in tumour volume, pH_i and NTP/P_i, for control and treated tumours are shown in Fig 4 A–C. As observed previously, pH_i decreased significantly in the control tumours as the tumour volume increased. However, a significant increase in pH_i (paired t-test, $P < 0.019$, $n = 8$) was seen following treatment with 5-FU, from 7.15 ± 0.07 to 7.38 ± 0.04 within 48 h. pH_e increased by more than 0.6 units in one tumour (Figure 3), which had both pH_e and pH_i below 6.8. Overall, however, there was no significant change in pH_e following 5-FU. Treatment with 5-FU also resulted in a small but significant increase in NTP/P_i by 48 h ($P < 0.05$).

As mentioned previously, the extracellular volume fraction within RIF-1 tumours before treatment was found to be similar ($35 \pm 6.7\%$) to those measured in London ($27 \pm 2.9\%$). When tumours were separated into treated and untreated groups, the extracellular volume fraction was $33 \pm 5.3\%$ at time 0, and $35 \pm 5.6\%$ at 48 h after treatment. The volume fraction for the untreated tumours was $38 \pm 8\%$ and $39.0 \pm 4.2\%$ for 0 and 48 h respectively.

DISCUSSION

Clarke et al (1994) have validated ^{31}P-MRS measurements of extracellular space in isolated rat hearts using phosphonates as

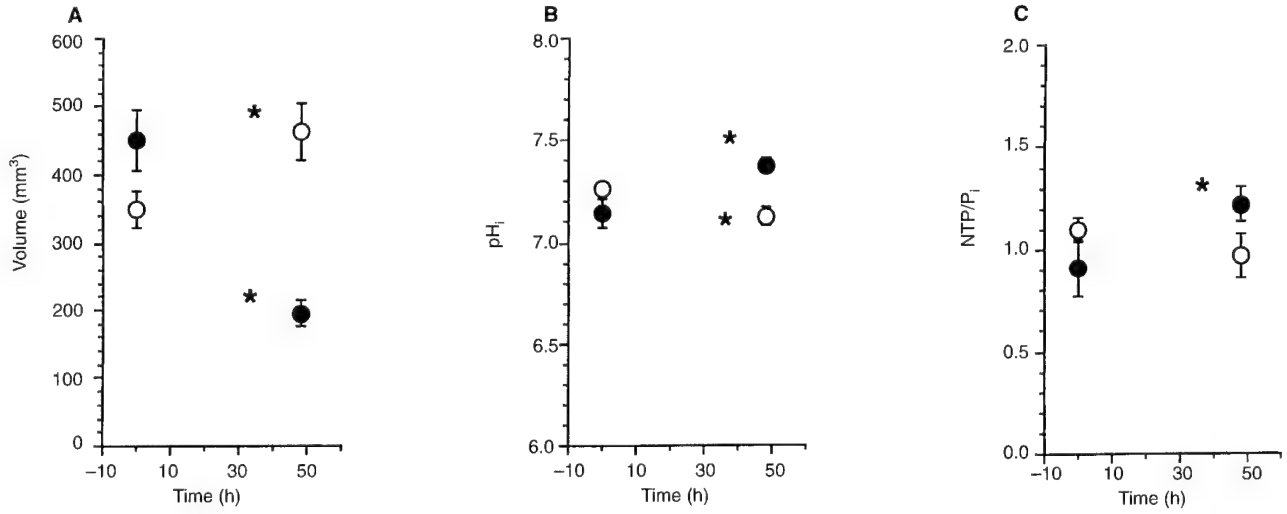

Figure 4 Changes in **A** tumour volume, **B** pH_i and **C** NTP/P_i at 0 and 48 h for (○) control tumours ($n = 7$) and (●) tumours treated with 165 mg kg^{-1} 5-FU

markers of different water spaces [DMMP for total water space and phenylphosphonic acid (PPA) as a marker of extracellular space]. Here we have shown that data obtained with the markers DMMP and 3-APP, which we have already shown is a useful marker of pH_e (Gillies et al, 1994), are in good agreement with values obtained using classical invasive methods for measuring volume fractions in an experimental tumour model. We also found that the extracellular volume fraction did not change significantly following 5FU treatment.

In contrast to the findings with 5FU in the present study, Braunschweiger (1988), using cyclophosphamide treatment and classical radiolabel methods that involved excising the tumours, demonstrated increases in RIF-1 tumour plasma and interstitial water volumes within 48 h of treatment. However, the modes of action of these two drugs are quite different, and therefore the observed differences in response are not totally unexpected. Changes in tissue water compartmentation after treatment involve complex physiological phenomena such as transient ischaemia, intermittent perfusion and vascular collapse, which occur in solid tumours, and these may contribute to the differences observed.

An additional interesting feature of cyclophosphamide treatment is that it causes an increase in the apparent diffusion coefficient (ADC) of water measured by diffusion weighted spectroscopy (Zhao et al, 1996), which is consistent with an increase in the fractional water content. However, the changes in ADC are difficult to interpret and the MRS method of measuring water spaces described in this paper may prove useful in conjunction with diffusion weighted spectroscopy measurements to aid in the interpretation of treatment-induced changes in the intensities of metabolite signals and as a potential predictor of response. Indeed other non-invasive MR methods such as multiexponential T_2 measurements may provide information on extracellular volume fractions at much higher spatial resolution (Whittall et al, 1997) in vivo. Determining whether the information obtained by such techniques does actually represent extracellular volume fractions is crucial to their potential usefulness, and comparisons made with the method described in this paper could be important.

A significant increase in pH_i at 4 h following a dose of 165 mg kg^{-1} 5-FU was observed consistently. As mentioned earlier, significant changes in pH_i have been observed following different forms of treatment such as radiation and chemotherapy in several other studies (Tozer et al, 1989; Li et al, 1991). These changes are usually attributed to an improvement in perfusion and bioenergetic status within the tumour (Tozer et al, 1989) following treatment. However, for such an effect to occur, one has to assume that pH regulation is energy limited in these tumours. Indeed, there is some evidence for this, both from Ehrlich ascites cells, in which pH homeostasis has been shown to be ATP dependent (Gillies et al, 1982), and from the study of Bhujwalla et al (1991), in which supplying glucose directly to RIF-1 tumours resulted in a significant increase in pH_i and NTP/P_i. This is also consistent with our observation that treated tumours showed a small but significant increase in NTP/P_i following 5FU. RIF-1 tumours have necrotic fractions of the order of 5–10% (Tozer et al, 1989).

The reasons for the differences in the absolute values of pH are not readily explained as measurements were made on machines of similar field strength, on the same tumour type and using the same standard curves for calculating pH. These differences have been apparent throughout our many years of collaboration and must be put down to some basic biological differences that have developed in the tumours over years of passage and/or to the differences in animal chow used in the USA and UK (e.g. 19% crude protein used in the US diet compared with 14.7% used in the UK diet). However, the absolute values are not so important and do not effect the experimental conclusions, as each animal serves as its own control.

With the exception of one tumour the results suggest that, as long as the initial pH_i was higher than 7.0, and pH_e higher than 6.8, the treatment-induced changes in pH_i were not accompanied by an increase in pH_e. All treated tumours decreased in size by more than 40% following treatment, but studies relating cell survival to changes in pH (intra- and extracellular) remain to be performed. It is possible that the increase in pH_i observed following 5FU may be related to attempts by the tumour cells to export the cytotoxic drug (Simon et al, 1994). An increase in pH_i in RIF-1 tumours 2 h after treatment with 5FU has also been observed (McSheehy et al, 1998). In conclusion, this study demonstrates the feasibility and the importance of tracking changes non-invasively in the content and quantity of tumour milieu following treatment.

ACKNOWLEDGEMENTS

The authors would like to acknowledge the surgical skills of Ms Loreta Rodrigues. We thank Professor JR Griffiths for his support and for useful discussions. This work was supported by the Cancer Research Campaign grant no. SP1971/0402 (CLM and MS), USAMRMC Breast Cancer grant DAMD17-94-J-4368 (RJG), NIH grants CA 51950 and CA 51935 (JDG and ZMB), DAMD-17-96-1-6131 and CA 73850 (ZMB). We thank Mr G Cromwell for transplanting the tumours and maintaining the cell line in Baltimore and the assistance of Dr VP Chacko in obtaining high-resolution spectra.

REFERENCES

Barry JA, McGovern KA, Lien YH, Ashmore B and Gillies RJ (1993) Dimethyl methylphosphonate (DMMP): a ^{31}P nuclear magnetic resonance spectroscopic probe of intracellular volume in mammalian cell cultures. *Biochemistry* **32**: 4665–4670

Bergmeyer HU (1974) *Methods of Enzymatic Analysis*. Verlag Chemie: Weinheim

Bhujwalla ZM, Constantinidis I, Chatham JC, Wehrle JP and Glickson JD (1991) Energy metabolism, pH changes, and lactate production in RIF-1 tumors following intratumoral injection of glucose. *Int J Radiat Oncol Biol Phys* **22**: 95–101

Braunschweiger P (1988) Effect of cyclophosphamide on the pathophysiology of RIF-1 solid tumors. *Cancer Res* **48**: 4206–4210

Braunschweiger P and Schiffer LM (1986) Effect of dexamethasone on vascular function in RIF-1 tumors. *Cancer Res* **46**: 3299–3303

Clarke K, Anderson RE, Nedelec J-F, Foster D and Ally A (1994) Intracellular and extracellular spaces and the direct quantification of molar intracellular concentrations of phosphorus metabolites in the isolated rat heart using ^{31}P NMR spectroscopy and phosphonate markers. *Magn Reson Med* **32**: 181–188

Gillies RJ, Ogino T, Shulman RG and Ward DC (1982) ^{31}P NMR evidence for regulation of intracellular pH by Ehrlich ascites tumour cells. *J Cell Biol* **95**: 24–28

Gillies R, Liu Z and Bhujwalla ZM (1994) ^{31}P MRS measurements of extracellular pH of tumors using 3-aminopropylphosphonate. *Am J Physiol* **267**: C195–C203

Hofer KG and Mivechi NF (1980) Tumour cell sensitivity to hyperthermia as a function of extracellular and intracellular pH. *J Natl Cancer Inst* **65**: 621–625

Hult RL and Larson RE (1976) Dissociation of 5-fluorouracil uptake from intracellular pH in Walker 256 carcinosarcoma. *Cancer Treat Rep* **60**: 867–873

Li SJ, Wehrle JP, Glickson JD, Kumar N and Braunschweiger PG (1991) Tumor bioenergetics and blood flow in RIF-1 murine tumors treated with 5-fluorouracil. *Magn Reson Med* **22**: 47–56

McCoy CL, Parkins CS, Chaplin DJ, Griffiths JR, Rodrigues LM and Stubbs M (1995) The effect of blood flow modification on intra- and extracellular pH measured by 31P magnetic resonance spectroscopy in murine tumours. *Br J Cancer* **72**: 905–911

McSheehy PJM, Robinson SP, Ojugo ACE, Cannell MB, Leach MO, Judson IR and Griffiths JR (1998) Carbogen breathing increases 5-fluorouracil uptake and cytotoxicity in hypoxic murine RIF-1 tumours: a magnetic resonance study in vivo. *Cancer Res* **58**(6): 1185–1194

Nissen E and Tanneberger ST (1981) Influence of pH and serum on the effectivity of antineoplastic agents in vitro. *Arch Geschwulstforsch* **51**: 152–156

Shungu DC, Bhujwalla ZM, Li S-J, Rose LM, Wehrle JP and Glickson JD (1992*a*) Determination of absolute phosphate metabolite concentrations in RIF-1 tumors in vivo by ^{31}P-^{1}H-^{2}H NMR spectroscopy using water as an internal intensity reference. *Magn Reson Med* **28**: 105–121

Shungu DC, Bhujwalla ZM, Wehrle JP and Glickson JD (1992*b*) ^{1}H NMR spectroscopy of subcutaneous tumors in mice: preliminary studies of effects of growth, chemotherapy and blood flow reduction. *NMR Biomed* **5**: 296–302

Simon S, Roy D and Schindler MV (1994) Intracellular pH and the control of multidrug resistance. *Proc Natl Acad Sci* **91**: 1128–1132

Stubbs M, Bhujwalla ZM, Tozer GM, Rodrigues LM, Maxwell RJ, Morgan R, Howe FA and Griffiths JR (1992) An assessment of ^{31}P MRS as a method of measuring pH in rat tumours. *NMR Biomed* **5**: 351–359

Thulborn KR and Ackerman JJH (1983) Absolute molar concentrations by NMR in inhomogeneous B1. A scheme for analysis of in vivo metabolites. *J Magn Reson* **55**: 357–371

Tozer GM, Bhujwalla ZM, Griffiths JR and Maxwell RJ (1989) Phosphorus-31 magnetic resonance spectroscopy and blood perfusion of the RIF-1 tumour following X-irradiation. *Int J Radiat Oncol Biol Phys* **16**: 155–164

Twentyman PR, Brown JM, Gray JW, Franko AJ, Scoles MA and Kallman RF (1980) A new mouse tumor system (RIF-1) for comparison of endpoint studies. *J Natl Cancer Inst* **49**: 735–749

Van der Veen JWC, De Beer R, Luyten PR and Van Ormondt D (1988) Accurate quantification of in vivo ^{31}P NMR signals using the variable projection method and prior knowledge. *Magn Reson Med* **6**: 92

Whittall KP, Mackay AL, Graeb DA, Nugent RA, Li DKB and Paty DW (1997) In vivo measurement of T_2 distributions and water contents in normal human brain. *Magn Reson Med* **37**: 34–43

Zhao M, Pipe JG, Bonnet J and Evelhoch JL (1996) Early detection of treatment response by diffusion-weighted ^{1}H-NMR spectroscopy in a murine tumor in vivo. *Br J Cancer* **73**: 61–64

British Journal of Cancer (1998) **78**(5), 612–615

Sequential loss of heterozygosity in the progression of squamous cell carcinoma of the lung

C Endo, M Sagawa, M Sato, Y Chen, A Sakurada, H Aikawa, S Takahashi, K Usuda, Y Saito and S Fujimura

Department of Thoracic Surgery, Institute of Development, Aging and Cancer, Tohoku University, 4-1 Seiryo-machi, Aoba-ku, Sendai 980-77, Japan

Summary Radiographically occult bronchogenic squamous cell carcinomas are early lung cancers that localize mainly in the bronchial wall, and are thought to be a good model for investigating genetic alterations through lung cancer progression. In order to elucidate sequential genetic changes in lung cancers, we analysed the incidence of allelic losses on chromosome regions 2q33, 3p21, 5q21, 7q31, 9p21 and 17p13 for 40 cases of radiographically occult bronchogenic squamous-cell carcinomas and 40 cases of advanced lung cancers microdissected. In this study we used eight microsatellite dinucleotide polymorphic markers. Frequent loss of heterozygosity (LOH) was observed on 3p21 (53%), 5q21 (44%) and 17p13 (61%) in roentgenographically occult bronchogenic squamous cell carcinomas. 2q, 7q and 9p were lost less frequently in both roentgenographically occult bronchogenic squamous cell carcinomas and advanced lung cancers. These results suggest that several tumour-suppressor genes are associated with lung cancer progression and that genetic changes on 3p21, 5q21 and 17p13 are early events.

Keywords: radiographically occult bronchogenic squamous-cell carcinoma; loss of heterozygosity; microdissection; microsatellite polymorphism; tumorigenesis

Rapid progress in molecular biology has made it clear that human cancers develop through an accumulation of genetic changes. A study of allelic losses is important to elucidate genetic alterations and in the search for tumour-suppressor genes. Numerous reports have been published concerning allelic losses in advanced lung cancers (Tsuchiya et al, 1992; Field et al, 1996). The first report of allelic losses in preneoplastic lesions of the lung was published by Sundaresan et al (1992) and a few investigators have reported allelic losses in early cancer or precancer of the lung in a few cases (Chung et al, 1995; Hung et al, 1995; Thiberville et al, 1995*a*). Therefore, for the further elucidation of multistep tumorigenesis of lung cancer, more cases of early cancer or precancer of the lung must be examined.

Radiographically occult bronchogenic squamous cell carcinomas (ROCs) are early lung cancers that are detected only by sputum cytology, and are located mainly in the bronchial wall (Saito et al, 1992). Non-treated ROCs develop into advanced lung cancers with radiologically abnormal shadows (radiographically non-occult squamous cell carcinomas; RNOCs) after several years (Saito et al, 1990).

Accordingly, the ROC is thought to be a good model for the purpose of elucidating the sequential genetic alterations in the progression of lung cancer. In this study, we analyse allelic losses on six chromosomes of 40 cases of ROC and 40 of RNOC.

Received 26 September 1997
Revised 5 January 1998
Accepted 16 January 1998

Correspondence to: C Endo, 3-3-14-8, Higashi-Tsukurimichi, Aomori-Shi, Aomori 030, Japan

MATERIALS AND METHODS

Forty cases of resected ROCs and 40 cases of resected RNOCs were examined. All cases were male. All cases of ROCs were classified as stage I. Resected specimens of ROCs were examined pathologically by serial block sectioning (2 mm block thickness) (Nagamoto et al, 1993). Depth and site of maximum invasion were decided by histopathological analysis (Nagamoto et al, 1993). ROCs were divided into two groups according to depth of invasion: intrabronchial wall invasion (25 cases) and extrabronchial wall invasion (15 cases). RNOCs were also divided into two groups: stage I (19 cases) and other stages (stage II–IV, 21 cases).

For RNOCs, tumours and corresponding normal tissues were stored frozen at – 80°C until DNA extraction could be performed. DNA was prepared by proteinase K digestion and phenol–chloroform extraction. For ROCs, eight 20-μm-thick sections of tumours and corresponding normal tissues were cut from formalin-fixed, paraffin-embedded blocks. These eight sections were used for microdissection according to the technique described elsewhere (Sundaresan et al, 1992). DNA was obtained by proteinase K digestion and phenol–chloroform extraction.

Polymorphic DNA markers used in this study were D2S116 on 2q33, D3S643 and D3S1298 on 3p21, D5S659 and L5.71 on 5q21, D7S522 on 7q31, D9S1748 on 9p21 and TP53 on 17p13. These markers were obtained from GenBank (accessions except for D9S1748 were Z16506, D01084, Z16860, Z24277, X78131, Z17100, and X61505, respectively). Sequences of primers for these markers were as follows: 5′-TGCTCATAATCCA-CAAAAAT-3′ and 5′-AAGGAGAAGAGGATTGGATT-3′ for D2S116; 5′-TCCAGGCTGGGTAACAGGAG-3′ and 5′-ACAGAACTGCCAAACCATCC-3′ for D3S643; 5′-GAGGT-GCTAGGGCTCCAG-3′ and 5′-TCCCCTGTGAAGCGTGTG-3′

BRIEF ARTICLE

Neoplasia • Vol. 1, No. 2, June 1999, pp. 113–117 113

Available On-line at http://www.neoplasia.org

Early Increases in Breast Tumor Xenograft Water Mobility in Response to Paclitaxel Therapy Detected by Non-Invasive Diffusion Magnetic Resonance Imaging

Jean-Philippe Galons[*], *Maria I. Altbach*[*], *Gillian D. Paine-Murrieta*[†], *Charles W. Taylor*[†] *and Robert J. Gillies*[*†]

[*] Department of Radiology, [†]Arizona Cancer Center, University of Arizona, Tucson, AZ

Abstract

An important goal in cancer chemotherapy is to sensitively and quantitatively monitor the response of individual patients' tumors to successful, or unsuccessful, therapy so that regimens can be altered iteratively. Currently, tumor response is monitored by frank changes in tumor morphology, yet these markers take long to manifest and are not quantitative. Recent studies suggest that the apparent diffusion coefficient of water (ADC_w), measured noninvasively with magnetic resonance imaging, is sensitively and reliably increased in response to successful CTx. In the present study, we investigate the combination chemotherapy response of human breast cancer tumor xenografts sensitive or resistant to Paclitaxel by monitoring changes in the ADC_w. Our results indicate that there is a clear, substantial, and early increase in the ADC_w after successful therapy in drug sensitive tumors and that there is no change in the ADC_w in p-glycoprotein–positive tumors, which are resistant to Paclitaxel. The mechanism underlying these changes is unknown yet is consistent with apoptotic cell shrinkage and a concomitant increase in the extracellular water fraction.

Introduction

Breast cancer is the second leading cause of death, after lung cancer, in American women. Paclitaxel, an inhibitor of microtubule depolymerization, is an effective chemotherapeutic agent in the adjuvant treatment of breast cancer, with a response rate ranging from 32% to 56% alone, or from 44% to 100% in combination chemotherapy (CTx) with anthracyclines [1]. An important goal in cancer CTx is to tailor treatment regimens to individual patients' genotype, tumor type, and physiology. In order to accomplish this, it will be essential to sensitively and quantitatively monitor the response of individual patients' tumors to successful, or unsuccessful, therapy so that regimens can be altered adaptively. Currently, tumor response is monitored by frank changes in tumor morphology, such as the size or margins of the tumor. However, these macroscopic markers take long to manifest and typically are not quantitative or quantified with modest precision. An intriguing potential improvement in therapeutic monitoring is the noninvasive measurement of the apparent diffusion coefficient of water (ADC_w) by magnetic resonance imaging (MRI). Recent studies have shown that diffusion-weighted MRI (DWI) can detect tumor response to CTx sensitively, quantitatively, and early [2–5]. In the present study, we investigate the CTx response of drug-sensitive and drug-resistant human tumor xenografts to Paclitaxel by monitoring changes in the ADC_w by DWI.

Paclitaxel is a microtubule depolymerization inhibitor commonly used in CTx. It was chosen because it is an extremely potent drug against tumors from MCF7/S cells. Its clinical antitumor activity has been demonstrated in patients with malignancies such as carcinoma of the ovaries, breast, lung, bladder, testes, esophagus, and endometrium [6]. It has also been shown to be more modestly active against Kaposi's sarcoma, lymphoma, and carcinoma of the cervix and stomach [6]. In contrast, taxanes do not have significant activity against neoplasms derived from tissues that overexpress p-glycoprotein (P-gp), including human breast tumor cells [7,8].

DWI is an early, noninvasive indicator of ischemic insult and can be used to successfully diagnose the extent of injury and the response to therapy in a variety of nontumor systems such as brain [9–11]. To date, it has been used primarily in neurological MRI examinations. The physiological mechanisms underlining the ADC_w changes in these systems are thought to involve a shift of water between extracellular and intracellular compartments that accompanies cell swelling or shrinkage. Recently published models have provided a theoretical framework wherein ischemic-associated changes in ADC_w can be interpreted [12,13]. In the case of stroke, decreases in ADC_w values are consistent with cell swelling, causing a shift of water from the extracellular to the intracellular space [14,15]. In the case of rapid hemodialysis of nephrectomized rats, the observed increases of ADC_w are consistent with hypernatremia-induced cell shrinkage and concomitant accumulation of water in the extracellular space [16]. The measurement of ADC_w has not been extensively applied to the study of cancer CTx. However, in the few extant studies, the results are extremely promising.

The use of DWI to monitor the response of tumors to CTx was first proposed by Ross and Chenevert [2,17]. Subsequently, Evelhoch's group [4,5] used ^1H MRS to measure the ADC_w in sarcoma xenografts to detect an early re-

Address correspondence to: Jean-Philippe Galons, Dept. Radiology, Arizona Health Sciences Center, Tucson, AZ 85724. E-mail: jgalons@u.arizona.edu

Received 31 December 1998; Accepted 22 January 1999.

sponse to cyclophosphamide (Cp) and 5-fluorouracil (5FU). In the case of Cp, ADC_w was measured before commencement of CTx and up to 9 days after treatment. Tumor ADC_w increased significantly within 2 days of treatment, which was prior to any observable change in tumor volume or other MRI visible changes. Results with 5FU were similar. Cp is a DNA alkylating agent and 5FU is an antimetabolite. In the present study, we use Paclitaxel, which acts via a distinct mechanism, to test the hypothesis that changes in ADC_w are a general response to successful CTx. In addition, our study measured the ADC_w by DWI, as compared to whole-tumor measurements. The advantage of using DWI is that spatial distribution of the ADC_w in the tumor is obtained. Thus, the responsiveness of various parts in the tumor to CTx can be analyzed.

Materials and Methods

Cell Lines and Tumors

In the current study Paclitaxel (MeadJohnson, Princeton, NJ) was used as CTx agent against tumors grown in severe combined immunodeficient (SCID) mice from MCF7/S and MCF7/D40 cell lines. MCF7/S cells are parental, drug sensitive, breast carcinoma cells that were originally obtained from American Type Culture Collection (ATCC #HTB-22, Rockville, MD). MCF7/D40 were generated *in vitro* by successive culturing in increasing concentrations of doxorubicin. These cells are (P-gp) positive and are 40-fold resistant to doxorubicin, compared to MCF7/S. The CTx responses of these cells to a variety of drugs have been demonstrated *in vitro* and *in vivo* [18].

SCID mice were obtained from the SCID mouse core facility at the University of Arizona Comprehensive Cancer Center. Tumors were grown by implanting 5×10^6 cells in Matrigel (Collaborative Research, Bedford, MA) into the mouse flanks. After 4 to 5 days, tumors reached a size (200–400 mm^3) appropriate for MRI analyses. Paclitaxel-treated animals were injected intraperitoneally with a single dose (27 mg/kg) immediately after the first MRI experiment and given subsequent booster injections (18 mg/kg) every other day. Control mice were injected an equivalent volume of a 0.9% saline solution.

SCID mice are a good system with which to examine the effects of chemotherapeutic agents on human tumor xenografts [19]. Melanoma, colon carcinoma, lung carcinoma, leukemia, prostate, and breast cell lines have all been successfully grown to tumors in SCID mice and successfully treated with CTx, e.g., tamoxifen (breast); Paclitaxel (breast); Cp (breast, leukemia); carmustine (colon), cisplatin (colon); and doxorubicin (leukemia). Therapeutic responses have been determined from tumor volumes, measured with calipers and calculated according to the formula (length $\times$ width^2)/2 [20].

Measurement of ADC_w

MRI was done on a 40 cm clear bore Bruker Biospec 4.7 Tesla (200 MHz ^{1}H) imaging spectrometer (Bruker, Karlsruhe, Germany). In all cases, animals were anesthetized with ketamine:acepromazine:xylazine at 72:6:6 mg/kg, and tumors were placed within a 1 cm diameter, 2-turn solenoidal coil. In DWI, the sample is pulsed with a strong magnetic field gradient, which imparts spatially dependent phase shifts on individual spins (e.g., water protons). After an evolution time, a refocusing pulse is imposed such that stationary spins (i.e., those with low diffusion coefficient, ADC_w) will completely refocus, whereas spins that have moved during the evolution time (i.e., those with high ADC_w) will not refocus, leading to signal attenuation. In DWI, the magnitude of signal is reduced by increasing the gradient strength or the evolution time Eq. (1). The parameters of gradient strength and evolution time are combined in the *b-factor*. DWI were obtained by using a diffusion-weighted stimulated echo pulse sequence [21] at 3 different *b* values. Other imaging parameters included TE, 10 ms; TR, 500 ms; diffusion time Δ, 50 ms; diffusion-weighting gradients duration δ, 4 ms; FOV 2.5 cm, matrix size 128×128).

DWI were then fit on a pixel-by-pixel basis to Eq. (1) by using a routine written for this purpose in interactive data language (IDL). Eq. (1) relates the decrease in signal intensity observed with increasing *b-factor* or ADC_w:

$$S = S_0 e^{-b(\mathrm{ADC})} \tag{1}$$

with

$$b = \gamma^2 G^2 \delta^2 (\Delta - \delta/3)$$

where S and S_0 are the signal intensities in each pixel with and without diffusion weighting, respectively; δ is the diffusion-weighting pulse duration; Δ the delay between the start of the diffusion-weighting pulse; γ the gyromagnetic ratio; and *G* the gradient strength. In the calculation of *b* values, cross terms between diffusion-weighting gradients and imaging gradients were taken into account. A possible source of error is the potential anisotropic nature of tumor tissue. In the presence of anisotropy the measured ADC_w

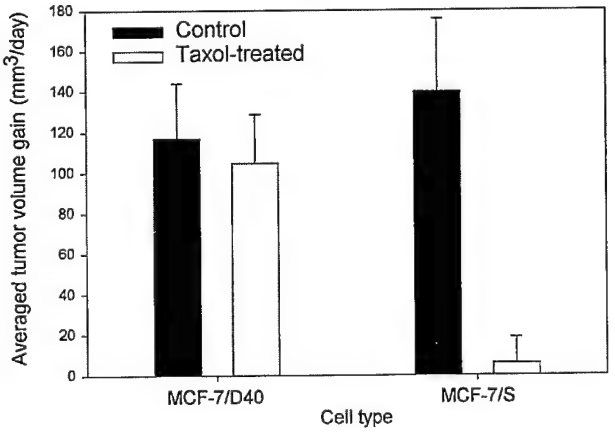

Figure 1. *Tumor volume–based response indexes to Paclitaxel for MCF7/S and MCF7/D40 tumors. In these experiments, the response indexes for the MCF7/D40 and MCF7/S tumors were calculated over a 7-day treatment regime.*

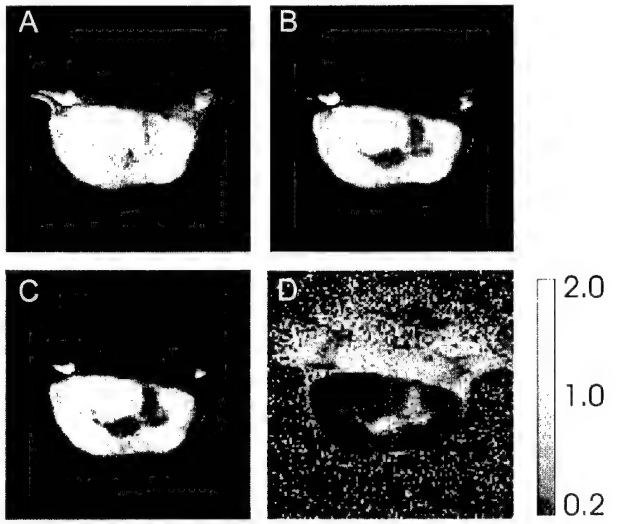

Figure 2. *DWI obtained from a 12-day-old tumor at different values of the diffusion-weighting factor, b. A. b = 0.027 × 10⁹ s/m², B. b = 0.249 × 10⁹ s/m², C. b = 0.442 × 10⁹ s/m². D. ADC_w map calculated from the images shown in A through C. Final ADC_w values were obtained by summing 3 ADC_w maps obtained with diffusion weighting in 3 orthogonal directions (see Materials and Methods).*

becomes a function of the orientation of the tumor relative to the direction of the diffusion gradients. To overcome this problem, we measured ADCs in 3 orthogonal directions and calculated the trace of the ADC_w, a parameter independent of orientation [22].

Results

Response of MCF-7 Tumors to Paclitaxel in Vivo

Figure 1 shows the responses of 8 MCF7/S and 8 MCF7/D40 tumors after treatment with Paclitaxel. Although tumor growth was exponential, data were expressed as the increase in tumor volumes by day 7, normalized to an average per-day basis. As shown in this figure, untreated tumors increase in volume at a rate of 115 to 140 mm^3 per day. In response to Paclitaxel, the drug-sensitive MCF7/S tumors uniformly halted tumor growth, with average volume gains near 5 mm^3 per day, whereas the drug-resistant tumors continued to grow, with volume gains greater than 105 mm^3 per day. The growth rate of the drug-resistant tumors was indistinguishable from the growth rate of untreated tumors. These data demonstrate that the SCID mouse model is relevant to study the response of Paclitaxel CTx in drug-sensitive and drug-resistant tumors grown from MCF7/S and MCF7/D40 cell lines, respectively.

Measurements of ADC_w in MCF7 Tumors

DWI images at different *b*-factors are shown in Figure 2A to C from a representative MCF7 tumor implanted in the

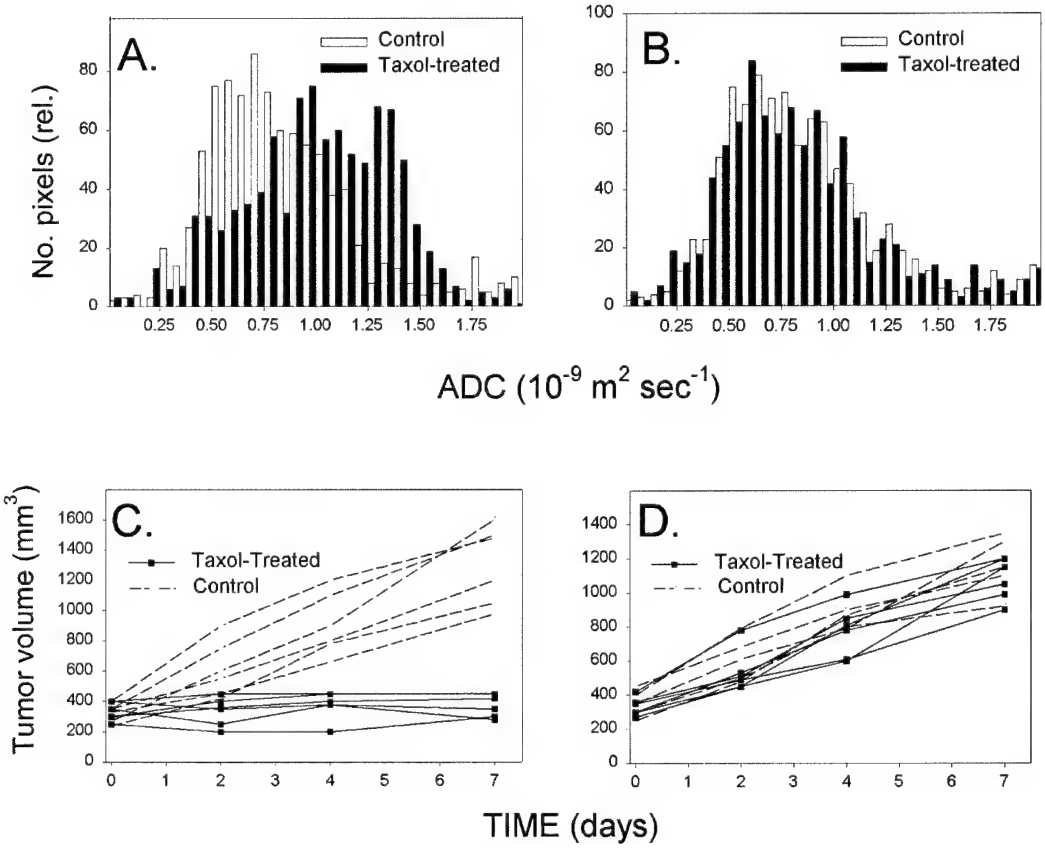

Figure 3. *(A,B) Effect of Paclitaxel on the distribution of ADC_w values in MCF7/S and MCF7/D40 tumors compared to untreated tumors. ADCw values were obtained 48 hours after the beginning of CTx. To allow for a direct comparison, the number of pixels in each tumor was normalized to a value of 1000 and the data averaged for each group (treated and control mice). (C,D) Effect of Paclitaxel on the growth of MCF7/S and MCF7/D40 tumors compared to untreated tumors.*

flanks of a SCID mouse. Note that the image shown was obtained 12 days after tumor inoculation to illustrate the diffusion behavior of necrosis. As the *b*-factor is increased, the pixel intensities inversely reflect the diffusion of the water molecules in the tumor (i.e., the higher the diffusion, the more rapidly the signal intensity is attenuated). Thus, signals originating from the necrotic spaces (dark regions within the tumor) lose intensity faster than the surrounding viable regions of the tumor. This is due to a higher diffusion of water in these regions of the tumor with lower cellularity. The ADC_w map shown in Figure 2D was generated by fitting the signal intensity of each pixel to Eq. (1), as described in Materials and Methods. The structural details seen in Figure 2A to C are also observed in the ADC_w map. However, the ADC_w map is a quantitative representation of absolute values wherein the higher D values are bright, and the DWI in Figure 2A to C show only relative values, with higher D values being dark due to signal attenuation.

Effect of Paclitaxel on the Distribution of ADC_w Values of Tumors

Twenty-four MCF7/S and MCF7/D40 tumors (6 treated and 6 controls of each type) were analyzed by tumor volume and DWI for 7 days after commencement of Paclitaxel CTx. As shown in Figure 3C and D, Paclitaxel arrested growth in all MCF7/S tumors and had no effect on the tumors from MCF7/D40 cells. After DWI examinations, the data were fit on a pixel-by-pixel basis, and ADC_w maps were generated for each tumor. These data were expressed as a histogram of pixel incidence versus ADC_w. As the tumors were remarkably homogeneous within a group, the ADC distribution was averaged for each group of tumors.

Figure 3A and B show histograms of ADC_w values in treated versus untreated tumors for both cell types 48 hours after the start of Paclitaxel CTx. In MCF7/S tumors, the ADC_w distribution in untreated tumors was $0.5 \sim 0.7 \times 10^{-9}$ m^2/s, which was not notably different from the range observed in tumors before treatment. However, in the treated tumors, the ADC_w values were 0.7 to 1.5×10^{-9} m^2/s. In contrast, both treated and untreated MCF7/D40 tumors exhibited ADC_w values similar to those observed in tumors before treatment. Note also that these changes in the ADC_w were apparent 2 days after commencement of CTx. Although there are observable differences in tumor volumes between treated and controls by day 2 (Figure 3C and D), these are not significant.

Discussion

Mechanism of ADC Changes

The mechanism underlying the change in ADC_w after chemotherapy is unknown. However, data from other systems (e.g., stroke) indicate a direct relationship between ADC_w and the extracellular volume fraction. If this mechanism also dominates the ADC_w values observed in tumors, then the higher values observed after CTx of the drug-sensitive tumors would be consistent with a decrease in the intracellular water after Paclitaxel-induced apoptosis. Paclitaxel is known to kill tumor cells via apoptosis [23–26]. A hallmark of apoptosis is a reduction of cell volume via blebbing. Benson et al. have shown that the decreases in cell volume during apoptosis are biphasic, with an early rapid phase that is reversible and a slower, irreversible phase associated with chromosome condensation and DNA hydrolysis [27]. A recent study by Hakumaki et al. (1998) showed a 219% increase in the ADC_w of water in viral thymidine kinase–containing tumors induced to apoptosis with ganciclovir [28]. In this system the relative fraction of extracellular water grew from 87% to 94% in response to CTx. The authors concluded that the measured nuclear magnetic resonance parameters could describe the biophysical signatures for apoptotic cell death.

Mechanism of Paclitaxel CTx

Previous studies investigating the response of ADC_w to CTx used exclusively cytotoxic drugs. It would be of interest to know if these changes also occur in modern cytostatic drugs. Paclitaxel has both cytostatic and cytotoxic properties. Clinically, Paclitaxel produces partial cytostasis (approximately 30% maximum) and apoptosis (maximum apoptotic index of 3.3% to 29%) in human breast tumors [23]. In SKOV3 ovarian carcinoma cells treated with Paclitaxel, the first cellular effect observed with continuous exposure to 50 ng/mL paclitaxel (ID50) was mitotic arrest, followed by DNA fragmentation, first detected at 24 hours and peaking at 48 hours. In this particular study, apoptosis was correlated with an induction and activation of the c-Mos gene product. [24]. Similar results were obtained in 3-dimensional histocultures of ovarian tumors surgically removed from patients ($n = 17$). Paclitaxel was shown to produce a partial inhibition of DNA precursor incorporation in about 40% of tumors and to induce apoptosis in about 90% of tumors, with a maximum apoptotic index of 15% [25]. Finally, in an extensive study of 6 differents cell lines, including bladder RT4, breast MCF7, pharynx FaDu, ovarian SKOV3, and prostate PC3 and DU145, Paclitaxel treatment for as brief a period as 3 hours was sufficient to induce apoptosis, which occurred with a lag time of about 24 hours. The intracellular and extracellular concentrations of the drug reached an equilibrium at approximately 5 hours after the beginning of treatment [26]. Thus, our results are consistent with the triggering of apoptosis by Paclitaxel in MCF7/S tumors, which induces a larger extracellular space, shifting the ADC_w to higher values.

ADC_w and MDR

An important aspect of the current study is that Paclitaxel-induced effects were not observed in MCF7/D40 cells, a P-gp-positive cell line. P-gp is an ATP-dependent drug efflux pump that increases drug efflux when overexpressed. P-gp expression renders cells cross-resistant to a wide variety of drugs [29,30]. The defective accumulation of Paclitaxel in P-gp overexpressing breast cancer cell lines was demonstrated with ^{14}C-Paclitaxel [7]. In another study Mechetner et al. showed a strong correlation between the degree of P-gp expression and *in vitro* resistance to Paclitaxel and doxorubicin in MCF-7/D40 cells [8]. Accordingly,

we did not see any effect of Paclitaxel treatment on the MCF7/D40 tumors in this study. It is noteworthy that Paclitaxel has also been shown to have antiangiogenic activity [31,32]. Presumably this could also have an effect on ADC values as it would decrease the perfusion of the tumor to induce hypoxia and subsequently trigger aptopotic cell death as well. This does not seems to be the case, however, because resistant and sensitive cells should have the same vascular beds, and yet there were distinct responses of ADC_w to CTx. The fact we do not see any Paclitaxel activity in MCF7/D40 tumors indicates that antiangiogenic effects are negligible at this stage of treatment (2 days after a 28 mg/kg Paclitaxel intraperitoneal injection).

Conclusions

The results presented herein show that DWI can identify CTx response and discriminate between sensitive and resistant breast carcinoma tumors at an early stage of chemotherapy, i.e., before frank changes in tumor volume are significant. Moreover, DWI can give a unique insight into the spatial distribution of CTx effects within a tumor over the course of treatment. This method can be easily adapted to the clinic and has the potential to become a noninvasive tool to evaluate the efficacy of CTx treatment in humans.

References

[1] Clemons M, Leahy M, Valle J, Jayson G, Ranson M, and Howell A (1997). Review of recent trials of chemotherapy for advanced breast cancer: The taxanes. *Eur J Cancer* **33**, 2183–2193.

[2] Chenevert TL, and Ross BD (1995). Diffusion, T1 and T2 as chemotherapeutic response predictors of experimental brain tumors. *Proc Int Soc Magn Reson Med* **2**, p. 924.

[3] Chenevert TL, McKeever PE, and Ross BD (1997). Monitoring early response of experimental brain tumors to therapy using diffusion magnetic resonance imaging. *Clin Cancer Res* **3**, 1457–1466.

[4] Zhao M, Pipe JG, Bonnett J, and Evelhoch JL (1996). Early detection of treatment response by diffusion-weighted 1H-NMR spectroscopy in a murine tumour *in vivo*. *Br J Cancer* **73**, 61–64.

[5] Zhao M, and Evelhoch JL (1996). Detection of response to 5-fluorouracil by diffusion-weighted 1H NMR spectroscopy in murine tumors *in vivo*. *Proc Int Soc Magn Reson Med* **2**, p. 1118.

[6] Rowinsky EK (1997). Paclitaxel pharmacology and other tumor types. *Semin Oncol* **24** [suppl 19], S19-1-S19-12.

[7] van Ark-Otte J, Samelis G, Rubio G, Lopez Saez JB, Pinedo HM, and Giaccone G (1998). Effects of tubulin-inhibiting agents in human lung and breast cancer cell lines with different multidrug resistance phenotypes. *Oncol Rep* **5**, 249–255.

[8] Mechetner E, Kyshtoobayeva A, Zonis S, Kim H, Stroup R, Garcia R, Parker RJ, and Fruehauf JP (1998). Levels of multidrug resistance (MDR1) P-glycoprotein expression by human breast cancer correlate with *in vitro* resistance to paclitaxel and doxorubicin. *Clin Cancer Res* **4**, 389–398.

[9] Moseley ME, Kucharczyk J, Mintorovitch J, Cohen Y, Kurhanewicz J, Derugin N, Asgari H, and Norman D (1990). Diffusion-weighted MR imaging of acute stroke: Correlation with T2-weighted and magnetic susceptibility-enhanced MR imaging in cats. *AJNR: Am J Neuroradiol* **11**, 423–429.

[10] Moseley ME, Cohen Y, Mintorovitch J, Chileuitt L, Shimizu H, Kucharczyk J, Wendland MF, and Weinstein PR (1990). Early detection of regional cerebral ischemia in cats: Comparison of diffusion- and T2-weighted MRI and spectroscopy. *Magn Reson Med* **14**, 330–346.

[11] Fischer M, Bockhorst K, Hoehn-Berlage M, Schmitz B, and Hossmann KA (1995). Imaging of the apparent diffusion coefficient for the evaluation of cerebral metabolic recovery after cardiac arrest. *Magn Reson Imaging* **13**, 781–790.

[12] Latour LL, Svoboda K, Mitra P, and Sotak CH (1994). Time-dependent diffusion of water in a biological model system. *Proc Natl Acad Sci USA* **91**, 1229–1233.

[13] Szafer A, Zhong J, and Gore JC (1995). Theoretical model for water diffusion in tissues. *Magn Reson Med* **33**, 697–712.

[14] van Gelderen P, de Vleeschouwer MH, DesPres D, Pekar J, van Zijl PC, and Moonen CT (1994). Water diffusion and acute stroke. *Magn Reson Med* **31**, 154–163.

[15] Warach S, Gaa J, Siewert B, Wielopolski P, and Edelman RR (1995). Acute human stroke studied by whole brain echo planar diffusion-weighted magnetic resonance imaging. *Ann Neurol* **37**, 231–241.

[16] Galons JP, Trouard T, Gmitro AF, and Lien YH (1996). Hemodialysis increases apparent diffusion coefficient of brain water in nephrectomized rats measured by isotropic diffusion-weighted magnetic resonance imaging. *J Clin Invest* **98**, 750–755.

[17] Ross BD, Chenevert TL, Kim B, and Ben-Yoseph O (1994). Magnetic Resonance Imaging and Spectroscopy: Application to Experimental Neuro-Oncology. *Q Magn Reson Biol Med* **1**, 85–102.

[18] Taylor CW, Dalton WS, Parrish PR, Gleason MC, Bellamy WT, Thompson FH, Roe DJ, and Trent JM (1991). Different mechanisms of decreased drug accumulation in doxorubicin and mitoxantrone resistant variants of the MCF7 human breast cancer cell line. *Br J Cancer* **63**, 923–929.

[19] Paine-Murrieta GD, Taylor CW, Curtis RA, Lopez MH, Dorr RT, Johnson CS, Funk CY, Thompson F, and Hersh EM (1997). Human tumor models in the severe combined immune deficient (scid) mouse. *Cancer Chemother Pharmacol* **40**, 209–214.

[20] Taetle R, Rosen F, Abramson I, Venditti J, and Howell S (1987). Use of nude mouse xenografts as preclinical drug screens: *in vivo* activity of established chemotherapeutic agents against melanoma and ovarian carcinoma xenografts. *Cancer Treat Rep* **71**, 297–304.

[21] Altbach MI, Mattingly MA, Brown MF, and Gmitro AF (1991) Magnetic resonance imaging of lipid deposits in human atheroma via a stimulated-echo diffusion-weighted technique. *Magn Reson Med* **20**, 319–324.

[22] Basser PJ, and Pierpaoli C (1996). Microstructural and physiological features of tissues elucidated by quantitative-diffusion-tensor MRI. *J Magn Reson B* **111**, 209–219.

[23] Gan Y, Wientjes MG, Lu J, and Au JL (1998). Cytostatic and apoptotic effects of paclitaxel in human breast tumors. *Cancer Chemother & Pharmacol* **42**, 177–182.

[24] Ling YH, Yang Y, Tornos C, Singh B, and Perez-Soler R (1998). Paclitaxel-induced apoptosis is associated with expression and activation of c-Mos gene product in human ovarian carcinoma SKOV3 cells. *Cancer Res* **58**, 3633–3640.

[25] Millenbaugh NJ, Gan Y, and Au JL (1998). Cytostatic and apoptotic effects of paclitaxel in human ovarian tumors. *Pharm Res* **15**, 122–127.

[26] Au JL, Li D, Gan Y, Gao X, Johnson AL, Johnston J, Millenbaugh NJ, Jang SH, Kuh HJ, Chen CT, and Wientjes MG (1998). Pharmacodynamics of immediate and delayed effects of paclitaxel: Role of slow apoptosis and intracellular drug retention. *Cancer Res* **58**, 2141–2148.

[27] Benson RS, Heer S, Dive C, and Watson AJ (1996). Characterisation of cell volume loss in CEM-C7A cells during dexamethasone-induced apoptosis. *Am J Physiol* **270**(4pt1), C1190–C1230.

[28] Hakumaki JM, Poptani H, Puumalainen AM, Loimas S, Paljarvi LA, Yla-Herttuala S, and Kauppinen RA (1998). Quantitative ^{1}H nuclear magnetic resonance diffusion spectroscopy of BT4C rat glioma during thymidine kinase-mediated gene therapy *in vivo*: Identification of apoptotic response. *Cancer Res* **58**, 3791–3799.

[29] Simon SM, and Schindler M (1994). Cell biological mechanisms of multidrug resistance in tumors. *Proc Natl Acad Sci USA* **91**, 3497–3504.

[30] Nielsen D, and Skovsgaard T (1992). P-glycoprotein as multidrug transporter: A critical review of current multidrug resistant cell lines. *Biochim Biophys Acta* **1139**, 169–183.

[31] Klauber N, Parangi S, Flynn E, Hamel E, and D'Amato RJ (1997). Inhibition of angiogenesis and breast cancer in mice by the microtubule inhibitors 2-methoxyestradiol and paclitaxel. *Cancer Res* **57**, 81–86.

[32] Belotti D, Vergani V, Drudis T, Borsotti P, Pitelli MR, Viale G, Giavazzi R, and Taraboletti G (1996). The microtubule-affecting drug paclitaxel has antigiogenic activity. *Clin Cancer Res* **2**, 1843–1849.

BIOGRAPHICAL SKETCH / CURRICULUM VITAE

ROBERT J. GILLIES
PROFESSOR OF BIOCHEMISTRY, RADIOLOGY AND PHYSIOLOGY
UNIVERSITY OF ARIZONA HEALTH SCIENCES CENTER
ARIZONA CANCER CENTER
1515 N. CAMPBELL AVE. TUCSON, AZ 85724-5024
520/626-5050 (vocal); 520/626-5051 (fax)
GILLIES@U.ARIZONA.EDU

EDUCATION

INSTITUTION AND LOCATION	DEGREE	YEAR CONFERRED	FIELD OF STUDY
University of California, Irvine	B.S.	1974	BIOLOGY
University of California, Davis	PHD.	1979	ZOOLOGY
Yale University	POST-DOC	1982	MOLECULAR BIOPHYSICS

PROFESSIONAL EXPERIENCE:

Appointments (mentor):

1970-1973	Lab Assistant, Neutrino Physics Lab, UC Irvine (F. Reines)
1973-1974	Lab Assistant, Developmental Biology, UC Irvine (H Bode)
1974-1975	Free Researcher, Neurochemistry Institute, U Pasteur, Strasbourg, FRANCE (P. Mandel)
1975-1979	Research and Teaching Assistant, Dept Zoology, UC Davis (DW Deamer)
1979-1981	Post-doctoral Associate, Dept Molec. Biophys. & Biochem., Yale U. (RG Shulman)
1981-1982	Research Associate, Dept. Molec. Biophys. & Biochem., Yale U.
1982-1988	Assistant Professor, Dept. Biochem., Colorado St. Univ.
1988-1996	Associate Professor, Depts. Biochemistry and Radiology, Univ. Arizona
1993-1996	Associate Professor, Dept. Physiology, Univ. Arizona
1994-1995	Guest Scientist, Max Planck Inst. For Biochemistry, Martinsreid, GERMANY (A Ullrich)
1994-pres	Member, Arizona Cancer Center
1996-pres	Professor, Depts. Biochem., Radiology and Physiology, Univ. Arizona
1997-pres	Executive Committee, Univ. Arizona Physiological Sciences Program

Teaching:

1989-pres	SPRING: BIOC 801: Medical Biochemistry (Course co-ordinator, 1996-1998)
1994-pres	FALL: PSIO 503 Graduate Cellular Physiology (8-12 Lectures and labs)
1995-pres	FALL: CBIO 595: Oncogenes and Signal Transduction Journal Club
1998-pres	SPRING: Problem-based Learning for 1st year Medical Students (Founder and Co-ordinator)

Memberships:

1980-pres	Am. Soc. of Biological Chemistry and Molecular Biology,
1982-pres	International Society for Magnetic Resonance in Medicine (ISMRM)
1988-pres	Am. Physiological Society

Society and Editorial Service:

1990-1991	Editor, Annual Reviews of Physiology, Special Section on NMR
1993-1996	Editorial Board, *Am. J. Physiology: Cell*
1995-pres	Editorial Board, *Magnetic Resonance in Medicine*
1996-1997	Chair, Subgroup on Cancer MR, ISMRM
1998-pres	Board of Trustees, ISMRM
1998-pres	Editorial board, *Neoplasia* (new journal)

Honors and Awards:

1992	Outstanding Achievement Award, ACS, Arizona Chapter;
1996, 1999	Basic Science Course Award, Medical Biochemistry
1996	Outstanding Mentor Award, Medical Student Res. Program, UA
1999	Finalist, Virginia Furrow award for Excellence in Basic Science Teaching, UA

National Service and Grant Review Panels

1992	Special Study Section, NCRR, NIH
1993-pres	Special Study Section, NCI Centers Program, NIH (4 x)
1997-1999	Ad Hoc member, Diagnostic Radiology Study Section, CSR, NIH
1996-1998	Member, Biotechnology Study Section, NCRR, NIH
1997-pres	Member, Path-1 Study Section, US Army Breast Cancer Research Program
2000-pres	Member, Diagnostic Radiology Study Section, CSR, NIH
1999	Workshop Consensus Panel on Emergent Imaging Technologies, NCI, NIH
1999	Workshop Consensus Panel on Clinical Applications of MRS
1999	Member, Special Emphasis Panels, CSR, NIH
1999	NCI panel on Bioengineering Consortia for Cancer Diagnosis
1999	Bioengineering Programs Review Panel, CSR, NIH

Meeting Organization

Oct. 9-10, 1993	Southwest Regional NMR Meeting, Tucson, AZ
Aug. 5-9, 1996	Int'l Workshop on "Applications of MR to Cancer", Baltimore, MD
Aug 12-16, 1996	APS Conference on "pHysiology of Acid-Base Regulation", Snowmass at Aspen, CO
October, 2000	Tumor pH (Novartis symposium) London, UK

Invited Presentations (1989-date):

<u>1989</u>	
2/16/89	University of Cincinnatti Dept. Biological Chemistry, Cincinnatti, OH
2/23/89	Hopkins Marine Station, Stanford Univ., Monterey, CA
4/5/89	Carnegie-Mellon U. Dept. Biology, Pittsburgh, PA
4/28/89	Univ. Basel, Dept. Medicinal Chemistry, Basel, Switz.
5/1/89	Univ. Marseilles Sch Med, Magnetic Resonance Unit., Marseilles, FRANCE
5/9/89	European Molecular Biology Organization, Heidelberg, GERMANY
5/11/89	Univ. Bordeaux, ICBN/CNRS, Bordeaux, FRANCE
7/14/89	Kinetek Corp., St. Louis, MO
9//5/89	Pan-American Physiology Meetings, Puebla, MEXICO
11/28/89	Microgon Corp., Laguna Nigel, CA
<u>1990</u>	
2/21/90	Dept. Radiology, Johns Hopkins Univ., Baltimore, MD
6/2/90	New Mexico Regional NMR meeting, Los Alamos, NM
9/10/90	Int'l Conf. Magnetic Resonance in Biological Systems, Warwick ENGLAND
9/18/90	Free University, Amsterdam, NETHERLANDS
9/21/90	Ludwigs Maximillian University, Munich, GERMANY
10/1/90	Instituto Investigaciones Biomedicas, Madrid, SPAIN
11/14/90	Pan American Biochemistry Meetings, San Louis Potosi, MEXICO
<u>1991</u>	
1/30/91	Univ. Calif. Dept. Med. Chem., San Francisco, CA
2/25/91	Dept. Biol. Chem. Univ. Calif., Davis, CA
4/24/91	Div. Biotechnology, Texas A & M Univ., College Station, TX
7/23/91	Aspen Cancer Conference, Aspen, CO
10/26/91	American Cancer Society Regional Mtg., Scottsdale, AZ
11/5/91	Course on In Vivo NMR, Madrid, SPAIN
11/9/91	Dept. Biochem. Physiology, Univ Nice, Nice, FRANCE
12/9/91	Eli Lilly Pharmaceuticals, Indianapolis, IN
12/13/91	NCI Workshop on NMR and Cancer, Bethesda, MD
12/14/91	Georgetown U., Washington, DC

Invited Presentations (cont)

1992

6/18/92 Carnegie-Mellon U. Dept. Biology, Pittsburgh, PA
7/24/92 International Cell Biology Conference, Madrid, SPAIN
10/22/92 American Cancer Society Regional Mtg., Scottsdale, AZ
11/9/92 Sandoz Pharmaceuticals, Newark, NJ

1993:

2/11/93 Dept. Molecular Physiology, Yale Univ., New Haven, CT
2/15/93 Dept. Pathology, Georgetown U., Washington, D.C.
4/13/93 Dept. Physiol., Univ. Alabama, Birmingham, AL
4/14/93 Dept. Radiology, Emory Univ., Atlanta, GA
4/15/93 Dept. Physiology, Emory Univ., Atlanta, GA
5/20/93 Int'l Congress on Biophysical Chemistry, San Luis Potosi, MEXICO
5/21/93 Int'l Congress on Biophysical Chemistry, San Luis Potosi, MEXICO
8/20/93 Dept. Radiology, Johns Hopkins Univ., Baltimore, MD
9/20/93 Int'l Conference on Lymphology, Bethesda, MD.

1994

4/25/94 APS annual meeting, Anaheim, CA
6/6/94 Dept. Physiol., Tufts Univ. Sch. Med, Boston, MA
10/7/94 Dept. Pediatrics and Cell. Biol., St. Louis U., St. Louis, MO.
11/994 Max Planck Inst. fuer Biochemistry, Munich, GERMANY
11/1194 Physiology Department, Univ. Tuebingen, GERMANY
11/1494 CNRS Centre Neurochemie, Univ. Grenoble, FRANCE
11/16/94 Dept. Biochemistry, U. Cambridge, GREAT BRITAIN
11/17/94 Dept. MR Res. St. George□s Hosp., London, GREAT BRITAIN
11/1894 London MR group, London, GREAT BRITAIN

1995 (sabbatical year began in July)

10/16/95 Int'l Conf. On Lipids and Cancer, Corfu, GREECE

1996 (sabbatical year ended in July)

2/16/96 Physiological Chemistry Inst., Ludwig Maximilian Universitaet, Munich, GERMANY
4/8/96 Dept. Biochemistry, U. Cambridge, GREAT BRITAIN
4/15/96 Dept. Chemistry. Kansas, Lawrence, KS
6/28/96 Instituto Investigaciones Biomedicas, Madrid, SPAIN
11/2/96 Dept. Biochemistry, Univ. Osaka, Osaka, JAPAN
11/5/96 Int'l Conf on Vacuolar H^+-ATPases, Shonan, JAPAN

1997 (tore rotator cuff while skiing. Out of commission for 6 months)

11/1/97 US Army Breast Cancer Research, Washington, DC
11/19/97 Tissue Engineering, Univ. N. Carolina, Chapel Hill, NC

1998

4/14/98 ISMRM, Sydney, AUSTRALIA
10/13/98 Working Group on Functional Imaging in Oncology, Bethesda, MD
11/14/98 Cancer MR Workshop, St. Louis, MO

1999

3/6/99 Angiogenesis workshop: Univ. Arizona Biomedical Engineering Program
4/6/99 Translational Research on Breast Cancer Imaging; Univ. Arizona Cancer Center
4/8/99 Dept. Radiology, Univ. Calif. Irvine, CA
4/22/99 Working Group on Clinical MRS, Nat'l Cancer Inst., Bethesda, MD
5/23/99 ISMRM, Philadelphia, PA
5/21/99 Niemann-Pick Type C, Parseghian Foundation, Tucson, AZ
7/27/99 Am. Assoc. Physicists in Medicine, Nashville, TN
9/28/99 Imaging in 2020, Jackson Hole, WY
10/8/99 Dept. Physiology, Texas Tech U., Lubbock, TX
10/14/99 Int'l Conf. on NP-C, Bethesda, MD

2000

2/15/00 Pan-Pacific NMR Conference, Brisbane, AUSTRALIA
4/2/00 ISMRM, Denver, COLO

PUBLICATIONS

Books or Monographs (1)

Gillies RJ, ed. (1994) *NMR in Physiology and Biomedicine*, RJ Gillies, editor. Academic Press. 471 pp, large format

Review Articles (13)

Gillies RJ and Deamer DW (1979) "Intracellular pH: Methods and Applications" *Curr. Top. Bioenergetics* 9, 63-89

Gillies RJ (1981) Intracellular pH and control of proliferation in animal cells. in *The Transformed Cell*, IB Cameron and TB Poole, eds, Academic Press.

Gillies RJ, Alger JR, den Hollander JA and RG Shulman(1981) "Intracellular pH measured by NMR: methods and results". *Kroc.Found.Ser.*, *15*:79-104.

Gillies RJ (1981) "Intracellular pH and proliferation in yeast, Tetrahymena and sea urchin eggs" *Kroc.Found.Ser.*, *15*:341-359.

Gillies RJ, Dale BE, Drury DD and Chresand TJ (1987) "Design and application of bioreactors for NMR Analyses of Mammalian Cells", *Rev. Mag. Reson. Med.* **1**, 155-179.

Gillies RJ and Okerlund LS (1988) "Determination of intracellular pH and sodium using NMR", pp. 23-48 IN: *Na^+/H^+ Exchange*, S Grinstein, ed., CRC press

Gillies RJ, NE MacKenzie and BE Dale (1989) "Analyses of Hollow fiber bioreactor Performance by Nuclear Magnetic Resonance Spectroscopy" *Bio/Technology* **7**, 50-54

Dale BE and **Gillies RJ** (1991) "Nuclear Magnetic Resonance Spectroscopy of Dense Cell Populations for Metabolic Studies and Bioreactor Engineering: A Synergistic Partnership" In *Animal Cell Bioreactors*, CS Ho and DI C Wang, eds., Butterworth-Heinemann, pp. 107-118

Martinez-Zaguilan R and **Gillies RJ** (1992) "A plasma membrane V-type H^+-ATPase may contribute to elevated intracellular pH in some human tumor cells". *Ann.N.Y.Acad.Sci*, *671*:478-480.

Gillies RJ, Martinez-Zaguilan RM, Peterson EP and Perona R (1992) "The role of intracellular pH in mammalian cell proliferation", *Cell Physiol. Biochem.* **2**, 159-179.

Gillies RJ (1992) "Physiological applications of NMR", *Ann. Rev. Physiol.* 54, 733-748.

Gillies RJ (1994) "Bioreactors for NMR" Encyclopedia of NMR, Wiley

Martinez-Zaguilan R, Tompkins LS, **Gillies RJ** and Lynch RM (1998) "Simultaneous analysis of Intracellular pH and Calcium from Cell Populations". *Meth. Molec. Biol.* 114: 287-306.

Refereed journal articles (62)

1976

Noble EP, **Gillies R**, Vigran R and Mandel P (1976) "The modification of the ethanol withdrawal syndrome in rats by di-n-propylacetate". *Psychopharmacologia*, *46*:127-131.

1979 (beginning of publications from UC Davis: graduate student)

Gillies RJ and Deamer DW (1979) "Intracellular pH changes during the cell cycle in Tetrahymena". *J Cell.Physiol*, *100*:23-31.

1980

Gillies RJ and Deamer DW (1980) "Endogenously produced CO_2 induces stationary phase in Tetrahymena cultures". *J Cell.Physiol*, *105*:221-225.

1981 (beginning of publications from YALE: post-doc)

Alger JR, Sillerud LO, Behar KL, **Gillies RJ**, Shulman RG, Gordon RE, Shae D and Hanley PE (1981) "In vivo carbon-13 nuclear magnetic resonance studies of mammals". *Science*, *214*:660-662.

Gillies RJ, Rosenberg MP and Deamer DW (1981) "Carbon dioxide efflux accompanies release of fertilization acid from sea urchin eggs". *J Cell.Physiol*, *108*:115-122.

Gillies RJ, Ugurbil K, den Hollander JA and Shulman RG (1981) "^{31}P NMR studies of intracellular pH and phosphate metabolism during cell division cycle of Saccharomyces cerevisiae". *Proc.Natl.Acad.Sci U S.A.*, *78*:2125-2129.

1982

Gillies RJ, Ogino T, Shulman RG and Ward DC (1982) "^{31}P nuclear magnetic resonance evidence for the regulation of intracellular pH by Ehrlich ascites tumor cells". *J Cell.Biol.*, *95*:24-28.

PUBLICATIONS (CONT.)

1983 (last publications from YALE)

Findly RC, **Gillies RJ** and Shulman RG (1983) *"In vivo* ^{31}P nuclear magnetic resonance reveals lowered ATP during heat shock of *Tetrahymena*." *Science, 219*:1223-1225.

Gillies RJ and Benoit AG (1983) "NMR analysis of a cell division cycle mutant of *Saccharomyces cerevisiae*." *Biochim.Biophys.Acta, 762*:466-470.

1986 (beginning of publications from Colorado State)

Gillies RJ, Didier N and Denton M (1986) "Determination of cell number in monolayer cultures". *Anal.Biochem, 159*:109-113.

1987

DeFronzo M and **Gillies RJ** (1987) "Characterization of methylphosphonate as a ^{31}P NMR pH indicator". *J Biol.Chem., 262*:11032-11037.

Gillies RJ, Cook J, Fox MH and Giuliano KA (1987) "Flow cytometric analysis of intracellular pH in 3T3 cells". *Am.J Physiol., 253*:C121-C125.

Giuliano KA and **Gillies RJ** (1987) "Determination of intracellular pH of BALB/c-3T3 cells using the fluorescence of pyranine". *Anal.Biochem, 167*:362-371.

Nelson TR, **Gillies RJ**, Powell DA, Schrader MC, Manchester DK and Pretorius DH (1987) "High resolution proton NMR spectroscopy of human amniotic fluid". *Prenat.Diagn., 7*:363-372.

1988

Chresand TJ, **Gillies RJ** and BE Dale (1988) "Optimum Fiber Spacing in a Hollow fiber Bioreactor". *Biotech. Bioengr.* **32**, 983-992

Drury DD, Dale BE and **Gillies RJ** (1988) "A Bioreactor to Maintain Mammalian Cells Under Defined Conditions Within a NMR Spectrometer" *Biotech. Bioengr.* **32**, 966-974

Chresand TJ, Dale BE, Hanson SL and **Gillies RJ** (1988) "A Stirred Bath Technique for Diffusivity Measurements in Cell Matrices" *Biotech. Bioengr.* **32**, 1029-1036

Lucas CA, **Gillies RJ**, Olson JE, Giuliano KA, Martinez R and Sneider JM (1988) "Intracellular acidification inhibits the proliferative response in BALB/c-3T3 cells". *J Cell.Physiol, 136*:161-167.

Martinez R, **Gillies RJ** and Giuliano KA (1988) "Effect of serum on the intracellular pH of BALB/c-3T3 cells: serum deprivation causes changes in sensitivity of cells to serum". *J. Cell.Physiol, 136*:154-160.

1989 (last publications from Colorado State)

Dale BE, Blute TR and **Gillies RJ** (1989) "Cell Density Measurements in Hollow fiber Bioreactors", *Biotech. Progress* **4**, 202-209

Martinez R and **Gillies RJ** (1989) "Dimethylsulfoxide modifies the sensitivity of BALB/c-3T3 cells to the activation of Na^+/H^+ exchange by phorbol esters". *J Cell.Physiol, 139*:131-135.

Gillies RJ, Martinez R, Sneider JM and Hoyer PB (1989) "Sphingosine inhibits phorbol 12-myristate 13-acetate-, but not serum-induced, activation of Na^+/H^+ exchange in mammalian cells". *J Cell.Physiol, 139*:125-130.

1990 (beginning of publications from Arizona)

Gillies RJ, Martinez-Zaguilan R, Martinez GM, Serrano R and Perona R (1990) "Tumorigenic 3T3 cells maintain an alkaline intracellular pH under physiological conditions". *Proc.Natl.Acad.Sci U S.A., 87*:7414-7418.

Wegner JA, Martinez-Zaguilan R, Wise ME, **Gillies RJ** and Hoyer PB (1990) "Prostaglandin $F_{2\alpha}$-induced calcium transient in ovine large luteal cells: I. Alterations in cytosolic-free calcium levels and calcium flux". *Endocrinology, 127*:3029-3037.

1991

Wegner JA, Martinez-Zaguilan R, **Gillies RJ** and Hoyer PB (1991) "Prostaglandin $F_{2\alpha}$-induced calcium transient in ovine large luteal cells: II. Modulation of the transient and resting cytosolic free calcium alters progesterone secretion". *Endocrinology, 128*:929-936.

Gillies RJ, Scherer PG, Raghunand N, Okerlund LS, Martinez-Zaguilan R, Hesterberg L and Dale BE (1991) "Iteration of hybridoma growth and productivity in hollow fiber bioreactors using ^{31}P NMR". *Magn.Reson.Med, 18*:181-192.

Gillies RJ and Martinez-Zaguilan R (1991) "Regulation of intracellular pH in BALB/c-3T3 cells. Bicarbonate raises pH via $NaHCO_3$/HCl exchange and attenuates the activation of Na^+/H^+ exchange by serum". *J Biol.Chem., 266*:1551-1556.

Martinez-Zaguilan R, Martinez GM, Lattanzio F and **Gillies RJ** (1991) "Simultaneous measurement of intracellular pH and Ca^{2+} using the fluorescence of SNARF-1 and FURA-2". *Am.J Physiol., 260*:C297-C307.

Dale BE and **Gillies RJ** (1991) "Nuclear magnetic resonance spectroscopy of dense cell populations for metabolic studies and bioreactor engineering: a synergistic partnership". *Biotechnology, 17*:107-118.

PUBLICATIONS (CONT.)

1992

Lien YH, Zhou HZ, Job C, Barry JA and **Gillies RJ** (1992) "In vivo ^{31}P NMR study of early cellular responses to hyperosmotic shock in cultured glioma cells". *Biochimie.*, *74*:931-939.

1993

Barry JA, McGovern KA, Lien YH, Ashmore B and **Gillies RJ** (1993) "Dimethyl methylphosphonate (DMMP): a ^{31}P nuclear magnetic resonance spectroscopic probe of intracellular volume in mammalian cell cultures". *Biochemistry.*, *32*:4665-4670.

Gillies RJ, Galons JP, McGovern KA, Scherer PG, Lien YH, Job C, Ratcliff R, Chapa F, Cerdan S and Dale BE (1993) "Design and application of NMR-compatible bioreactor circuits for extended perfusion of high-density mammalian cell cultures". *NMR. Biomed.*, *6*:95-104.

Martinez-Zaguilan RM, Martinez GM, Lynch R and **Gillies RJ** (1993) "A vacuolar-type H^+ ATPase is expressed in the plasma membranes of tumor cells" *Am J. Physiol. 265*, C1015-C1029

1994

Wegner JA, Martinez-Zaguilan R, **Gillies RJ** and Hoyer PB (1994) "Prostaglandin F2[illegible], releases intracellular calcium from a thapsigargin-sensitive pool in ovine large luteal cells." Am. J. Physiol: *Endocrinology*, 50-56

Sanchez-Armass S, Martinez-Zaguilan R, Martinez GM and **Gillies RJ** (1994) "Regulation of pH in rat brain synaptosomes: role of bicarbonate and potassium". *J. Neurophysiol.* 71, 2236-2248

Martinez-Zaguilan, R, **Gillies, RJ**, Zapata N and Sanchez-Armass S (1994) "Regulation of pH in rat brain synaptosomes: role of chloride". *J Neurophysiol.* 71, 2249-2257

Gillies RJ, Liu Z andBhujwalla Z (1994) "^{31}P MRS Measurement of extracellular in tumors using 3-aminopropylphosphonate". *Am. J. Physiol.:* Cell 267:C195-C203

Gillies RJ, Barry JA and Ross BD (1994) *"In vitro* and *in vivo* ^{13}C and ^{31}P NMR analyses of phosphocholine metabolism in rat glioma cells". *Magn. Reson. Med.* 32: 310-318

Peterson EP, Martinez-Zaguilan R, Martinez GM, Perona R and **RJ Gillies** (1994) "NIH-3T3 cells transfected with a yeast H^+ ATPase have altered sensitivity to insulin, IGF-1 and PDGF" *J. Cell. Physiol.* 159: 551-560

Lax D, Martinez-Zaguilan R and **Gillies RJ** (1994). "Effects of furazolidone on intracellular pH and calcium homeostasis in chick cardiac myocytes." *Am. J. Physiol* 267 (Heart and Circulatory 36): H734-H741

Wiskinsky AM, Martinez-Zaguilan R, Alden C, Gandolfi AJ and **Gillies RJ** (1994). "Phenobarbital induces cytosolic acidification in an established liver epithelial cell line" *Toxicol. Lett.* 74, 157-166

Martinez GM, Martinez-Zaguilan R and **Gillies RJ** (1994) "Effect of glucose on pH^{in} and $[Ca^{2+}]_{in}$ in NIH-3T3 cells transfected with the yeast P-type-H^+-ATPase". *J. Cell Physiol.* 161: 129-141

Martinez-Zaguilan R, Wegner JA, **Gillies RJ** and Hoyer PB (1994). "Differential regulation of Ca^{2+} homeostasis in ovine large and small luteal cells". *Endocrinology* 135: 2099-2108

Gunn M, Martínez-Zaguilán R, Wald-Hopkins S, Woolridge D and **Gillies RJ** (1994). "NIH-3T3 cells transfected with a yeast H^+-ATPase have altered rates of protein turnover". *Arch. Biochem. Biophys.*314, 268-275

1995

Galons JP, Job C, and **Gillies RJ**. (1995) Increase of GPC levels in cultured mammalian cells during acidosis. A 31P MR spectroscopy study using a continuous bioreactor system. *Magnetic Resonance in Medicine*, *33*:422-6

Lien YH, Wang X, **Gillies RJ**, and Martinez-Zaguilan R. (1995) Modulation of intracellular Ca2+ by glucose in MDCK cells: role of endoplasmic reticulum Ca(2+)-ATPase. *American Journal of Physiology*, *268*:F671-9

Wang W, Lien Y-H, **Gillies RJ** and Martinez-Zaguilan R (1995) Glucose decreases intracellular free calcium and pH in cultured rat aortic vascular smooth muscle cells: role of Ca-ATPase. *Cell. Physiol. Biochem.* 5, 299-312

1996

Martinez-Zaguilan R, Chinnock BF, Wald-Hopkins S, Bernas M. Way D, Weinand M, Witte MH and **Gillies RJ**. (1996) Calcium and pH homeostasis in Kaposi sarcoma cells. *Cell. Physiol. Biochem.* 6, 169-184

Aiken NR and **Gillies RJ**. (1996) Phosphomonoester metabolism as a function of cell proliferative status and exogenous precursors. *Anticancer Research*, *16*:1393-7

*Martinez-Zaguilan R, Seftor EA, Seftor RE, Chu YW, **Gillies RJ**, and Hendrix MJ (1996) Acidic pH enhances the invasive behavior of human melanoma cells. *Clinical & Experimental Metastasis, 14*:176-86

1997

Xie X, **Gillies RJ**, Gerner EW. (1997) Characterization of a diamine exporter in Chinese hamster ovary cells and identification of specific polyamine substrates. *J. Biol. Chem. 272*:20484-20489

PUBLICATIONS (CONT.)

1998

*Martinez-Zaguilan R, Martinez GM, Gomez A and **Gillies RJ** (1998) Distinct regulation of pH and Ca by cells of differing metastatic potential. *J. Cell. Physiol* 176:196-205

*Bhujwalla ZM, McCoy CL, Glickson JD, **Gillies RJ** and Stubbs M (1998) Non-invasive estimations of intra- and extracellular volume and pH by 31-P MRS: applications to untreated and 5-FU treated RIF-1 tumors. *Br. J. Cancer.* 78, 606-611

1999

*Martinez-Zaguilan R. Raghunand N, Lynch RM, Bellamy W, Martinez GM, Rojas B, Smith DJ, Dalton WS and **Gillies RJ** (1999) pH and Drug Resistance I. Plasmalemmal V-type H+-ATPase is expressed in drug resistant human breast carcinoma cell lines. *Biochem. Pharmacol.* 57, 1037-1046.

* Martinez-Zaguilan R. Raghunand N, Lynch RM, Bellamy W, Martinez GM, Rojas B, Smith DJ, Dalton WS and **Gillies RJ** (1999) pH and Drug Resistance II. Turnover of acidic vesicles and resistance to weakly basic chemotherapeutic drugs. *Biochem. Pharmacol.* 57, 1047-1058.

*van Sluis R, Bhujwalla Z, Raghunand N, Ballesteros P, Alvarez J, Cerdan S, and **Gillies RJ** (1999) Imaging of extracellular pH of tumors using 1H MRSI. *Magnetic Resonance in Medicine* 41:743-750.

*Bhujwalla ZM, Aboagye EO, **Gillies RJ**, Chacko VP, Mendola CE and Backer JM (1999) Nm23-transfected MDA-mb-435 human breast carcinoma cells form tumors with altered phospholipid metabolism and pH: A 31-P NMR study in vivo and in vitro. Magn. Reson. Med. 41, 897-903

*Raghunand N, He X, van Sluis R, Mahoney B, Baggett B, Taylor CW, Paine-Murrietta G, Roe D, Bhujwalla ZM and **Gillies RJ** (1999) Enhancement Of Chemotherapy By Manipulation Of Tumor pH. *Br. J. Cancer* 80, 1005-1011.

Gillies RJ (1999) Angiostatin's partners (letter). *Science* 284, 434-434

*Raghunand N, Altbach MI, van Sluis R, Baggett B, Taylor CW, Bhujwalla ZM and **Gillies RJ** (1998) Plasmalemmal pH-gradients in Drug-Sensitive and Drug-Resistant MCF-7 Human Breast Carcinoma Xenografts Measured by ^{31}P MR Spectroscopy. *Biochem. Pharmacol.* 57, 309-312.

*Galons J-P, Altbach MI, Taylor CW, Payne-Murrietta G and **Gillies RJ** (1999) Early Increases in Breast Tumor Xenograft Water Mobility in Response to Paclitaxel Therapy Detected by Non-Invasive Diffusion Magnetic Resonance Imaging. *Neoplasia* 1(2), 113-117.

Gillies RJ, Schornack PA, Secomb TW and Raghunand N (1999) The Hemodynamic and Nutritive Aspects of Blood Flow in Tumors. *Neoplasia* 1(3), 197-207.

*Supported by DAMD 17-94-J-4368.

CURRENT GRANT SUPPORT:

Flinn Foundation

"Biological Magnetic Resonance Facility"	RJ Gillies and A Gmitro, Co-PI
9/1/97-8/31/02	0% effort
Direct costs- Year 01	$94,778
Total Direct costs	$492,234

The Flinn Foundation is an Arizona-based philanthropic organization that supports biomedical research centers. This grant is used to support scientific infrastructure, salaries of young investigators and outreach.

NIH-DRR S10 RR13048-01

"Microimaging Upgrade of AMX 400 WB"	RJ Gillies, PI
4/1/98-3/31/00	0% effort
Total Direct costs:	$270,800

This is a shared instrument proposal for the upgrade of our current AX400 WB spectrometer to include microimaging capabilities.

NIH-R01 GM84238-01a1

"MRI and MRS of Model Stroke in Perfused Cell Cultures"	T Trouard, P.I.
1/1/99-12/31/04	4% effort
Requested Annual Direct Costs - Year 01	$119,854
Requested Total Direct Costs	$306,016

This proposal aims to investigate the molecular mechanisms behind the changes in the apparent diffusion coefficient of water in stroke. The major technique to be employed is MR analyses of cultured cells in bioreactors.

NIH-RO1 CA80130-01

"Control of PME Metabolism in Metastasis and Chemotherapy"	NR Aiken, PI
1/1/99-07/31/02	15% effort
Requested Annual Direct Costs – Year 01	$125,392
Requested Total Direct Costs	$530,591

The aims of this proposal is to define the biochemical regulation of phosphomonoester levels and to determine how these metabolic pathways are affected by chemotherapy in a series of metastatic and non-metastatic breast cancer cells..

Parseghian Foundation

"Noninvasive monitoring of NP-C Progression and therapy with MRS/MRI"	RJ Gillies, PI
1/1/99-12/31/00	15% effort
Total direct costs	$94,526

The goal of this research is to develop a non-invasive and quantitative method to monitor the progression of NP-C disease and its response to successful therapy.

*NIH-RO1 CA77575-01

"Causes and Consequences of Acid pH in Tumors"	RJ Gillies, PI
7/1/99-6/30/03	30% effort
Requested Annual Direct Costs – Year 01	$226,259
Requested Total Direct Costs	$1,021,795

The aims of this proposal are to develop more sophisticated techniques to monitor pH of tumors, to define mechanisms leading to the acidic tumor environment, and to examine the effect of manipulating tumor pH on chemotherapy.

NIH-R24CA83148-01

"Small Animal Imaging Facility"	RJ Gillies, PI
7/1/99-6/30/04	20% effort
Requested Annual Direct Costs – Year 01	$1,004,113
Requested Total Direct Costs	$4,215,093

The aims of this proposal are to establish a small animal imaging facility dedicated to cancer research employing MRI, SPECT and OCT imaging modalities.

*Resulting from Army Support.